

POST-MAGMATIC MODIFICATION OF THE SULPHIDE DEPOSITS FROM
THE THOMPSON NICKEL BELT, MANITOBA, CANADA

BY

JANICE LIWANAG

A Thesis Submitted to the Faculty of Graduate Studies
in Partial Fulfillment of the Requirements for the Degree of

MASTER OF SCIENCE

Department of Geological Sciences

University of Manitoba

Winnipeg, Manitoba, Canada

© April, 2001



National Library
of Canada

Acquisitions and
Bibliographic Services

395 Wellington Street
Ottawa ON K1A 0N4
Canada

Bibliothèque nationale
du Canada

Acquisitions et
services bibliographiques

395, rue Wellington
Ottawa ON K1A 0N4
Canada

Your file Votre référence

Our file Notre référence

The author has granted a non-exclusive licence allowing the National Library of Canada to reproduce, loan, distribute or sell copies of this thesis in microform, paper or electronic formats.

The author retains ownership of the copyright in this thesis. Neither the thesis nor substantial extracts from it may be printed or otherwise reproduced without the author's permission.

L'auteur a accordé une licence non exclusive permettant à la Bibliothèque nationale du Canada de reproduire, prêter, distribuer ou vendre des copies de cette thèse sous la forme de microfiche/film, de reproduction sur papier ou sur format électronique.

L'auteur conserve la propriété du droit d'auteur qui protège cette thèse. Ni la thèse ni des extraits substantiels de celle-ci ne doivent être imprimés ou autrement reproduits sans son autorisation.

0-612-76790-6

Canada

**THE UNIVERSITY OF MANITOBA
FACULTY OF GRADUATE STUDIES

COPYRIGHT PERMISSION PAGE**

Post-Magmatic Modification of the Sulphide Deposits from the Thompson Nickel Belt,

Manitoba, Canada

BY

Janice Liwanag

A Thesis/Practicum submitted to the Faculty of Graduate Studies of The University

of Manitoba in partial fulfillment of the requirements of the degree

of

Master of Science

JANICE LIWANAG © 2001

Permission has been granted to the Library of The University of Manitoba to lend or sell copies of this thesis/practicum, to the National Library of Canada to microfilm this thesis/practicum and to lend or sell copies of the film, and to Dissertations Abstracts International to publish an abstract of this thesis/practicum.

The author reserves other publication rights, and neither this thesis/practicum nor extensive extracts from it may be printed or otherwise reproduced without the author's written permission.

ABSTRACT

Disseminated to massive sulphides from the Thompson Nickel Belt, Manitoba, show textural and geochemical evidence of being modified by deformation and fluid alteration. Samples of massive sulphide horizons, hosting metasediments, sulphide-bearing ultramafic rocks, and sulphide breccias were collected from the Thompson, Birchtree, and William Lake deposits. Sulphide minerals from these samples were examined petrographically and analyzed by electron microprobe analysis (EMPA) and proton-induced X-ray emission (PIXE). Representative samples were analyzed by whole-rock geochemical techniques.

Compositional zonation occurs in and around massive sulphide horizons hosted by metasediments. Disseminated pyrrhotite grains in metasediments occurring within ~20 metres of a massive sulphide horizon are enriched in Ni relative to pyrrhotite grains that are more distal to the massive sulphide horizon. These Ni-enriched disseminated pyrrhotite grains co-exist with Ni-enriched pentlandite. Chalcopyrite tends to be concentrated into stringers at the contacts between massive sulphide horizons and hosting metasediments. During high-grade metamorphism, Cu may have migrated to the contacts. During final cooling of the sulphides, fluid-assisted diffusion of Ni from the massive ores to the metasediments may have occurred.

Massive ores from the Thompson, Birchtree, and Pipe deposit are very depleted in Pt relative to other platinum group elements (PGE). The Pt depletion may be the result of 1) the fractionation of Pt from the other PGE under reducing conditions or 2) mobilization of Pt from the massive ores due to metamorphic or metasomatic processes. The most deformed (i.e. remobilized) massive ores in the Thompson Nickel Belt contain higher Ni

tenors, Ni/Co ratios, Se/S ratios, and Pd/Ir ratios than less deformed ores. Furthermore, the most remobilized ores contain higher As, Bi, and Pd concentrations than less remobilized ores; these elevated trace element concentrations coincide with the paragenetically late mineralization of gersdorffite (NiAs), As-bearing pyrite, and Pd-bearing bismuthotellurides. Monoclinic pyrrhotite grains comprising extremely deformed massive sulphide horizons contain higher Ni concentrations than less deformed pyrrhotite grains; co-existing pentlandite grains also contain higher Ni concentrations and higher Ni/Co ratios. Nickel may be complexed by As-, Pd-, and Bi-enriched fluids travelling through stress-induced weaknesses in deformed ores, then subsequently re-deposited in massive sulphides distal to ultramafic sills and incorporated into thermally metamorphosed sulphides. Economic concentrations of sulphide ore in the Thompson Nickel Belt are considered to be structurally, stratigraphically, and metamorphically controlled.

ACKNOWLEDGEMENTS

This thesis could not have been completed without the collaboration of many geoscientists. I would like to thank my thesis advisor, Norman Halden, for his guidance, encouragement, and criticism. The financial support from the following CAMIRO Exploration Division sponsors is gratefully acknowledged: INCO Ltd., Falconbridge Ltd., Hudson Bay Exploration and Development Co. Ltd., Western Mining International Ltd., Billiton International Metals B.V., and NSERC. I would also like to acknowledge the following people and their contributions to my thesis:

INCO Limited, Thompson:

Exploration

- Rick Somerville and Scott Mooney – access to drill core for Thompson, Birchtree, and Soab North deposits
- Larry Larson and Rob Stewart – assistance with drill core from Soab North
- Mars Napoli – assistance with structural interpretation of Thompson deposits

Mines

- Gary Sorensen – access to Thompson and Birchtree Mines
- John Lutz and Brennan Gerlinsky – interpretation of Birchtree Mine and underground technical support
- Hadi Mahony – interpretation of T1 Mine and underground technical support
- Dave Owens and Boris Shepetycky – interpretation of 1C and 1D ore bodies (T3 Mine) and underground technical support
- Marcia Hay and Ian Fieldhouse – interpretation of 1D ore body (T3 Mine) and underground technical support

Falconbridge Limited, Winnipeg:

- Jamie Robertson – access to William Lake information
- Patricia Tirschmann and Kevin Wells – access to and interpretation of William Lake core, maps, and data
- Jack der Weduwen – access to and interpretation of Bucko core, maps, and data
- Jack Giroux and Sandra King – technical assistance

Manitoba Energy and Mines, Winnipeg:

- Dave Peck – organization of CAMIRO TNB Project, and assistance with interpretation of geochemical data
- Josef Macek – interpretation of Thompson Nickel Belt stratigraphy
- Chris Freund and Carl Chandler - assistance with sampling

University of Manitoba, Winnipeg:

- Sergio Mejia – imaging and computer software support
- Ron Chapman – electron microprobe analysis (EMPA) technical support
- Lorne Ayres – assistance with petrography and thesis writing
- Al Turnock – assistance with sample preparation
- Adrienne Larocque – review of thesis draft and discussions of thesis content

Laurentian University, Sudbury:

- Mike Leshner – assistance in the interpretation of petrography and geochemistry
- Marcus Burnham – assistance with acquisition and interpretation of geochemical data
- Daniel Layton-Matthews – assistance with sampling and acquisition of geochemical data

University of Guelph, Guelph:

- William Teesdale – access to proton-induced X-ray emission (PIXE)
- Zdenek Nejedly – PIXE technical support

I would also like to thank my family and friends for their support and encouragement throughout the writing of my thesis.

This document is dedicated to my husband, Gregor Brandt, whose never-ending support and patience helped me to obtain my personal, professional, and academic goals in geology.

TABLE OF CONTENTS

Abstract.....	ii
Acknowledgements.....	iv
Table of Contents	vi
List of Figures	x
List of Tables.....	xv
Chapter 1: Introduction	1
1.1 Overview	1
1.2 Previous Work.....	1
1.3 Purpose and Scope of Study.....	4
Chapter 2: Thompson Nickel Belt.....	6
2.1 Regional Setting.....	6
2.2 Thompson Nickel Belt Geology.....	8
2.3 Lithostratigraphy of the Ospwagan Group.....	8
2.4 Structural and Metamorphic History of the Belt	12
Chapter 3: Nickel Deposits	16
3.1 Model for the Formation of TNB Sulphide Deposits.....	16
3.2 Thompson Deposit.....	18
3.3 Birchtree and Pipe Deposits	23
3.4 William Lake Deposit.....	25
Chapter 4: Sampling and Methodology	27
4.1 Sampling Technique.....	27

4.2 Analytical Techniques	28
4.2.1 Overview.....	28
4.2.2 EMPA and PIXE.....	30
Chapter 5: Sulphide Textures and Mineralogy.....	32
5.1 Classification of Sulphide Textures.....	32
5.1.1 Overview.....	32
5.1.2 Disseminated sulphides in metasediments (DS-SED).....	34
5.1.3 Disseminated and interstitial sulphides in ultramafic rocks (DS-U, IS-U).....	34
5.1.4 Barren massive sulphides in metasediments (BMS-SED).....	34
5.1.5 Massive sulphides in ultramafic breccia (MS-UB)	38
5.1.6 Massive and semi-massive sulphides in metasediments (MS-SED, SMS-SED)	
40	
5.2 Characteristics of Mineralized Massive Sulphides from TNB Deposits.....	43
5.3 Textural Variations Across Strike of a Deformed Ore Zone.....	52
5.4 Textural Variations Along Strike of a Deformed Ore Zone	56
Chapter 6: Sulphide Mineral Chemistry.....	64
6.1 Chemistry of Pyrrhotite	64
6.2 Chemistry of Variably Deformed Sulphide Minerals.....	68
6.3 Diffusion of Nickel.....	74
6.4 Major Element Concentrations of TNB Sulphide Minerals (EMPA data).....	79
6.4.1 Nickel in Pyrrhotite	79
6.4.2 Ni and Co in Pentlandite.....	85
6.5 Trace Element Concentrations in TNB Sulphide Minerals (PIXE data).....	91

6.6	Magmatic <i>versus</i> Hydrothermal Se Concentrations in Sulphide Minerals.....	92
Chapter 7: Whole-rock geochemistry of Thompson Nickel Belt Sulphides		97
7.1	Ni Concentration of Massive Sulphides	97
7.2	Ni/Co Ratios	98
7.3	Se/S Ratios	98
7.4	Platinum Group Element (PGE) Concentrations	103
7.5	Trace Element Concentrations.....	115
Chapter 8: Discussion.....		123
8.1	Metamorphic Textures in the TNB sulphides.....	123
8.2	Discussion of Chalcophile Element Data.....	124
8.2.1	Platinum Anomaly in TNB Massive Sulphides.....	124
8.2.2	Effect of <i>R</i> Factor on the Distribution of Chalcophile Elements.....	127
8.2.3	Platinum Group Element Ratios.....	130
8.2.4	PGE as Discriminants of Ore Genesis	132
8.3	Fluid-Assisted Migration of Metals.....	133
8.3.1	Alteration of Thompson 1D ores	133
8.3.2	The Role of Deformation in Fluid Movement.....	136
8.3.3	Compositional and Mineralogical Haloes	137
8.4	Revised Model for the Thompson Nickel Belt Sulphides.....	139
Chapter 9: Conclusion		145
9.1	Summary.....	145
9.2	Implications for Exploration.....	145
References.....		147

Appendix 1: Summary of Thin Sections	153
Appendix 2: Conditions of Microprobe Techniques	157
Appendix 3: EMPA Data.....	158
Appendix 4: PIXE Data.....	197
Appendix 5: Whole-Rock Geochemical Data	201
Appendix 6: Whole-Rock Geochemical Techniques	208

LIST OF FIGURES

Figure 1.1. Map showing the location of the Thompson Nickel Belt in Manitoba (inset) and its position relative to other geological domains (modified from CAMIRO, 2000a).	2
Figure 2.1. Geological map of northern Manitoba, showing the location of the Thompson Nickel Belt (TNB) along the northwestern margin of the Archean Superior province.	7
Figure 2.2. Geological map of the exposed portion of the Thompson Nickel Belt, showing the major nickel deposits (CAMIRO, 2000a).	9
Figure 2.3. Composite lithostratigraphic section of the Ospwagan Group and its tectonic setting in the early development of the Thompson Nickel Belt (from Bleeker, 1990).	10
Figure 2.4. Structural map of the Ospwagan Group supracrustal belt from Moak Lake to Pipe Lake (from Bleeker, 1990).	13
Figure 2.5. 3D sketch showing the refolded nappe structure from Moak Lake to Pipe Lake (from Bleeker, 1990).	14
Figure 3.1. Typical stages in the formation of a magmatic sulphide deposit (from Naldrett, 1989).	17
Figure 3.2. Schematic model for the emplacement of magmatic sulphides in the Thompson Nickel Belt (after Bleeker, 1990).	19
Figure 3.3. Schematic representation of stretched and folded ultramafic sills of the Thompson Nickel Belt deposits.	20
Figure 3.4. Cross section through the downward facing Thompson structure, looking NE (from Bleeker, 1990).	21
Figure 3.5. Orthographic block diagram of the Thompson structure (after Bleeker, 1990).	22
Figure 3.6. Typical cross section from the Birchtree Mine.	24
Figure 3.7. Schematic geological map of the William Lake deposit showing the relationship between the ultramafic rocks and what are interpreted to be Ospwagan Group metasediments.	26

Figure 5.1. Relative location of the sulphide classes within folded and stretched sequence of Ospwagan Group supracrustals in the Thompson Nickel Belt (after Bleeker 1990).	33
Figure 5.2. Textures representing sulphide class DS-SED (disseminated sulphides in metasediments).	35
Figure 5.3. Textures representing sulphide classes DS-U (disseminated sulphides in ultramafic rocks) and IS-U (interstitial sulphides in ultramafic rocks).	36
Figure 5.4. Textures representing sulphide class BMS-SED (barren sulphides in metasediments).	37
Figure 5.5. Textures representing sulphide class MS-UB (massive sulphides in ultramafic breccia).	39
Figure 5.6. Textures representing sulphide class MS-SED (massive sulphides in metasediments) and SMS-SED (semi-massive sulphides in metasediments).	41
Figure 5.7. BSE image showing semi-massive sulphides hosted in biotite gneiss from the 1D ore body, Thompson Mine.	42
Figure 5.8. Brecciated silicate fragments along contact between garnet biotite schist and massive sulphides.	44
Figure 5.9. Stringer sulphides in garnet biotite gneiss from the Thompson T1 Mine.	45
Figure 5.10. Example of chalcopyrite occurring adjacent to porphyroblastic silicates in massive sulphides.	46
Figure 5.11. Pyrite-chalcopyrite symplectites.	47
Figure 5.12. Massive sulphides from the Thompson T1 Mine.	49
Figure 5.13. Massive sulphides from the Thompson 1C ore body.	50
Figure 5.14. Semi-massive sulphides from the Thompson 1D ore body.	51
Figure 5.15. Massive sulphide horizon in contact with biotite schist from the William Lake deposit.	53
Figure 5.16. Schematic diagram of an ore zone in the 1C ore body, Thompson Mine.	54
Figure 5.17. Reflected light photomicrographs of typical sulphide-bearing samples from a Ni ore zone in the 1C ore body, Thompson Mine.	58
Figure 6.1. Phase relations involving pyrrhotite below 350°C (Kissin and Scott, 1982). ..	66

Figure 6.2. Relative concentrations of Fe, Ni, and Co in pentlandite grains from a range of sulphide types from the Thompson 1C ore body.	69
Figure 6.3. Relative concentrations of Fe, Ni, and S in pentlandite grains from a range of sulphide types from the Thompson 1C ore body.	71
Figure 6.4. Relative concentrations of Fe, Ni, and S in pyrrhotite grains from a range of sulphide types from the Thompson 1C ore body.	72
Figure 6.5. Electron microprobe point analyses across an equant porphyroblastic pentlandite grain and adjacent pyrrhotite grains in two dimensions.	75
Figure 6.6. Concentration of Ni in co-existing sulphide minerals from samples along section I-I' in Figure 5.16, Thompson 1C ore body.	76
Figure 6.7. Concentration of Ni in pyrrhotite grains from sulphide-bearing samples along section J-J' in Figure 5.16, Thompson 1C ore body.	78
Figure 6.8. Nickel and sulphur concentrations in monoclinic pyrrhotite grains from the Thompson Mine (T1 Mine, 1C ore body, and 1D ore body).	80
Figure 6.9. Ni and sulphur concentrations in monoclinic pyrrhotite grains from massive sulphides.	81
Figure 6.10. Nickel and sulphur concentrations in monoclinic pyrrhotite grains from sulphide class MS-UB (massive sulphides in ultramafic breccia).	83
Figure 6.11. Nickel and sulphur concentrations in monoclinic and hexagonal pyrrhotite grains from sulphide class DS-U (disseminated in ultramafic rocks).	84
Figure 6.12. a) Nickel and sulphur concentrations in pentlandite grains from massive sulphides. b) Ni/Co ratios and S concentrations in pentlandite grains shown in graph a).	87
Figure 6.13. a) Nickel and sulphur concentrations in pentlandite grains from sulphide class MS-UB (massive sulphides in ultramafic breccia). b) Ni/Co ratios and S concentrations in pentlandite grains shown in graph a).	88
Figure 6.14. a) Nickel and sulphur concentrations in pentlandite grains from sulphide class DS-U (disseminated sulphides in ultramafic rocks). b) Ni/Co ratios and S concentrations in pentlandite grains shown in graph a).	89
Figure 6.15. Nickel and selenium concentrations in monoclinic pyrrhotite grains from massive sulphides.	93
Figure 6.16. Nickel and selenium concentrations in pentlandite grains from massive sulphides.	94

Figure 7.1. Ni concentration of massive and semi-massive sulphides from the TNB, normalized to 100% sulphides.	99
Figure 7.2. Ni/Co ratios of ultramafic bodies from the TNB with the following geochemical parameters: MgO > 24%, S < 5000 ppm, and Se/S x 10 ⁶ < 1000.	100
Figure 7.3. Ni/Co ratios of massive and semi-massive sulphides from the TNB.	101
Figure 7.4. Se/S and δ ³⁴ S data for nickel sulphide ore and barren sedimentary sulphides from the TNB (from Eckstrand <i>et al.</i> , 1989).	102
Figure 7.5. Se/S ratios of massive and semi-massive sulphide samples from the TNB. .	104
Figure 7.6. Se/S of ultramafic bodies from the TNB with the following geochemical parameters: MgO > 24%, S < 5000 ppm, and Se/S x 10 ⁶ < 1000.	105
Figure 7.7. Chondrite-normalized plot of chalcophile element concentrations in massive and semi-massive sulphide samples from the TNB, this study.	106
Figure 7.8. Chondrite-normalized plot of chalcophile element concentrations in samples from Birchtree Mine, this study.	108
Figure 7.9. Chondrite-normalized plot of chalcophile element concentrations in samples from Thompson Mine.	109
Figure 7.10. Chondrite-normalized plot of chalcophile element concentrations in samples from the Pipe deposit.	110
Figure 7.11. Analytical data for Co, Ni, Cu, and the PGE for Proterozoic komatiite-related deposits (from Naldrett, 1989).	111
Figure 7.12. Chondrite-normalized plot for Archean komatiite-related deposits from the Kambalda mining camp, Western Australia (from Naldrett, 1989).	112
Figure 7.13. Pd and Bi concentrations in massive and semi-massive sulphide samples from the TNB.	117
Figure 7.14. Bismuthotellurides in massive sulphides from the 1D ore body, Thompson Mine.	118
Figure 7.15. Ni and As concentration in massive and semi-massive sulphides from the TNB.	120
Figure 7.16. Ni and Pd concentration in massive and semi-massive sulphides from the TNB.	121
Figure 7.17. Ni and Bi concentration in massive and semi-massive sulphides from the TNB.	122

Figure 8.1. Solubility of Pd and Pt in a hydrous silicate melt *versus* oxygen fugacity (from Bezmen *et al.*, 1998). 126

Figure 8.2. Schematic representation of the variation of the metal content of a sulphide melt as a function of R (magma/sulphide ratio) and D (Nernst distribution coefficient) (from Naldrett, 1989). 128

Figure 8.3. An ore deposit model representing the history of the deposition and post-magmatic modification of the ores from the Thompson Nickel Belt. 143

LIST OF TABLES

Table 5.1. Mesoscopic textures and relative locations of representative sulphide samples from the 1C ore body, Thompson Mine.	55
Table 6.1. EMPA data of sulphide minerals (pn = pentlandite, po = pyrrhotite, py = pyrite) in samples from the Thompson 1C ore body.	70
Table 7.1. Chalcophile element and PGE data for massive and semi-massive sulphides from the TNB, normalized to 100% sulphides.	114
Table 7.2. Trace element data (un-normalized) for massive and semi-massive sulphides from the TNB.	116

CHAPTER 1: INTRODUCTION

1.1 Overview

The Thompson Nickel Belt (TNB) is a northeasterly trending mobile belt of reworked Archean basement gneisses and Early Proterozoic cover rocks separating the Churchill and Superior Provinces in northern Manitoba, Canada (Figure 1.1). This belt contains several world-class Fe-Ni-Cu sulphide deposits (e.g. Thompson, Pipe) hosted by complexly deformed and metamorphosed volcanic, subvolcanic, and sedimentary rocks. The complex geological processes involved in creating these sulphide deposits have obscured the stratigraphic relationships between ore and host rocks, thus making the TNB a difficult exploration target. To further complicate exploration, rocks in the northern part of the belt are poorly exposed and those in the southern part are covered by up to 130 m of Paleozoic carbonate rocks. Refinement of existing exploration tools and ore deposit models for the Belt is needed to ensure cost-effective exploration and extraction of Ni ore.

1.2 Previous Work

The TNB has been a focus for exploration in northern Manitoba since the discovery of major Ni deposits in the 1950's and early 1960's, and has also been a focus for research because of its genetic relationship to the Churchill-Superior boundary zone. Zubrigg (1963) presented the geology and mineralization within the Thompson Mine. Coats (1966) examined the serpentinized ultramafic rocks that host the Ni deposits in the Belt. Peredery *et al.* (1982) mapped the Thompson and Pipe mines and outlined the stratigraphy of the Ni ore-bearing supracrustal rocks of the TNB, which are now known

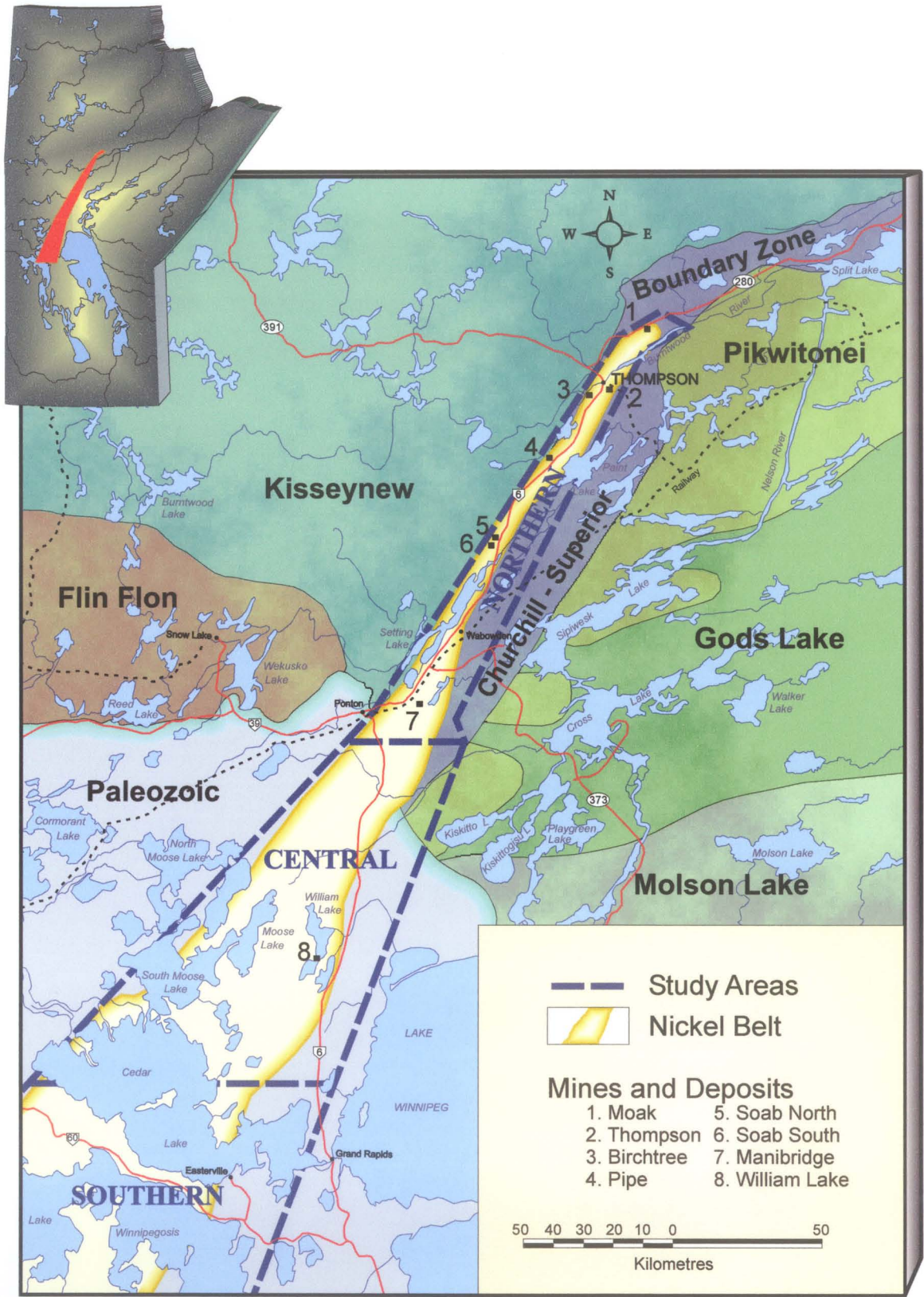


Figure 1.1. Map showing the location of the Thompson Nickel Belt in Manitoba (inset) and its position relative to other geological domains (modified from CAMIRO, 2000a).

as the Ospwagan Group, a term first introduced by Scoates *et al.* (1977). Cranstone and Turek (1976) and Machado *et al.* (1990) summarized geochronological relationships in the TNB. Bleeker (1990) presented interpretations of the tectonic evolution of the TNB and its Ni deposits. These interpretations are based on detailed mapping, structural analysis, petrography, and geochemistry of rocks within the exposed portion of the Belt. Although the basic elements of the geology in and around the TNB was established by the late 1980's, the interpretation of the tectonic setting of the Belt and its ore deposits continues to evolve.

Much work has been done to support the interpretation that the TNB Ni sulphide ores are magmatic in character, but little has been published to show the possible effects of metamorphism and/or metasomatism on the composition of the sulphide minerals and the ores themselves. Boulet and Larocque (1997) examined massive and brecciated ores from the Birchtree deposit that have been affected by metamorphism and brittle deformation. The authors observed metamorphic textures such as reaction rims on pyrrhotite grains and Ni-arsenides, fracturing of pyrrhotite and pentlandite, and veinlets of chalcopyrite in fractures and grain boundaries. Larocque and Boulet (1998) observed that deformed and metamorphosed sulphides from the Birchtree deposit can be distinguished from primary (magmatic) sulphides by their trace element contents, as determined by electron microprobe analysis (EMPA) and proton-induced X-ray emission (PIXE) analysis. The authors showed that massive brecciated pentlandite had lower concentrations of Ni but higher concentrations of Co than massive magmatic pentlandite.

Bleeker (1990) observed "nickel haloes" surrounding magmatic stratabound ore zones in the TNB, specifically in the Pipe II and Thompson open pit mines. Bleeker

(1990) found that sedimentary sulphides, which are Ni barren at a considerable distance away from an ore zone, show increasing Ni content in proximity to the ore zone. This suggests that weak Ni enrichment in sedimentary sulphides might be an indication of nearby magmatic sulphides. The Ni zonation was attributed to the local remobilization of Ni from massive sulphide ore to barren sedimentary sulphides by metamorphic processes, the mechanics of which are not well understood. This thesis describes the Ni zonation with respect to sulphide mineral textures and chemistry.

1.3 Purpose and Scope of Study

In 1997, the Thompson Nickel Belt Project was established by the Canadian Mining Industry Research Organization (CAMIRO) Exploration Division to aid mineral exploration in the TNB. The project was designed as a 4-year collaborative study by geoscientists from academia, government, and industry to 1) define the geology, stratigraphy, structure, geochronology, petrogenesis, and metallogenesis of the TNB, 2) refine existing geological, geochemical, and geophysical exploration tools used in the TNB, and 3) aid in the identification of new exploration targets.

This Master's thesis was designed as a sub-project of the Thompson Nickel Belt Project to: 1) assess the mobility of Ni as a result of metamorphism, metasomatism, and deformation in ore zones throughout the Thompson Nickel Belt, and 2) physically and chemically characterize spatially distinct ore zones in the Belt. This was done by comparing and contrasting the textures and compositions of sulphide minerals in ultramafic rocks, massive sulphide horizons, and sulphide-hosting metasediments throughout ore zones in the Thompson Nickel Belt. Textural analysis of sulphide ores, in

conjunction with chemical analyses of sulphide minerals and sulphide-bearing rocks, provides a better understanding of the mobility of metals within sulphide ore zones, and helps to define the scales at which this mobility occurs.

CHAPTER 2: THOMPSON NICKEL BELT

2.1 Regional Setting

The Thompson Nickel Belt of northern Manitoba, Canada, is a 10-35 km wide complexly deformed mobile belt trending 033°. The eastern margin of the belt marks the approximate limit of Hudsonian overprinting on unworked Archean crust; the western margin, the Churchill-Superior boundary fault, marks the contact with the Early Proterozoic Kiseynew domain (Weber, 1990)(Figure 2.1). The Kiseynew domain comprises paragneisses, metasedimentary rocks, and metavolcanic rocks that are typically metamorphosed to upper amphibolite-grade (Peredery, 1982). The unworked Archean crust to the southeast of the Belt includes low- to medium-grade granite-greenstone terrains, and the high-grade Pikwitonei granulite belt. Mafic to ultramafic dykes of the Molson swarm (Ermanovics and Fahrig, 1975; Scoates and Macek, 1978), dated at 1883 Ma (Heaman *et al.*, 1986) further characterize the Archean crust. These dykes intrude rocks of the Thompson Nickel Belt (Cranstone and Turek, 1976), but not those to the northwest.

The Belt marks part of the boundary between the Churchill and Superior provinces. To the north-northeast, the Thompson Nickel Belt extends into the Split Lake Block (Weber and Scoates, 1978), a region of primarily polymetamorphic gneisses (Corkery, 1985). East of this Block is the Fox River Belt, which consists of Aphebian supracrustals and related intrusions (Scoates, 1981). The southern extension of the Thompson Nickel Belt has been delineated below Phanerozoic platformal cover to as far south as South Dakota.

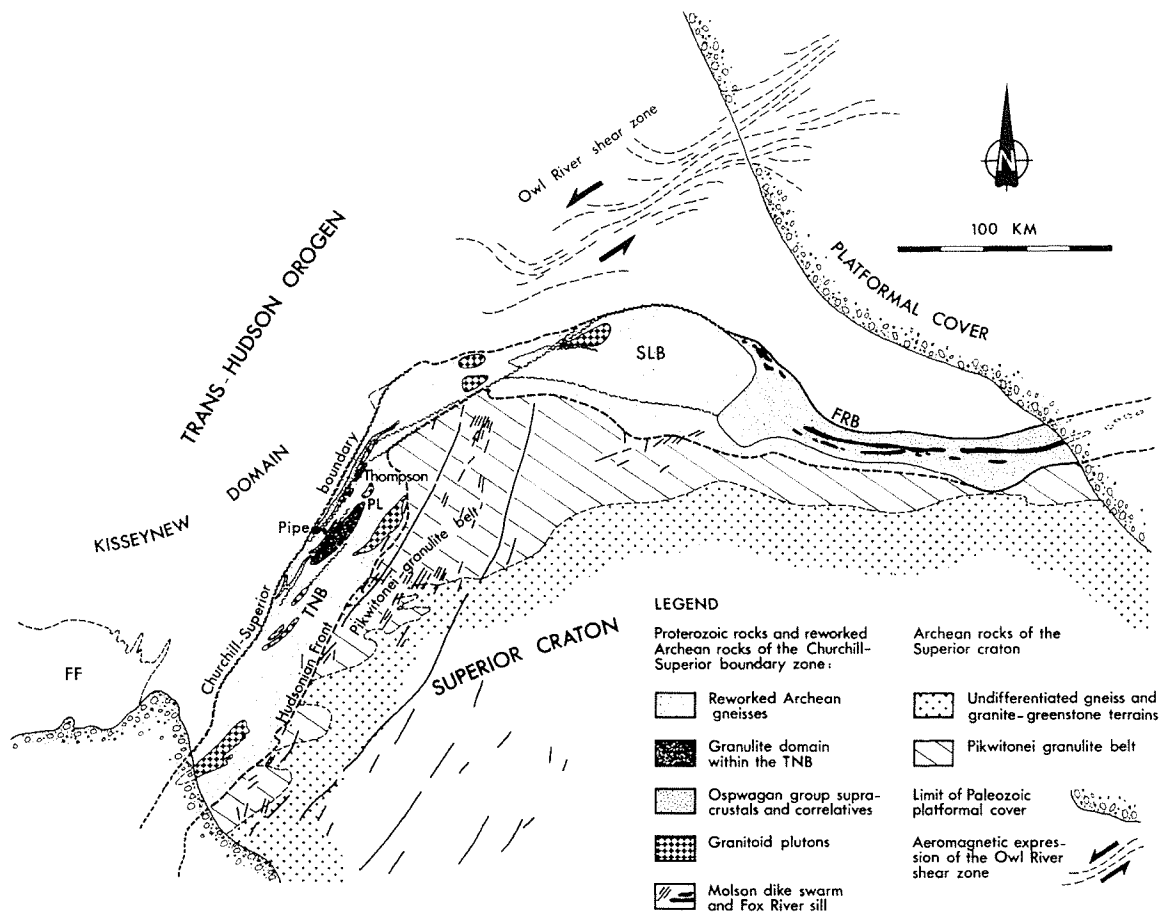


Figure 2.1. Geological map of northern Manitoba, showing the location of the Thompson Nickel Belt (TNB) along the northwestern margin of the Archean Superior province. Towards the northeast, the Belt extends into the Split Lake Block (SLB) and the Fox River Belt (FRB). PL = Paint Lake granulitic domain; FF = Flin Flon-Snow Lake volcanic belt (from Bleeker, 1990).

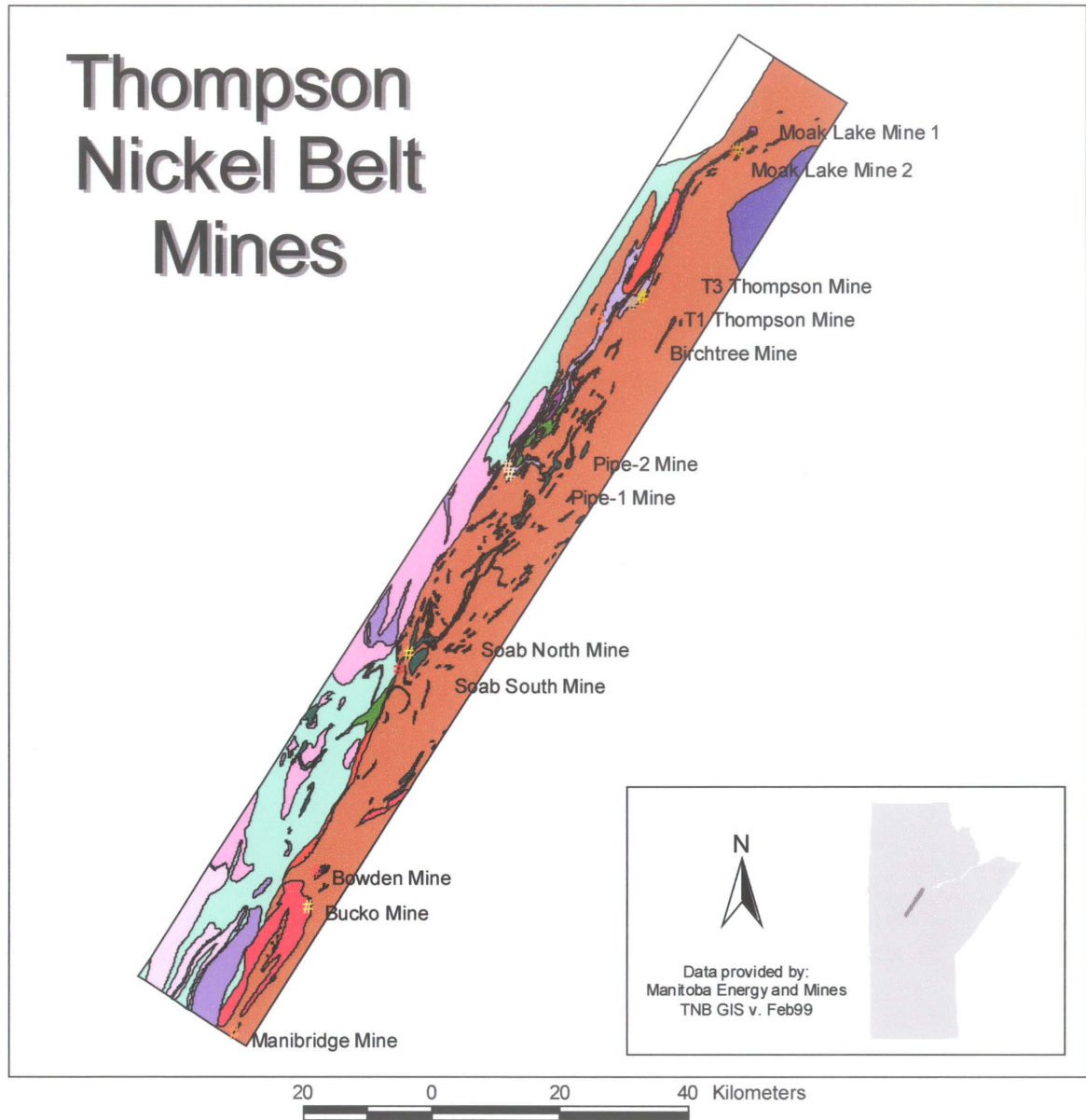
2.2 Thompson Nickel Belt Geology

The Thompson Nickel Belt consists of about 80% or more variably reworked Archean gneisses (Bleeker, 1990). Early Proterozoic supracrustal rocks, commonly referred to as the Oswagan Group (Scoates *et al.*, 1977), are in narrow, structurally controlled belts on the western part of the Belt (Figure 2.2). The gneisses and Oswagan Group supracrustals are intruded by dikes and sills of dunitic to pyroxenitic composition. These ultramafic bodies, and the Ni sulphide deposits that associated with them, also occur on the western portion of the Belt (Figure 2.2). The reworked basement gneisses, Oswagan Group, and Molson dykes are intruded by Hudsonian felsic plutons, which are characterized by the occurrence of garnet and muscovite in addition to biotite (Bleeker, 1990). Several generations of pegmatite dykes, dated between 1687 and 2667 Ma (Potrel, 2000 – Table 3.3) occur throughout the TNB.

2.3 Lithostratigraphy of the Oswagan Group

The Early Proterozoic Oswagan Group cover sequence is of great interest to both exploration geologists and researchers alike, as it contains the world-class Ni deposits of the TNB and records the early tectonic evolution of the Belt. The lithostratigraphic map of the Oswagan Group, summarized by Bleeker (1990), is shown in Figure 2.3. The lower portion of the Oswagan Group (Manasan Formation), is a clastic sequence consisting of a thin quartz and feldspar conglomerate, overlain by arkosic to quartz-arenitic rocks. These rocks fine upwards into quartz-rich siltstones, which are overlain by arenites. Overlying the Manasan Formation is a sequence of chert and siliceous dolomite

Thompson Nickel Belt Mines



- Gac_geol.shp
- 0
 - 13) Pyroxene-granulite facies gneiss, charnockitic (hypersthene) granites, mafic granulites, and retrograded equivalents.
 - 11) Ultramafic rocks. Serpentinized to partly serpentinized ultramafics, usually of peridotitic composition. May be mineralized by disseminations and stringers of pyrrhotite and pentlandite.
 - 10) Biotite-hornblende quartz monzonite. Medium-grained and foliated.
 - 9) Granodiorite, porphyritic granodiorite, massive to poorly foliated. (e.g. Burrwood Granite)
 - 8) Amphibolite, plagioclase-hornblende gneiss. Foliated to layered. Quartz, K-feldspar and sphene locally significant.
 - 7) Layered migmatite gneiss, lit-par-lit gneiss. Probably derived from former sedimentary-volcanic rocks. Local areas contain hypersthene (granulite facies) toward east side of map-area.
 - 6) Meta-volcanics. Mainly fine-grained greenstones(?) with felted amphibole matrix. Some with pillow structures. May include tuffs.
 - 5) Metasediments. Quartzite, meta-arkose, marble, diopside-phi-logopite-carbonate rocks (called skam), garnet-amphibole-magnetite/pyrrhotite-quartz rocks (called iron-formation). Possible tuffs.
 - 4) Agmatite, granodiorite. Grey, buff and orange-pink granodiorite, related apite and pegmatite dikes and stockworks intruding units 1 and 2. Local stocks of granodiorite.
 - 3) Quartz monzonite, granodiorite. Massive to slightly foliated, orange-pink, buff, grey-buff, and grey.
 - 2) Granitized paragneisses, porphyroblastic gneiss and augen gneiss. Probably formed by potash metasomatism of paragneiss. Quartz diorite to potassic quartz monzonite in composition.
 - 1) Paragneiss, including lower amphibolite facies metasediments and minor stretched pebble conglomerate on west shore of Setting Lake.

Figure 2.2. Geological map of the exposed portion of the Thompson Nickel Belt, showing the major nickel deposits (CAMIRO, 2000a).

LEGEND

-  Mafic to ultramafic metavolcanics
 -  Rare felsic metavolcanics
 -  Metamorphosed conglomerates, greywackes and minor pelitic sediments
 -  Interlayered quartzites and schists
 -  Pelitic schists
 -  Silicate facies iron formation
 -  Sulphide facies iron formation
 -  Dolomitic marble
 -  Impure calcareous metasediments
 -  Semipelitic schists or gneiss
 -  Basal quartzite
 -  Local basal conglomerate
- } Oswagan group
-
-  Angular unconformity with local relics of a regolith
 -  Archean basement gneisses

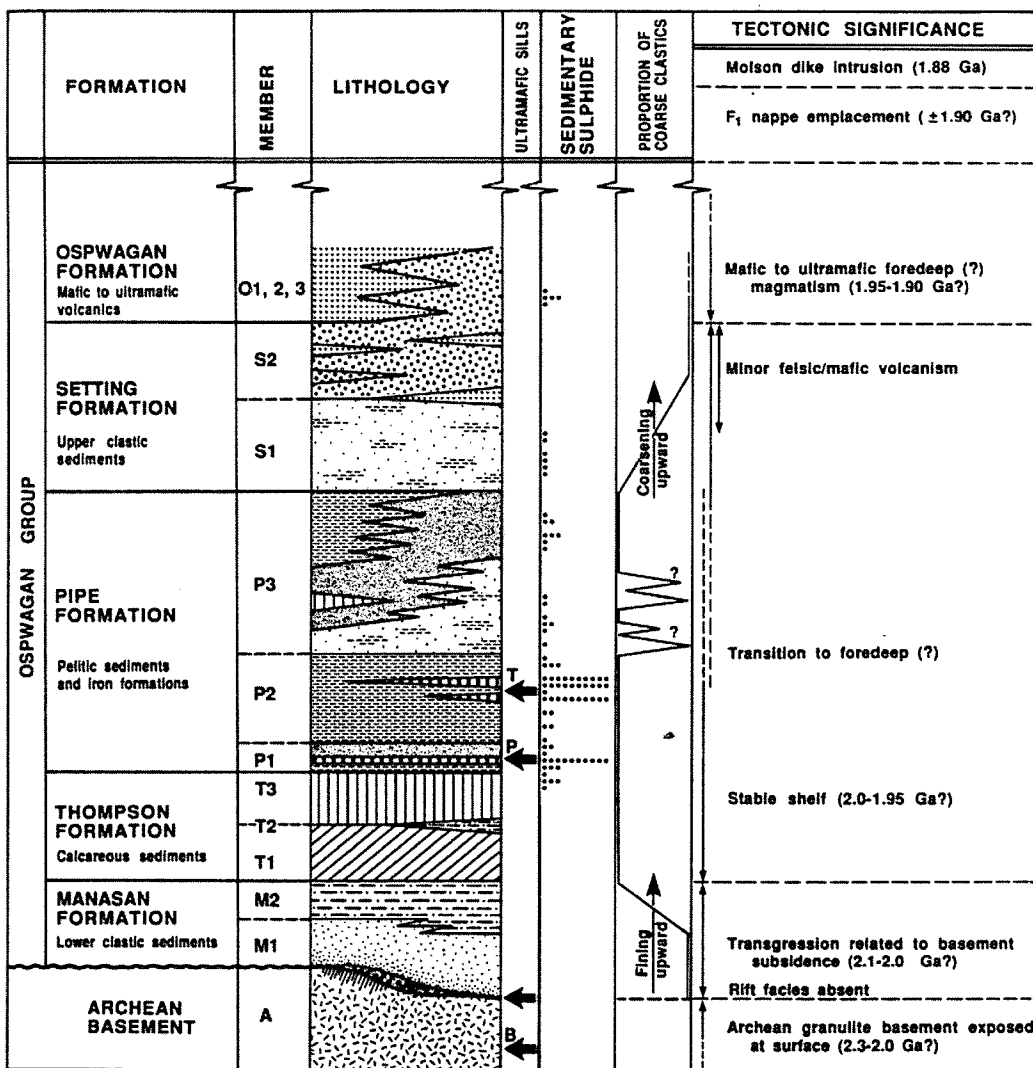


Figure 2.3. Composite lithostratigraphic section of the Oswagan Group and its tectonic setting in the early development of the Thompson Nickel Belt (from Bleeker, 1990).

(Thompson Formation), and a sequence of graphitic sulphide facies iron formation, silicate facies iron formation, and pelitic schists (Pipe Formation). As used here, the term “iron formation” signifies a ferruginous metasediment that is characteristic to the TNB, rather than a conventional sedimentary iron formation. The Pipe Formation is overlain by the Setting Formation, a sequence of interlayered quartzites and schists, followed by a mixture of metamorphosed conglomerates, greywackes, and minor pelitic sediments. At the top of the Oswagan Group is the Oswagan Formation, which consists of mafic to ultramafic volcanic rocks. Several ultramafic sills intruded the cover sequence at various levels (e.g. Thompson, Pipe, and Birchtree) and also intruded within Archean basement rocks (e.g. Bucko Lake). The sulphide ores of the Thompson deposit occur near the top of the pelitic schist unit of the Pipe Formation, while the ores of the Pipe and Birchtree deposits occur within the graphitic sulphide facies iron formation of the Pipe Formation (Figure 2.3).

Bleeker (1990) interpreted the Oswagan Group as a record of sedimentation and magmatism that occurred in response to changing tectonic regimes in the early evolution of the TNB. The clastic rocks of the Manasan Formation represents deposition related to the transgression of an Early Proterozoic basin onto the Superior plate margin. The calcareous sediments of the Thompson Formation marks the advent of a stable shelf environment following the transgression. The graphitic schists and graphitic cherts of the overlying Pipe Formation are characteristic of a deeper, euxinic environment, and could indicate renewed subsidence due to an approaching foredeep. This period of deepening was followed by a period of shallowing or infilling of the foredeep as indicated by the metaturbiditic sequences of the Setting Formation. The mafic to ultramafic volcanic rocks

of the Oswagan Formation indicate that such a foredeep environment was magmatically active.

2.4 Structural and Metamorphic History of the Belt

Bleeker (1990) established seven fold and several fault generations in the TNB, based largely on structural analyses of the Oswagan Group rocks between Moak Lake and Pipe Lake (Figure 2.4). The first three fold generations and associated faulting episodes provide evidence that the Belt was a major collision zone. According to a recent compilation of geochronological data for the adjacent parts of the Trans-Hudson Orogen and the Superior Boundary Zone, the major period of collisional tectonics between these two terranes occurred between ca. 1820 and 1780 Ma (CAMIRO, 2000b).

Compressional tectonism likely produced isoclinal F_1 folds with northeast trending fold axes, such as the nappe-like F_1 fold that dominates the Moak Lake-Pipe Lake region (Figure 2.5). The core of this nappe structure comprises intensely reworked basement rocks that locally overlie downward-facing supracrustals, such as at Thompson Mine. The incorporation of the basement rocks into the structure suggests that at least lower amphibolite facies metamorphism occurred during F_1 . F_1 folds are crosscut by mafic dykes interpreted to be part of the 1883 Ma Molson dike swarm. Tight to isoclinal F_2 folds overprint F_1 and fold Molson dikes. The F_2 folds were probably recumbent and provide evidence for a second period of ductile thrusting during which the Kisseynew gneisses may have been emplaced onto the TNB. F_1 and F_2 folding may record a phase of crustal thickening along the margin of the Superior plate. The thermal peak of regional metamorphism, which has been interpreted to occur around 1820 Ma, overprints F_2 .

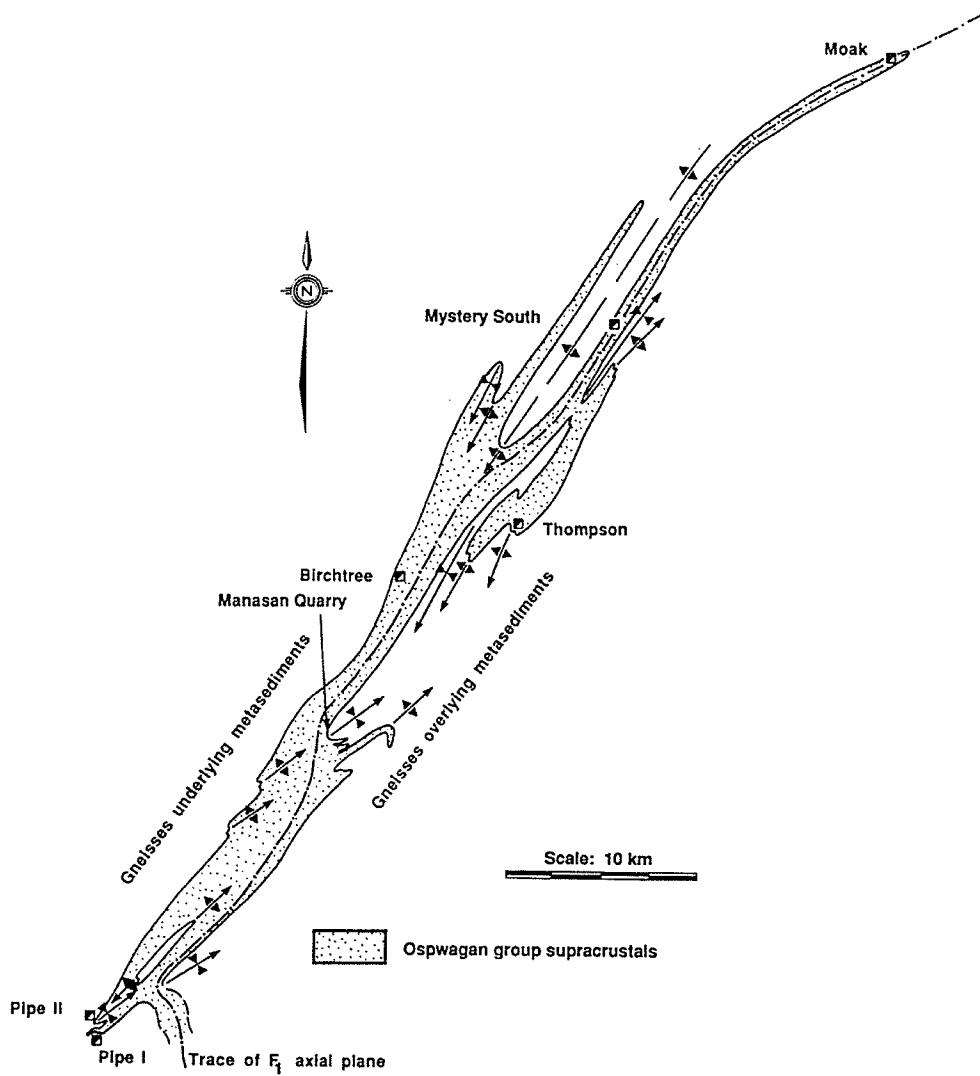


Figure 2.4. Structural map of the Oswagan group supracrustal belt from Moak Lake to Pipe Lake (from Bleeker, 1990).

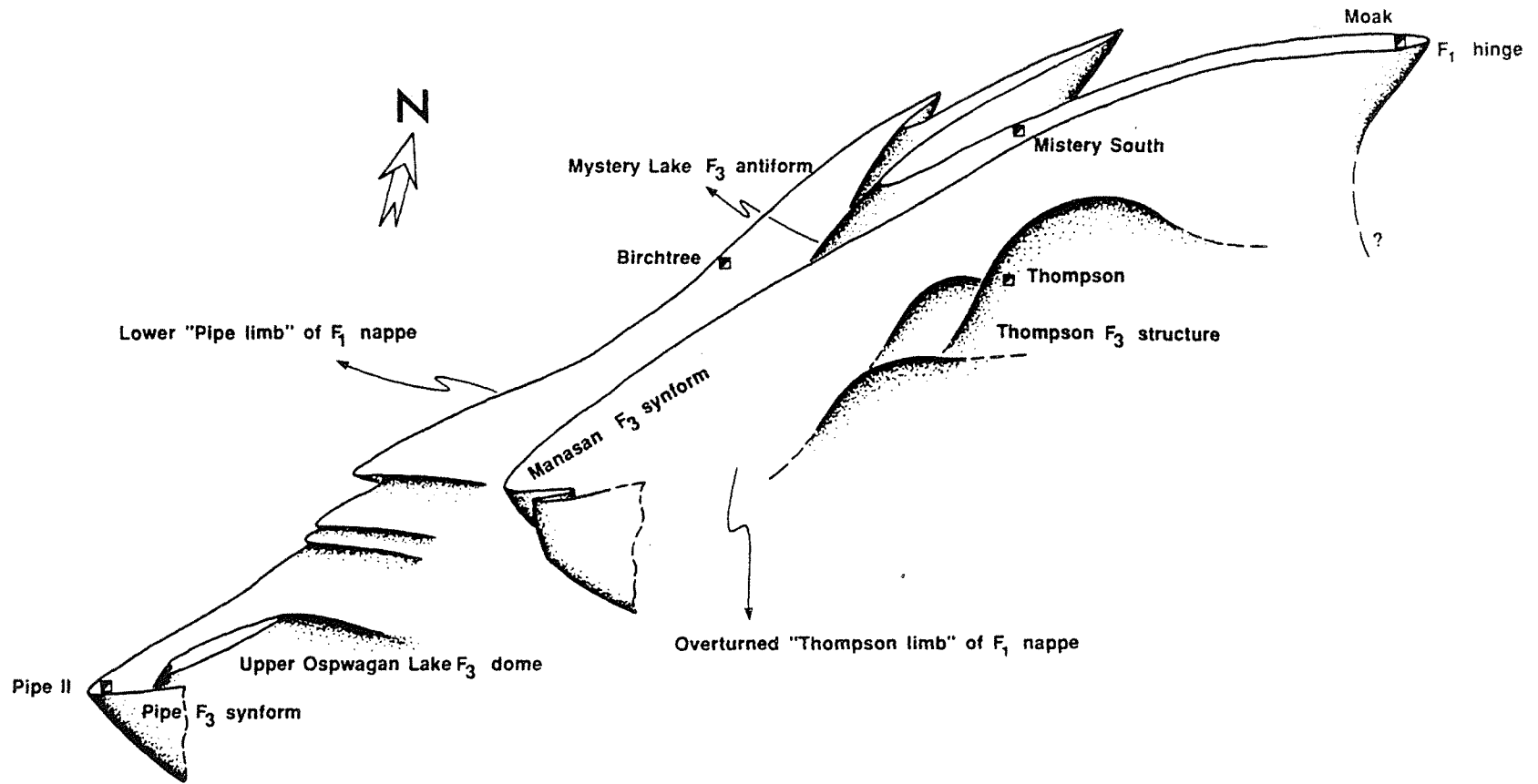


Figure 2.5. 3D sketch showing the refolded nappe structure from Moak Lake to Pipe Lake (from Bleeker, 1990).

Average garnet-biotite geothermometric data for deposits discussed in this thesis are as follows: Thompson, 740°C, 6 kbars; Birchtree 680°C, 5 kbars; Pipe, 635°C, 5 kbars (Bleeker, 1990). Peak metamorphism of these deposits could have been generated by the thermal relaxation of a thickened crust, during which anatectic granites intruded the TNB.

High amplitude, nearly upright, doubly-plunging F_3 folds are the result of intense sinistral transpression of the nappe that was produced during F_1 - F_2 history. F_3 folds transformed the preexisting fold pile into a steep belt of gneisses and metasediments. Axial planes of the F_3 folds dip steeply to the SE, trend N35-50E, and form a left-stepping en-echelon pattern; the axial traces of these folds trend 0-15° from the N35E trend of the TNB. Mylonitization is confined to ductile shear zones that are generally parallel to steeply dipping limbs of the F_3 folds, in keeping with the en-echelon trends of the Belt. These shear zones are overprinted by steep brittle-ductile and brittle faults that are (sub)parallel to, and are concentrated on, the western margin of the Belt. Early movement along these faults indicates sinistral strike-slip displacement, whereas later movement is dextral. This dextral movement occurred in conjunction with transcurrent brittle faults that are pervasive throughout the belt.

CHAPTER 3: NICKEL DEPOSITS

3.1 Model for the Formation of TNB Sulphide Deposits

The stages in the formation of a magmatic sulphide ore are shown in Figure 3.1 (Naldrett, 1989). Partial melting of the mantle gives rise to ultramafic or basaltic magma, which rises upward and intrudes the crust or extrudes as lava. Either before or while the magma is cooling, immiscible sulphide droplets start to segregate from the silicate melt. Chalcophile metals tend to be scavenged by the sulphide melt. The droplets, being much denser than the silicate magma, settle to the base of the magma, coalesce, and solidify. Alteration, deformation, and/or metamorphism can modify the composition of the sulphides after they have solidified.

The Thompson Nickel Belt deposits are categorized as magmatic Ni deposits related to low-Mg komatiites at rifted (Proterozoic) continental plate margins (Naldrett, 1989; Eckstrand, 1996). The Cape Smith Belt deposits in the Ungava Peninsula of Northern Quebec also fall into this category. Both deposits are within Hudsonian fold and thrust belts, and occur at the base of a komatiite sequence along a sedimentary-volcanic contact. These deposits are typically located in the lowest, thickest, most magnesian of flows, where MgO contents range from about 20-35%. The sulphide ores are often massive at the base of the flows, and grade upwards into matrix sulphides and disseminated sulphides.

A model for the mineralization in the Thompson Nickel Belt is presented here, after the work of Bleeker (1990), Peredery (1982) and Naldrett *et al.* (1979). Ultramafic magmatism, which occurred as a result of a Proterozoic rifting event, led to the intrusion

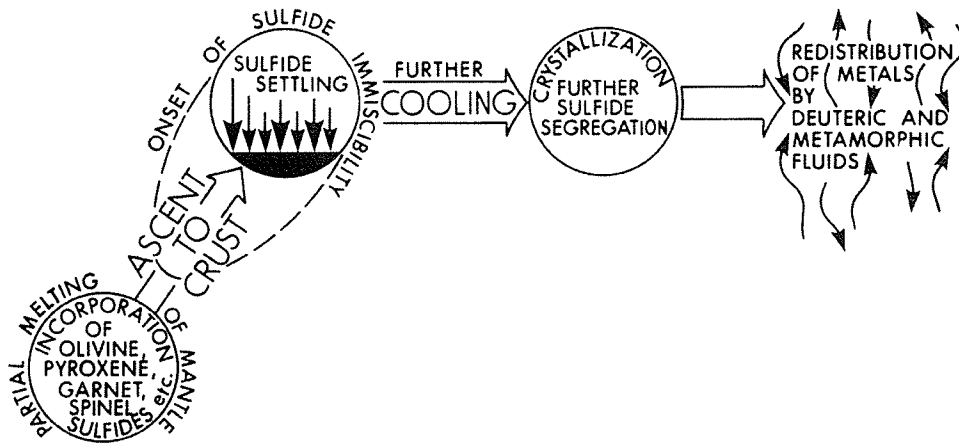


Figure 3.1. Typical stages in the formation of a magmatic sulphide deposit (from Naldrett, 1989).

of large ultramafic sills in the Oswagan Group metasediments (Figure 3.2). The ultramafic sills intruded the Oswagan Group metasediments and locally assimilated sedimentary sulphides. The ultramafic magmas subsequently became saturated with respect to sulphide, and large quantities of immiscible sulphide melt coalesced at the base of the ultramafic bodies. The ultramafic sills and the localized magmatic sulphide concentrations were then stretched and folded (Figure 3.3). Whereas the ultramafic sills accommodated the deformation by boudinage, the sulphides were remobilized within the metasedimentary host. Locally, the sulphides were remobilized into late shear zones and late tension gashes.

3.2 Thompson Deposit

The Thompson ore is stratabound and occurs within the pelitic schist unit of the Pipe Formation (Figure 3.4). The Thompson structure consists of nearly upright, variably plunging, high-amplitude folds interpreted to have formed during an F_3 folding event in the Thompson Nickel Belt (Bleeker, 1990). Reworked basement gneisses occur on the outer limbs of the structure, while the Oswagan Group supracrustals occur in the core.

The block diagram in Figure 3.5 illustrates the structure and geological setting of the Thompson nickel sulphide ore body (Bleeker, 1990). The reference horizon in the diagram represents the pelitic schist unit that hosts the Thompson sulphide ore and the associated ultramafic boudins. The subvertical attitudes of the rocks are interpreted to be the result of doubly plunging F_3 folds, which dominate the Thompson Nickel Belt (Bleeker, 1990). Also shown in the block diagram are the locations of the T1 shaft, which

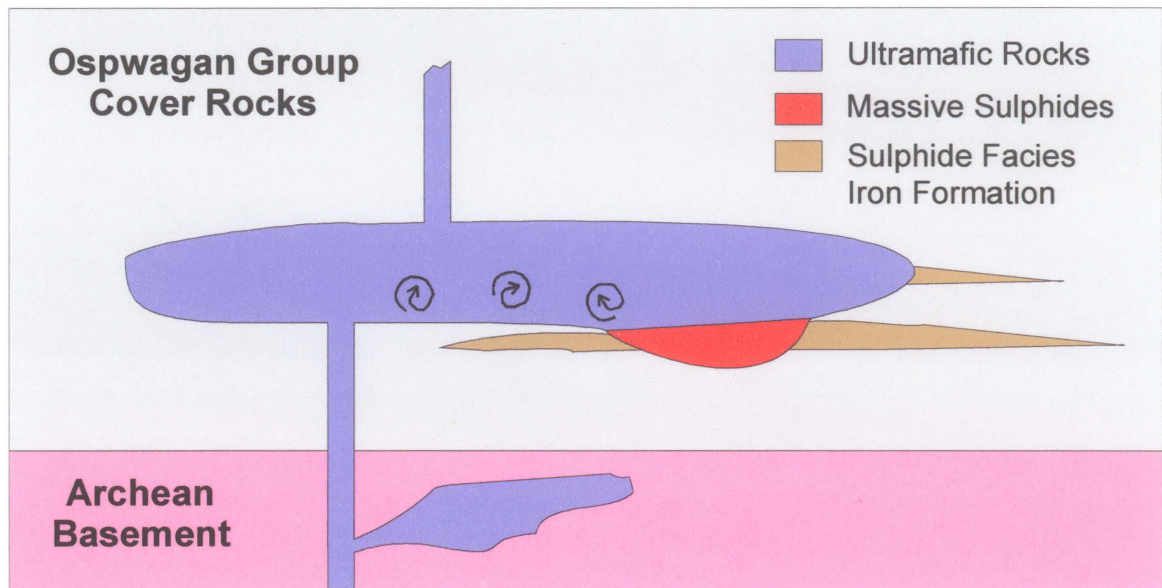


Figure 3.2. Schematic model for the emplacement of magmatic sulphides in the Thompson Nickel Belt (after Bleeker, 1990). Ultramafic magmatism near the end of Ospwagan Group deposition led to the intrusion of ultramafic sills within Archean basement rocks (e.g. Bucko Lake) and the Ospwagan Group metasediments (e.g. Thompson, Birchtree, Pipe, William Lake). These ultramafic sills may have differentiated at higher levels in the sequence to produce extrusive mafic volcanic rocks and intrusive subvolcanic gabbro/picrite sills throughout the TNB.

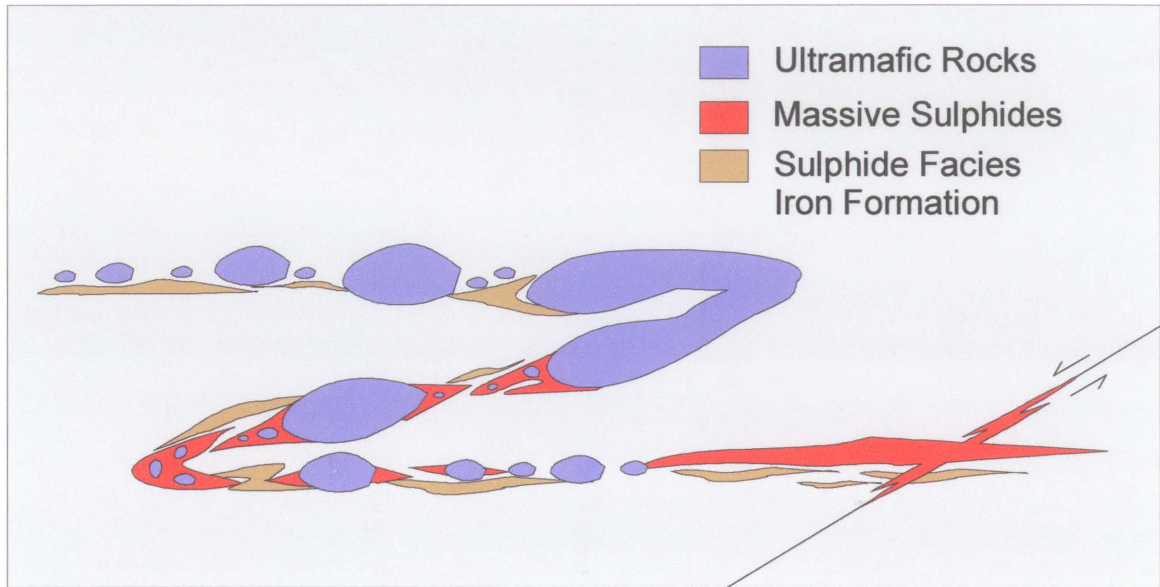


Figure 3.3. Schematic representation of stretched and folded ultramafic sills of the Thompson Nickel Belt deposits. Massive sulphide horizons are located within boudin necks, metasediments, and late shear zones and tension gashes (after Bleeker, 1990).

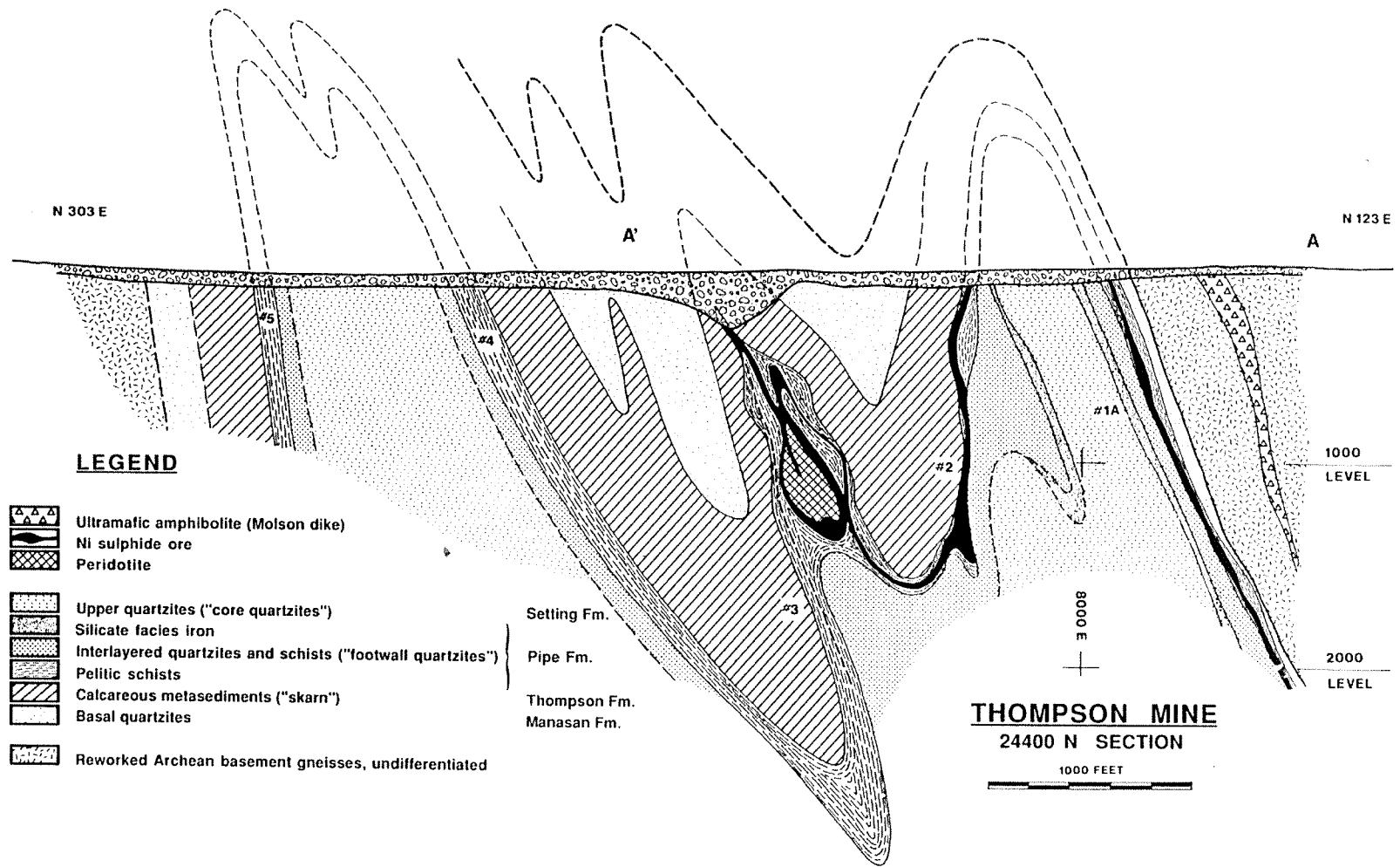


Figure 3.4. Cross section through the downward facing Thompson structure, looking NE (from Bleeker, 1990).

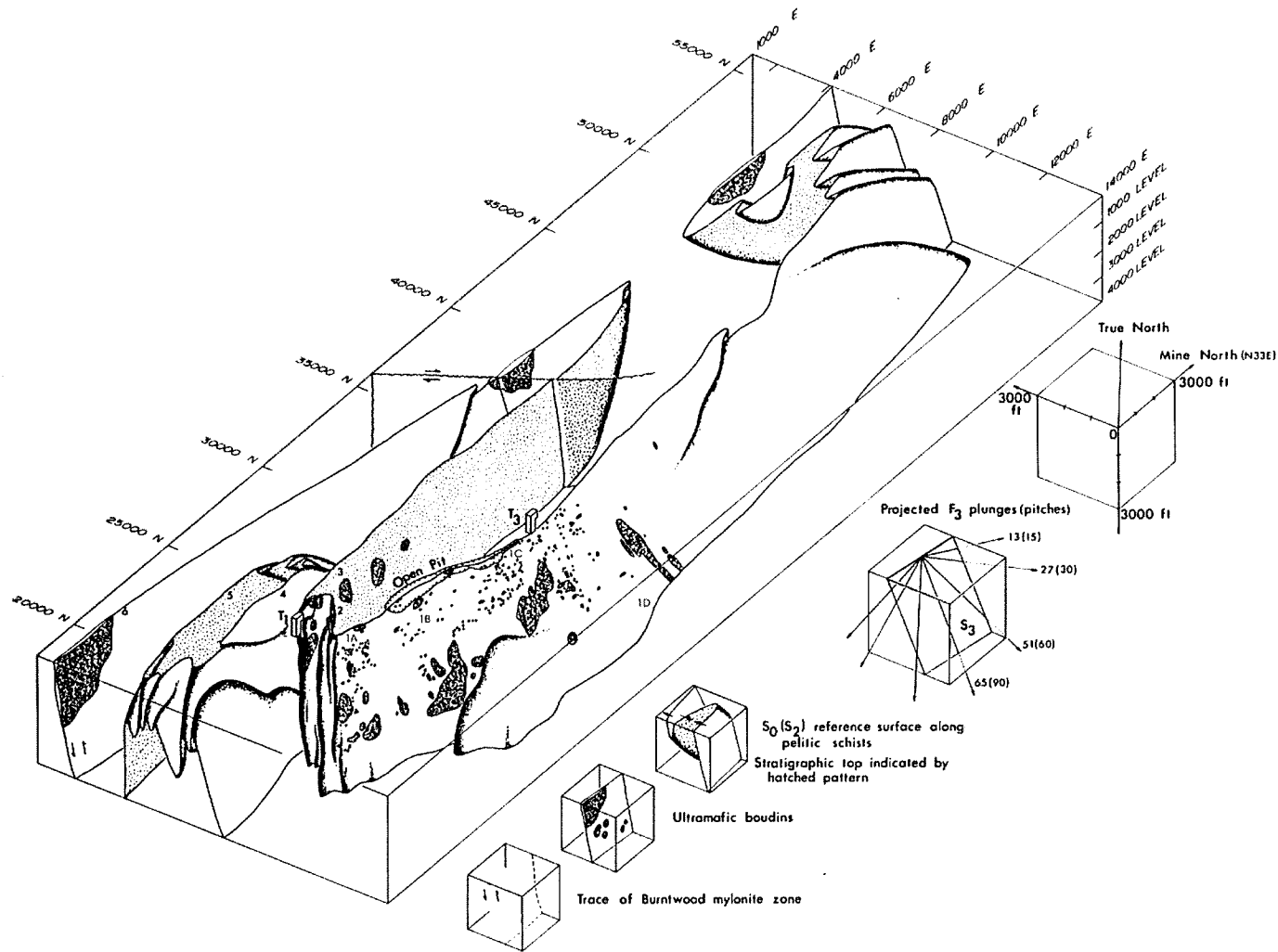


Figure 3.5. Orthographic block diagram of the Thompson structure (after Bleeker, 1990). View towards N358°E, 35°down. Coordinates refer to Thompson Mine grid. Note the location of the 1A, 1B, 1C, and 1D ore bodies along the reference horizon, which represents the pelitic schists of the Pipe Formation. Also note the location of the T1 mine shaft at the apex of an F3 fold structure, and the location of the T3 mine shaft on the main F3 hinge.

marks the T1 fold nose area that was sampled for this study, and the 1C and 1D ore bodies that were also sampled for this study.

3.3 Birchtree and Pipe Deposits

The Birchtree and Pipe deposits share similar lithological and structural settings. The ultramafic rocks of the Birchtree deposit are interpreted to be part of a discontinuous array of ultramafic bodies that stretch from Pipe II Open Pit to Birchtree Mine (Bleeker, 1990)(Figure 2.2). The ultramafic sills from the Birchtree deposit and the Pipe deposit occur in the same stratigraphic position within the Ospwagan Group cover sequence, i.e. within the graphitic sulphide facies iron formation of the Pipe Formation (Figure 3.6). The massive and semi-massive sulphides at Birchtree and Pipe have not undergone the same degree of deformation as the Thompson deposits. Massive sulphide accumulations tend to occur as breccias consisting of peridotitic clasts in a sulphide matrix. These breccias are typically proximal to ultramafic boudins and are not stretched within the metasedimentary horizon to the same extent as in Thompson.

Of the two deposits, only the Birchtree Mine was sampled for this thesis. However, due to the similarities of these deposits, data from Pipe deposit, as listed in the Thompson Nickel Belt Database (CAMIRO 2000a), is also presented for comparison. For more detailed stratigraphic, structural, and geochemical analyses of the Pipe deposit, the reader is referred to Bleeker (1990) and Peredery (1982).

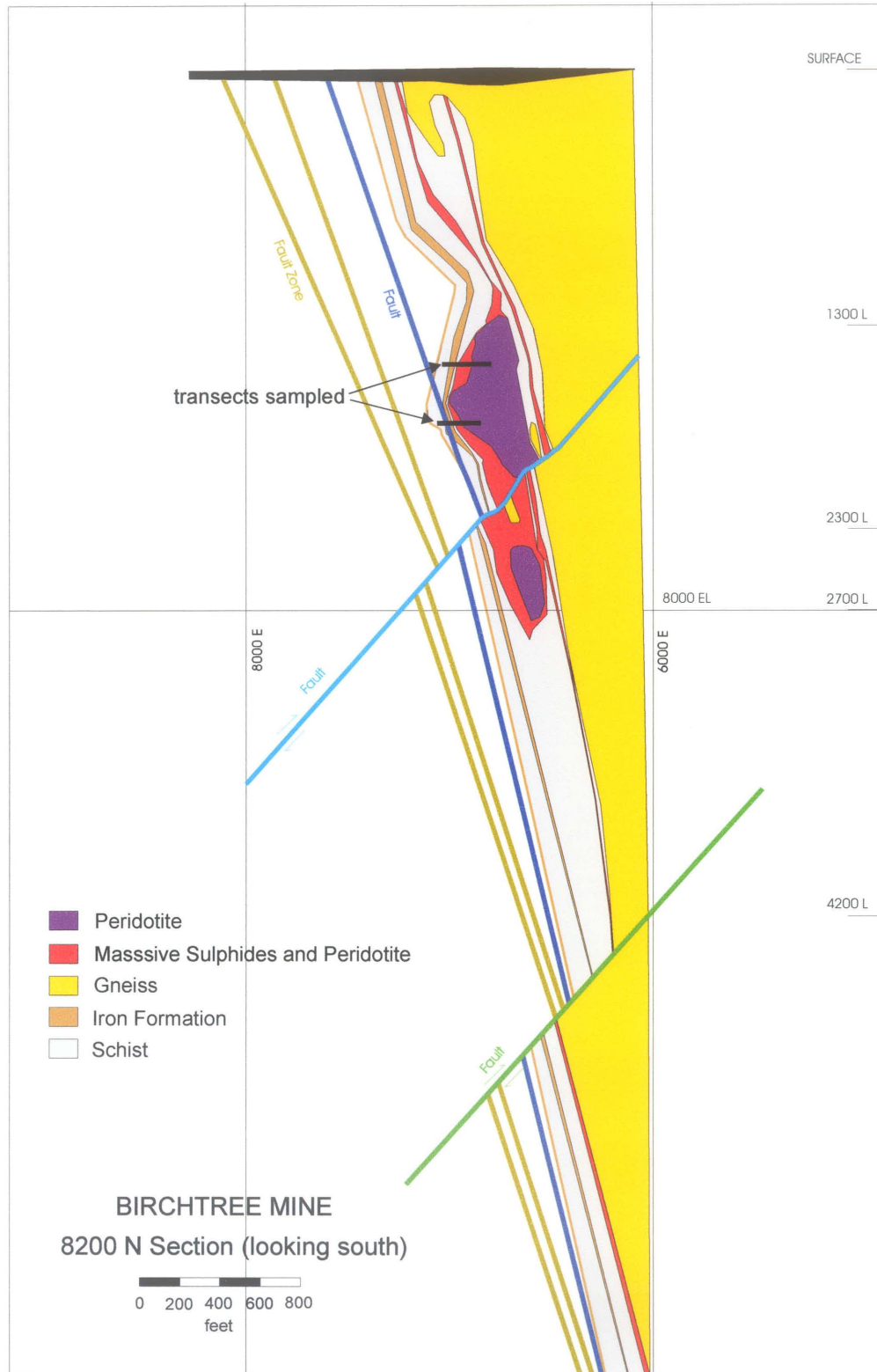


Figure 3.6. Typical cross section from the Birchtree Mine. Geological interpretation by INCO geologists. Samples analyzed from the mine were taken from transects at the 1500 Level and 1800 Level, as marked.

3.4 William Lake Deposit

The William Lake deposit lies beneath Paleozoic carbonate rocks in the southern portion of the Thompson Nickel Belt. Like the Thompson and Birchtree deposits, the ultramafic bodies are interpreted as being hosted by the Ospwagan Group metasediments (Figure 3.7). These metasediments include quartzites, pelites, calcareous metasediments, iron formations, and graphitic schists. The ultramafic bodies consist of pyroxenite, peridotite, and dunite. No work has been published to place the position of the bodies within the Ospwagan Group lithostratigraphic section of Bleeker (1990)(Figure 2.3). The ultramafic bodies and the hosting metasediments are concentrated on the southeastern margin of a granitic intrusion, the William Lake Dome. Centimetre- to metre-scale granitic pegmatite veins, interpreted to be related to the intrusion of the William Lake Dome, cross-cut the older Ospwagan Group rocks in many drill-core samples.

The mineralization in the deposit typically occurs as disseminated sulphides within the ultramafic bodies, and locally grades to centimetre- to decimetre-scale massive and semi-massive sulphide accumulations toward the base of bodies. Banded sulphides, sulphide stringers, and disseminated sulphides within metapelites and iron formations are commonly encountered in drill core.

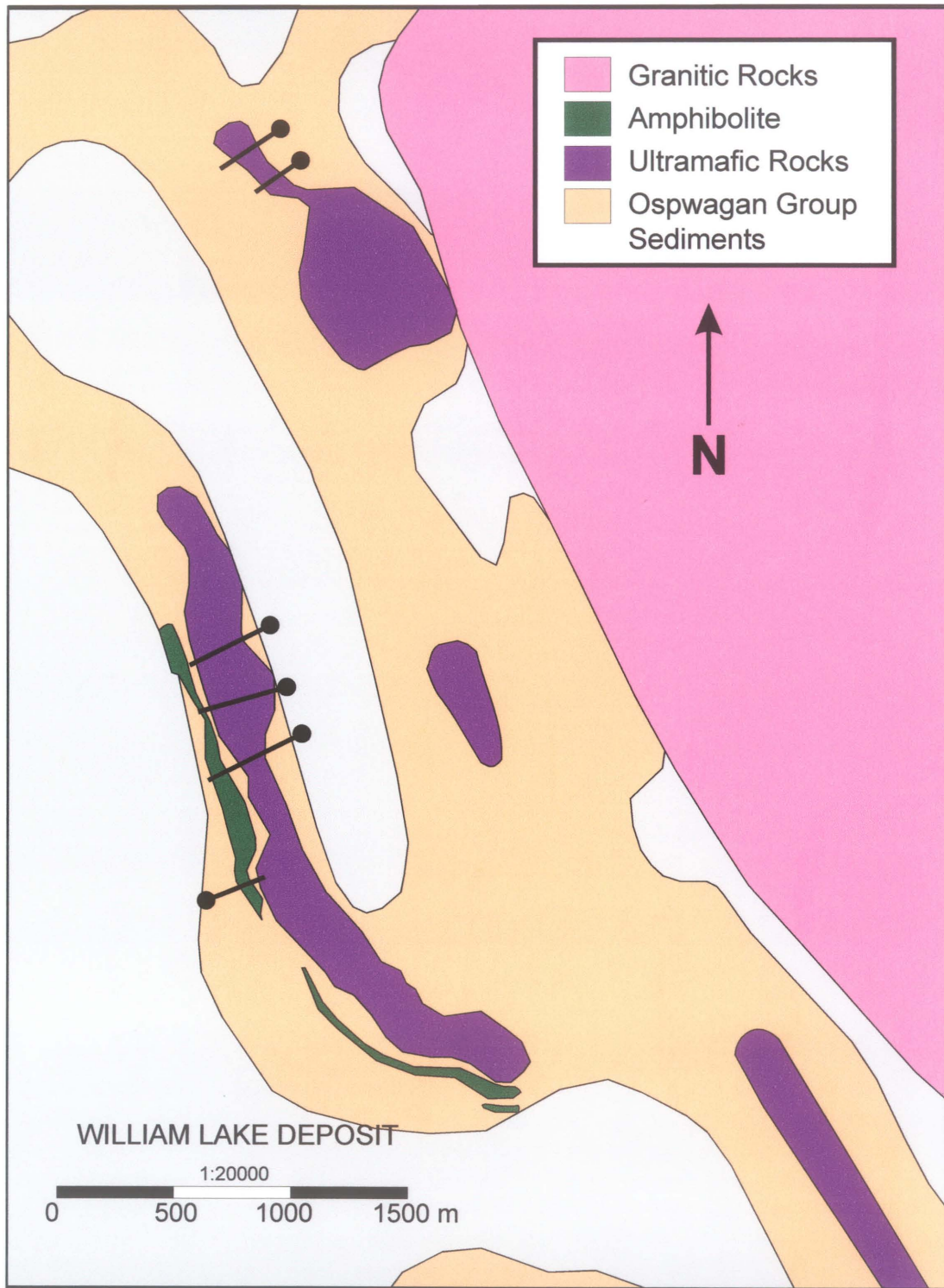


Figure 3.7. Schematic geological map of the William Lake deposit showing the relationship between the ultramafic rocks and what are interpreted to be Oswagan Group metasediments. Geological interpretation by J. Macek (CAMIRO, 2000a). Samples analyzed from the deposit were taken from drill hole intersections, as marked.

CHAPTER 4: SAMPLING AND METHODOLOGY

4.1 Sampling Technique

The majority of rocks sampled for this study were from the Thompson, Birchtree, and William Lake deposits; several samples from Bucko Lake, and Soab North deposits were analyzed by electron microprobe for comparison. Suites of sulphide-bearing rocks were collected as either grab samples from underground mines (Thompson T1 Mine, Thompson T3 Mine, and Birchtree Mine) or as saw cuts from exploration drill core (William Lake, Bucko Lake, and Soab North deposits). Sulphide-bearing intersections were collected with the guidance and technical assistance of INCO and Falconbridge geologists. Each sample suite consists of massive to semi-massive nickeliferous sulphides, and disseminated to stringer sulphides in the adjacent lithological units. These units were anywhere from centimetres to hundreds of metres away from the massive sulphides, the majority of the samples being tens of metres away. Semi-massive to massive Ni-barren sulphides (those sulphide-bearing rocks reported to contain less than 0.1% Ni) were also collected for comparison with nickeliferous ore. The relative locations of all samples were documented in order to establish trends in the compositions of the sulphides with respect to distance from massive ore bodies.

Several limitations in the sampling technique are presented here. Underground sampling in the Thompson and Birchtree mines was limited to available drifts that either cross-cut sulphide ore bodies and bounding strata, or that cut along strike of sulphide ore. The stratigraphy within and between the drifts is largely interpreted from AutoCAD maps provided by INCO geologists. Another limitation was encountered in the sampling of

exploration drill core from the Soab North deposit; drill core from these deposits is reduced to abbreviates, which are decimetre-sized remnants of lithologies that were intersected at 10- to 50-foot intervals.

4.2 Analytical Techniques

4.2.1 Overview

Microscopic textures of sulphide minerals in over 200 polished thin sections were examined by ore petrography. Major and minor element concentrations of sulphide minerals in 108 samples were determined by electron microprobe analysis (EMPA). Brief field descriptions and classifications of those samples that were analyzed by EMPA are listed in Appendix 1. Trace element concentrations of sulphide minerals from 33 samples were determined by proton-induced X-ray emission (PIXE). Whole-rock geochemical analyses of 81 sulphide samples complemented microprobe data in defining the chemical character of the Ni deposits. Whole-rock geochemical techniques that were used in this study are described in detail in Appendix 6. By relating the textures of sulphide-bearing rocks to the chemistry of the sulphide minerals in the rocks, one can better interpret these textures with respect to the timing of sulphide mineralization.

Applications of electron and proton microprobe analyses in sulphide mineralogy have been documented by Cabri (1988), Cabri *et al.* (1985), and Ryan and Griffin (1993). Microprobe analyses of sulphide minerals from Ni-Cu, Pt-Pd-Ni-Cu, and Pb-Zn-Cu-Ag ores can indicate the existence of valuable elements within certain mineral phases. These elements may occur as fine microscopic or submicroscopic inclusions, or in the form of a solid solution. Microprobe analyses can be very valuable from a mineral processing

perspective, in that they can determine which desirable elements (e.g. Ag, Au, PGE) can be liberated by metallurgical extraction and which undesirable elements (e.g. Se, As) may hamper the extraction. Major and trace element patterns in sulphide minerals can be diagnostic of physical conditions and geological processes in which the minerals were formed. Such data can be very valuable in determining the effects of metamorphism and metasomatism on a microscopic, macroscopic and, possibly, a regional scale. By complementing data from microprobe techniques with data from bulk analytical techniques, the exploration geologist can have a better understanding of where both desirable and undesirable elements are likely to reside within a deposit.

Czamanske *et al.* (1992) analyzed Cu-Fe-Ni sulphide minerals in a suite of ore samples from the Cu-Ni-PGE deposits of the Noril'sk-Talnakh district, Russia, by proton and electron microprobes. They found that the spatial distribution of the mineral assemblages, ore textures, bulk-composition, and experimental studies of the Cu-Fe-Ni-S system indicate that fractional crystallization of monosulphide solid solution (*mss*) and migration of resultant Cu-rich sulphide liquids were key processes in the evolution of the Noril'sk-Talnakh ores. These processes led to the crystallization of pentlandite from *mss* in ores that ultimately became pyrrhotite-bearing, and from trace-element enriched, intermediate solid solution (*iss*) in ores that ultimately became pyrrhotite-free. The work of Czamanske *et al.* (1992) showed the concentrations and mineral residency of both valuable and deleterious elements. Their work served as a preliminary guide to the use of EMPA and PIXE in this thesis.

4.2.2 EMPA and PIXE

The chemical compositions of pyrrhotite ($\text{Fe}_{(1-x)}\text{S}$), pentlandite ($\text{Fe, Ni}_9\text{S}_8$), chalcopyrite (CuFeS_2), pyrite (FeS_2), and gersdorffite (NiAsS) were determined by microprobe techniques. Sulphide minerals in polished thin sections and polished rounds were first analyzed by EMPA at University of Manitoba to determine major and minor element compositions. A selection of representative samples was then analyzed by PIXE at University of Guelph to determine trace element compositions. Operating parameters for EMPA and PIXE analyses are summarized in Appendix 2. Both techniques use a focussed beam of charged particles to excite characteristic X-rays and use energy-dispersive X-ray spectroscopy in the form of Si (Li) detectors. EMPA is widely used for mineralogical studies, as it provides nondestructive *in situ* analysis of mineral grains with $1\mu\text{m}$ spatial resolution and detection limits of a few hundred ppm. PIXE can be used to extend these detection limits to only a few ppm. However, the PIXE technique can be somewhat problematic in that more sample volume is required for PIXE analysis in comparison to EMPA. This sample volume must be large enough to accommodate a beam spot of $5 \times 10 \mu\text{m}^2$, which travels at a 45° angle downward from the surface of the sample, to a depth of 10-20 μm . The volume analyzed by EMPA is only $1\mu\text{m}^3$. It is recommended that grains analyzed by the PIXE technique at the University of Guelph are no smaller than about $50 \mu\text{m}^2$ to ensure that the proton beam only penetrates the grain of interest, and not surrounding grains. This poses a problem when analyzing very fine-grained disseminated sulphides, as the resulting data may partially record the chemistry of host silicates. Thus, the majority of samples analyzed by PIXE were semi-massive to massive sulphide ores. Furthermore, the majority of the sulphide phases analyzed by PIXE

were pyrrhotite and pentlandite, as these were the coarsest grains in the samples. This problem of grain size has resulted in a scant representation of trace element chemistry for disseminated sulphides, particularly in metasediments.

CHAPTER 5: SULPHIDE TEXTURES AND MINERALOGY

5.1 Classification of Sulphide Textures

5.1.1 Overview

Nickel sulphide deposits that form at high temperatures undergo various re-equilibration steps during slow cooling (Naldrett *et al.*, 1967a). Present sulphide mineral assemblages may reflect equilibrium attained and then preserved at one or more intermediate stages in the cooling process. Thus, the mineral assemblages in sulphide ore do not necessarily reflect the conditions at which the ore was emplaced. In this study, a classification scheme of sulphide-bearing rocks collected from the Thompson Nickel Belt was developed to assess the chemistry of the sulphides as they relate to their textures. The Thompson Nickel Belt sulphides have been classified previously by Zubrigg (1963), Peredery (1982), Bleeker (1990), and Larocque and Boulet (1998).

The classification scheme presented in this thesis is based on the macroscopic, mesoscopic, and microscopic texture of the sulphide component, and the character of the host rock in which the sulphides reside. The abbreviations for the nomenclature in this classification scheme are divided into a prefix, which reflects the texture of the sulphides, and a suffix that reflects the character of the host rock. For example, the sulphide class “disseminated sulphides in metasediments” is abbreviated as “DS–SED”; the sulphide class “massive sulphides in ultramafic breccia” is abbreviated as “MS–UB”. Figure 5.1 shows the general location of the sulphide classes, in relation to the Thompson Nickel Belt ore deposit model after Bleeker (1990).

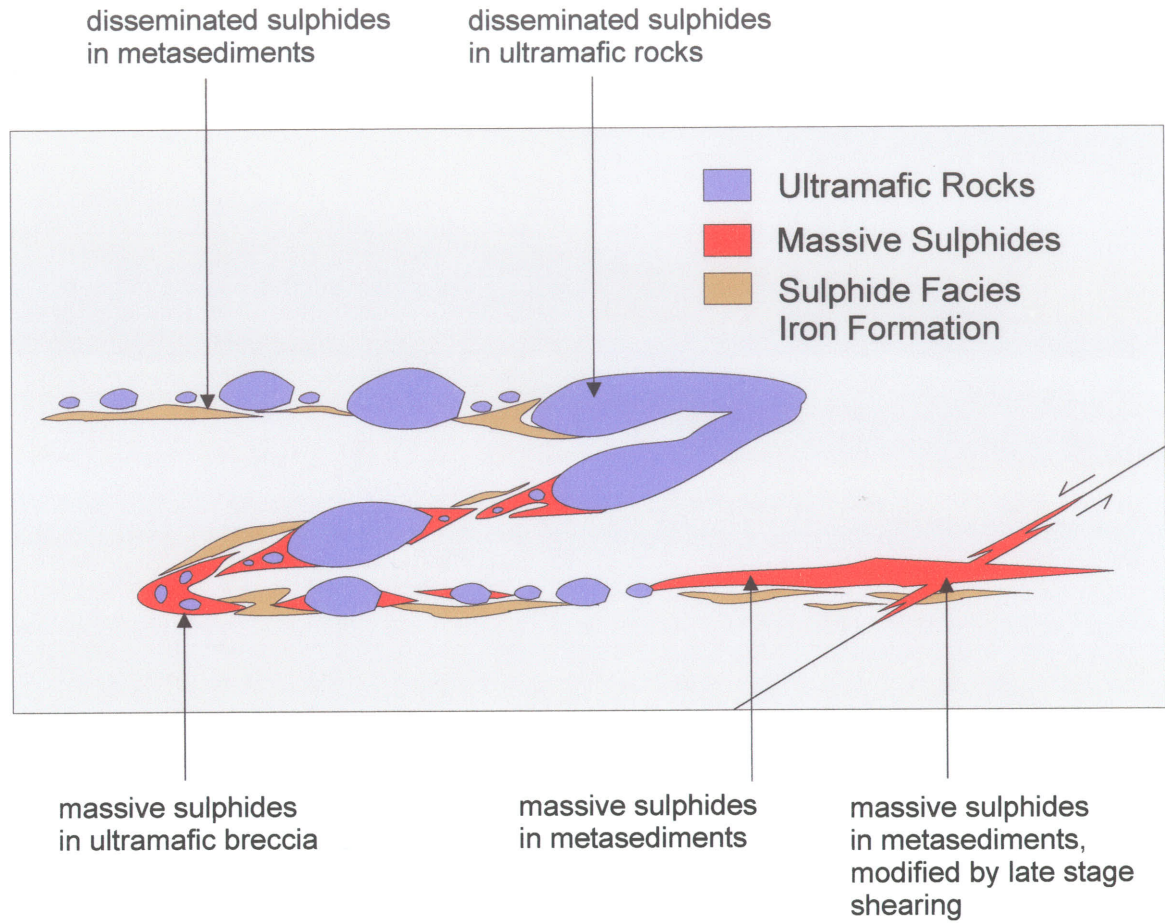


Figure 5.1. Relative location of the sulphide classes within folded and stretched sequence of Oswagan Group supracrustals in the Thompson Nickel Belt.

5.1.2 Disseminated sulphides in metasediments (DS-SED)

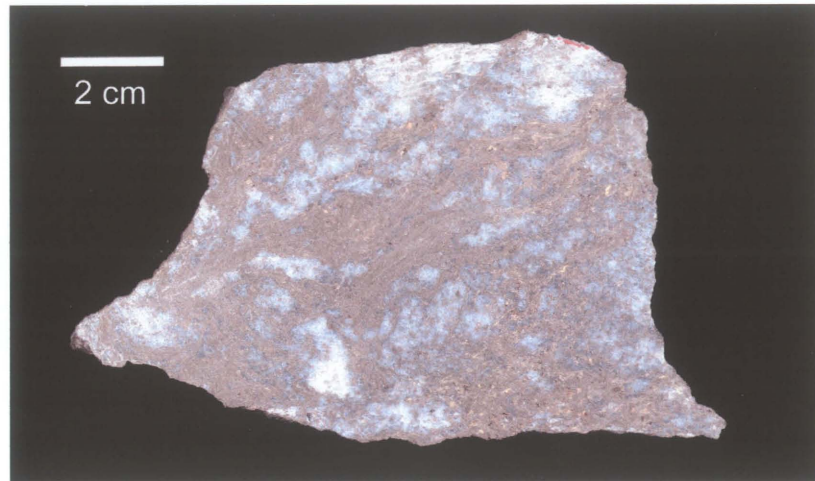
The sulphides in this class are disseminated, fine- to medium-grained, and constitute trace amounts to 15 percent (average ~5%) of gneisses, schists, or quartzites (Figure 5.2a). These sulphides are typically foliated pyrrhotite grains hosting very fine-grained angular to rounded patches of pentlandite and/or chalcopyrite (Figure 5.2b and c).

5.1.3 Disseminated and interstitial sulphides in ultramafic rocks (DS-U, IS-U)

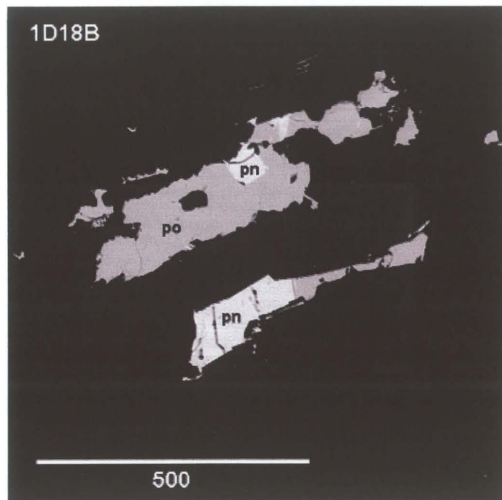
These sulphides range from fine-grained disseminated blebs to coarse-grained networks of interstitial grains (Figure 5.3a) in altered ultramafic rocks. The disseminated blebs typically constitute trace amounts to 7% sulphides of the ultramafic rocks, while interstitial grains typically constitute 7-25% sulphides in the rocks. Typically, the disseminated grains are in the interior of serpentinized ultramafic bodies, while the interstitial grains are toward the exterior of the bodies. The minerals comprising this sulphide type are pyrrhotite and pentlandite, with minor chalcopyrite and magnetite. The pentlandite and chalcopyrite typically form subangular to subrounded patches along the edges of pyrrhotite grains (Figure 5.3b). Magnetite typically occurs as fine anhedral grains adjacent to the sulphides and as lamellae in silicate minerals (Figure 5.3c).

5.1.4 Barren massive sulphides in metasediments (BMS-SED)

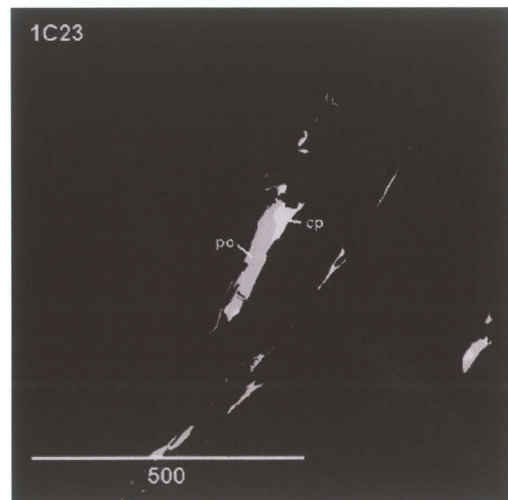
This sulphide class typically comprises massive horizons or cm-scale bands of pyrrhotite within biotite-rich schists and gneisses, and graphitic schists (Figure 5.4a). The term “barren” refers to the low abundance of Ni in the sulphides (<1500 ppm Ni on a 100% sulphide basis). The pyrrhotite is typically fine-grained and annealed, and comprises



a

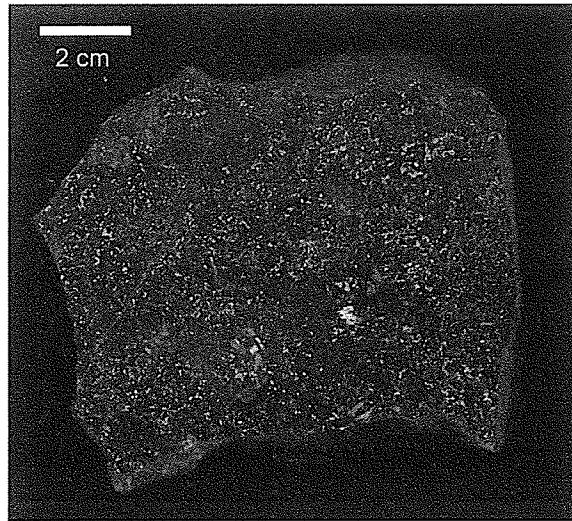


b

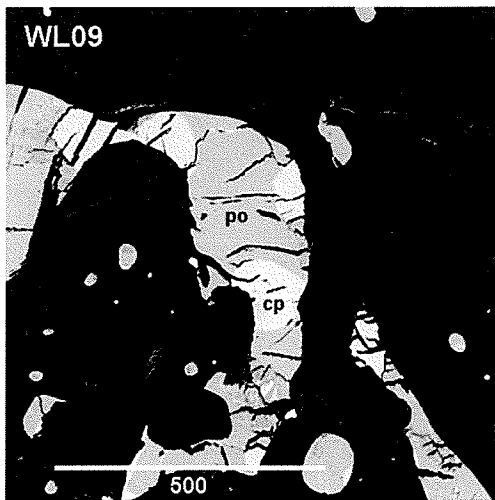


c

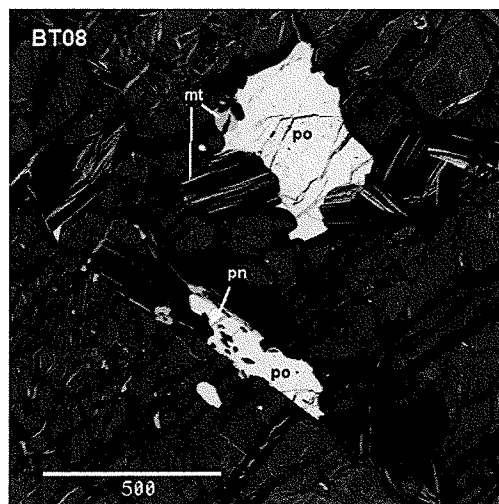
Figure 5.2. Textures representing sulphide class DS-SED (disseminated sulphides in metasediments). a) Mineralized biotite schist from the Thompson 1D ore body. b) BSE (backscatter electron) image of disseminated sulphides in a sillimanite-garnet-biotite schist from the Thompson 1D ore body, T3 Mine. pn = pentlandite, po = pyrrhotite, black background = silicates. Scale bar in μm . c) BSE image of disseminated sulphides in garnet-biotite schist from the 1C ore body, T3 mine. cp = chalcopyrite, po = pyrrhotite, black background = silicates. Scale bar in μm .



a



b

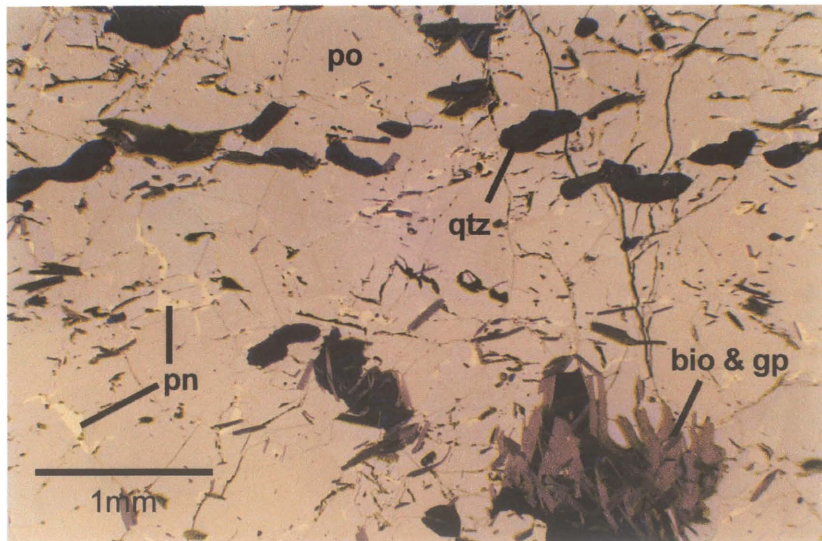


c

Figure 5.3. Textures representing sulphide classes DS-U (disseminated sulphides in ultramafic rocks) and IS-U (interstitial sulphides in ultramafic rocks). a) Serpentinized peridotite containing interstitial sulphides from Birchtree Mine. b) BSE image of disseminated sulphides in serpentinized peridotite from the William Lake deposit. Note the blebby texture of the sulphides that are interstitial to serpentinized olivine grains (dark grey and black). cp = chalcopyrite, po = pyrrhotite. Scale bar in μm . c) BSE image of disseminated sulphides in serpentinized peridotite from the Birchtree mine. Magnetite (mt) occurs as fine grains along the edges of pyrrhotite grains (po), and also as lamellae in silicates (dark grey and black). Pentlandite (pn) occurs as fine angular patches in pyrrhotite. Scale bar in μm .



a



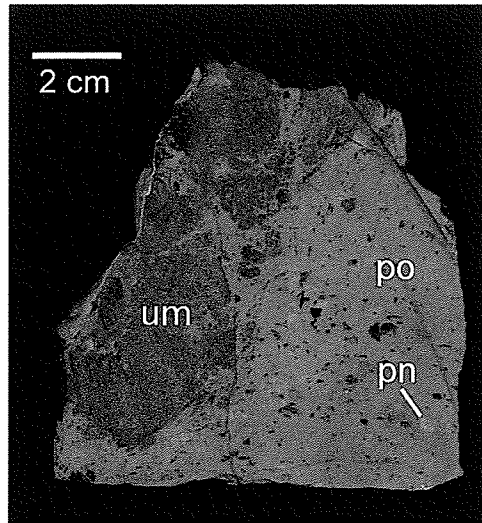
b

Figure 5.4. Textures representing sulphide class BMS-SED (barren sulphides in metasediments). a) Sample from the Thompson T1 Mine, showing massive pyrrhotite with foliated single crystal inclusions of graphite and biotite, and ovoid aggregates of plagioclase, quartz, graphite, and biotite. b) Photomicrograph showing massive pyrrhotite (po) and flame-textured to fine chain-textured pentlandite (pn) with inclusions of graphite (gp), biotite (bio), and quartz (qtz).

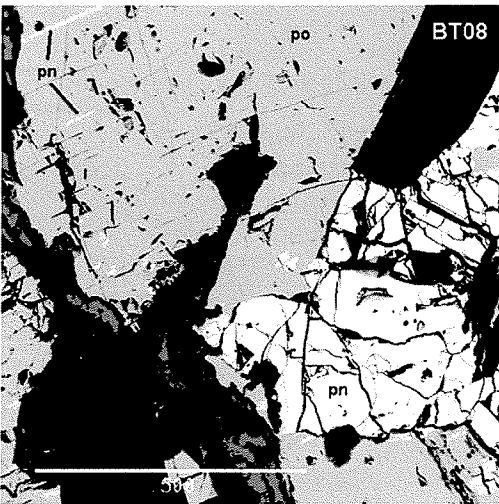
both hexagonal and monoclinic varieties. This sulphide class lacks visible pentlandite mineralization on a hand-sample scale and is particularly graphitic, containing up to 25% graphite. The graphite occurs as foliated single inclusions or as aggregates associated with foliated biotite flakes and rounded to ovoid quartz and plagioclase (Figure 5.4b). Chalcopyrite, pyrite, and magnetite are minor to trace minerals. The chalcopyrite typically occurs as very fine-grained blebs within the pyrrhotite grains, and as “porous masses” adjacent to silicate inclusions. Pyrite occurs as subhedral aggregates replacing pyrrhotite. Magnetite occurs as randomly distributed, fine anhedral grains. In several samples (JL99-1D-37, JL99-1D-38, JL99-1D-39), up to 5% pentlandite was observed to occur microscopically as “flames” and very fine-grained “chains” at the boundaries of annealed pyrrhotite grains (Figure 5.4b); no coarse-grained pentlandite was found in this sulphide type.

5.1.5 Massive sulphides in ultramafic breccia (MS-UB)

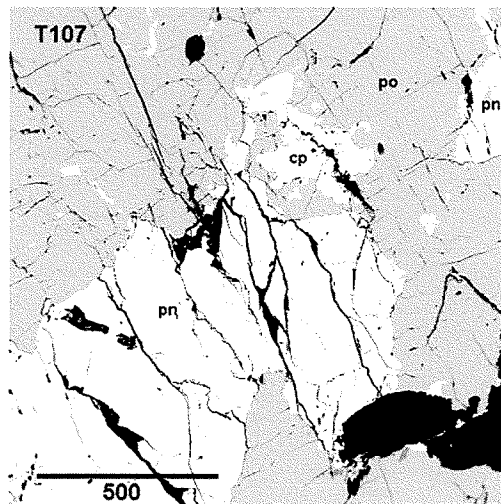
These sulphides are semi-massive (25-70% sulphide component) to massive (70-100% sulphide component) accumulations forming the matrix to ultramafic breccias (Figure 5.5a). Fine- to very coarse-grained, tectonized inclusions of the hosting ultramafic bodies are typical of this sulphide type. The mineralogy is dominated by pyrrhotite and pentlandite, with minor amounts of chalcopyrite, pyrite, chromian spinel and gersdorffite. Pyrrhotite occurs as annealed medium- to coarse-grained polygonal grains. Pentlandite occurs as 1) very fine lamellae (Figure 5.5b), 2) elongated, wispy “chains”, and 3) coarse-grained, subangular to subrounded “eyes” (Figure 5.5b and c). The pentlandite eyes are typically <1mm to 5 mm in size. On a microscopic scale, the sulphide textures and



a



b



c

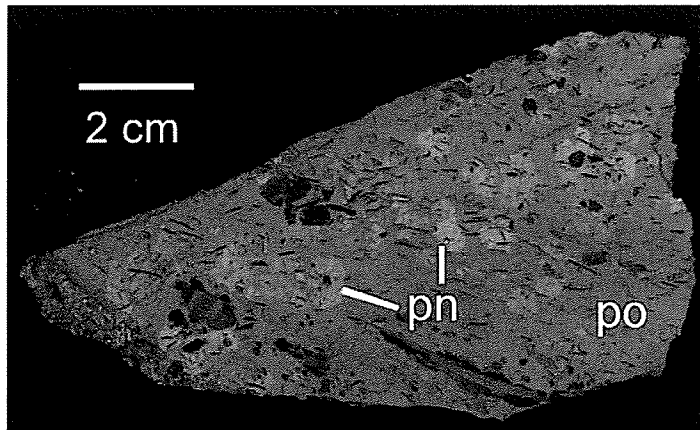
Figure 5.5. Textures representing sulphide class MS-UB (massive sulphides in ultramafic breccia). a) Massive sulphide breccia sample from Birchtree Mine, showing cm-scale inclusions of serpentinite (um) and single crystal inclusions of mafic mica grains, quartz, and feldspar in massive pyrrhotite (po). Pentlandite (pn) occurs as medium-grained light-coloured “eyes”. b) BSE image of sulphides hosted in a serpentinized peridotitic breccia from the Birchtree mine. Pentlandite (pn) occurs as lamellae and subrounded to subangular “eyes” in massive pyrrhotite (po). black areas = silicates and pits. Scale bar in μm . c) BSE image showing massive breccia sulphides from the T1 mine. cp = chalcopyrite, pn = pentlandite, po = pyrrhotite, black areas = silicates and pits. Scale bar in μm .

mineralogy in this sulphide class are similar to those of massive sulphides in metasediments (MS-SED – described below).

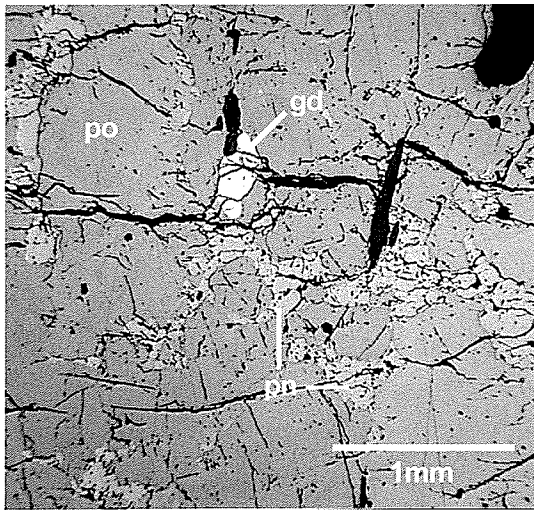
5.1.6 Massive and semi-massive sulphides in metasediments (MS-SED, SMS-SED)

These sulphides are semi-massive (25-70% sulphide component) to massive (70-100% sulphide component) horizons at the base of ultramafic bodies, or within gneisses, schists, and quartzites. The sulphides in this class consist mainly of pyrrhotite and pentlandite (Figure 5.6a). Minor amounts of chalcopyrite, pyrite, magnetite, chromian spinel and gersdorffite occur in this sulphide type. As in the massive sulphides in ultramafic breccia (MS-UB), pyrrhotite occurs as annealed polygonal grains and pentlandite occurs as 1) very fine lamellae, 2) elongated, wispy “chains” (Figure 5.6b), and 3) coarse-grained, subangular to subrounded “eyes” (Figure 5.6c). The pentlandite eyes are typically <1mm to 5 mm in size, but can be up to 2 cm wide in some horizons. In many massive sulphide horizons throughout the Thompson Mine, pentlandite eyes are often segregated into cm-scale bands within a coarse-grained, annealed pyrrhotite matrix (Figure 5.13b).

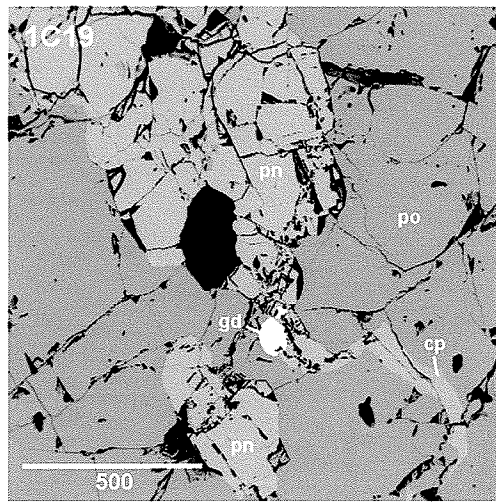
Pyrite typically occurs as aggregates of subhedral grains that replace both pentlandite and pyrrhotite (Figure 5.7). Gersdorffite, which occurs as very fine, anhedral to subhedral grains (Figure 5.7), was most often found in this sulphide class; however, the mineral also occurs in massive sulphides in ultramafic breccia (MS-UB) (Figure 5.6b and c). Magnetite and chromian spinel occur as very fine-grained euhedral to subhedral grains randomly oriented in a sulphide matrix.



a



b



c

Figure 5.6. Textures representing sulphide class MS-SED (massive sulphides in metasediments) and SMS-SED (semi-massive sulphides in metasediments). a) Massive sulphide sample from the Thompson T1 Mine, showing coarse grained annealed pyrrhotite and lighter-coloured pentlandite eyes. Inclusions are foliated mafic mica grains and aggregates of biotite, quartz, and plagioclase. b) Photomicrograph showing fractured massive sulphides hosted in biotite schist from the Birchtree Mine. Pentlandite (pn) occurs as “chains” at the boundaries of annealed pyrrhotite grains (po). The bright ovoid mineral in the centre of the figure is gersdorffite (gd). c) BSE image of semi-massive sulphides hosted in sillimanite-garnet-biotite gneiss from the 1C ore body, Thompson mine. Note the subrounded gersdorffite grain (gd) that has crystallized over pentlandite (pn). Chalcopyrite (cp) and pentlandite have the same grey levels in backscatter electron images; the typically fractured texture of pentlandite distinguishes it from chalcopyrite. po = pyrrhotite, black grains = silicates. Scale bar in μm .

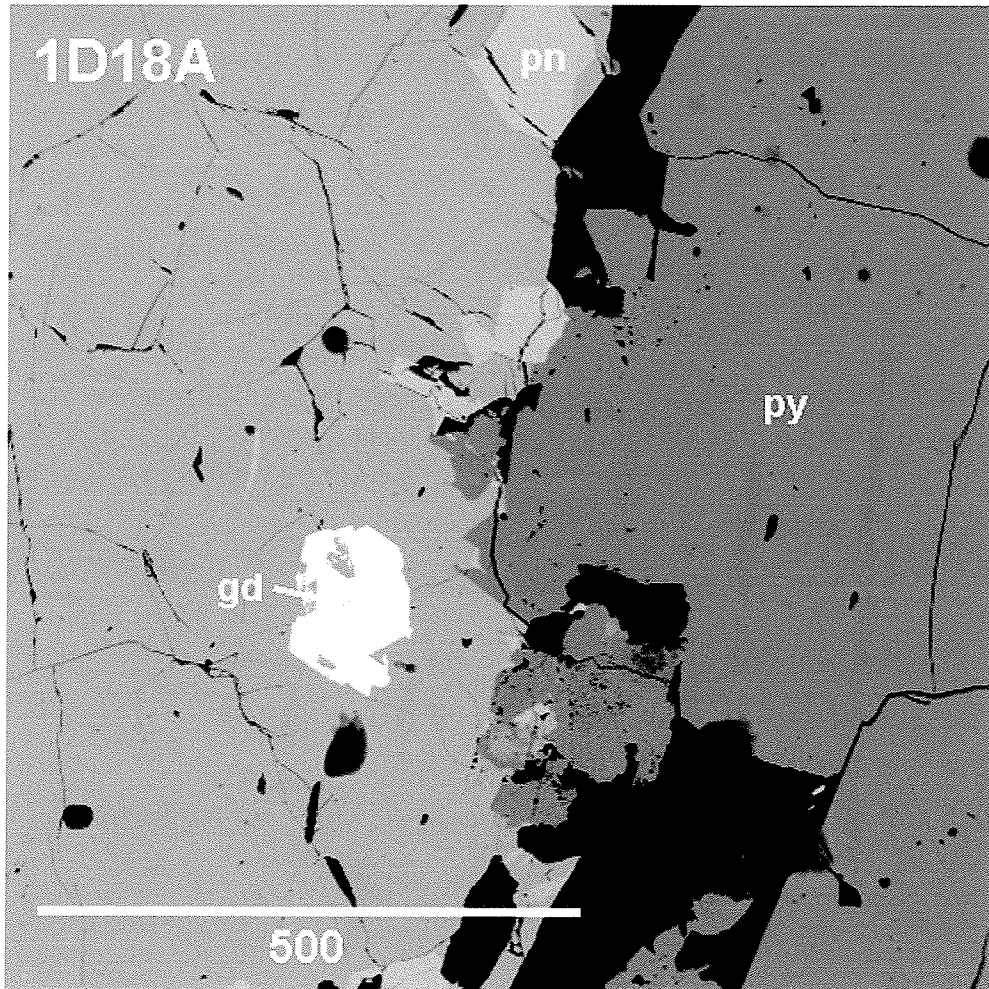


Figure 5.7. BSE image showing semi-massive sulphides hosted in biotite gneiss from the 1D ore body, Thompson mine. Note the subhedral gersdorffite grain (gd) within massive pyrrhotite. Pyrite (py) occurs as aggregates of subhedral grains replacing pyrrhotite. pn = pentlandite, black grains = silicates. Scale bar in μm .

The margins of massive sulphide horizons show evidence of brecciation along the contact with hosting metasediments (Figure 5.8). Fine- to coarse-grained chalcopyrite is typically distributed adjacent to pentlandite in stringers projecting into the metasediments along this contact (Figure 5.9). Chalcopyrite also tends to be concentrated proximal to silicate inclusions (Figure 5.10). Pyrite-chalcopyrite symplectites are irregularly distributed within and along the margins of the massive sulphide horizons (Figure 5.11).

5.2 Characteristics of Mineralized Massive Sulphides from TNB Deposits

The mineralized massive sulphide samples (MS-UB, SMS-SED and MS-SED) collected from various deposits in the Thompson Nickel Belt can be characterized in terms of their host, their relative proximity to ultramafic boudins, their inclusion population (which can comprise up to 60% of the sample), and the macroscopic texture of pentlandite grains. Of all samples collected in this study, the following were mineralized semi-massive to massive sulphides: 8 from Birchtree, 10 from T1 Mine, 10 from 1C ore body, 15 from 1D ore body, and 12 from William Lake.

Ore samples from the Birchtree Mine consist of massive sulphides that occur in ultramafic boudin necks and at the base of ultramafic bodies, thereby representing sulphide class (MS-UB). They contain randomly oriented to oriented, medium- to coarse-grained brecciated ultramafic inclusions and minor pelitic inclusions. Pyrrhotite, the main sulphide mineral, is associated with up to 10% fine- to medium-grained pentlandite (Figure 5.5a). Due to the proximity of the ore to the ultramafic boudins, samples from Birchtree are interpreted to be closer in textural character to “primary” magmatic massive sulphides, in comparison to samples from Thompson.

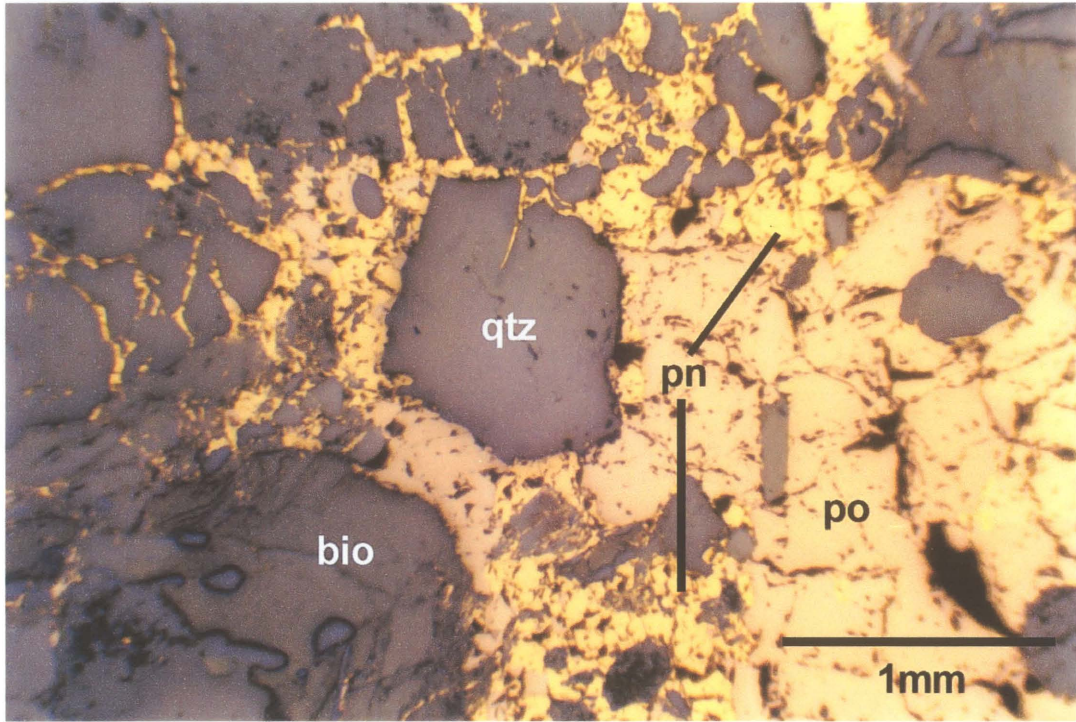


Figure 5.8. Brecciated silicate fragments along contact between garnet biotite schist and massive sulphides. Sample is from the Thompson 1C ore body.

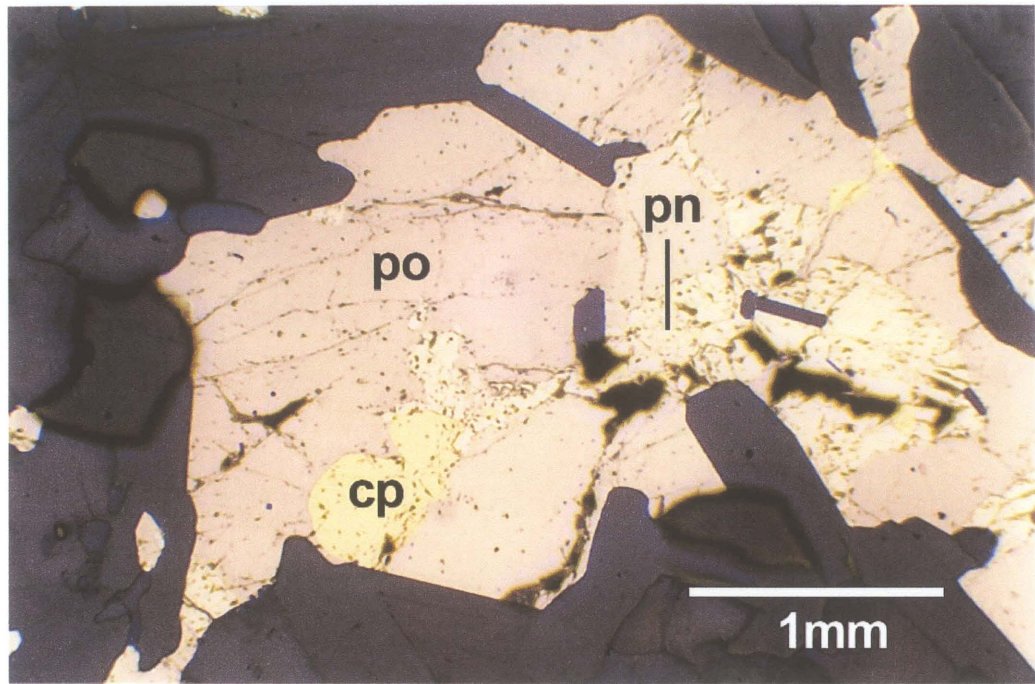


Figure 5.9. Stringer sulphides in garnet biotite gneiss from the Thompson T1 Mine. Chalcopyrite tends to be concentrated in such stringers throughout the Thompson Mine.

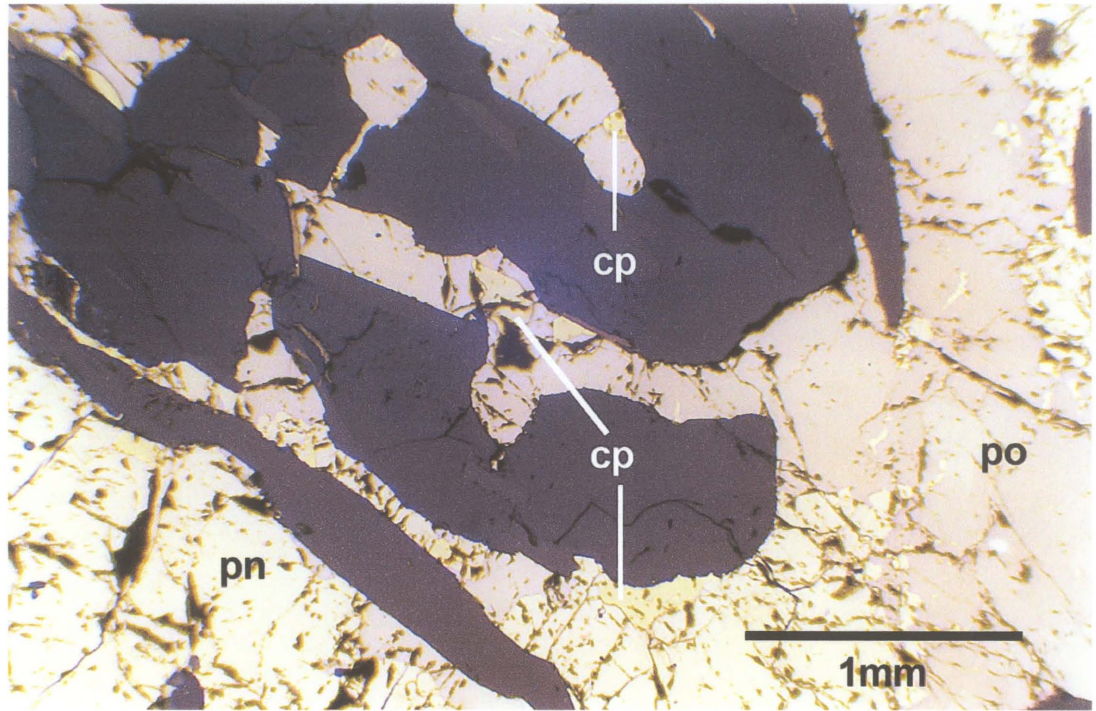
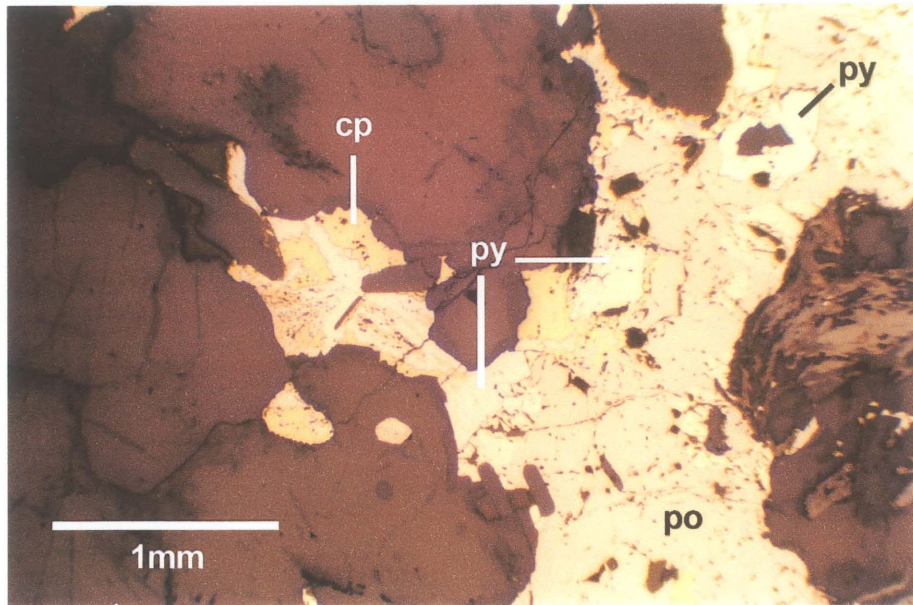
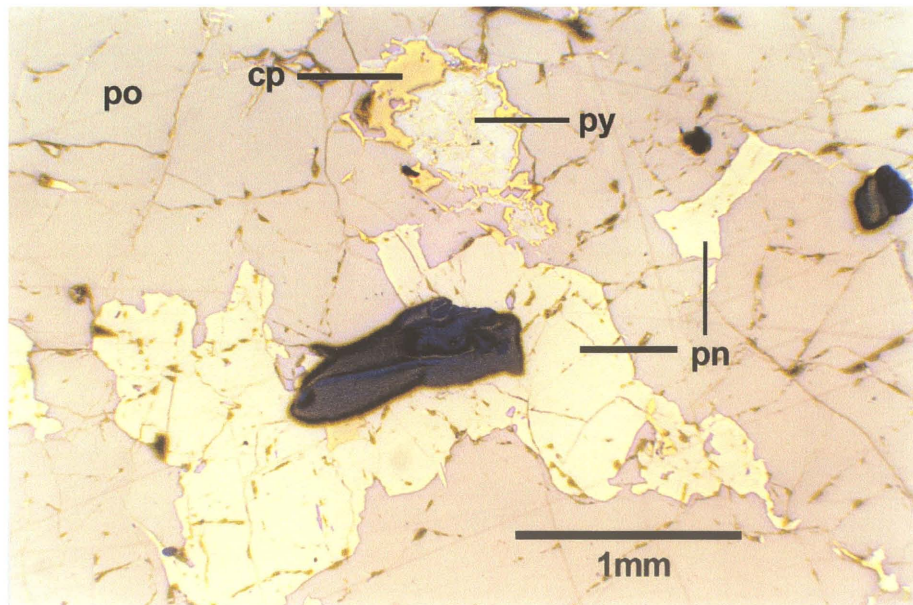


Figure 5.10. Example of chalcopyrite occurring adjacent to porphyroblastic silicates in massive sulphides. Silicates are embayed aggregates of quartz and feldspar oriented parallel to foliated biotite porphyroblasts. Sample is from the Thompson T1 Mine.



a



b

Figure 5.11. Pyrite-chalcopyrite symplectites. a) Symplectite in stringer sulphides from the Thompson 1D ore body. b) Symplectite in annealed massive sulphides from the Thompson T1 Mine.

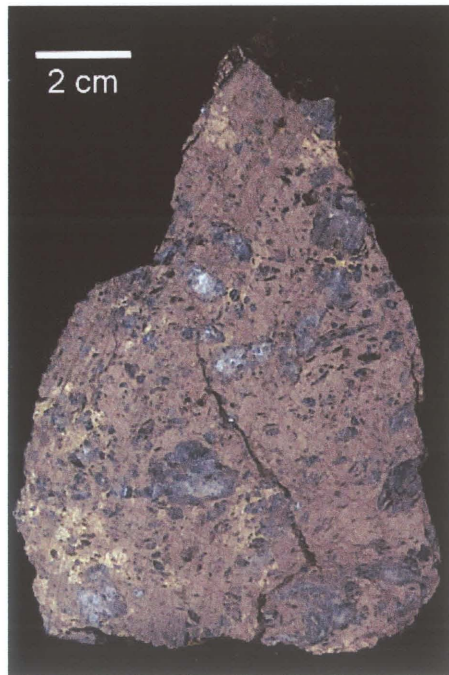
Ore samples from the Thompson Mine, which present a spectrum of textures, are best separated in terms of the area from which they were sampled (T1 fold nose, 1C ore body, and 1D ore body). Most ore samples from the T1 fold nose are very similar in texture to the Birchtree MS-UB samples described above (Figure 5.12a). One from the T1 fold nose area (Sample JL98-T1-19) represents sulphide class MS-SED. This sample is from a concordant massive sulphide lens hosted in pelitic schist that is more distal to ultramafic boudins (at least 50 ft away from, and along strike of, an ultramafic body). T1 ore typically contains randomly oriented to oriented, medium- to coarse-grained ultramafic and pelitic inclusions, and contain up to 25% medium- to coarse-grained pentlandite grains (Figure 5.12b). Single crystal inclusions also occur in the T1 massive sulphides; the most abundant crystal inclusions are fine- to medium-grained foliated biotite flakes, and rounded quartz and plagioclase grains.

Ore samples from the 1C ore body largely represent sulphide class MS-SED (Figure 5.13a). The 1C samples differ from the T1 MS-SED samples above in that the pentlandite grains tend to be coarse and distributed into parallel, cm-scale bands within the ore horizons (Figure 5.13b). Furthermore, single crystals of biotite, quartz, and plagioclase dominate the inclusion population.

Ore samples from the 1D ore body represent massive sulphides hosted in pelitic and quartz-rich sediments that have been intruded by late pegmatitic granite (Figure 5.14a). Although the samples from this part of the Thompson Mine fall largely under the category SMS-SED, the ore is unique in character with respect to other Thompson Nickel Belt sulphides. The 1D ore body has undergone extreme and complex deformation, which is evident from undulating contacts between rock units, numerous metre-scale shear zones,



a

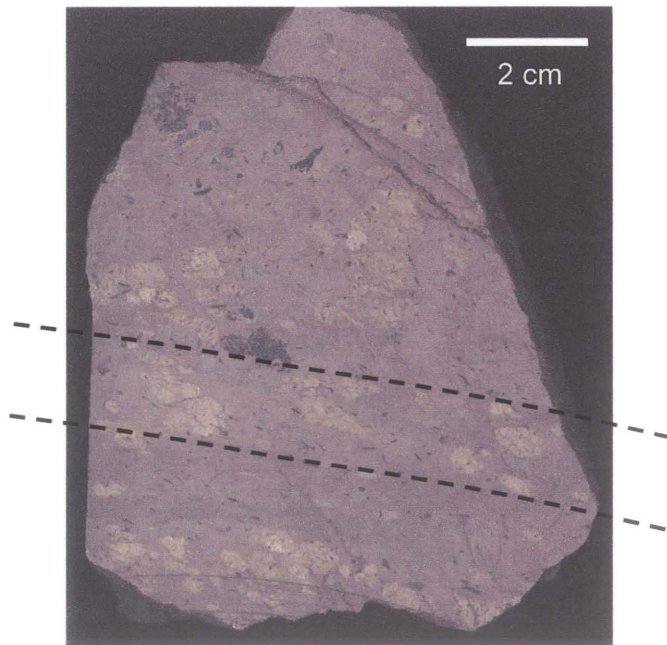


b

Figure 5.12. Massive sulphides from the Thompson T1 Mine. a) Massive sulphides in the matrix of serpentized ultramafic breccia. Ultramafic boudins have talc-carbonate envelopes. Field of view is 12 feet (3.7m). b) Massive sulphides consisting of medium to coarse grained annealed pyrrhotite and pentlandite, and inclusions of pelitic schist fragments and serpentized peridotite.

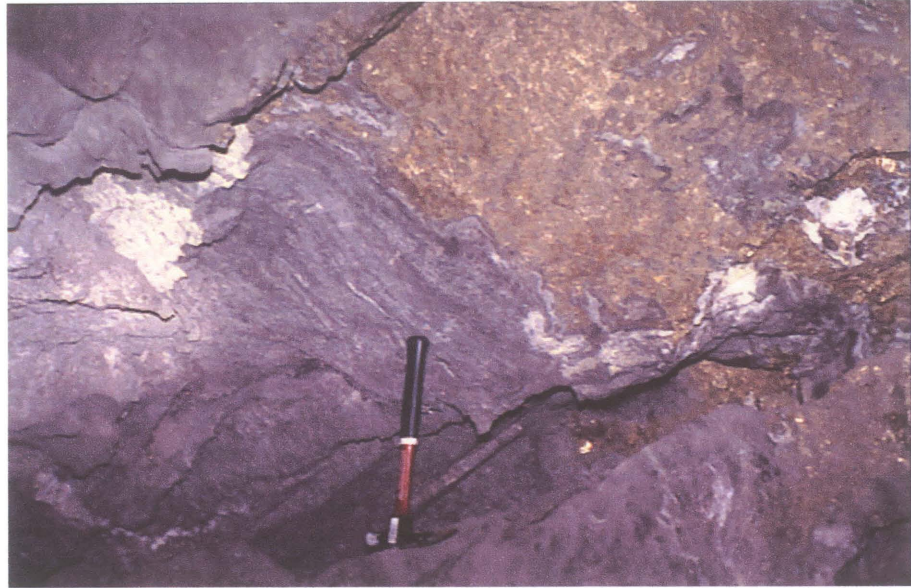


a

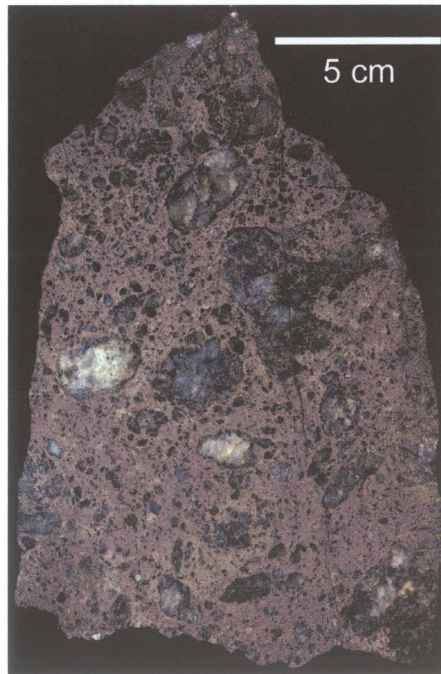


b

Figure 5.13. Massive sulphides from the Thompson 1C ore body. a) Concordant massive sulphides hosted in biotite schist. Field of view is 7.5 feet (2.3m). (b) Massive sulphides consisting of coarse pyrrhotite grains and pentlandite eyes oriented parallel to foliated mica inclusions and schistose aggregates.



a



b

Figure 5.14. Semi-massive sulphides from the Thompson 1D ore body. a) Semi-massive sulphides at the contact with biotite schist. Schist and sulphides contain decimetre-scale pegmatitic veins. b) Semi-massive sulphide sample containing fine to medium grained pyrrhotite, pentlandite, and chalcopyrite, and coarse ovoid inclusions of pegmatitic granite.

and abundant pegmatitic/tonalitic inclusions. The samples from this part of the Thompson Mine are also relatively more distal to ultramafic boudins than aforementioned samples; no interpreted ultramafic parent rocks were observed within 800 ft along strike of the ore bodies in 1D. The samples contain up to 40% well-rounded, medium- to coarse-grained pegmatitic/tonalitic inclusions, and typically contain up to 10% fine- to medium-grained pentlandite grains (Figure 5.14b). Locally, the pentlandite grains are as coarse-grained as the 1C ore; however, these are interpreted to occur in relatively more preserved (i.e. less deformed) portions of the ore body.

William Lake massive sulphide samples, all taken as core samples (Figure 5.15), have similar macroscopic textures to those from Birchtree, T1 fold nose, and 1C ore body; no textural equivalents of 1D ore body samples were observed.

5.3 Textural Variations Across Strike of a Deformed Ore Zone

A detailed investigation of an ore-bearing stratigraphic section in the 1C ore body, Thompson Mine (Figure 5.16), was conducted to assess the textural variation of sulphides across and along the strike of a deformed ore zone. The mesoscopic textures of the sulphides within the 1C ore zone are summarized in Table 5.1.

The textures of sulphides across strike of the 1C ore zone vary with the location of the sulphides in the stratigraphic pile. Figure 5.17 (A to D) shows the transition from disseminated sulphides in the interior of the ultramafic body to interstitial, net-textured sulphides at the edges of the body. This transition coincides with increasing serpentinization of the ultramafic host, which was likely caused by hydration of the ultramafic body from the exterior to the interior.

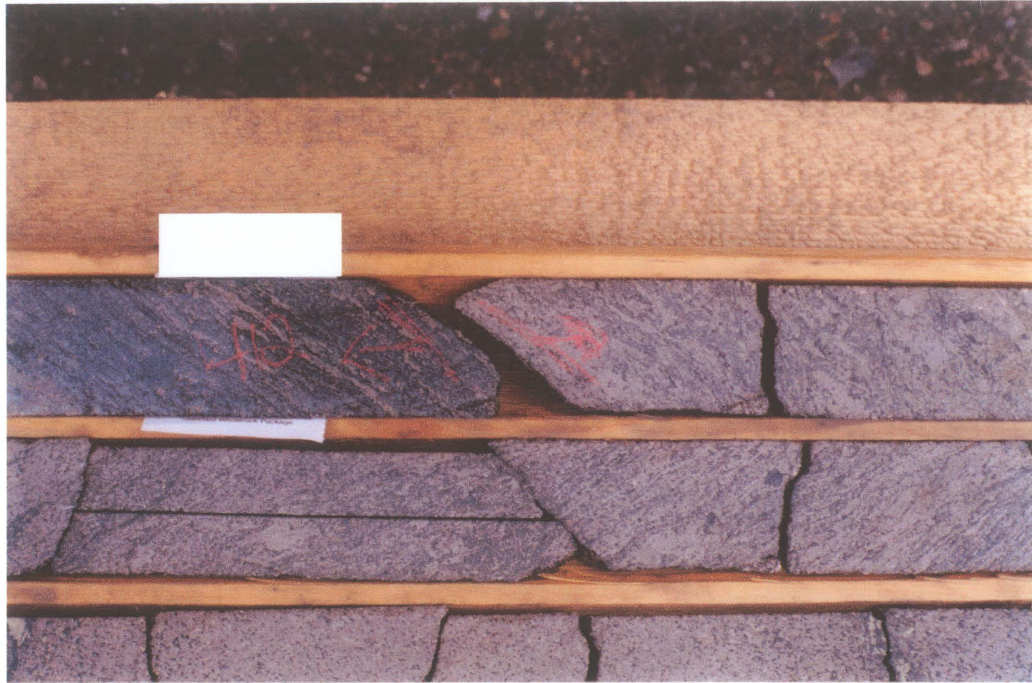


Figure 5.15. Massive sulphide horizon in contact with biotite schist from the William Lake deposit. Down-hole contact of massive sulphide (not shown) is with a serpentinized ultramafic body. Massive sulphide consists of fine to medium grained pyrrhotite, minor chalcopyrite, foliated biotite inclusions, and fine-grained quartz. Width of core is 5 cm.

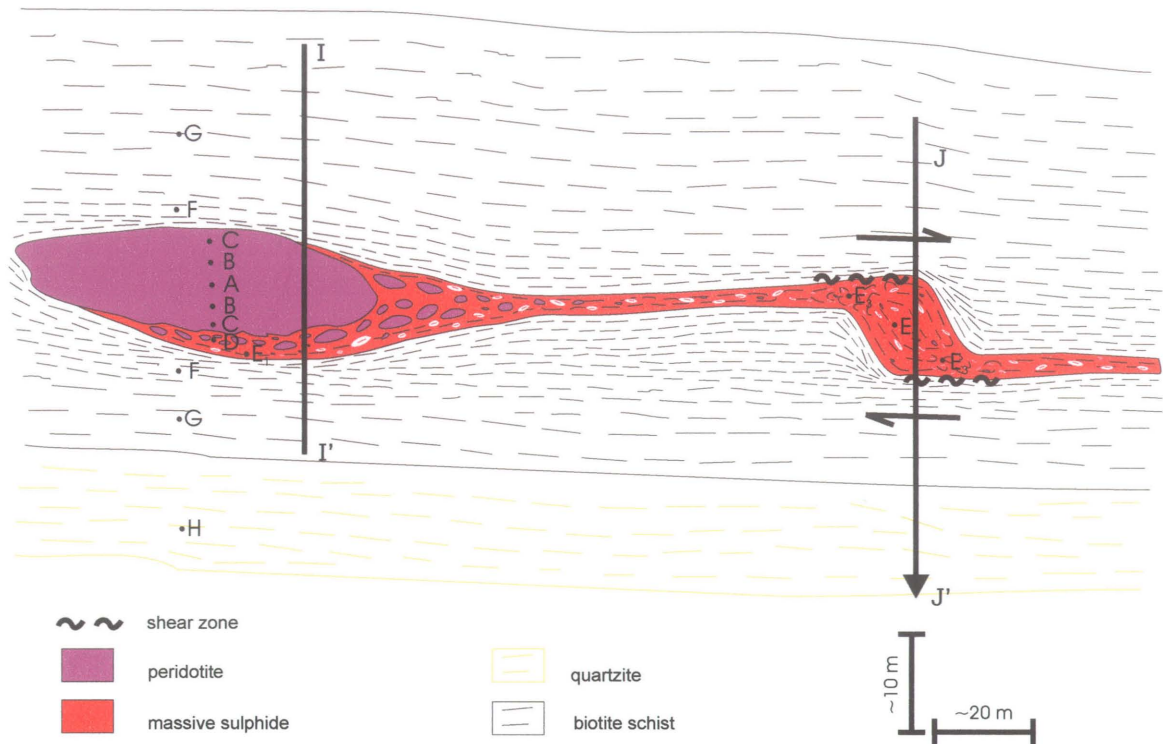


Figure 5.16. Schematic diagram of an ore zone in the 1C ore body, Thompson Mine. Letters A to H refer to relative locations of representative sulphide textures in the mine. Photomicrographs of these textures are shown in Figure 5.17; descriptions of the textures are summarized in Table 5.1. Section I-I' and J-J' are traverses along which sulphide-bearing samples were collected for electron microprobe analyses (Figures 6.6 and 6.7).

Table 5.1. Mesoscopic textures and relative locations of representative sulphide samples from the 1C ore body, Thompson Mine.

Symbol in Figure 1	Sulphide Texture (po, pn, cp combined)	Relative Location in Ore Zone	Mesoscopic Textures	
			Pentlandite Grains	Typical Inclusion Population
A, B	disseminated (tr-7%)	hosted in ultramafic body	not observed	na
C	interstitial (7-25%)	typically toward edges of ultramafic body	not observed	na
D	sulphide breccia (25-70%)	adjacent to ultramafic body	up to 30%; equant to ovoid eyes up to 1cm size	serpentinized ultramafic clasts: up to 50%; cm- to dm-scale; angular to rounded; often contain stringer sulphides mafic mica grains: up to 20% biotite, phlogopite, and/or chlorite; rounded laths up to 5 mm long; oriented parallel with contact to metasediments quartz and feldspar grains: up to 5%; up to 5mm size; rounded to ovoid; sometimes partially rimmed by rounded garnet grains or mafic mica grains
E ₁	semi-massive (50-70%) to massive (70-100%)	proximal to (< ~60m from) ultramafic body	up to 20%; equant to ovoid eyes up to 1cm size	rafts of adjacent metasedimentary host: up to 30%; cm- to dm-scale, rounded to ovoid; irregular boundaries; sometimes contain stringer sulphides mafic mica grains: up to 20% biotite, phlogopite, and/or chlorite; rounded laths up to 1 cm long, oriented parallel to contact with metasediments quartz and feldspar grains: up to 10%; up to 5mm size; rounded
E ₂	semi-massive (50-70%) to massive (70-100%)	distal to (> ~ 60m from), and along strike of, ultramafic body	up to 20%; equant to ovoid eyes up to 1cm size; also chain-like mm-scale aggregates producing mottled texture w/ pyrrhotite	rafts of adjacent metasedimentary host: up to 30%; cm- to dm-scale, rounded to ovoid; irregular boundaries; sometimes contain stringer sulphides mafic mica grains: up to 20% biotite, phlogopite, and/or chlorite; rounded laths up to 1 cm long, oriented subparallel to contact with metasediments quartz and feldspar grains: up to 10%; up to 5mm size; rounded
E ₃	massive (70-100%)	distal to (> ~ 60m from), and along strike of, ultramafic body	up to 35%; equant eyes up to 1mm size	mafic mica grains: up to 20% biotite, phlogopite, and/or chlorite; rounded laths up to 3mm long; randomly oriented quartz and feldspar grains: up to 10%, up to 3mm size; rounded
F	disseminated to stringer (5-15%)	a) proximal to (< ~20m from) ultramafic body b) proximal to (< ~ 20m from) massive sulphides	not observed	na
G,H	disseminated (tr-7%)	distal to (> ~20m from) ultramafic body and massive sulphides	na	na

Evidence for shearing of the massive sulphide horizon can be seen throughout the 1C stratigraphic section. At the base of the ultramafic body, pentlandite porphyroblasts are flattened and embayed; pyrite aggregates are segregated into mm-scale bands oriented parallel to the foliation of the hosting metasediments (Figure 5.17, E₁). Shearing is also indicated in the well-foliated nature of the mineralized schists adjacent to the massive sulphides (Figure 5.17, F). Further away from the massive sulphide horizon, non-mineralized metasediments have a lesser degree of foliation (Figure 5.17, G and H).

5.4 Textural Variations Along Strike of a Deformed Ore Zone

The textures of the massive sulphides in the Thompson 1C type section preserve several episodes of sulphide deformation and metamorphism (Figure 5.17; E₁, E₂, and E₃). The degree of deformation of the massive sulphides is best preserved in the pentlandite grains. The elongated and corroded pentlandite porphyroblasts in location E₁, Figure 5.17, are interpreted to be the result of pentlandite exsolution from a cooling *mss*, followed by flattening of the porphyroblasts. The ovoid porphyroblasts are oriented parallel to the foliation of the hosting metasediments (Figure 5.17, E₁), suggesting that a shearing and/or compressional event may have occurred. The embayed nature of the porphyroblasts suggests that the sulphides had not fully equilibrated after deformation.

The equant and chain-textured pentlandite grains in location E₂, Figure 5.17, are interpreted to have exsolved from *mss* after the sulphides were mobilized away from the ultramafic sill. Porphyroblastic growth of the pentlandite after mobilization is inferred by the presence of coarse-grained sulphide minerals enclosing foliated porphyroblastic mica inclusions (<1mm to 1 cm)(Figure 5.17, E₂).

The sulphides in the massive ore at location E₃, Figure 5.17, are interpreted to have been milled or have undergone cataclasis. Evidence for cataclasis is suggested by the fine-grained texture of both the sulphides and silicate inclusions; the undulating boundaries of the sulphides; and the lack of orientation of the mica inclusions (Figure 5.17, E₃). The sulphide sample at location E₃ contains secondary pyrite grains that mimic the texture of pentlandite grains, and in places look like overgrowths on pentlandite grains. The occurrence of these pyrite “overgrowths” is common within massive sulphides from the Thompson Mine. The cataclastic texture of the pyrite indicates that the pyrite formed prior to the brittle deformation of the sulphides. The equant, equigranular texture of the all the sulphide minerals at location E₃ suggests that the deformed sulphides were subsequently recrystallized.

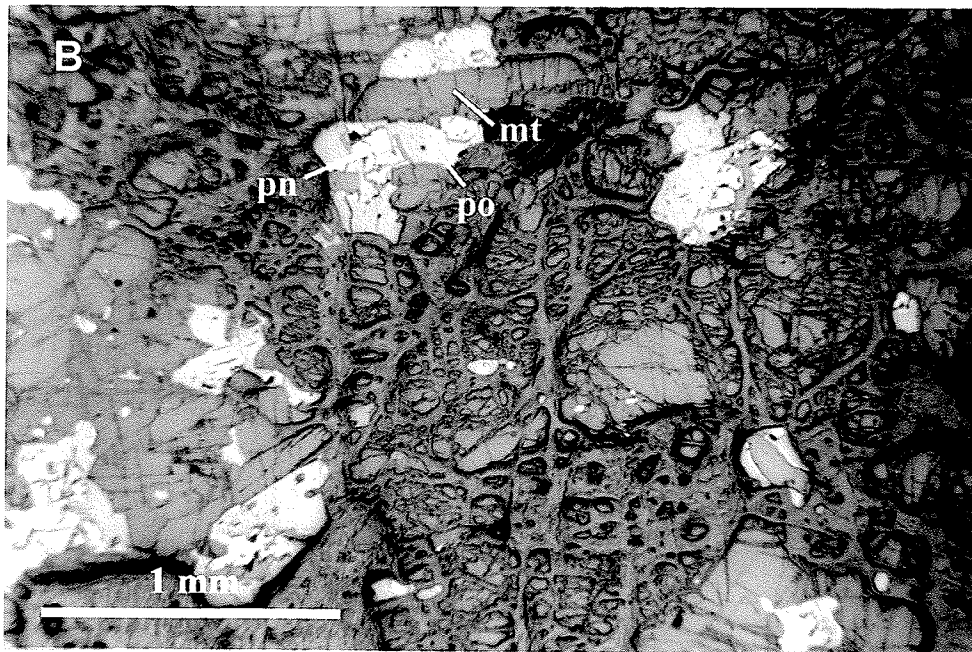
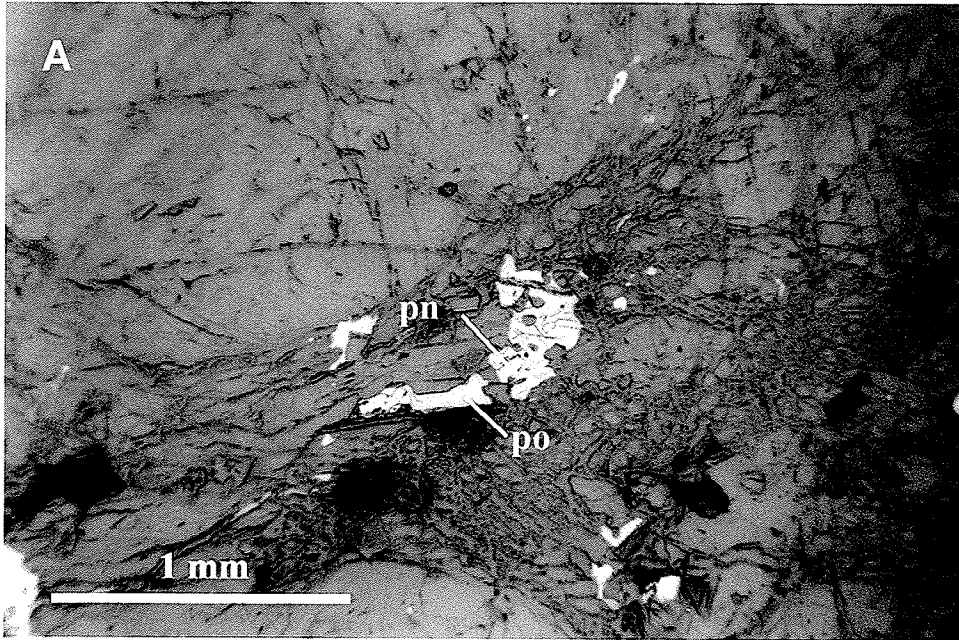


Figure 5.17. Reflected light photomicrographs of typical sulphide-bearing samples from a nickel ore zone in the 1C ore body, Thompson Mine. Letter symbols in the left-hand corner of all photomicrographs correspond to sample locations in Figure 5.16. Summary descriptions of the sulphide types are shown in Table 5.1. Abbreviations: po=pyrrhotite, pn=pentlandite, py=pyrite, mt=magnetite. Darkest phases in photomicrographs are silicates. (A) Disseminated sulphides in interior of ultramafic sill. Major silicate phase is pyroxene. Fibrous silicate phase is serpentine. (B) Disseminated sulphides toward exterior of ultramafic sill, where serpentinization is more pervasive.

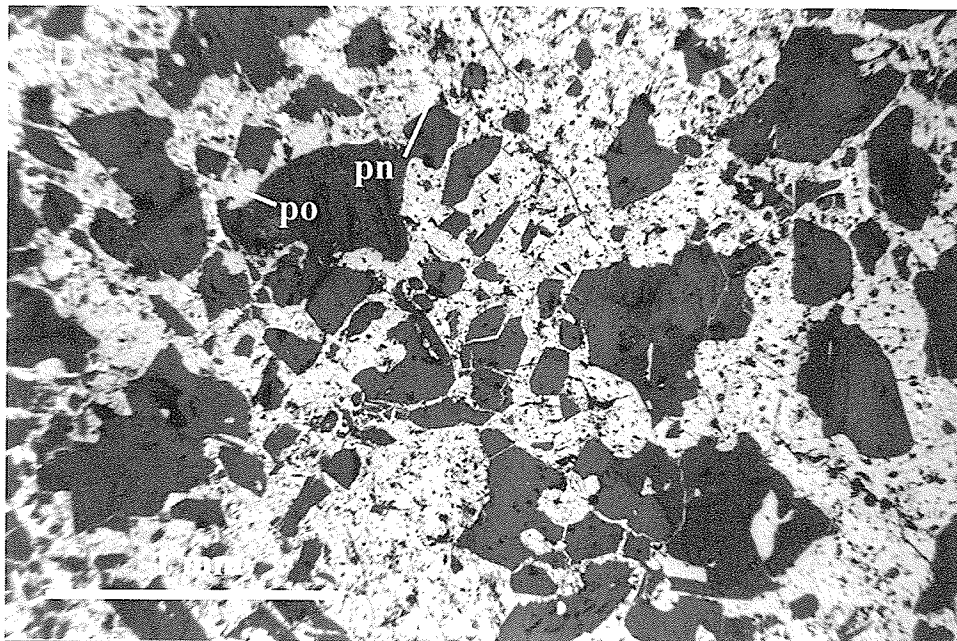
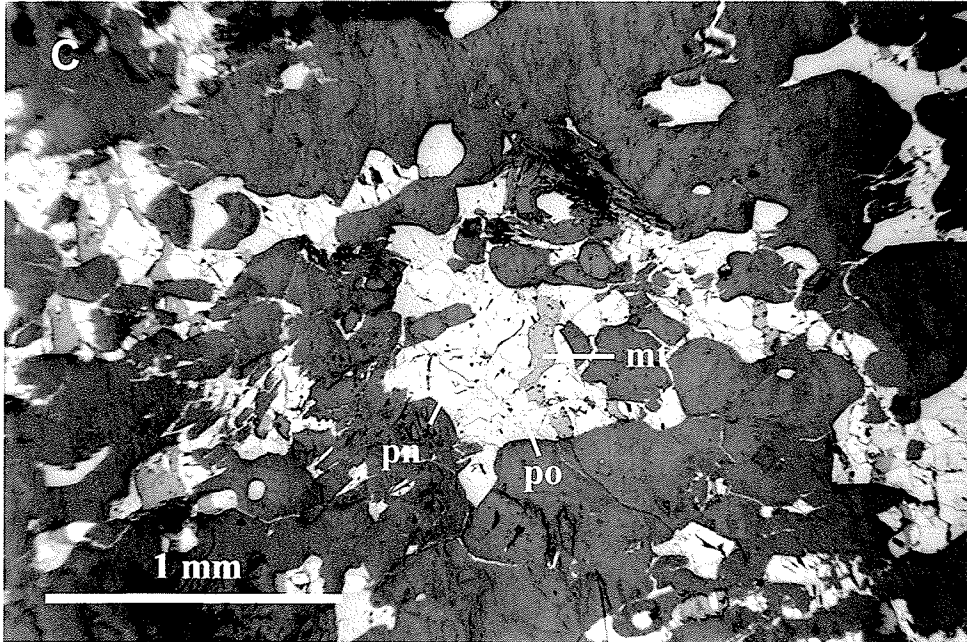


Figure 5.17 (continued). (C) Interstitial sulphides towards exterior of ultramafic sill, where serpentinization prevails. (D) Massive sulphides with subangular inclusions of altered ultramafic sill.

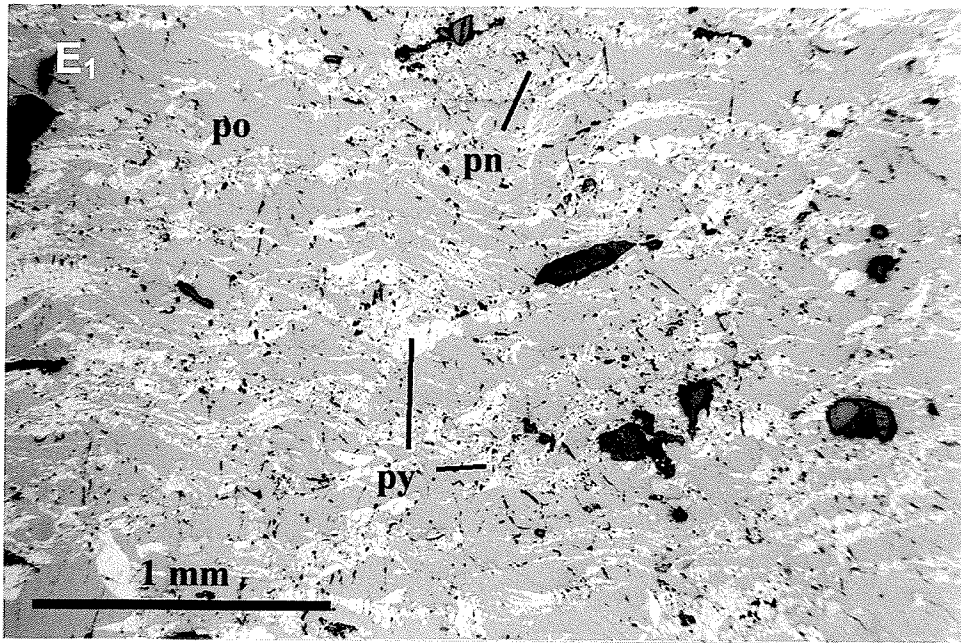
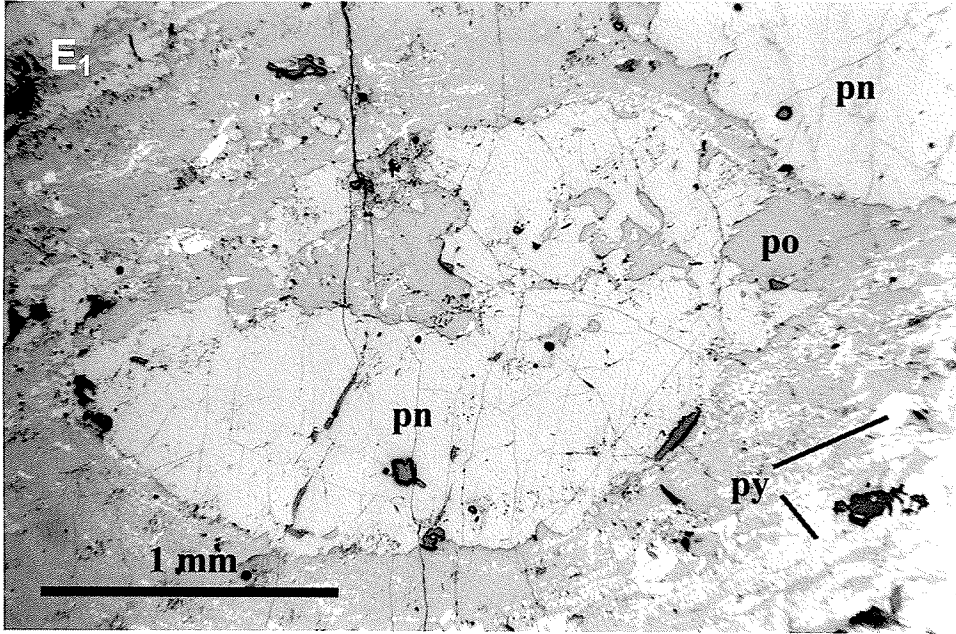


Figure 5.17 (continued). (E₁) Sulphides from the massive sulphide horizon, proximal to ultramafic sill. Ovoid and embayed pentlandite porphyroblasts are associated with pyrrhotite and foliated pyrite.

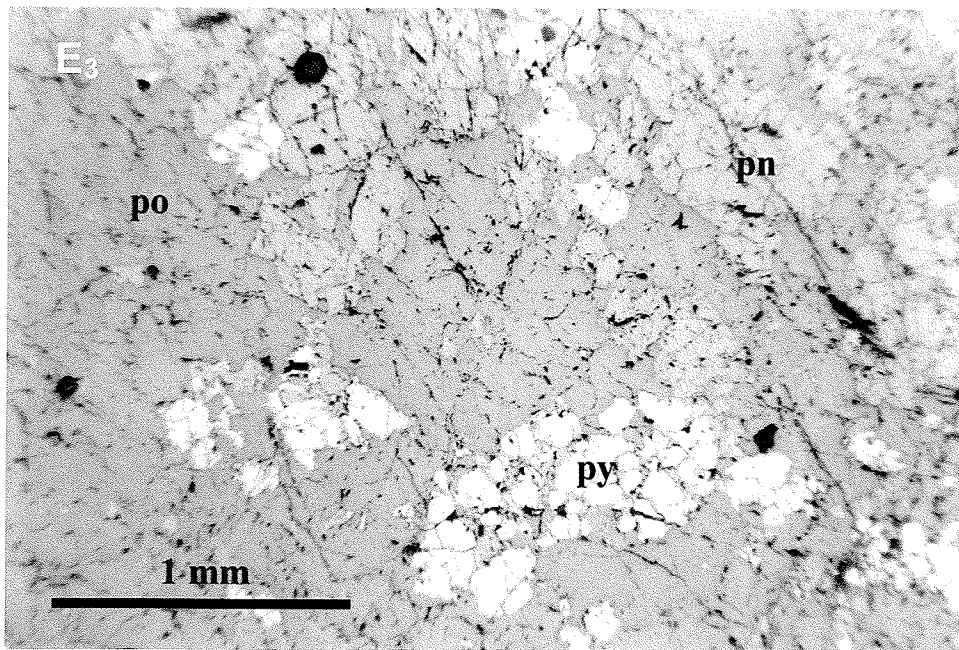
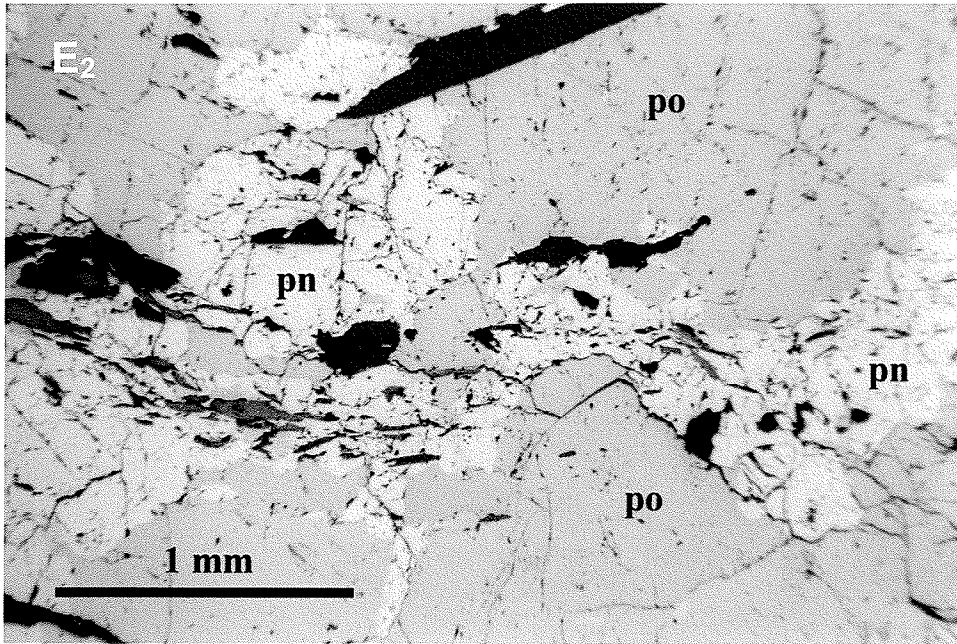


Figure 5.17 (continued). (E₂) Sulphides from the massive sulphide horizon, located ~100m along strike from ultramafic sill. Equant pentlandite porphyroblasts and chain-textured pentlandite are associated with equant pyrrhotite grains. Dark grains are foliated mica inclusions (E₃) Milled sulphides within the massive sulphide horizon, distal to ultramafic sill.

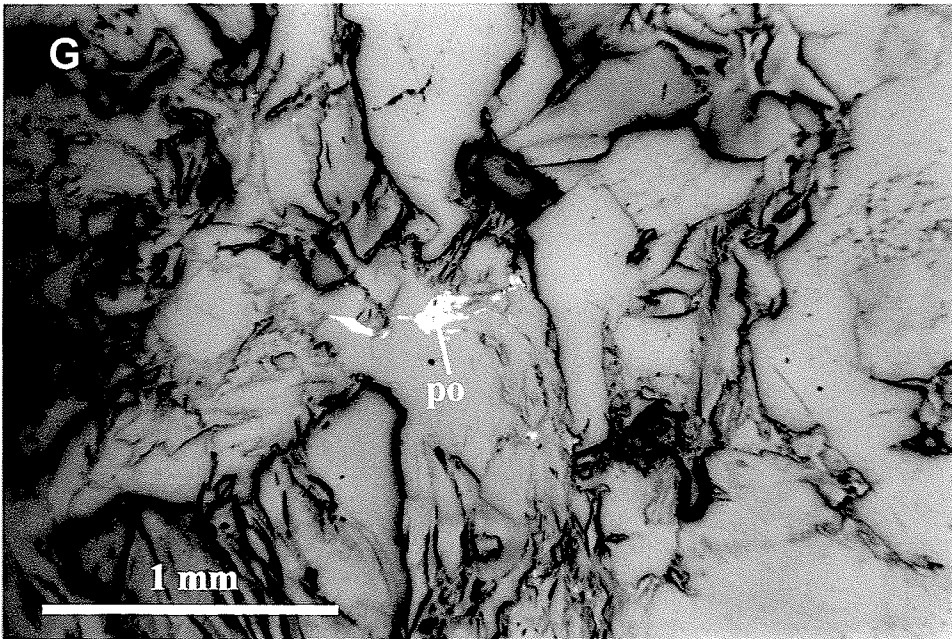
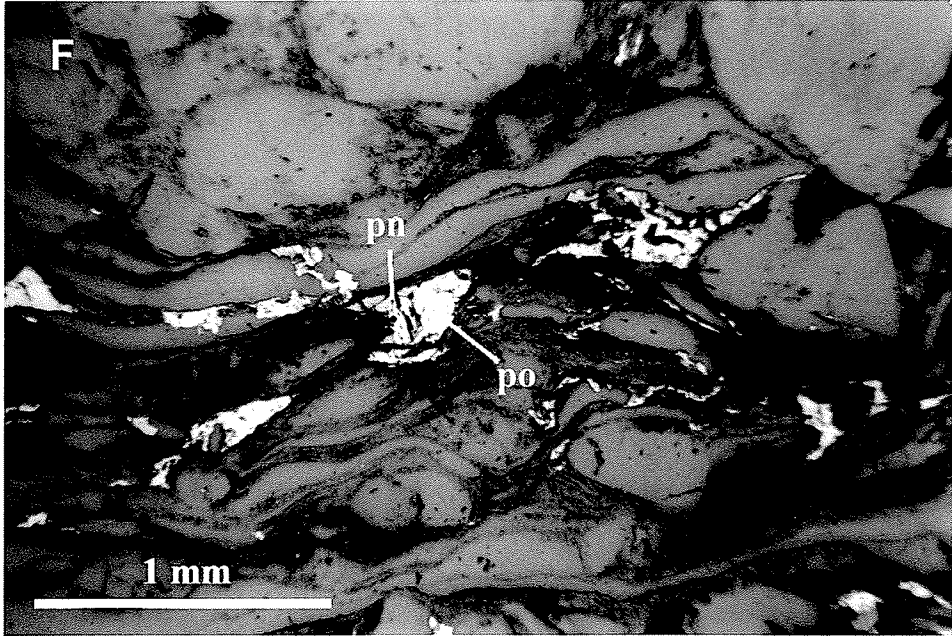


Figure 5.17 (continued). (F) Nickeliferous sulphides hosted in well-foliated sillimanite-biotite schist, proximal to massive ore. (G) Disseminated nickel-enriched pyrrhotite (>0.2 wt% Ni) in weakly foliated biotite schist, more distal to (>~20m away from) massive ore.

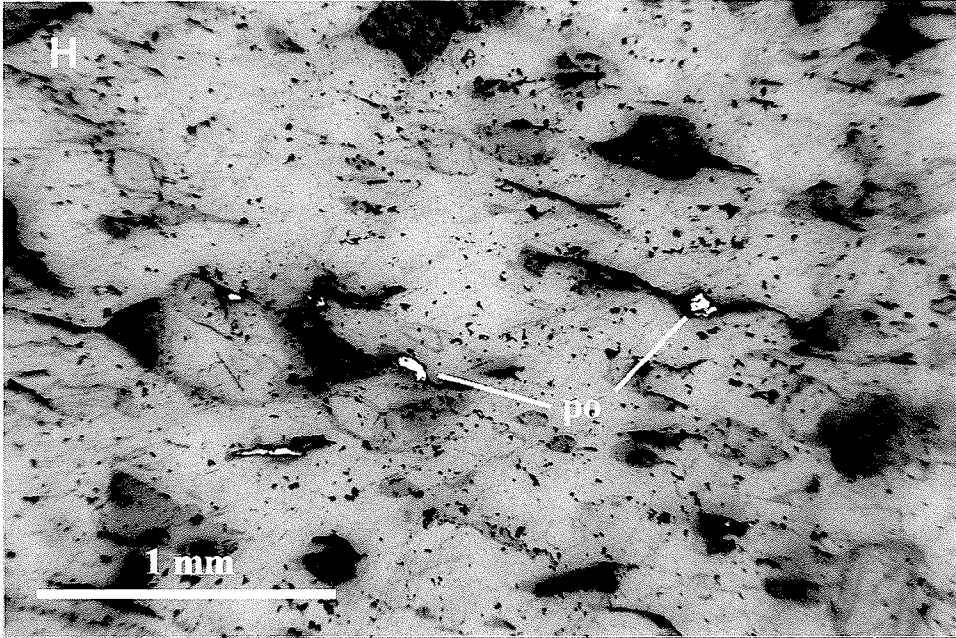


Figure 5.17 (continued). (H) Disseminated nickel-barren pyrrhotite ($<0.2\text{ wt\% Ni}$) in foliated quartzite.

CHAPTER 6: SULPHIDE MINERAL CHEMISTRY

6.1 Chemistry of Pyrrhotite

Minerals of the pyrrhotite group are considered by Kissin and Scott (1982) to be all iron monosulphides of the general formula $\text{Fe}_{(1-x)}\text{S}$ ($0 < x < 0.125$) that possess the NiAs (B8) substructure (Carpenter and Desborough, 1964), however, the term “pyrrhotite” is generally given to all members of the pyrrhotite group excluding troilite (FeS). Both pyrrhotite and troilite have structures in which the metals occur in octahedral coordination and anions in trigonal prismatic coordination. Layers of metals and anions occur parallel to the basal plane; the metal atoms can be omitted to leave vacancies in the structure. The pyrrhotite structure can allow for one-eighth of its Fe atoms to be omitted, giving rise to an omission solid solution. Solid solution is complete at higher temperatures ($\geq 350^\circ\text{C}$), where the vacancies are randomly distributed in the structure. At lower temperature, the vacancies are ordered, resulting in the development of superstructures based on the NiAs structure.

The best known of these superstructures is that of monoclinic pyrrhotite. Monoclinic pyrrhotite exhibits a monoclinic symmetry, whereas hexagonal pyrrhotite exhibits a hexagonal symmetry. In the field, monoclinic pyrrhotite is difficult to distinguish from hexagonal pyrrhotite, except that monoclinic pyrrhotite is magnetic and the hexagonal variety is not. Petrographically, monoclinic pyrrhotite can be distinguished from hexagonal pyrrhotite after a thin section has been etched with an acid solution (Naldrett and Kullerud, 1967, p. 497). However, it is not an advantage to etch and stain samples that will ultimately be probed by EMPA and PIXE, as etching would result in

alteration of the sample surface. In this thesis, the distinction between monoclinic and hexagonal pyrrhotite is based on the atomic metal:sulphur ratio (M/S) of pyrrhotite grains that were analyzed by electron microprobe.

The technique of using atomic M/S ratios to distinguish the pyrrhotite types was used by Czernanske *et al.* (1992) in their study of magmatic sulphide ores from the Noril'sk-Talnakh district, Russia. In their study, M/S ratios were calculated from electron microprobe data, where monoclinic pyrrhotite M/S = 0.858-0.883, hexagonal pyrrhotite M/S = 0.909-0.923, and troilite M/S = 0.980-1.003. In this thesis, the work of Kissin (1974), and Arnold (1971) are taken into account with Czernanske's data, to include broader ranges of M/S values for monoclinic and hexagonal pyrrhotite. The distinction between the pyrrhotite types for this thesis is as follows:

Monoclinic pyrrhotite: M/S = 0.858 – 0.898

Hexagonal pyrrhotite: M/S = 0.899 – 0.996

Troilite: M/S = 0.997 – 1.000

Kissin and Scott (1982) summarized the phase relations involving pyrrhotite below 350°C (Figure 6.1). These authors concluded that monoclinic pyrrhotite can form by several ways in the pure Fe-S system: 1) continuous re-equilibration of pyrite and pyrrhotite as they cool from high temperature; 2) direct deposition in the stability field of monoclinic pyrrhotite; 3) incomplete quenching of hexagonal pyrrhotite that is oversaturated with respect to pyrite, resulting in the metastable formation of monoclinic pyrrhotite. The third explanation, observed in experimental work by Kissin and Scott (1982) is unlikely in nature, as cooling would have to occur in a matter of hours. In the

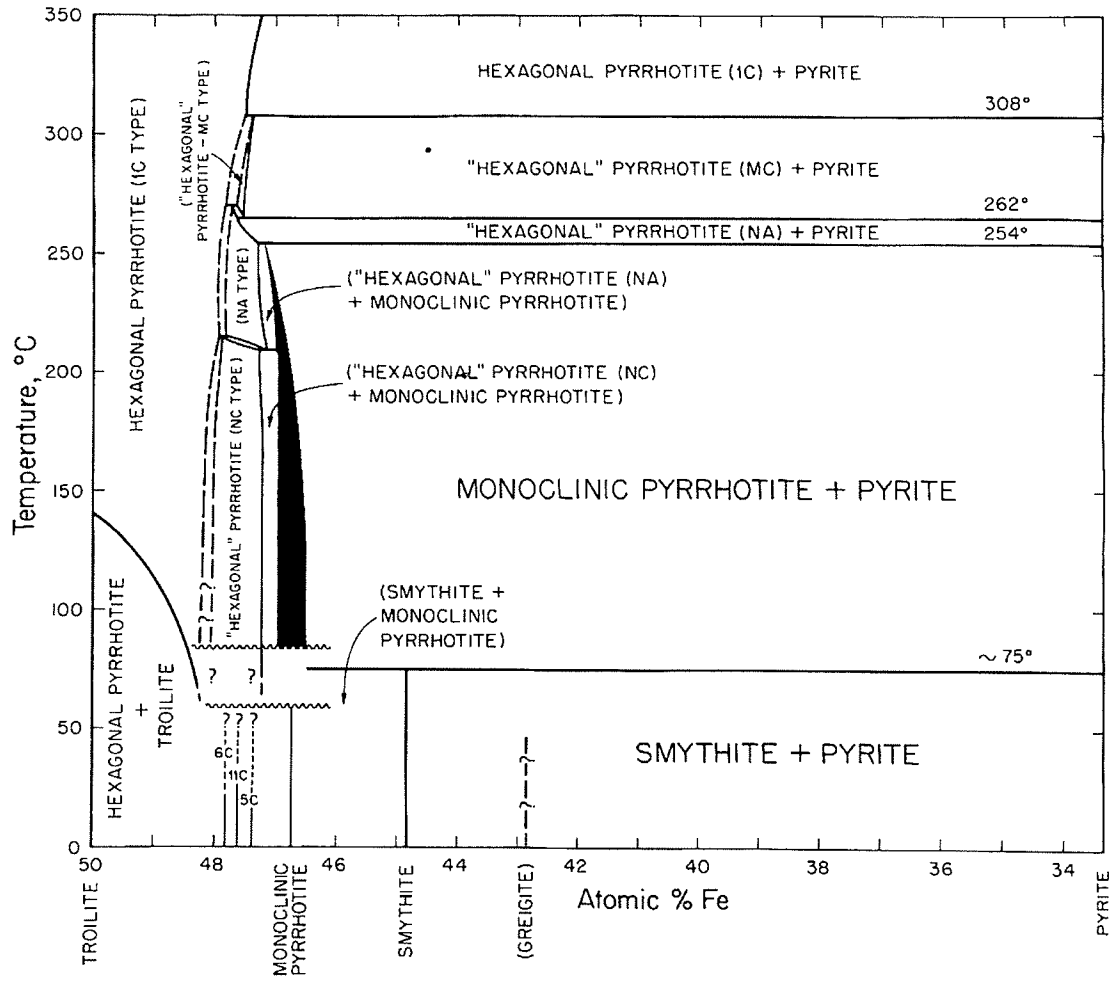


Figure 6.1. Phase relations involving pyrrhotite below 350°C (from Kissin and Scott, 1982).

natural environment, the Fe-S system may be open to oxygen, as well as to sulphur.

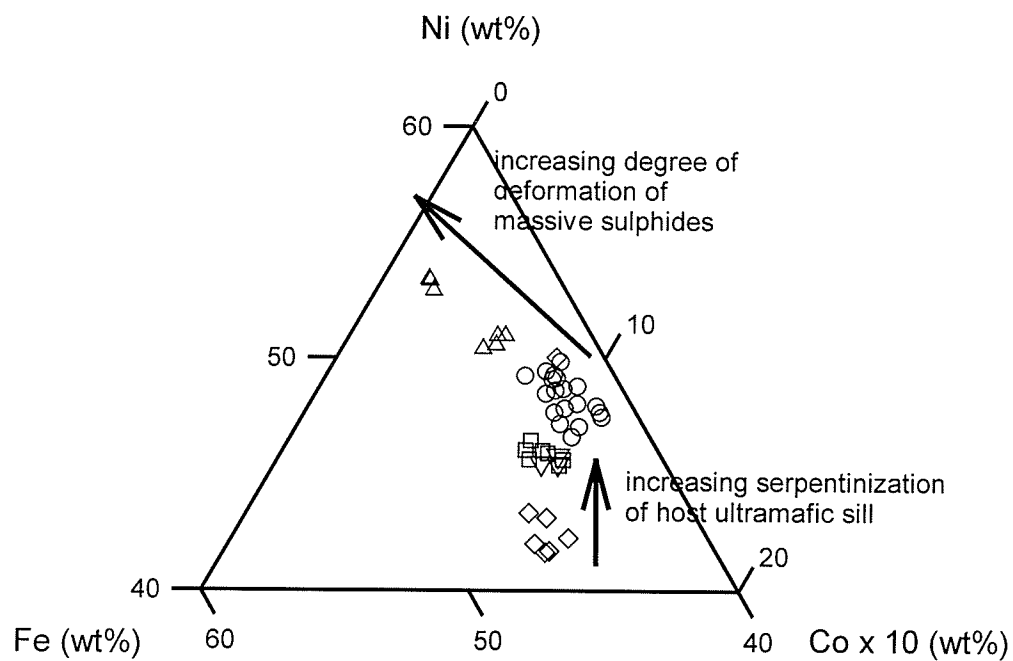
Sulphurization could convert a hexagonal pyrrhotite to monoclinic pyrrhotite; however, this process may be difficult to distinguish from the process of oxidation (Kissin and Scott, 1982).

Nickel can occur in significant concentrations within hexagonal and monoclinic pyrrhotite. Batt (1972) showed a correlation between the Ni content of pyrrhotite and its structural form and magnetic susceptibility; electron microprobe analyses of a representative pyrrhotite sample from the Sudbury area showed that magnetic monoclinic pyrrhotite contained 0.4-0.5% Ni and the hexagonal paramagnetic phase contained 0.8-0.9% Ni. Similarly, Vaughan *et al.* (1971) showed that hexagonal pyrrhotite grains from a massive sulphide ore body in the Strathcona Mine, Sudbury, had about twice the amount of Ni as monoclinic pyrrhotite (where the range of Ni concentrations in both pyrrhotite types was 0.3-1.0%). The consistently higher Ni concentrations in hexagonal pyrrhotite were attributed to Ni having higher site preference for the hexagonal pyrrhotite coordination site. In this same study, however, the highest Ni concentrations occurred in the center of the ore body, where largely monoclinic pyrrhotite and only trace hexagonal pyrrhotite was observed. This could indicate that, during the formation of massive sulphide accumulations, conditions are more favorable for the formation of monoclinic pyrrhotite over hexagonal pyrrhotite.

6.2 Chemistry of Variably Deformed Sulphide Minerals

The major element chemistry of the sulphide minerals within a massive sulphide horizon from the Thompson 1C ore body was investigated. The sulphides in the massive ore horizon shown in Figure 5.16 record progressively higher degrees of deformation from locations E₁ to E₃. Figure 6.2 shows the relative distribution of the major cations (Fe, Ni, and Co) in pentlandite grains from locations E₁, E₂, and E₃ in the ore horizon. With increasing degree of deformation of the massive sulphides, there is an increase in Ni concentration in pentlandite grains, accompanied by a decrease in Co concentration (Figure 6.2). Table 6.1 shows that the milled pentlandite grains at location E₃ (Figure 5.16) have Ni/Co ratios that are an order of magnitude higher than non-milled pentlandite grains located proximal to the ultramafic sill (location E₁, Figure 5.16). Conversely, the Ni/Co ratios of milled pyrite grains at location E₃ are an order of magnitude lower than the ratios of foliated pyrite aggregates at location E₁. These data suggest that, prior to the recrystallization of the milled sulphides at location E₃, Ni was upgraded in the pentlandite grains and Co was expelled. Some of the Co that is released from pentlandite can be taken up by coexisting pyrite, as Co commonly substitutes stoichiometrically in the pyrite lattice (Huston *et al.*, 1995). The data demonstrate that increasing Ni/Co ratios in pentlandite grains from a massive sulphide horizon could reflect increasing degrees of sulphide remobilization and/or recrystallization.

Figure 6.3 shows the relative distribution of Fe, Ni, and S in pentlandite grains from the Thompson 1C ore body. Pentlandite grains show an increase in Ni concentration with increasing serpentinization of the ultramafic host rock, and with increasing degree of deformation of the massive sulphide ore. Figure 6.4 shows a similar increase in Ni

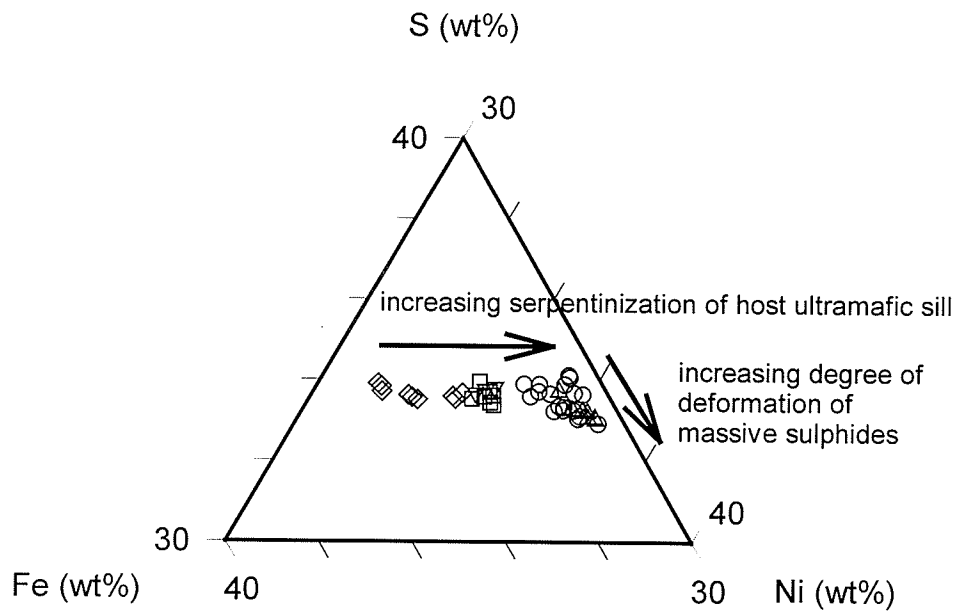


- ◇ location A: disseminated grains in ultramafic sill
- ▽ location C: interstitial grains in ultramafic sill
- location E₁: ovoid porphyroblasts, proximal to ultramafic sill
- location E₂: equant porphyroblasts, distal to ultramafic sill
- △ location E₃: milled porphyroblasts, distal to ultramafic sill

Figure 6.2. Relative concentrations of Fe, Ni, and Co in pentlandite grains from a range of sulphide types from the Thompson IC ore body. Locations A to E refer to the sample locations shown in Figure 5.16. All sulphide types are described in detail in Table 5.1.

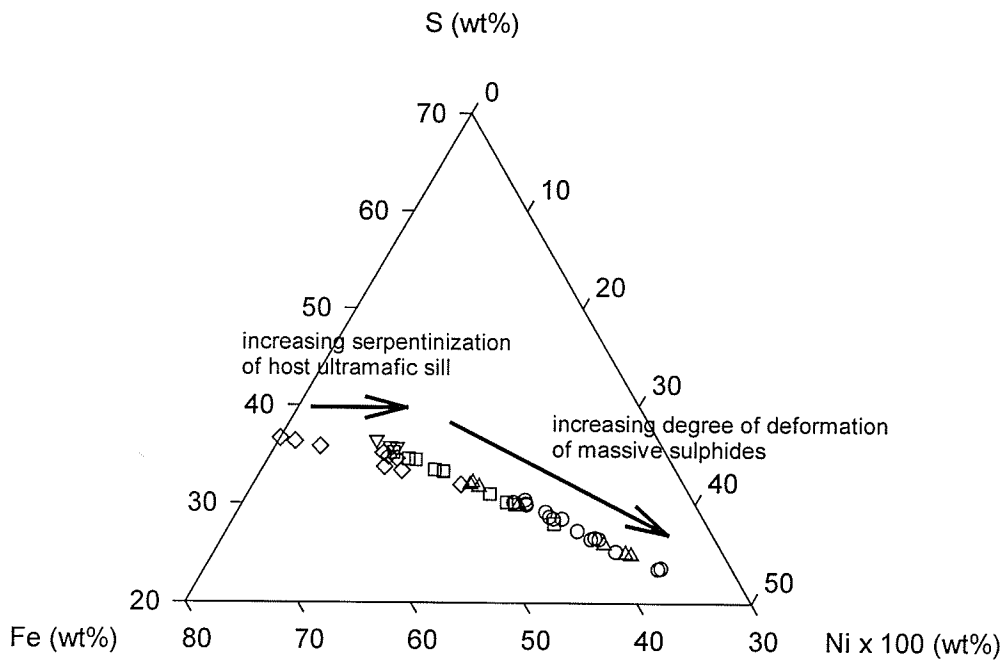
Table 6.1. EMPA data of sulphide minerals (pn = pentlandite, po = pyrrhotite, py = pyrite) in samples from the Thompson 1C ore body. Relative location of samples shown in Figure 5.16.

Location in Figure 5.16	Sample Name	Mineral	S (wt%)	Fe (wt%)	Co (wt%)	Ni (wt%)	Ni/Co	
E1	DM98-1C-07	pn	33.19	31.24	0.41	35.09	85.31	
	DM98-1C-07	pn	33.28	31.30	0.47	34.86	74.68	
	DM98-1C-07	pn	33.00	30.73	0.39	35.73	90.57	
	average		33.16	31.09	0.42	35.23	83.52	
	DM98-1C-07	po	39.29	60.36	0.04	0.27	6.71	
	DM98-1C-07	po	39.30	60.22	0.03	0.32	12.69	
	DM98-1C-07	po	39.05	60.49	0.05	0.40	7.81	
	average		39.21	60.36	0.04	0.33	9.07	
	DM98-1C-07	py	53.13	45.84	0.64	0.35	0.56	
	DM98-1C-07	py	52.82	45.46	0.77	0.86	1.11	
	DM98-1C-07	py	52.80	44.78	1.90	0.42	0.22	
	average		52.92	45.36	1.10	0.54	0.63	
	E3	JL98-1C-20	pn	33.06	30.57	0.14	36.02	251.36
		JL98-1C-20	pn	32.92	30.51	0.12	36.35	314.35
		JL98-1C-20	pn	32.94	30.49	0.12	36.27	301.83
average			32.98	30.52	0.13	36.21	289.18	
JL98-1C-20		po	39.51	60.08	0.06	0.25	4.18	
JL98-1C-20		po	39.40	60.30	0.06	0.24	3.69	
JL98-1C-20		po	39.52	60.08	0.02	0.32	14.89	
average			39.48	60.15	0.05	0.27	7.59	
JL98-1C-20		py	53.00	45.88	0.93	0.05	0.06	
JL98-1C-20		py	52.90	45.49	1.48	0.03	0.02	
JL98-1C-20		py	52.87	45.55	1.48	0.05	0.03	
average			52.92	45.64	1.29	0.04	0.04	



- ◇ location A: disseminated grains in ultramafic sill
- ▽ location C: interstitial grains in ultramafic sill
- location E₁: ovoid porphyroblasts, proximal to ultramafic sill
- location E₂: equant porphyroblasts, distal to ultramafic sill
- △ location E₃: milled porphyroblasts, distal to ultramafic sill

Figure 6.3. Relative concentrations of Fe, Ni, and S in pentlandite grains from a range of sulphide types from the Thompson 1C ore body. Locations A to E refer to the sample locations shown in Figure 5.16. All sulphide types are described in detail in Table 5.1.



- ◇ location A: disseminated grains in ultramafic sill
- ▽ location C: interstitial grains in ultramafic sill
- location E₁: ovoid porphyroblasts, proximal to ultramafic sill
- location E₂: equant porphyroblasts, distal to ultramafic sill
- △ location E₃: milled porphyroblasts, distal to ultramafic sill

Figure 6.4. Relative concentrations of Fe, Ni, and S in pyrrhotite grains from a range of sulphide types from the Thompson 1C ore body. Locations A to E refer to the sample locations shown in Figure 5.16. Pyrrhotite grains from location A are hexagonal; all other grains are monoclinic. All sulphide types are described in detail in Table 5.1.

concentration in pyrrhotite grains co-existing with the pentlandite grains. Notably, pyrrhotite grains from the interstitial and massive sulphides of the IC ore zone were all monoclinic, while pyrrhotite grains that were disseminated in the ultramafic sill were hexagonal.

There may be a change in the structure of pyrrhotite upon the formation of massive sulphides, i.e. from hexagonal pyrrhotite in the ultramafic host to monoclinic pyrrhotite in interstitial and massive accumulations. This change from hexagonal to monoclinic pyrrhotite may be the result of metamorphic and/or metasomatic processes accompanying massive sulphide formation. According to Kissin and Scott (1982), sulphurization or oxidation could convert hexagonal pyrrhotite to monoclinic pyrrhotite. In the Thompson IC type section, pyrite occurs proximal to the ultramafic sill as aggregates that are oriented parallel to stress-induced foliation (Figure 5.17, E₁). The pyrite could have formed during an increase in sulphur fugacity or oxidation of pyrrhotite. The lack of magnetite occurring with the sulphides suggests that oxidation was not a dominant process, and that sulphurization of pyrrhotite most likely produced the pyrite. The oriented nature of the pyrite could indicate that S was mobilized into the ores by fluids travelling through stress-induced weaknesses in the deposits. The embayed nature of the sheared pentlandite grains in Figure 5.17, E₁, as well as the pyrite-poor halo around the pentlandite grains (Figure 5.17, E₁), may indicate that both Ni and S were mobilized from the massive ore proximal to the ultramafic sill. These observations support the suggestion that fluid-assisted mobilization of metals may have occurred in the massive sulphide deposits (Marshall *et al.*, 2000).

6.3 Diffusion of Nickel

During re-equilibration of massive sulphides that are cooling from high temperatures, diffusion of Ni can occur on a microscopic scale. McQueen (1987) concluded that rapid diffusion rates facilitate sulphide deformation during metamorphism above 500°C. During post-peak retrogression, solid-state diffusion of metals can occur as sulphides re-equilibrate. Electron microprobe analyses across an equant pentlandite porphyroblast from a metasediment-hosted massive sulphide horizon in Thompson show that pyrrhotite that is most proximal to the pentlandite porphyroblast is enriched in Ni (Figure 6.5). Nickel concentrations in pyrrhotite can vary by 0.3 wt% within 50 µm of the pentlandite porphyroblast. This local Ni enrichment in pyrrhotite suggests that solid-state diffusion of Ni has occurred during cooling and re-equilibration of the sulphides.

Ni concentrations in pentlandite and pyrrhotite grains from an ultramafic sill increase from the interior to the exterior of the body; this increase coincides with an increasing degree of serpentinization in the sill (Figures 6.2, 6.3, and 6.4). The introduction of metasomatic fluids to the exterior of the ultramafic sill likely caused the serpentinization. The serpentinization could have facilitated the release of Ni from the mafic silicate phase and the subsequent incorporation of Ni into the disseminated sulphides within the ultramafic sill (c.f. Donaldson, M.J., 1981; Barrett *et al.*, 1977).

Figure 6.6 shows the concentration of Ni in pyrrhotite grains from section I-I', Figure 5.16. The sections shows a depletion of Ni in disseminated ultramafic-hosted pyrrhotite grains relative to pyrrhotite grains in the adjacent massive sulphide horizon. Figure 6.6 shows a similar trend in pentlandite grains co-existing with the pyrrhotite. The

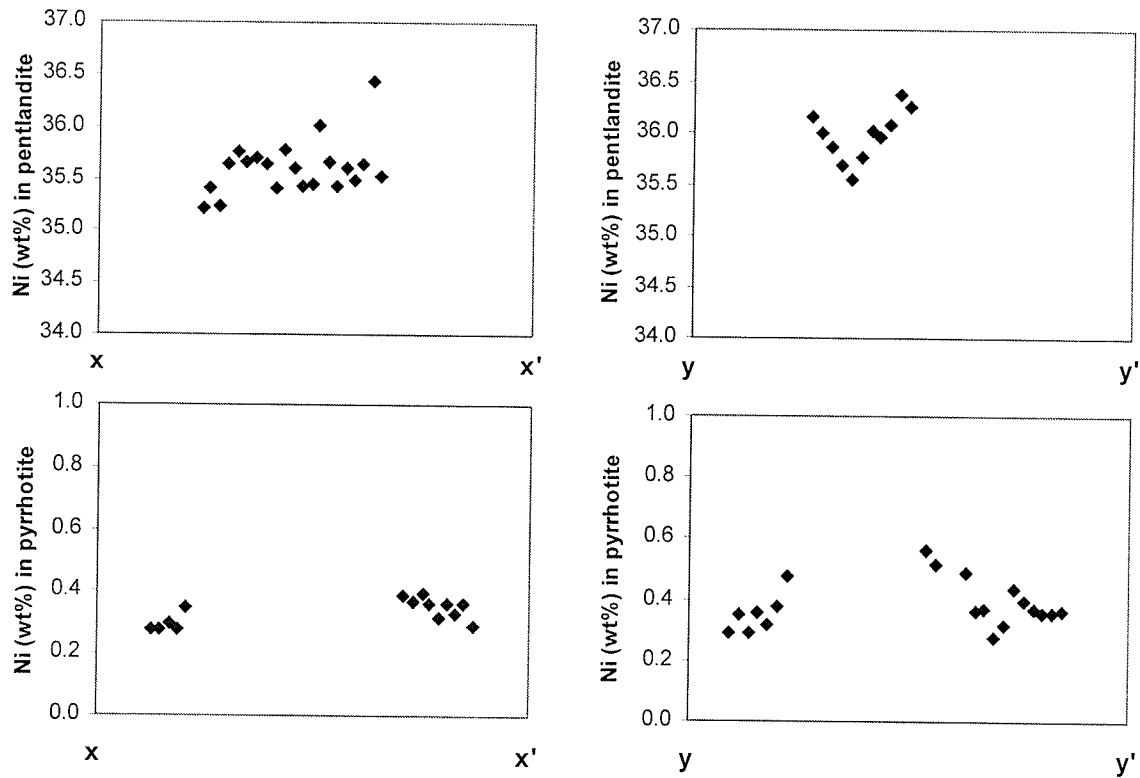
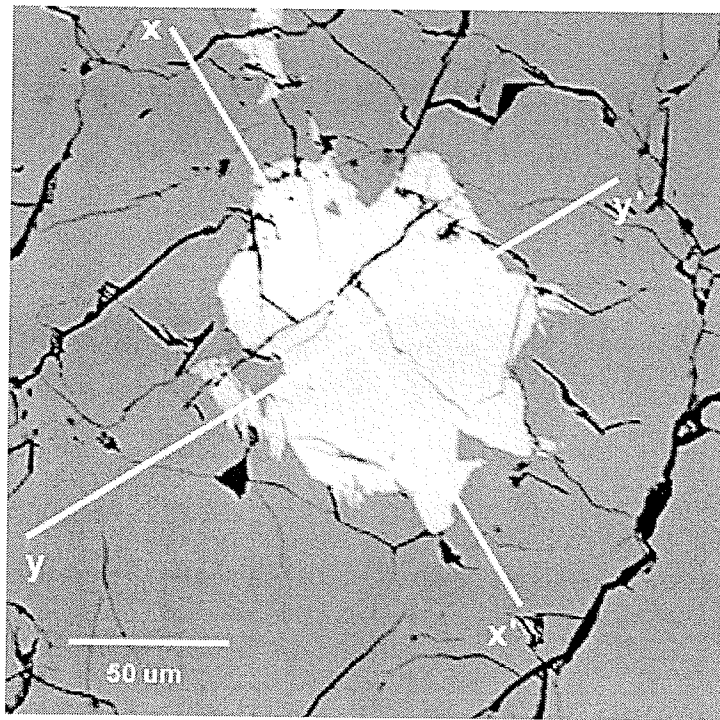


Figure 6.5. Electron microprobe point analyses across an equant porphyroblastic pentlandite grain and adjacent pyrrhotite grains in two dimensions. There is Ni enrichment within pyrrhotite grains adjacent to the pentlandite porphyroblast. Sample is from a massive sulphide horizon hosted by metasediments from the Thompson Mine.

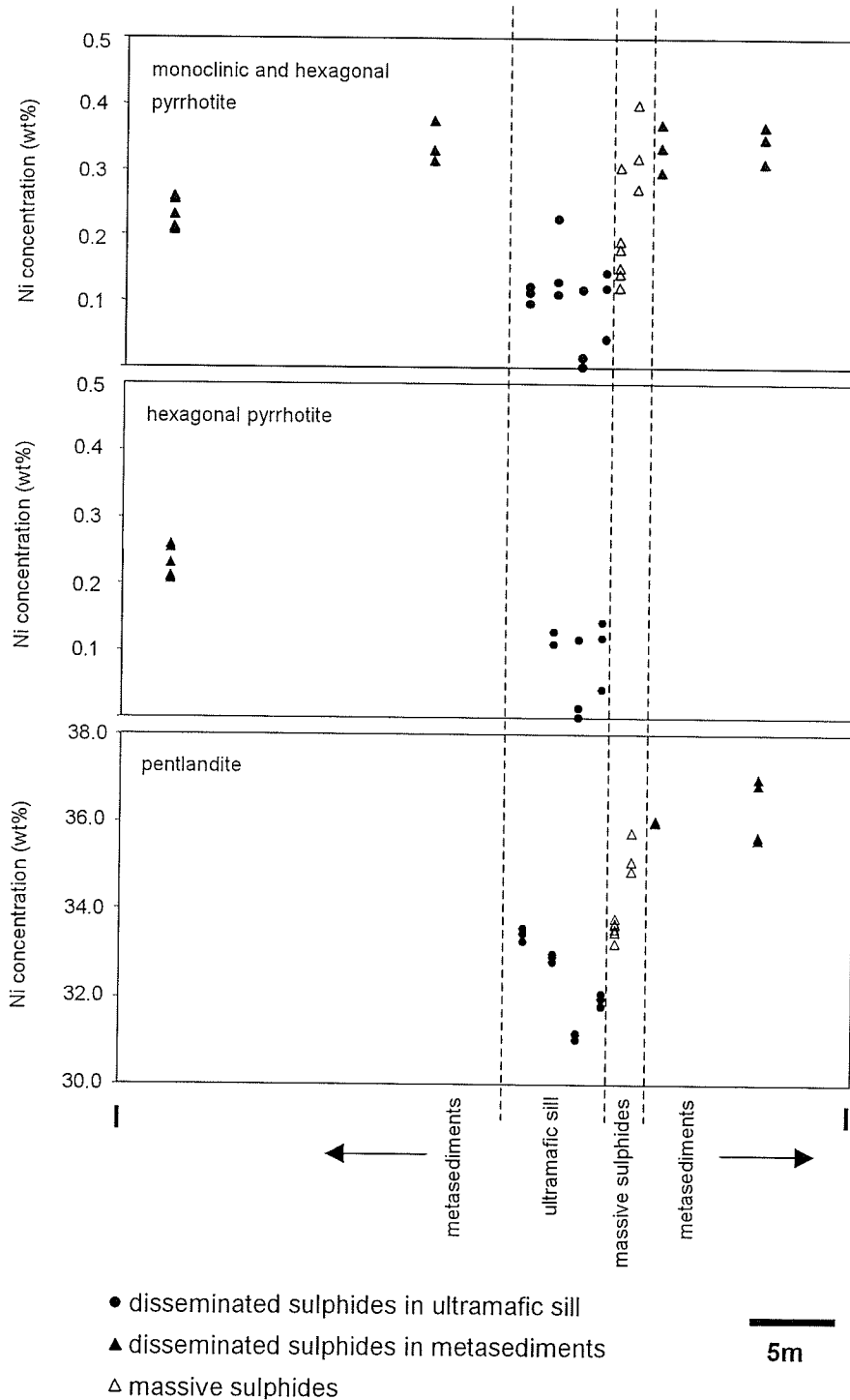


Figure 6.6. Concentration of nickel in co-existing sulphide minerals from samples along section I-I' in Figure 5.16, Thompson 1C ore body. For each sample collected along the section, at least 3 pyrrhotite grains were analyzed by electron microprobe. Results show 1) nickel enrichment in pyrrhotite grains from metasediments that are proximal to the massive ore and the parent sill, and 2) nickel depletion in pyrrhotite grains within the ultramafic sill. Nickel enrichment in pyrrhotite coincides with the mineralization of pentlandite and with nickel enrichment in pentlandite.

stark contrast in Ni concentrations between the ultramafic-hosted sulphides and the massive sulphides may be due to post-magmatic processes that enriched the massive ore in Ni relative to the ultramafic-hosted sulphides. Alternatively, Ni could have been remobilized from the disseminated ultramafic-hosted sulphides into the massive sulphides.

It is possible that post-tectonic diffusion of Ni can occur across strike of an ore zone. Electron microprobe analyses of pyrrhotite grains along section I-I' and section J-J' (Figure 5.16), shows that sediment-hosted pyrrhotite grains are enriched in Ni; such grains are proximal to (within ~20 metres of) the massive ore horizons (Figure 6.6 and 6.7). The relationship between the concentration of Ni in pyrrhotite and its hexagonal or monoclinic character is not entirely clear from the sections in Figure 6.6 and 6.7; however, monoclinic pyrrhotite dominates over hexagonal pyrrhotite within the massive sulphide horizons and within metasediments nearest to the massive sulphide horizons.

Ni enrichment in pyrrhotite (>0.2 wt% Ni) coincides with a Ni enrichment in co-existing pentlandite grains (Figure 6.6). The Ni enrichment in pyrrhotite also coincides with increasing modal percentage of pentlandite. Notably, pentlandite in disseminated metasedimentary sulphides is always associated with Ni-enriched pyrrhotite, and only occurs proximal to the ore zone (within ~20 m). Therefore, Ni enrichment around the horizon is interpreted to be a local phenomenon. The observed Ni halo suggests that Ni diffused away from the massive sulphide horizon and entered sulphide blebs within the metasediments. Nickel may have been mobilized from the ore horizon to the metasediments with the assistance of fluids. The presence of fluids is inferred by the serpentinization of the ultramafic sill and the apparent sulphurization of the massive sulphide horizon.

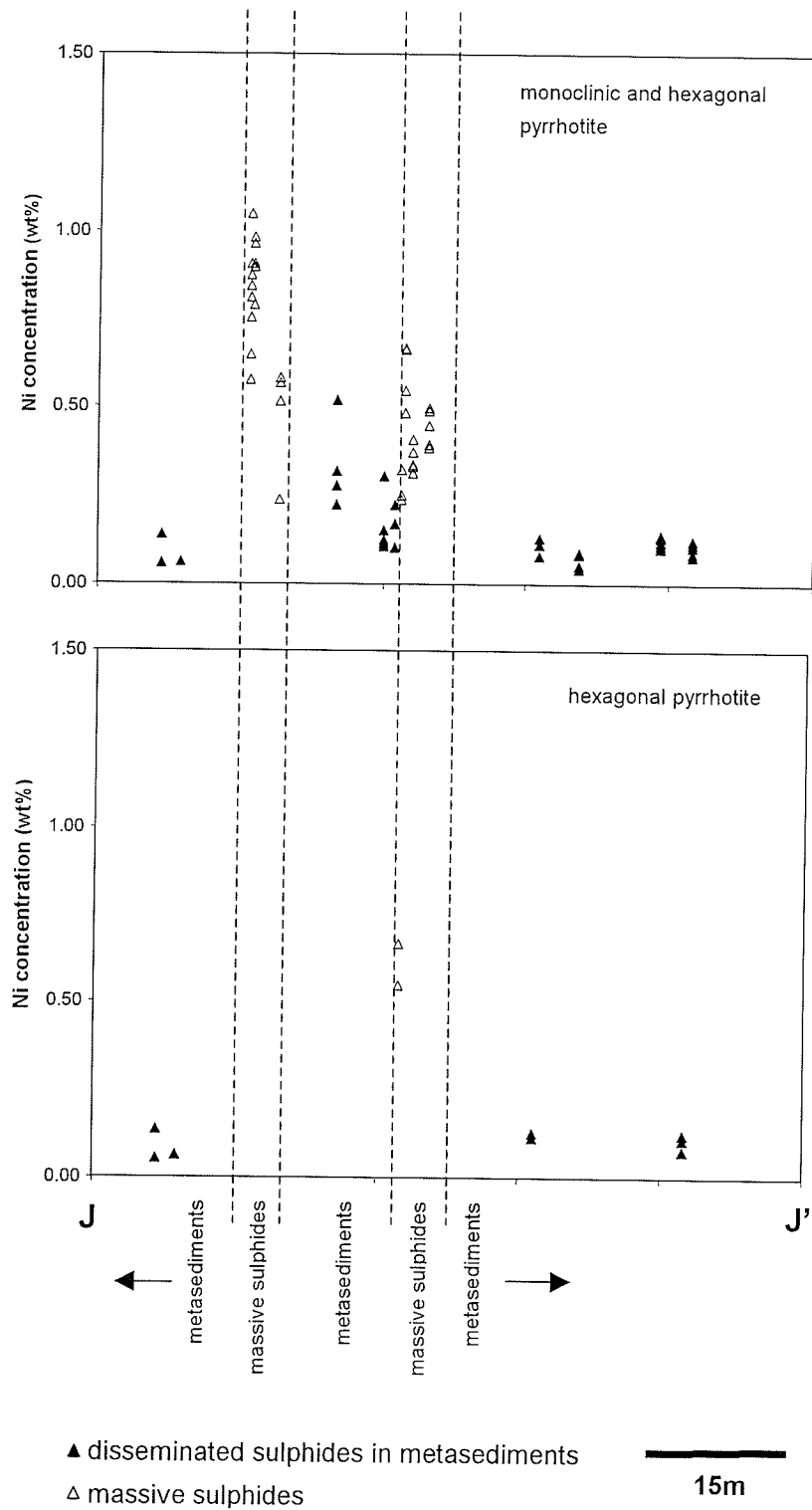


Figure 6.7. Concentration of nickel in pyrrhotite grains from sulphide-bearing samples along section J-J' in Figure 5.16, Thompson 1C ore body. Results show nickel enrichment in pyrrhotite grains from metasediments that are proximal to the massive ore.

6.4 Major Element Concentrations of TNB Sulphide Minerals (EMPA data)

6.4.1 Nickel in Pyrrhotite

Nickel concentrations in pyrrhotite from the Thompson, Birchtree, William Lake, Bucko, and Soab North deposits were determined by electron microprobe analysis (EMPA) (Appendix 3). Special care was taken to probe pyrrhotite grains at least 50 μm away from pentlandite porphyroblasts, in order to avoid those grains that may have inherited Ni by solid-state diffusion (see Figure 6.5).

Pyrrhotite grains in massive sulphide horizons within metasediments are shown to be predominantly monoclinic. Analyses of monoclinic pyrrhotite grains from the Thompson Mine indicate that pyrrhotite in massive and semi-massive sulphides hosted in metasediments (MS-SED, and SMS-SED, respectively) are enriched in Ni in comparison to pyrrhotite that is disseminated in metasediments (DS-SED)(Figure 6.8). MS-SED pyrrhotites range from 0.24-1.11 wt% Ni and SMS-SED pyrrhotites range from 0.31-0.91 wt% Ni. Pyrrhotite grains in sulphide class DS-SED contain up to 0.77 wt% Ni. DS-SED pyrrhotites from samples that contain 1 - 5 modal% sulphides, and are located less than 1 metre away from massive sulphide horizons, have Ni concentrations that overlap those of MS-SED and SMS-SED. These data could indicate that Ni enrichment in disseminated pyrrhotite grains may be a function of their proximity to massive sulphide horizons. Comparison of data from William Lake, Bucko Lake, and Soab North show that monoclinic pyrrhotite grains from these localities have Ni concentrations that fall within the range of the Thompson massive sulphides (0.24-1.11 wt% Ni) (Figure 6.9).

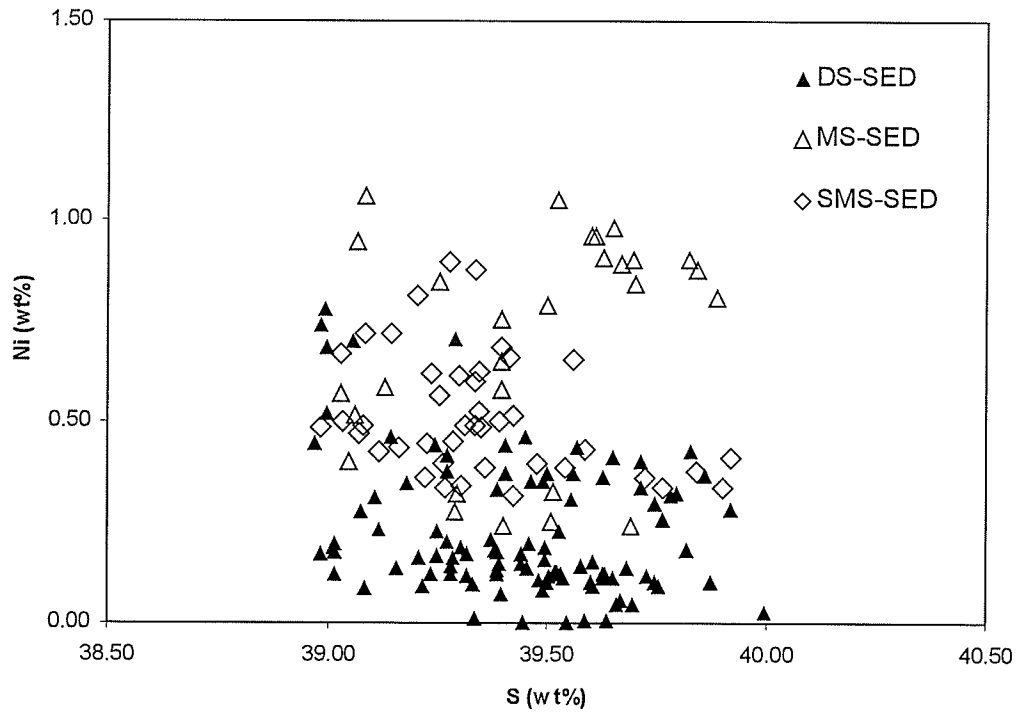


Figure 6.8. Nickel and sulphur concentrations in monoclinic pyrrhotite grains from the Thompson Mine (T1 mine, 1C ore body, and 1D ore body). Sulphide classes represented: DS-SED = disseminated sulphides in metasediments, SMS-SED = semi-massive sulphides in metasediments, MS-SED = massive sulphides in metasediments.

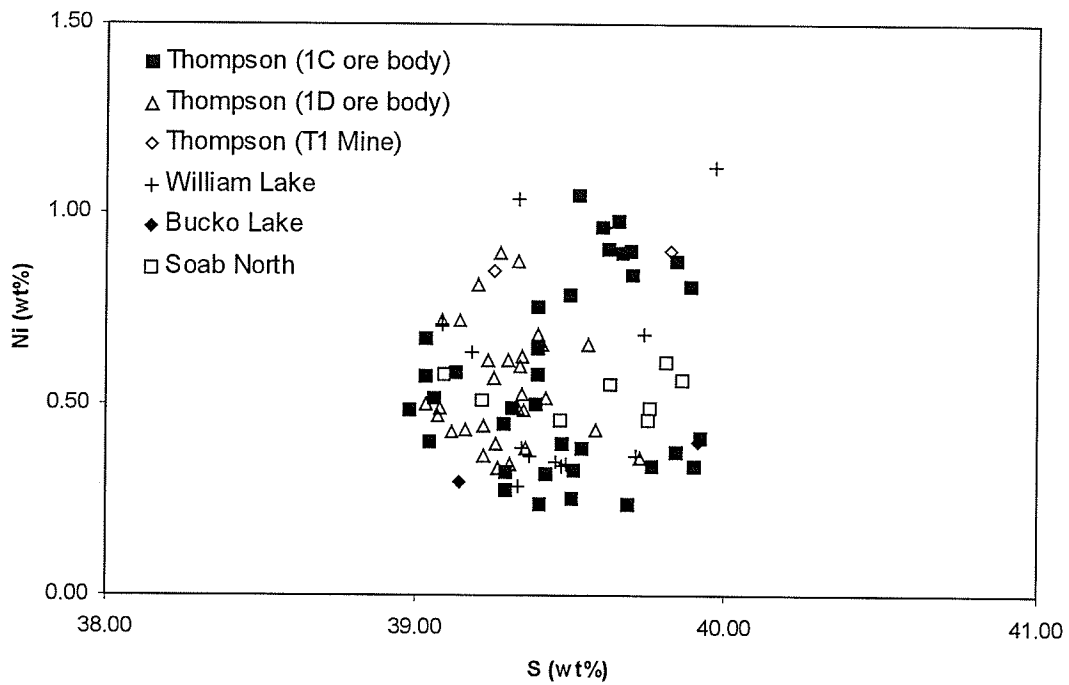


Figure 6.9. Ni and sulphur concentrations in monoclinic pyrrhotite grains from massive sulphides. Sulphide classes represented: SMS-SED (semi-massive sulphides in metasediments); MS-SED (massive sulphides in metasediments), SMS-ARC (semi-massive sulphides in Archean Basement – Bucko only).

In sulphide class MS-UB (massive sulphides in ultramafic breccia), monoclinic pyrrhotite grains predominate over hexagonal grains. Monoclinic pyrrhotites from William Lake contain elevated Ni concentrations (0.69–0.80 wt% Ni) in comparison to the Thompson and Birchtree pyrrhotites (0.12–0.50 wt% Ni) (Figure 6.10).

Both monoclinic and hexagonal pyrrhotite grains from sulphide class DS-U (disseminated sulphides in ultramafic rocks) show increasing Ni concentrations with increasing sulphur (Figure 6.11). The highest Ni concentrations in pyrrhotites from this category occur in hexagonal grains from the William Lake and Birchtree deposits (>0.50 wt% Ni). The lowest Ni concentrations occur in monoclinic grains from the Thompson deposit (<0.50 wt% Ni).

The Ni tenors of pyrrhotite grains from William Lake remain elevated in sulphide classes DS-U, MS-UB, and MS-SED (>0.30 wt% Ni). These data show that, at William Lake, pyrrhotites from massive sulphides are similar in character to the disseminated sulphides in the ultramafic sills. Birchtree pyrrhotites appear to lose Ni in the transition from disseminated ultramafic-hosted sulphides (DS-U) to massive breccia sulphides (MS-UB). Thompson pyrrhotite grains, on the other hand, appear to increase in Ni tenor in the transition from disseminated ultramafic-hosted sulphides (DS-U) to massive sulphides (MS-SED).

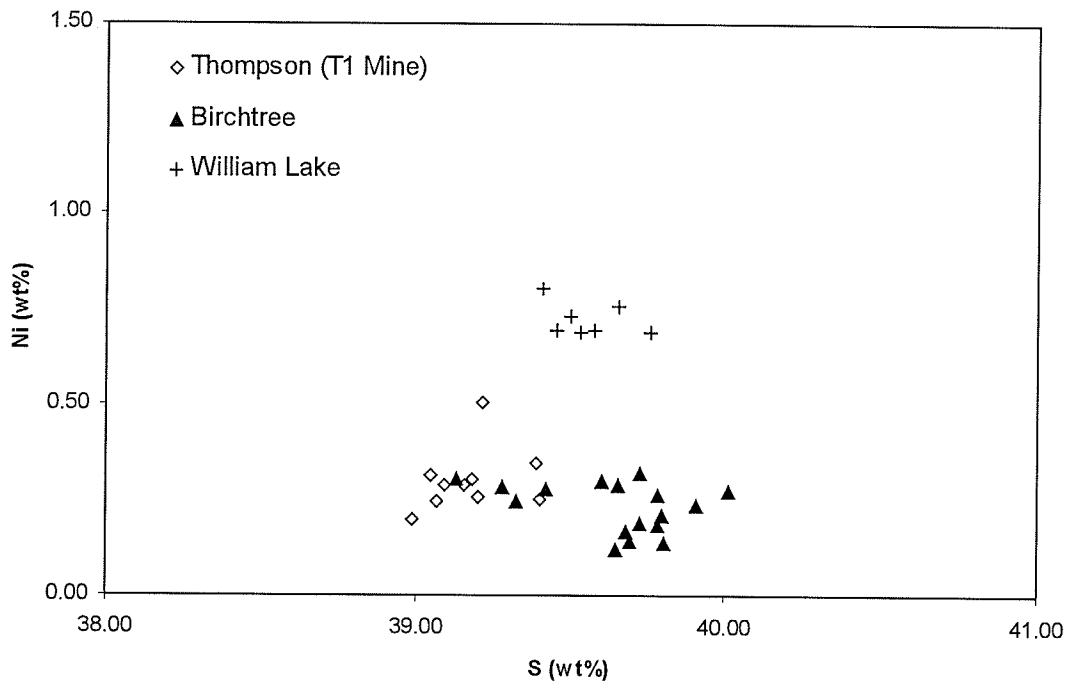


Figure 6.10. Nickel and sulphur concentrations in monoclinic pyrrhotite grains from sulphide class MS-UB (massive sulphides in ultramafic breccia).

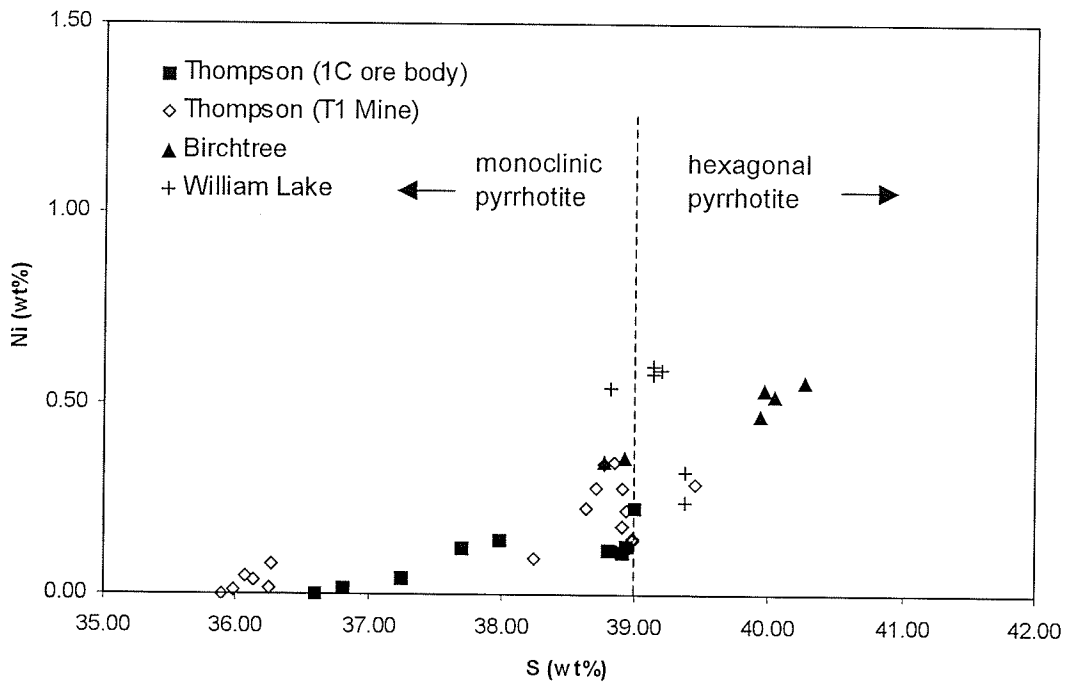


Figure 6.11. Nickel and sulphur concentrations in monoclinic and hexagonal pyrrhotite grains from sulphide class DS-U (disseminated in ultramafic rocks). All host rocks are serpentized.

6.4.2 Ni and Co in Pentlandite

Based on isothermal and controlled cooling experiments on *mss* by Durazzo and Taylor (1982), pentlandite grains occurring as equant blebs, or as chain-like aggregates along the boundaries between annealed pyrrhotite grains (e.g. Figure 5.17, E₂), form from *mss* that cools from temperatures between 610°-250°C. At temperatures below 250°C, the lower diffusion rates of Fe and Ni may prevent continuous re-equilibration, and produce higher degrees of supersaturation than were possible at higher temperatures (Durazzo and Taylor, 1982). Coarsened linear pentlandite, which includes wedges and elongated aggregates developed along one direction within the *mss* matrix, exsolves from *mss* between 250°-150°C. Thin, fine-grained, linear pentlandite, commonly referred to as pentlandite “flames” (e.g. Figure 5.5 b) exsolves at 150°C or slightly below. The occurrence of a combination of these pentlandite textures within a sulphide sample may indicate several generations of equilibration within the history of an orebody. The above textures have been observed in various combinations and abundances throughout the Thompson Nickel Belt deposits. These observations indicate that the sulphides in these deposits have undergone a complex equilibration history, with several generations of melting and cooling.

When pentlandite grains were analysed by electron microprobe, results were not categorized in terms of the pentlandite textures (e.g. chains, eyes, or blebs); rather, the results were categorized in terms of the classification scheme in Section 5, and in terms of the ore body from which they were collected. Microprobe analysis of flame-textured pentlandite was avoided, as the Fe and Ni from hosting pyrrhotite grains often obscured

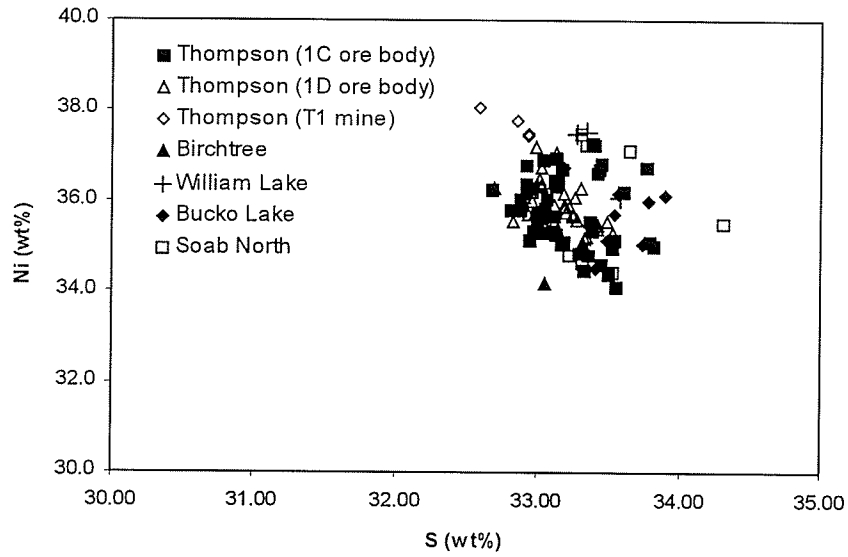
the metal concentrations in pentlandite. Care was also taken to avoid cracks in pentlandite.

Nickel tenors of pentlandite grains from the TNB deposits (Figures 6.12a, 6.13a, and 6.14a) show similar trends to the Ni tenors of co-existing pyrrhotite grains (Figures 6.9, 6.10, and 6.11). Pentlandite grains in massive sulphides from several TNB deposits have Ni tenors ranging from ~34 to 38 wt% Ni (Figure 6.12a). William Lake pentlandites from sulphide class MS-UB contain elevated Ni concentrations (~38 wt% Ni) in comparison to the Thompson and Birchtree pentlandites (~33 to 35 wt% Ni) (Figure 6.13a). William Lake and Birchtree pentlandites from sulphide category DS-U are characterized by high Ni tenors (>35 wt% Ni), while Thompson pentlandites have relatively lower Ni tenors (Figure 6.14a). Pyrrhotite grains co-existing with the DS-U pentlandites from William Lake and Birchtree also have high Ni tenors (Figure 6.11).

The Ni tenors of pentlandite grains from William Lake remain elevated in sulphide classes DS-U, MS-UB, and MS-SED (>35 wt% Ni). These data further support the suggestion that the William Lake massive sulphides closely resemble the character of disseminated sulphides in the ultramafic sills. Birchtree pentlandites, like the coexisting pyrrhotites, appear to lose Ni in the transition from disseminated ultramafic-hosted sulphides (DS-U) to massive sulphides (MS-UB). Thompson pentlandite grains show an opposite trend, increasing in Ni tenor from disseminated ultramafic-hosted sulphides (DS-U) to massive sulphides (MS-SED).

Ni/Co ratios of pentlandite grains further distinguish the chemical character of the TNB deposits. As shown in Chapter 6.2, Thompson pentlandites that were subjected to higher degrees of deformation showed increasing Ni concentrations and decreasing Co

a



b

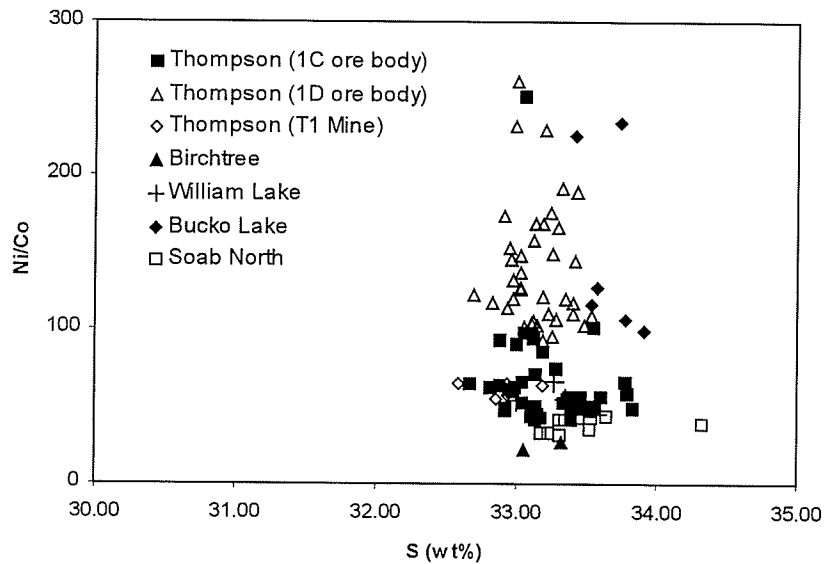
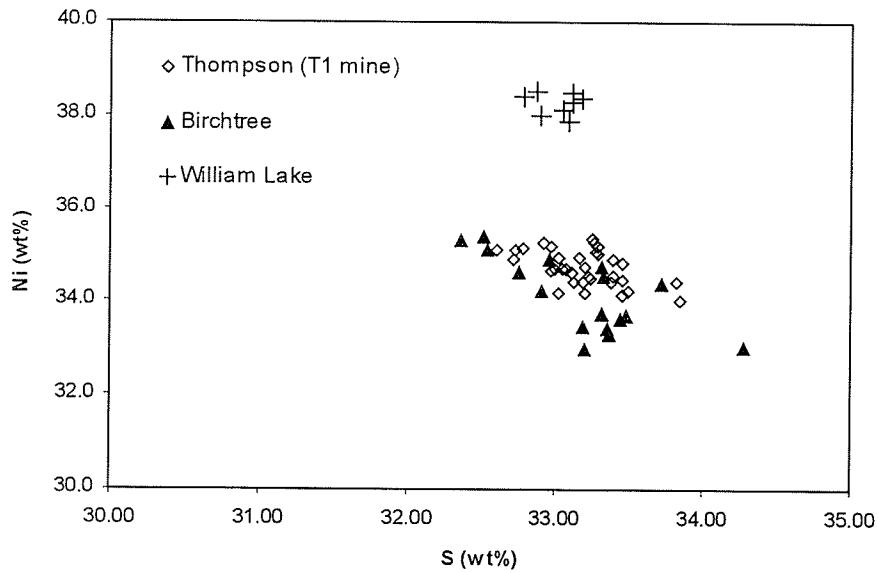


Figure 6.12. a) Nickel and sulphur concentrations in pentlandite grains from massive sulphides. Sulphide classes represented: SMS-SED (semi-massive sulphides in metasediments); MS-SED (massive sulphides in metasediments), SMS-ARC (semi-massive sulphides in Archean Basement – Bucko samples only). b) Ni/Co ratios and sulphur concentrations in pentlandite grains shown in graph a).

a



b

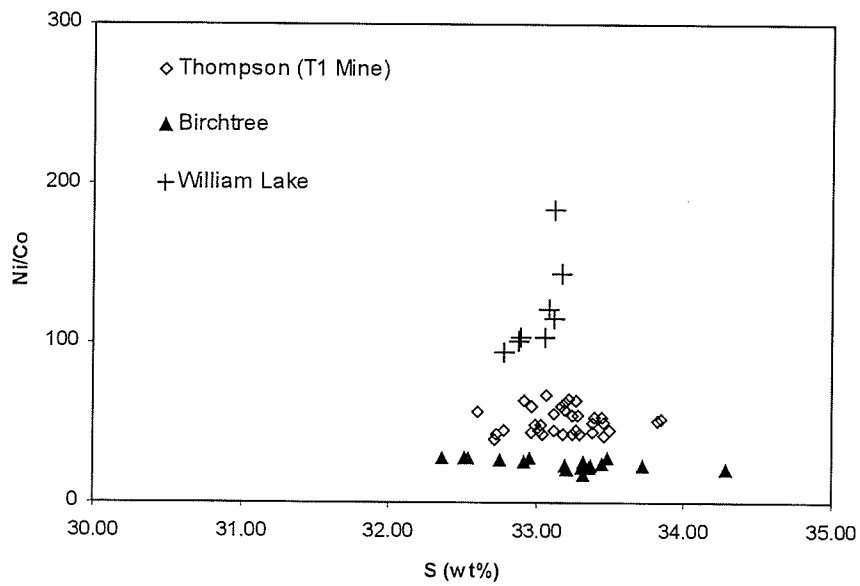
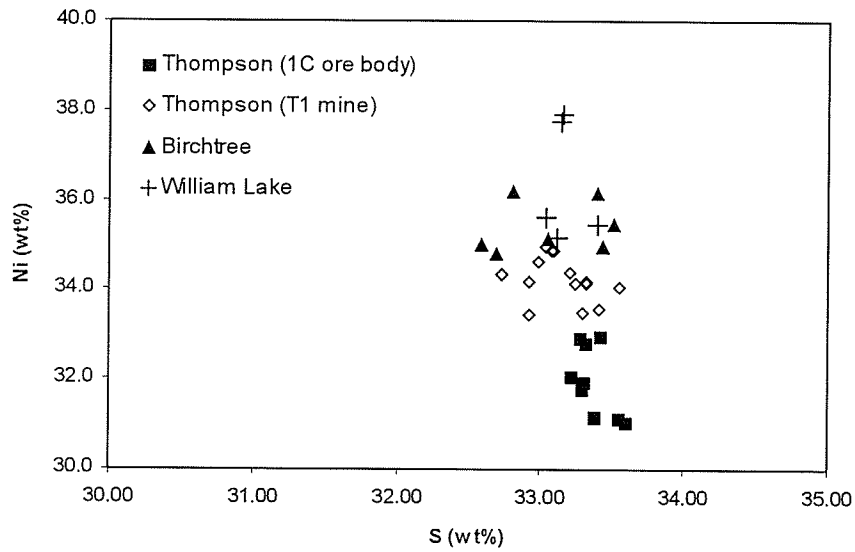


Figure 6.13. a) Nickel and sulphur concentrations in pentlandite grains from sulphide class MS-UB (massive sulphides in ultramafic breccia). b) Ni/Co ratios and sulphur concentrations in pentlandite grains shown in graph a).

a



b

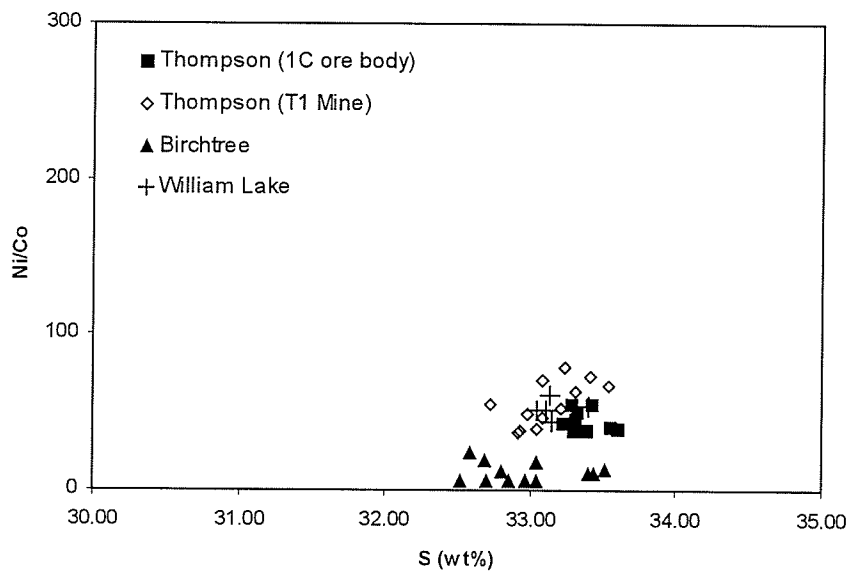


Figure 6.14. a) Nickel and sulphur concentrations in pentlandite grains from sulphide class DS-U (disseminated sulphides in ultramafic rocks). b) Ni/Co ratios and sulphur concentrations in pentlandite grains shown in graph a). All host rocks are serpentinized.

concentrations. Thus, more progressively deformed pentlandite grains have higher Ni/Co ratios than their less deformed counterparts. The massive sulphides from Thompson 1D ore body and Bucko Lake have the highest Ni/Co ratios among the TNB deposits (>100) (Figure 6.12b). Given that the Ni concentrations in the pentlandites from the 1D ore body and Bucko Lake are within the same range as the other deposits (Figure 6.12a), the high Ni/Co ratios can be attributed to relatively lower Co abundances in the two deposits. It can be argued that the lower Co abundances reflect an initially low magmatic Co concentration. However, given the extent of deformation in the Thompson 1D ore body, it is possible that the 1D pentlandites have experienced a loss in Co due to deformation. The Bucko pentlandites, although also deformed, are quite distinct from the other TNB ores in that they are hosted in Archean basement gneisses, and not in Oswagan Group metasediments. The high Ni/Co ratios in Bucko ore may therefore be a function of the interaction between the parent magma and the host rocks.

In sulphide class MS-UB, pentlandite grains from the William Lake deposit are characterized by elevated Ni/Co values (~100 to 200) in comparison to the Birchtree and Thompson ores (<100) (Figure 6.13b). However, in sulphide class DS-U, William Lake pentlandites have Ni/Co ratios that fall within the range of Thompson pentlandites (35 to 80)(Figure 6.14b).

In samples from the Thompson Mine, Ni/Co ratios and Ni tenors from pentlandites in ores proximal to the ultramafic hosts (MS-UB)(Figure 6.13) were markedly lower than those ratios from their distal equivalents (MS-SED)(Figure 6.12). These data further support the theory that the more deformed or attenuated ores have higher Ni/Co ratios and higher Ni concentrations in comparison to less deformed ores (refer to Section 6.2).

In all sulphide classes (DS-U, MS-UB, and MS-SED), Ni/Co ratios for pentlandite grains from the Birchtree Mine are the lowest of the ore bodies (<40) (Figures 6.12b, 6.13b, 6.14b). These relatively low Ni/Co ratios are due to the fact that pentlandite grains from Birchtree Mine are characterized by elevated Co values (1.01 to 3.28 wt% Co) in comparison to the other ore bodies (typically <1.00 wt% Co) (Appendix 3). The elevated Co values in all the sulphide classes of the Birchtree deposit may largely be a function of primary magma composition. However, the narrow range in Ni/Co ratios in Birchtree pentlandites may be a function of the lower degrees of deformation in the Birchtree deposit relative to the Thompson deposit.

6.5 Trace Element Concentrations in TNB Sulphide Minerals (PIXE data)

Trace element chemistry of sulphide minerals in 33 thin sections was determined by proton-induced X-ray emission (PIXE) (Appendix 4). These thin sections represented samples from Thompson Mine (1C and 1D ore bodies), Birchtree Mine, and the William Lake deposit.

Some general observations from the PIXE data are as follows:

- Zinc tends to be elevated in chalcopyrite (47 to 505 ppm Zn).
- Arsenic is concentrated in secondary subhedral to euhedral pyrite grains within the massive sulphide ores (MS-UB, SMS-SED, MS-SED). Secondary pyrite has been noted to occur with late paragenetic gersdorffite (NiAsS) in the Thompson ores, suggesting that As is brought into the system in the late stages of ore formation and crystallizes in both pyrite and gersdorffite. Pyrite grains analyzed in this study contained up to 409 ppm As.

- Appreciable concentrations of Co also occur in secondary pyrite grains (up to 1.4% Co)
- No measurable quantities of platinum group elements were detected in the sulphide minerals by PIXE.

Selenium concentrations in pentlandite grains from TNB massive sulphides increase with increasing selenium concentrations in co-existing pyrrhotite grains. This correlation indicates that Se does not preferentially partition into any one sulphide mineral in the pyrrhotite-pentlandite assemblage. There is a positive correlation between Ni and Se in both pyrrhotite and pentlandite grains from TNB massive sulphide ore (Figures 6.15 and 6.16). Pentlandite and pyrrhotite grains within massive sulphide ore from the Thompson 1D ore body contain higher Se concentrations in comparison to the Birchtree, 1C ore body, and William Lake ores (Figures 6.15 and 6.16). The elevated Se values from the 1D ore body sulphide minerals may record a primary magmatic Se signature or an upgrading of Se within the deposit.

6.6 Magmatic *versus* Hydrothermal Se Concentrations in Sulphide Minerals

Selenium data reported by previous workers (Hawley and Nichol, 1959; and Jonasson and Sangster, 1975) show that Se contents in a given sulphide mineral vary widely within and among individual ore deposits. These variations in Se concentration can be attributed to the extent of hydrothermal activity that took place during deposition of the ores.

Selenium contents in chalcopyrite from the Thompson Nickel Belt massive sulphides range from about 14 to 48 ppm. Selenium concentrations in chalcopyrite grains

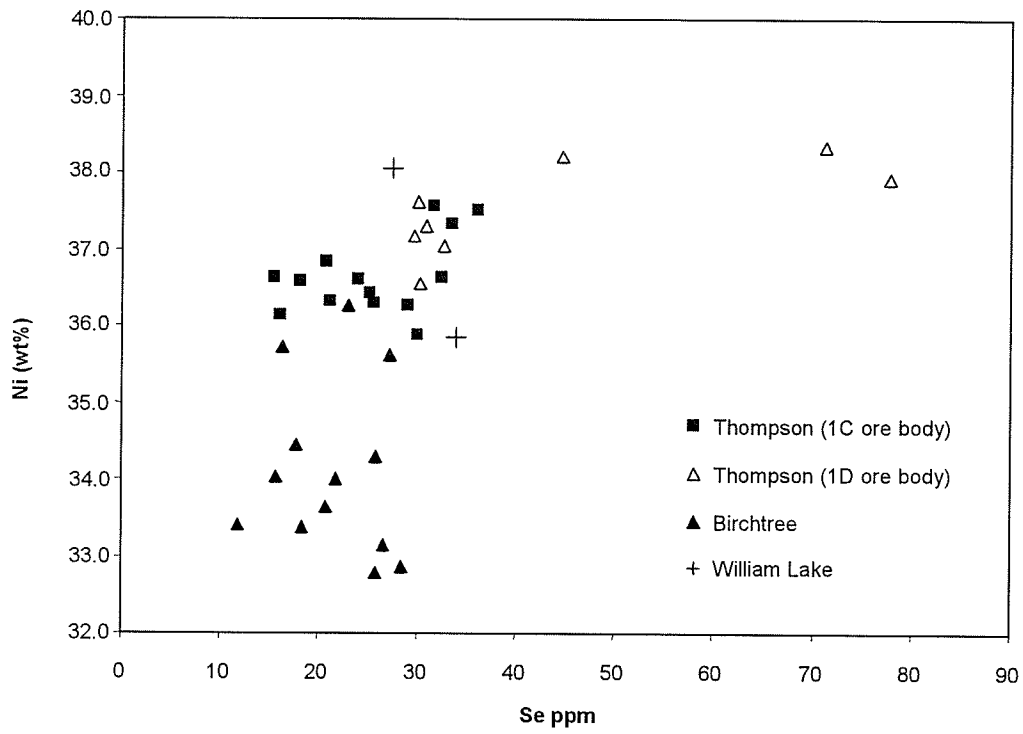


Figure 6.16. Nickel and selenium concentrations in pentlandite grains from massive sulphides. Sulphide classes represented: SMS-SED (semi-massive sulphides in metasediments); MS-SED (massive sulphides in metasediments).

from other deposits are as follows: 33 to 165 ppm from nickeliferous copper sulphide ores from Sudbury (Hawley and Nichol, 1959); 23 to 540 ppm from non-nickeliferous Cu-Fe-Zn hydrothermal replacement ores from Quebec (Hawley and Nichol, 1959); and 159 to 537 ppm from Canadian volcanogenic type ores of Archean and Proterozoic age (Jonasson and Sangster, 1975). It is important to note that the Se concentrations from Hawley and Nichol (1959) were obtained by x-ray spectrographic analysis of mineral separates; those from Jonasson and Sangster (1975) were also obtained from mineral separates, but analysis was by a colorimetric method that utilizes the reagent, 3,3'-diamino-benzidine. Selenium concentrations from the Thompson Nickel Belt were obtained by PIXE. The narrow range in Se concentrations from the TNB samples can be partially attributed to the fact that PIXE is an *in situ* method of analysis and, therefore, involves less sample modification in comparison to the methods used by the previous authors.

Selenium concentrations in pyrite from the TNB massive sulphides range from about 7 to 57 ppm, compared to a range of 25 to 60 ppm in pyrite from Sudbury ores, and <15 to 1000 ppm in the Quebec ores (Hawley and Nichol, 1959).

Selenium concentrations in pyrrhotite from the TNB massive sulphides range from about 13 to 61 ppm, compared to a range of 17 to 230 ppm in pyrrhotite from Sudbury ores, and <15 to 595 ppm in the Quebec ores (Hawley and Nichol, 1959).

Selenium concentrations in pentlandite from the TNB massive sulphides range from about 12 to 78 ppm, compared to a range of 30 to 160 ppm in the Sudbury ores (preliminary values, Hawley and Nichol, 1959).

The highest Se concentrations in chalcopyrite, pyrite, and pyrrhotite (>500 ppm) are those found in the non-nickeliferous copper ores of hydrothermal and volcanogenic origin. The range of Se values for the TNB sulphides tend to be relatively low, leaning toward a more magmatic signature. However, Se concentrations in pyrrhotite and pentlandite grains from the Thompson 1D massive ores are elevated with respect to grains in the massive ores from the Thompson 1C ore body, Birchtree Mine, and William Lake (Figures 6.15 and 6.16). If fluid-assisted movement of Se is possible, as inferred by Hawley and Nichol (1959), then elevated Se concentrations in the 1D sulphide minerals could record hydrothermal alteration of the 1D ores.

CHAPTER 7: WHOLE-ROCK GEOCHEMISTRY OF THOMPSON NICKEL BELT SULPHIDES

7.1 Ni Concentration of Massive Sulphides

In order to compare the metal concentration in samples with widely varying sulphide contents and textures, it is appropriate to normalize the metal concentration to 100% sulphides (MacDonald and Cherry, 1988). This normalization technique assumes that the trace elements were incorporated into magmatic sulphides and that the original magmatic sulphide assemblage consisted of monoclinic pyrrhotite, pentlandite (36 wt% Ni) and stoichiometric chalcopyrite.

It is important to note that the normalization of element concentrations to 100% sulphides can be problematic in determining the amount of Ni in ultramafic rock samples with very low weight percent sulphides. By normalizing the concentration of Ni in a whole rock to the amount of S in that rock, one assumes that all the Ni resides in the sulphide phases. However, in a serpentinized dunite or peridotite, Ni may reside in olivine as well as pyrrhotite and pentlandite. If the total Ni concentration in such a rock is normalized to the amount of S in that rock, then the entire rock will have an artificially high Ni tenor, i.e. a high amount of Ni for the amount of sulphide present. Therefore, it may not be very meaningful to assess the concentration of Ni (if normalized to 100% sulphides) in a weakly mineralized ultramafic body (< 1% S). It is more appropriate to normalize Ni concentrations to 100% sulphide when comparing the Ni tenor of massive sulphide samples, since the Ni will largely reside in the sulphide phases in these samples.

The Thompson 1D massive ores have generally higher Ni tenors in comparison to the Birchtree and Pipe ores (Figure 7.1). Whole-rock Ni concentrations in the ores show a positive correlation with Ni concentrations in the sulphide minerals comprising the ores; pyrrhotite and pentlandite grains from the sediment-hosted Thompson massive sulphides contain higher Ni concentrations than the Birchtree breccia ores (Figures 6.1 and 6.4).

7.2 Ni/Co Ratios

Ni/Co ratios of ultramafic bodies associated with the Thompson, Birchtree, and Pipe massive ores are very similar (mean = 20 to 25) (Figure 7.2). However, the massive sulphides specifically from the Thompson 1D ore body have elevated Ni/Co ratios (24 to 113) with respect to the massive sulphides from Birchtree and Pipe (Birchtree = 6 to 64; Pipe = 20 to 32) (Figure 7.3). The Birchtree and Pipe massive ores appear to have retained similar ratios to their ultramafic host rocks. The higher Ni/Co ratios of the Thompson ores are largely attributed to lower Co concentrations, as well as higher Ni concentrations, in comparison to Birchtree and Pipe ores (Appendix 5).

7.3 Se/S Ratios

Eckstrand *et al.* (1989) showed that Se/S ratios of the Thompson ores ($\sim 28 \times 10^6$ to 170×10^6) resembled ratios of barren wall rock sulphides ($\sim 28 \times 10^6$ to 78×10^6) much more closely than ratios of the mantle ($\sim 228 \times 10^6$ to 350×10^6) (Figure 7.4). These data support the theory that the magma yielding the Thompson ores was contaminated by barren sedimentary sulphides.

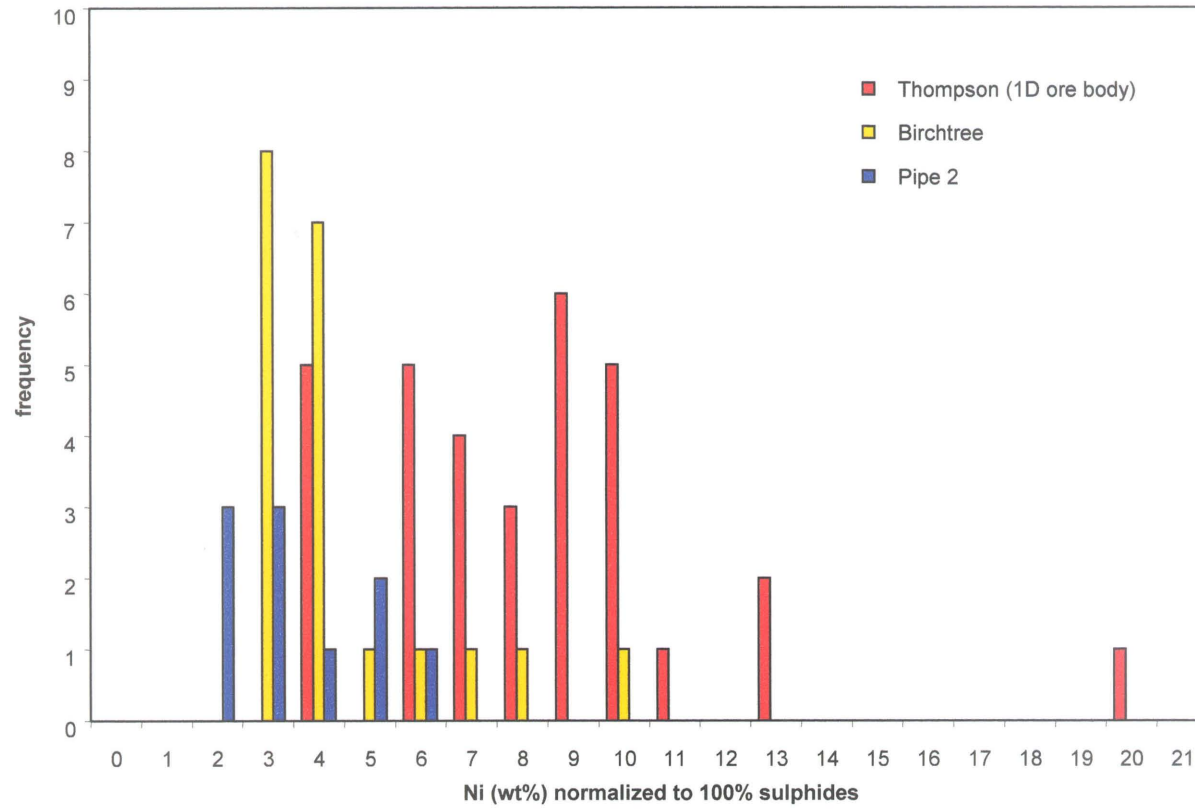


Figure 7.1. Ni concentration of massive and semi-massive sulphides from the TNB, normalized to 100% sulphides. Sulphide classes represented: MS-UB, MS-SED, SMS-SED.

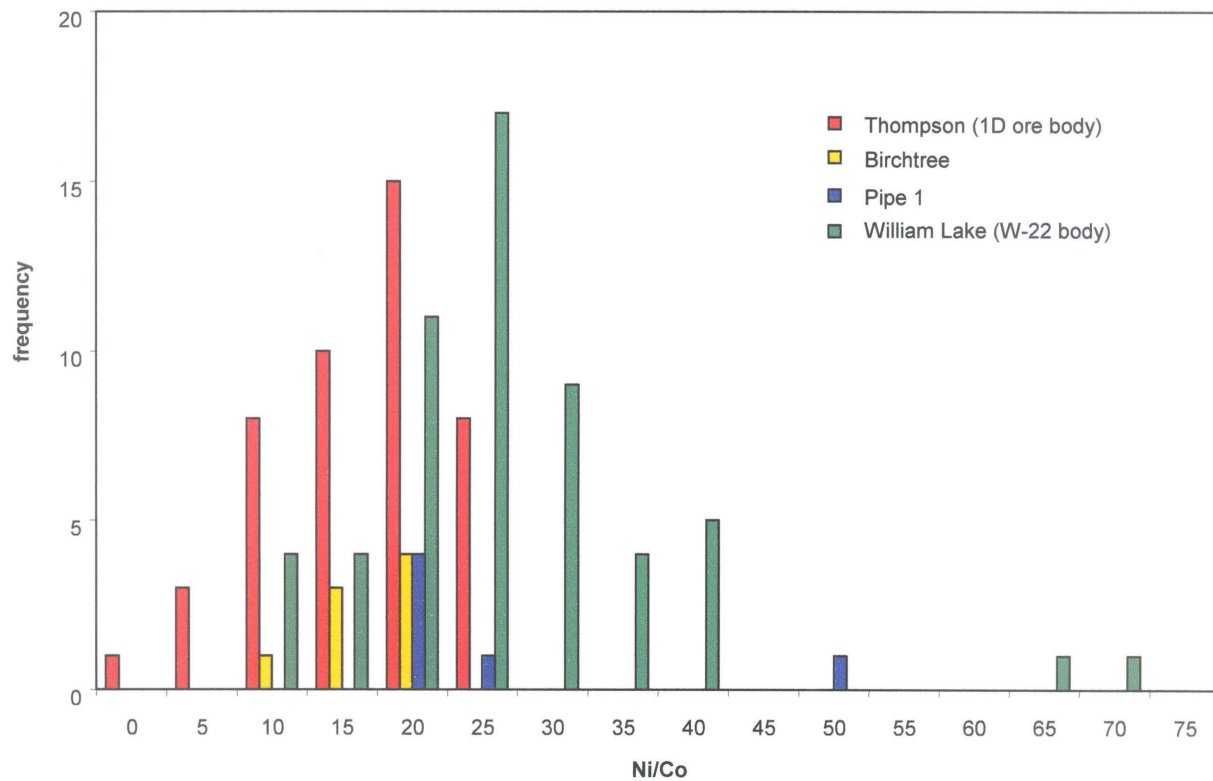


Figure 7.2. Ni/Co ratios of ultramafic bodies from the TNB with the following geochemical parameters: MgO > 24%, S < 5000 ppm, and Se/S x 10⁶ < 1000. Data from CAMIRO (2000a).

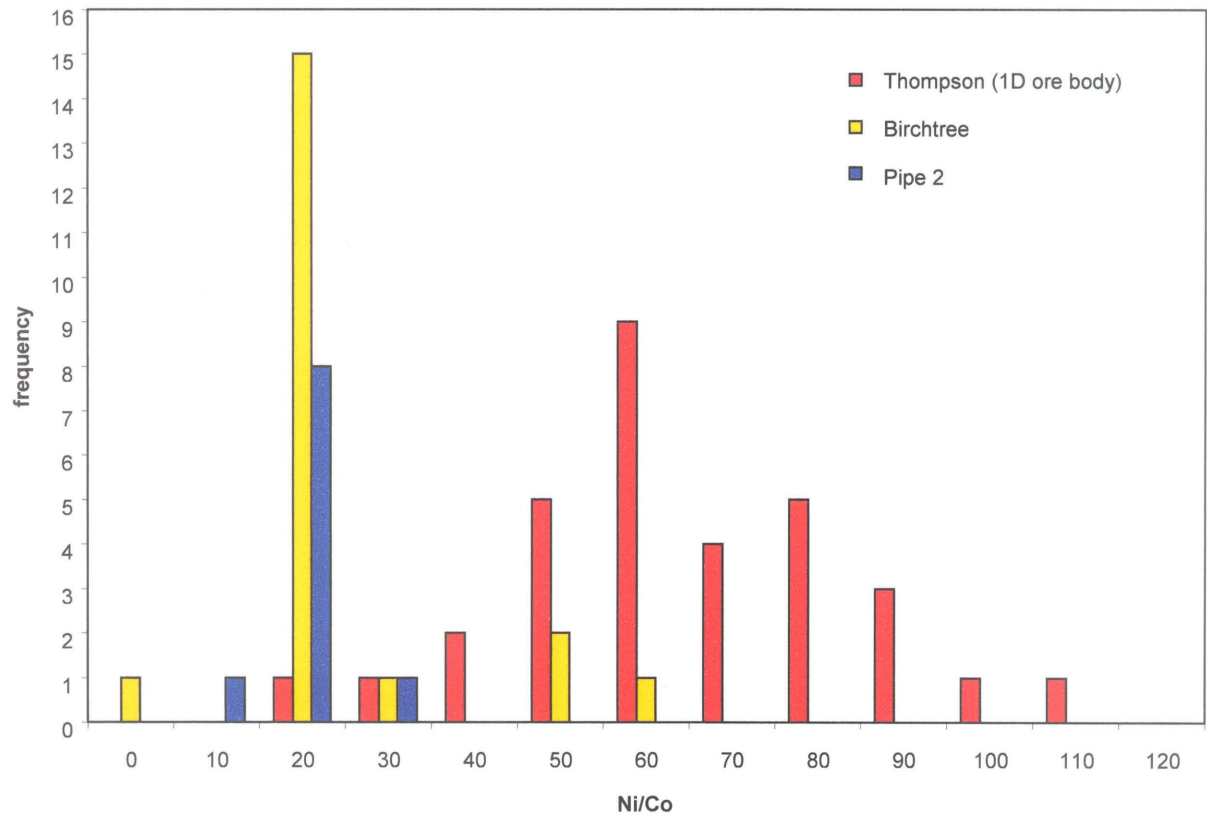


Figure 7.3. Ni/Co ratios of massive and semi-massive sulphides from the TNB. Sulphide classes represented: MS-UB, MS-SED, SMS-SED.

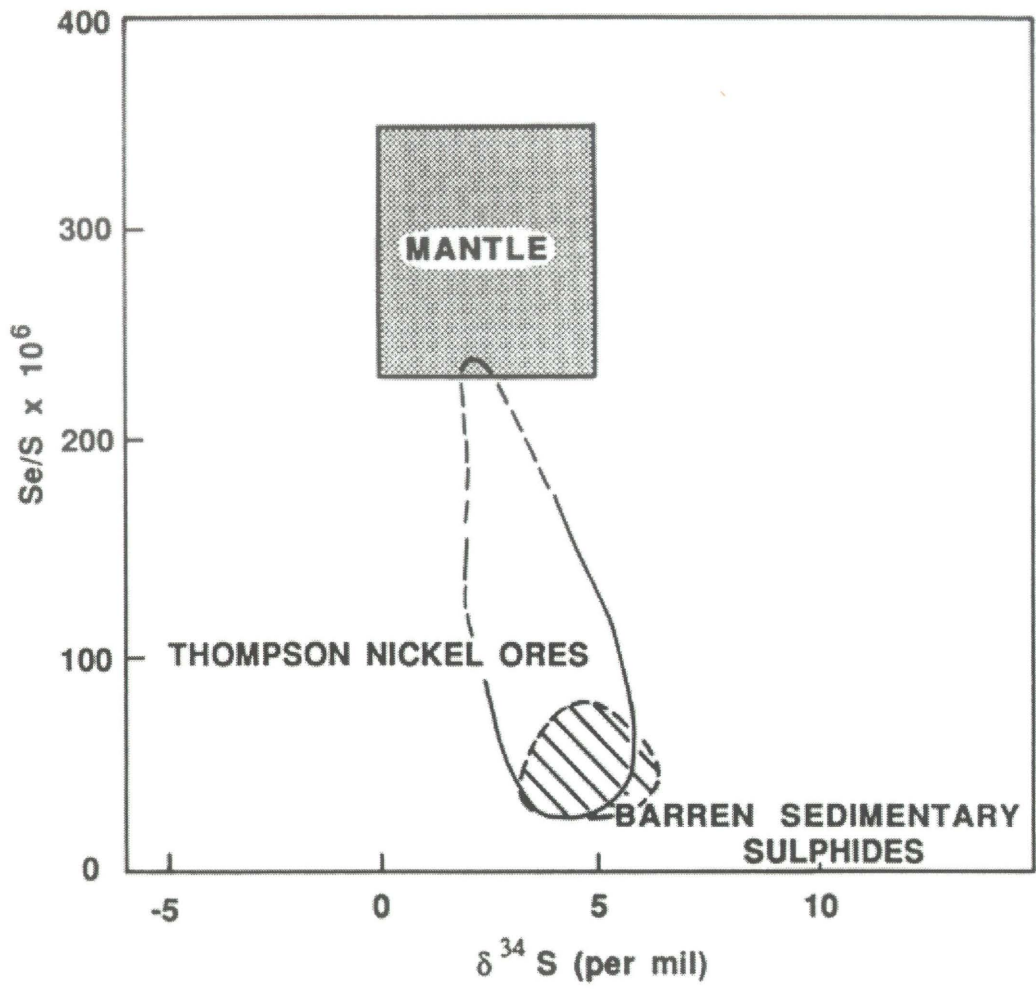


Figure 7.4. Se/S and $\delta^{34}\text{S}$ data for nickel sulphide ore and barren sedimentary sulphides from the TNB (from Eckstrand *et al.*, 1989).

Se/S ratios for massive and semi-massive sulphide samples from this study are consistent with there being a sedimentary sulphur component in the ores of the Thompson 1D ore body, Birchtree Mine, and Pipe 2 deposit ($< 120 \times 10^6$)(Figure 7.5). Thompson massive ores have slightly elevated values of Se/S ($\sim 60 \times 10^6$) in comparison to the Birchtree and Pipe 2 ores ($\sim 40 \times 10^6$), although there is considerable overlap in the Se/S values. Figure 7.6 shows the Se/S ratios for ultramafic rocks associated with the massive ores above. The similarity in Se/S ratios of the massive ores with the ratios of associated ultramafic rocks suggests that the Thompson, Birchtree, and Pipe ores were largely derived from ultramafic magma that was contaminated by sedimentary sulphides.

A striking distinction can be made between the William Lake W-22 ultramafic body and its northern counterparts, based on Se/S ratios (Figure 7.6). William Lake Se/S ratios (40×10^6 to 240×10^6) are significantly higher than the Birchtree, Pipe, and Thompson ratios (10×10^6 to 130×10^6). This may suggest that William Lake ultramafic rocks, particularly those from the W-22 ultramafic body, are more juvenile than the Birchtree and Thompson ultramafic rocks.

7.4 Platinum Group Element (PGE) Concentrations

The chondrite-normalized chalcophile-element plots of the Thompson and Birchtree massive and semi-massive samples from this study show a distinct Pt depletion (Figure 7.7). This Pt depletion is also shown in similar plots of the Pipe deposit by Naldrett *et al.* (1979), and in plots of massive magmatic sulphide samples from the Pipe II and Thompson deposits (Bleeker, 1990). The Pt depletion is anomalous for a magmatic sulphide deposit, as it is even more depleted than the typically immobile Ir, Ru, and Rh.

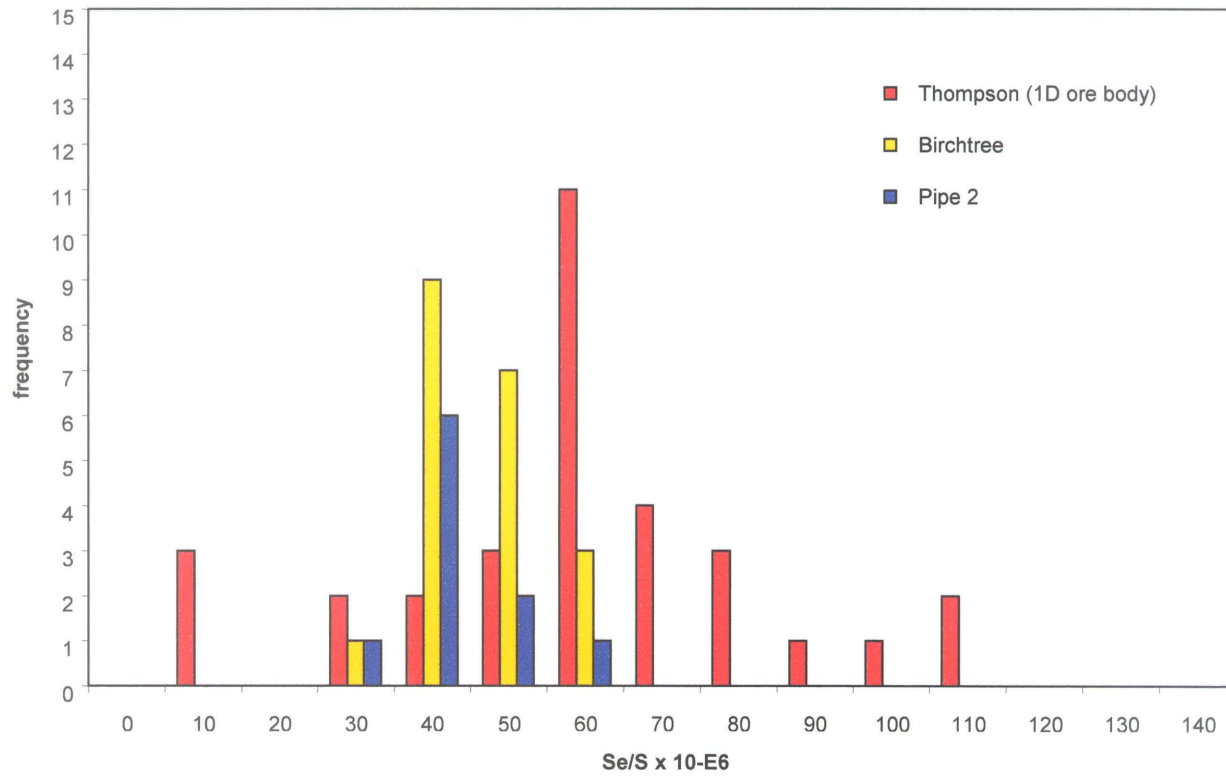


Figure 7.5. Se/S ratios of massive and semi-massive sulphide samples from the TNB. Data from CAMIRO (2000a).

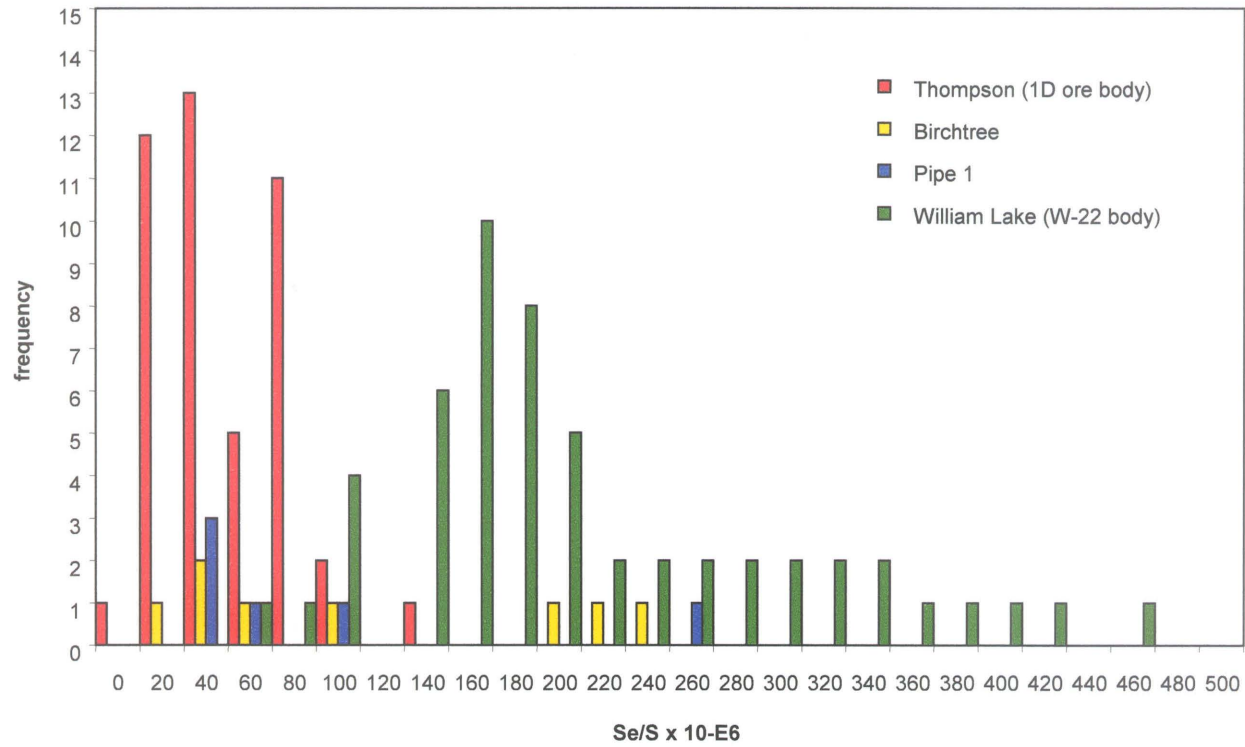


Figure 7.6. Se/S of ultramafic bodies from the TNB with the following geochemical parameters: MgO > 24%, S < 5000 ppm, and Se/S x 10⁶ < 1000. Data from CAMIRO (2000a).

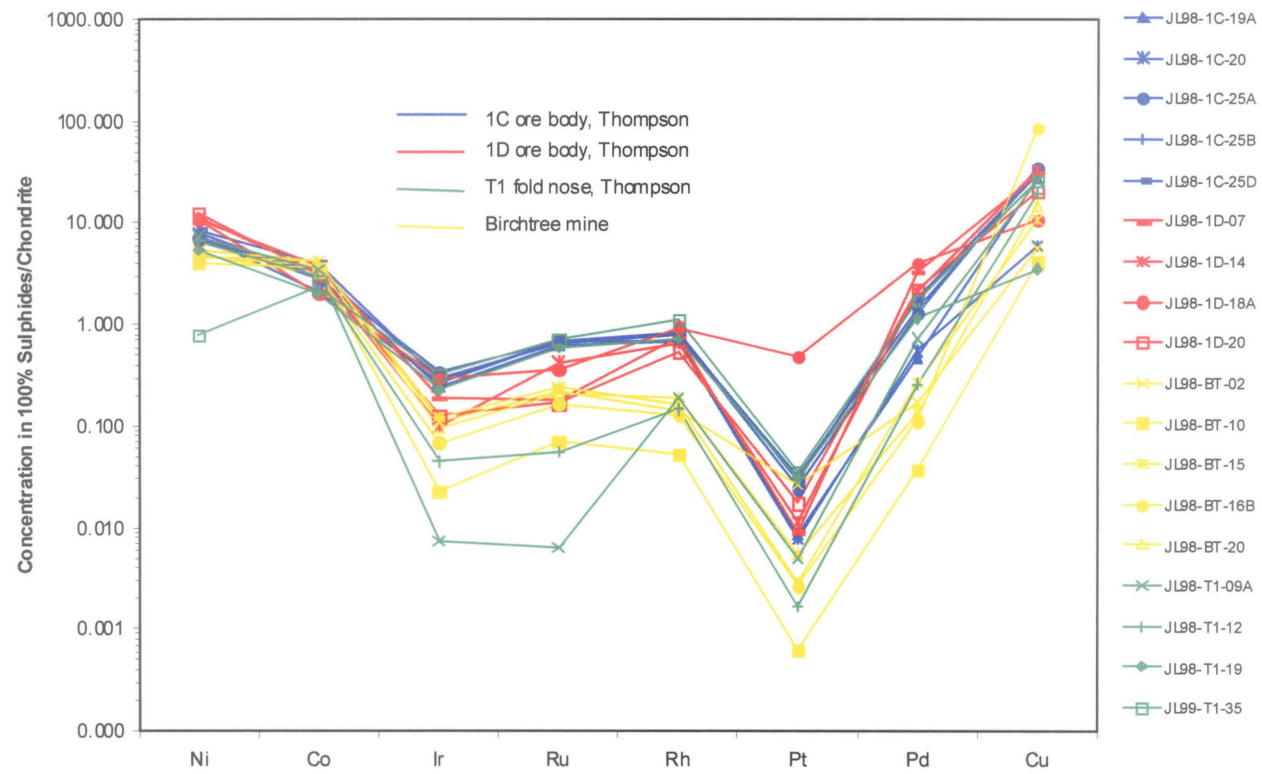


Figure 7.7. Chondrite-normalized plot of chalcophile element concentrations in massive and semi-massive sulphide samples from the TNB, this study. Data are recalculated to 100% sulphide and then normalized by the chondritic abundances for each element.

One would expect the concentration of Pt in the massive sulphides to fall between the concentration of Rh and Pd (average ~125 ppb). The Pt anomaly in the massive sulphide samples from this study can be quantified in the equation:

$$\begin{aligned} & \% \text{ Pt concentration below expected Pt concentration} \\ & = [(\text{average observed Pt concentration} - \text{average expected Pt concentration}) / \\ & \text{average observed Pt concentration}] \times 100 \\ & = (41.6 \text{ ppb} - 125.8 \text{ ppb} / 41.6 \text{ ppb}) \times 100 \\ & = - 202\% \text{ depletion in Pt} \end{aligned}$$

Chondrite-normalized plots of sulphide-bearing Birchtree, Thompson, and Pipe samples (Figure 7.8, 7.9, and 7.10, respectively) show that the Pt anomaly is only found in massive sulphide samples; the disseminated and net-textured sulphides from the three localities show no Pt anomaly. This Pt anomaly does **not** occur in spider plots of other Proterozoic ultramafic-hosted sulphide ores, which include the predominantly net-textured Donaldson and Katiniq ores from the Ungava belt, and the disseminated and net-textured ores of the Bucko Lake deposit (Figure 7.11); nor does the Pt anomaly occur in the Archean ores of the Kambalda mining camp, which are predominantly net-textured (Figure 7.12).

The Pt anomaly in the Birchtree, Thompson and Pipe massive sulphides may indicate that the Thompson Nickel Belt deposits may have been subjected to a different series of metamorphic events in comparison to other ultramafic-associated ore deposits. The komatiitic rocks from the Kambalda mining camp have been metamorphosed to lower amphibolite facies. In contrast to the Thompson Nickel Belt deposits, Kambalda ore consists of about 80% net-textured sulphides, while massive sulphide ore is commonly

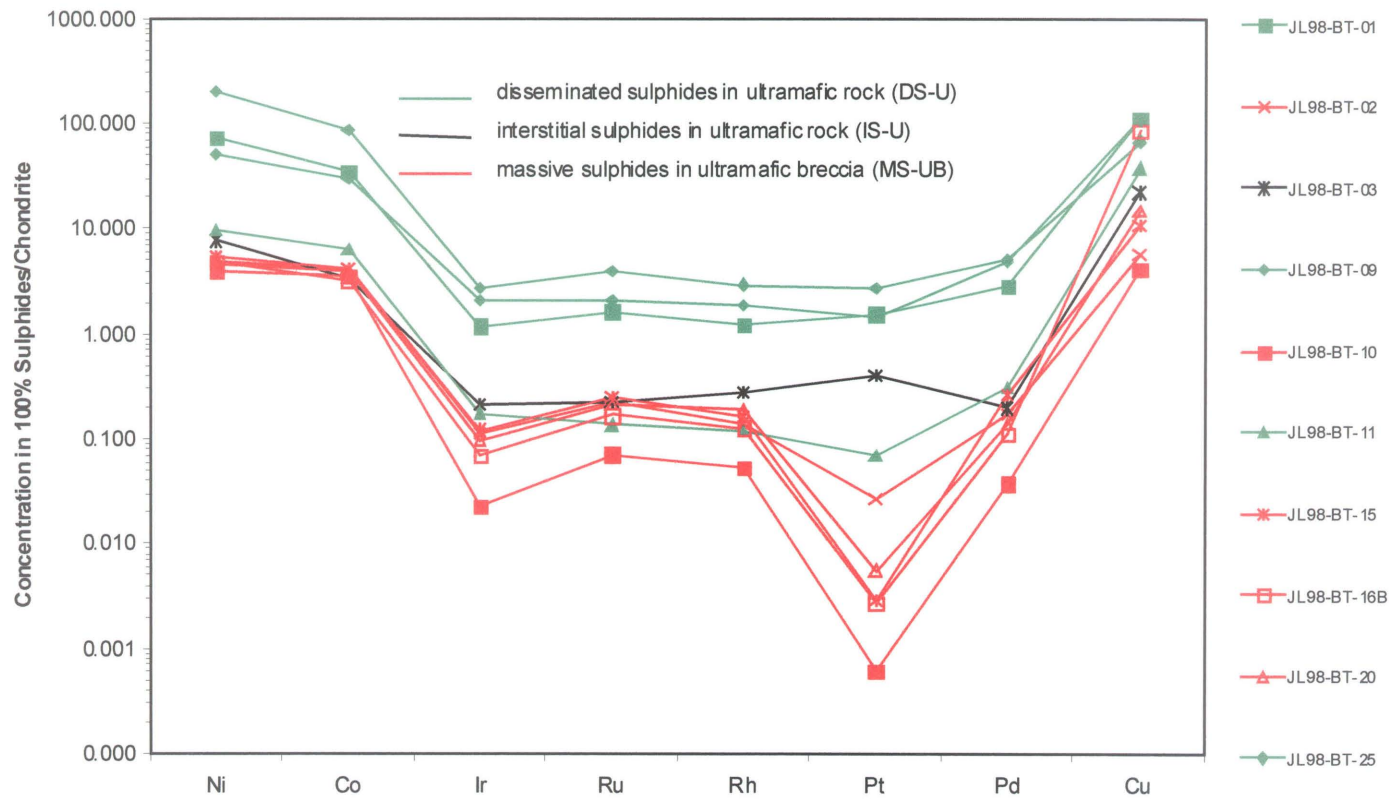


Figure 7.8. Chondrite-normalized plot of chalcophile element concentrations in samples from Birchtree Mine, this study.

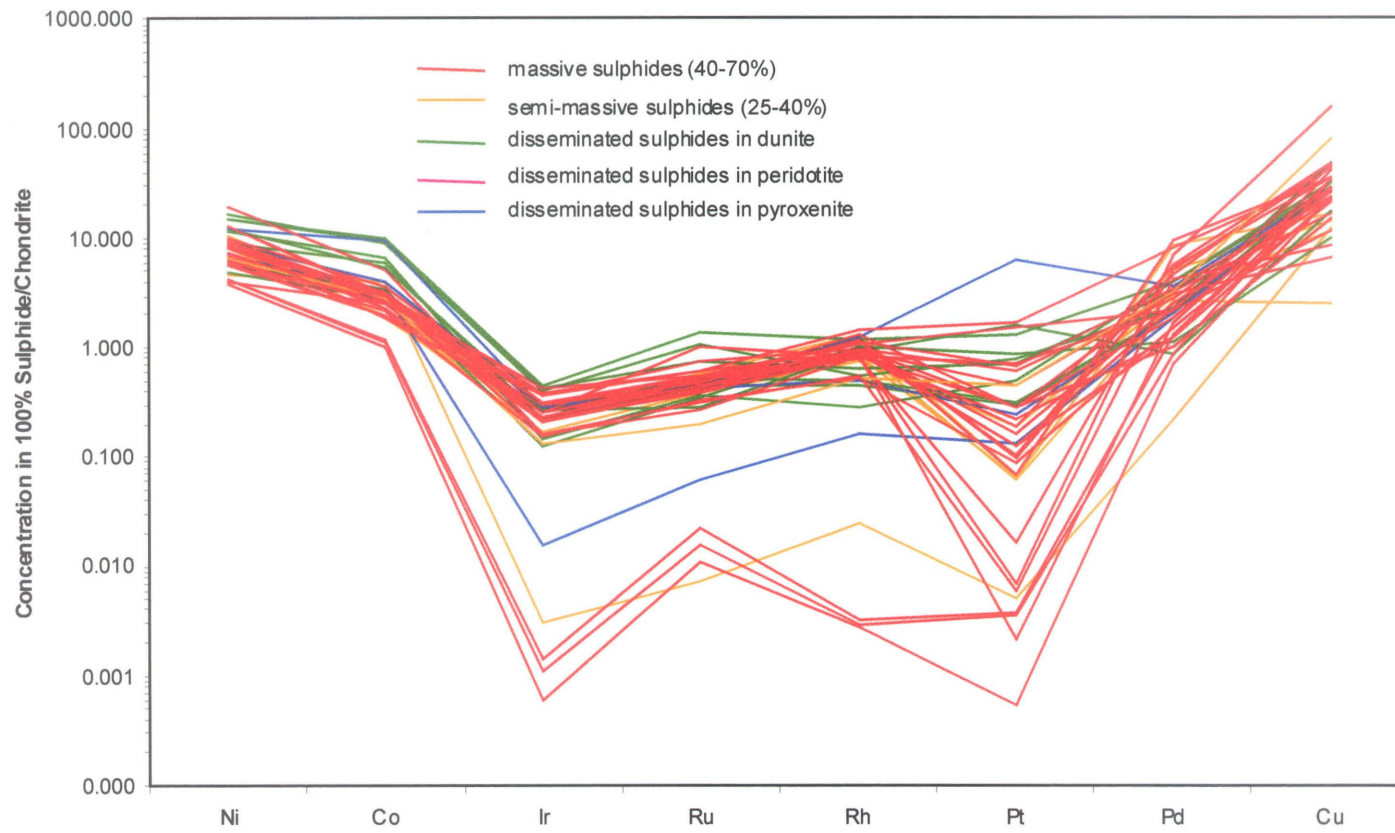


Figure 7.9. Chondrite-normalized plot of chalcophile element concentrations in samples from Thompson Mine. Data from CAMIRO (2000a).

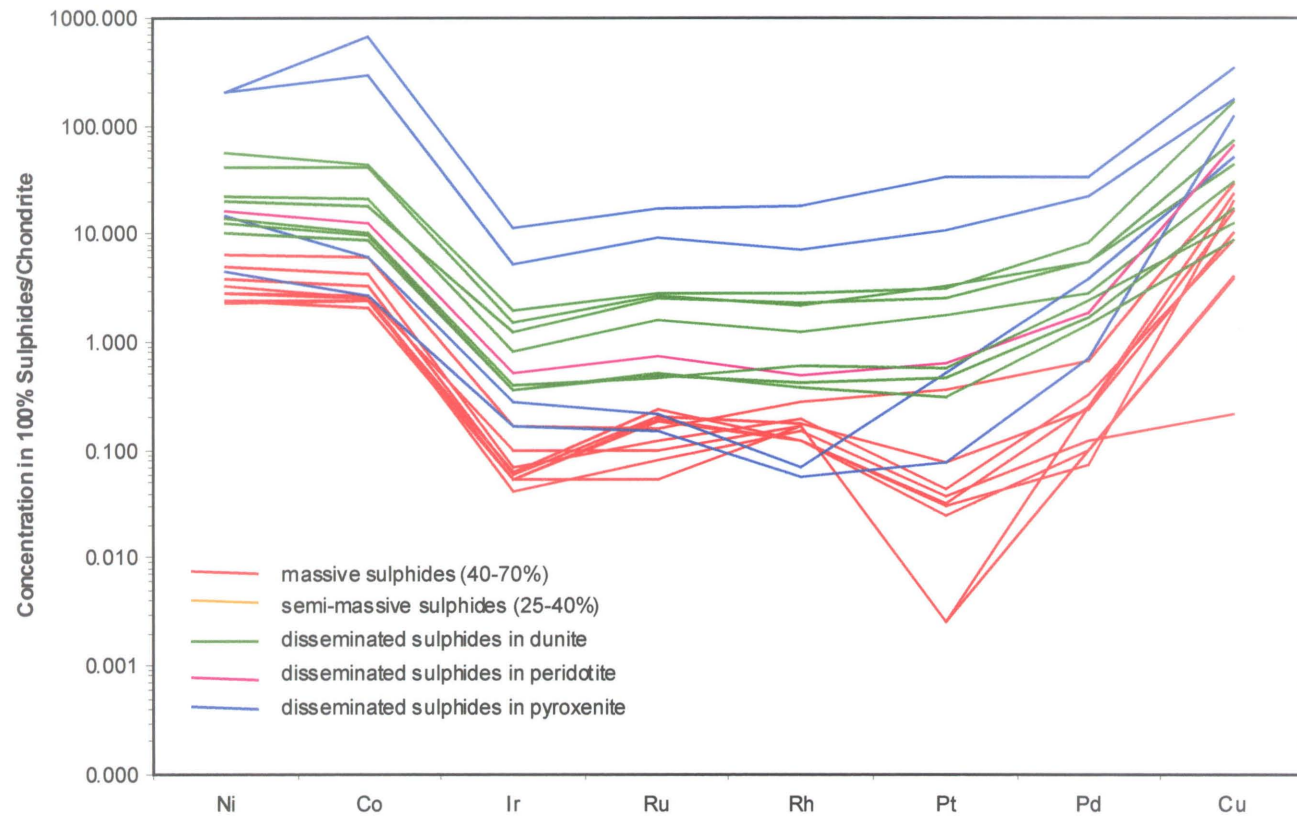


Figure 7.10. Chondrite-normalized plot of chalcophile element concentrations in samples from the Pipe deposit. Data from CAMIRO (2000a).

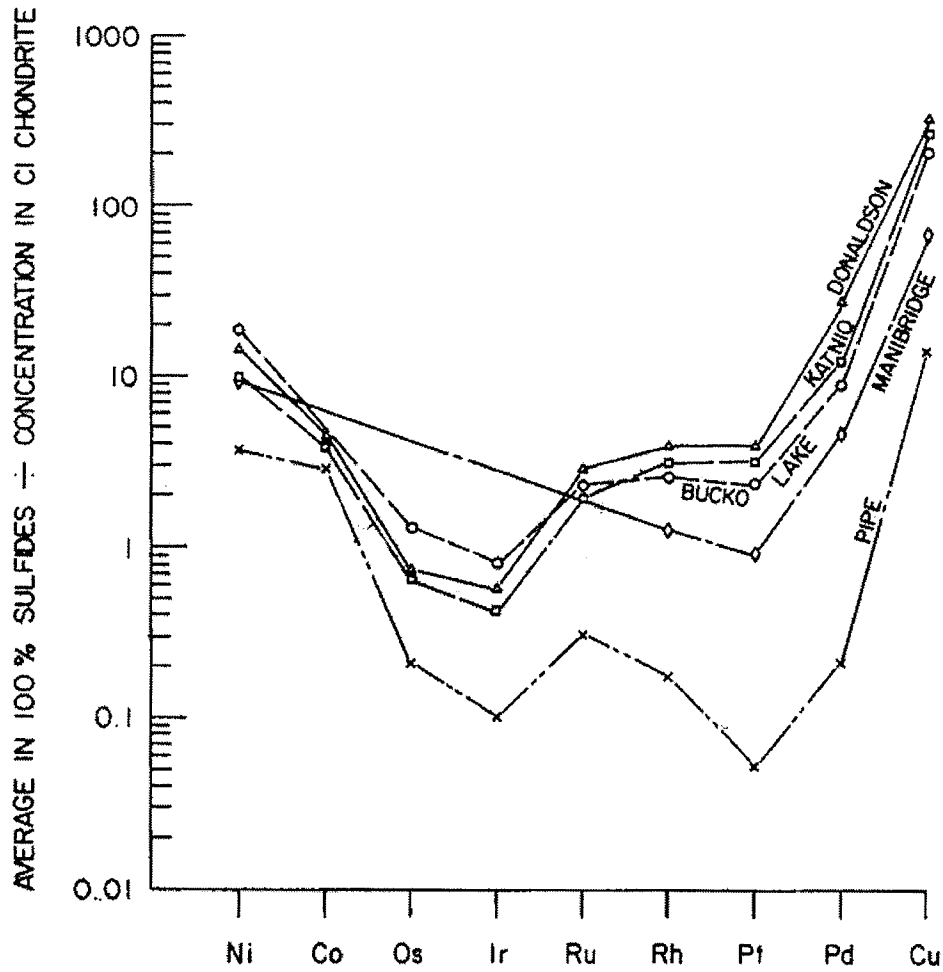


Figure 7.11. Analytical data for Co, Ni, Cu, and the PGE for Proterozoic komatiite-related deposits (from Naldrett, 1989). Data are recalculated to 100% sulphide and then normalized by the chondritic abundances for each element. Data from Naldrett and Duke (1980), Naldrett (1981), and Good (1985).

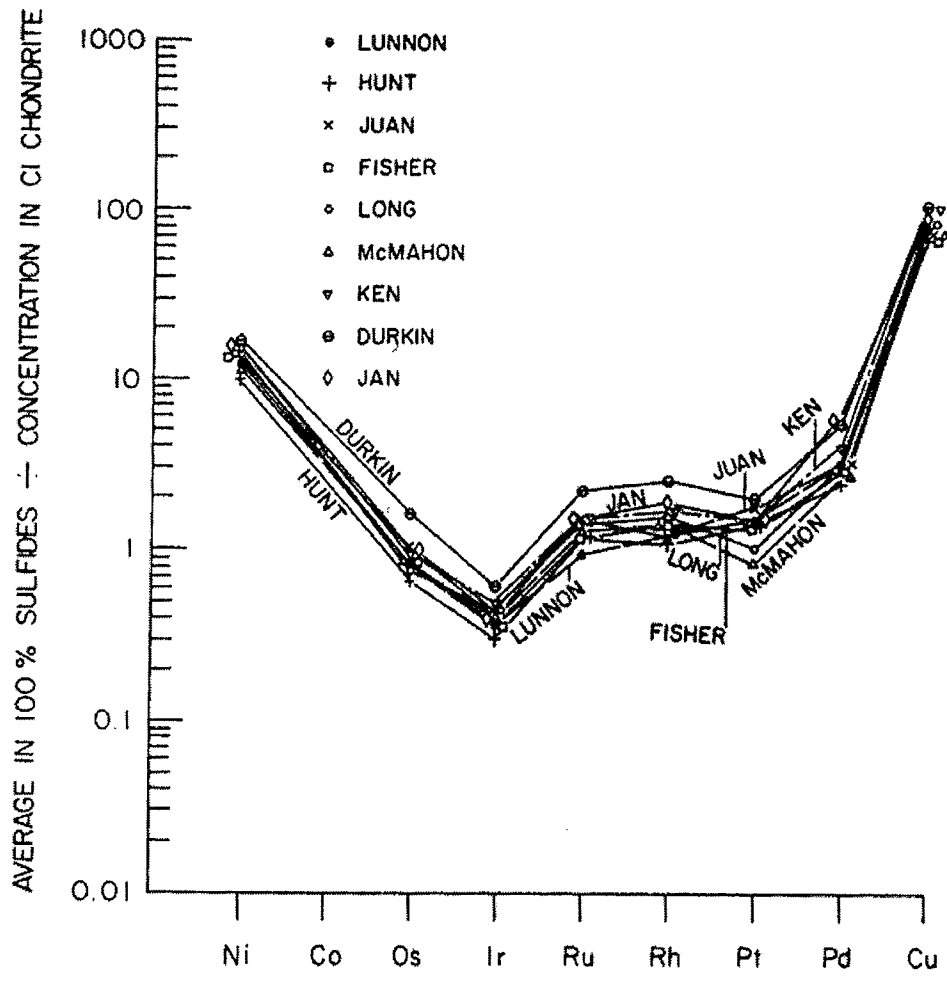


Figure 7.12. Chondrite-normalized plot for Archean komatiite-related deposits from the Kambalda mining camp, Western Australia (from Naldrett, 1989). Data from Cowden *et al.* (1986).

absent (Naldrett, 1989). If the net-textured ores from Kambalda were subjected to the same metamorphic events as the massive Thompson, Birchtree, and Pipe ores, then they would have a negative Pt anomaly. However, this is not the case (see Figure 7.12). The lack of a negative Pt anomaly in Kambalda ores, as well as the lack of massive accumulations of sulphides, is consistent with the theory that the Kambalda ores were metamorphosed *in situ*, with little post-metamorphic deformation (Barrett *et al.*, 1977). The occurrence of boudinaged ultramafic bodies and remobilized massive sulphide horizons in the Thompson Nickel Belt deposits are a clear indication that the TNB ores have undergone more severe deformational events than the Kambalda ores. Therefore, the Pt anomaly in the TNB ores could possibly record post-magmatic modification (especially deformation and/or metamorphism) of the massive sulphide ores.

Geochemical data for massive mineralized sulphides in this study (Table 7.1), indicate that the Thompson 1D ores are chemically distinct from the other Thompson ores and the Birchtree ores. The 1D ore body has the highest Pd/Pt ratios, which average 92.90 (compared to 30.29 in 1C samples, 51.45 in T1 samples, and 24.22 in Birchtree samples). The 1D samples also have the highest Pd/Ir ratios, which average 17.90 (compared to 3.83 in 1C samples, 5.47 in T1 samples, and 1.69 in Birchtree samples). In light of the fact that the rocks from the 1D ore body have undergone extensive brittle deformation, the elevated Pd/Pt and Pd/Ir ratios could further indicate some post-magmatic modification of the massive ores from this part of the Thompson deposit.

Table 7.1. Chalcophile element and PGE data for massive and semi-massive sulphides from the TNB, normalized to 100% sulphides.

Sample	sulphide class	wt% Ni	wt% Co	ppb Ir	ppb Ru	ppb Rh	ppb Pt	ppb Pd	ppb Au	wt% Cu	wt% S	Pd/Ir	Pd/Pt	Ni/Co	Ni/Cu	Pd/Ir av	Pd/Pt av
Thompson 1C ore body																	
JL98-1C-19A	SMS-SED	8.57	0.15	129	421	137	9	259	4	0.29	33.30	2.00	29.31	56.21	29.34	3.83	30.29
JL98-1C-20	MS-SED	8.40	0.11	144	468	134	8	298	14	0.06	37.30	2.07	37.38	76.82	131.02		
JL98-1C-25A	MS-SED	7.36	0.15	180	477	158	25	693	11	0.37	34.60	3.85	27.77	50.33	19.73		
JL98-1C-25B	MS-SED	7.53	0.17	157	451	160	33	765	21	0.35	33.60	4.87	23.43	44.27	21.78		
JL98-1C-25D	MS-SED	9.22	0.21	154	477	166	29	977	16	0.33	35.50	6.36	33.54	44.19	28.07		
Thompson 1D ore body																	
JL98-1D-07	MS-SED	11.42	0.20	102	127	148	9	1799	36	0.33	39.90	17.71	197.38	57.76	34.83	17.90	92.90
JL98-1D-14	SMS-SED	12.03	0.17	53	294	128	11	1162	55	0.35	33.80	22.12	102.00	70.90	34.01		
JL98-1D-18A	SMS-SED	11.50	0.10	156	249	186	494	2173	131	0.12	27.40	13.93	4.40	113.03	98.18		
JL98-1D-20	SMS-SED	13.45	0.16	67	115	108	18	1199	34	0.22	31.50	17.86	67.84	86.15	61.95		
Thompson T1 mine																	
JL98-T1-09A	MS-UB	7.98	0.18	4	4	38	5	395	10	0.28	38.20	100.65	77.11	44.78	28.44	5.47	51.45
JL98-T1-12	MS-UB	7.10	0.15	24	38	29	2	140	1	0.21	37.90	5.87	82.98	46.18	34.20	(n=3)	
JL98-T1-19	MS-SED	5.81	0.10	121	408	143	32	622	57	0.04	35.00	5.13	19.54	55.41	152.81		
JL99-T1-35	MS-SED	0.85	0.12	174	489	220	36	942	19	0.28	35.50	5.41	26.17	7.01	3.06		
Birchtree Mine																	
JL98-BT-02	MS-UB	5.11	0.21	60	154	28	27	92	22	0.06	37.30	1.54	3.35	24.22	83.81	1.69	24.22
JL98-BT-10	MS-SED	4.35	0.18	12	49	10	1	20	0	0.04	37.70	1.64	32.25	23.83	99.25		
JL98-BT-15	MS-SED	5.85	0.21	65	169	32	3	143	5	0.12	33.30	2.20	49.63	27.70	50.06		
JL98-BT-16B	MS-UB	5.17	0.16	37	115	25	3	61	1694	0.91	32.60	1.65	22.59	31.94	5.67		
JL98-BT-20	MS-UB	5.07	0.20	52	147	38	6	74	14	0.16	37.00	1.42	13.28	25.53	31.55		

7.5 Trace Element Concentrations

In addition to elevated platinum group element ratios, the Thompson 1D ores contain As, Bi, and Pd concentrations that are an order of magnitude higher than the ores from the Thompson 1C ore body, Thompson T1 fold nose, and Birchtree Mine (Table 7.2). Arsenic concentrations in the 1D ore body range from 411 to 510 ppm, compared to 34 to 97 ppm in 1C samples, 13 to 114 ppm in T1 samples, and 8 to 96 ppm in Birchtree samples. The elevated As in the 1D samples correlates with the occurrence of paragenetically late pyrite, which can contain up to 409 ppm As in the massive ores (Appendix 4), and the occurrence of euhedral to subhedral grains of gersdorffite (NiAsS). The rare mineralization of niccolite (NiAs) associated with gersdorffite has also been noted in the Thompson ores (e.g. thin section T119 from the T1 Mine).

There is a positive correlation between Bi and Pd in the Thompson and Birchtree massive sulphide samples (Figure 7.13). Bismuth concentrations are elevated in the 1D samples (28 to 41 ppm) in comparison to 1C samples (1 to 5 ppm), T1 samples (4 to 6 ppm), and Birchtree samples (0 to 2 ppm). Palladium concentrations are also elevated in the 1D samples (1162 to 2173 ppb) in comparison to 1C samples (259 to 977 ppb), T1 samples (140 to 942 ppb), and Birchtree samples (20 to 143 ppb). The elevated Bi and Pd concentrations in the 1D ores can largely be attributed to the late mineralization of Pd-bearing bismuthotellurides, which were identified by scanning electron microscope (Figure 7.14). The exact composition of these minerals was not determined. The observed bismuthotellurides are typically associated with pentlandite; however, they are also hosted

Table 7.2. Trace element data (un-normalized) for massive and semi-massive sulphides from the TNB.

Sample	sulphide class	wt% S	ppb Se	Se/S	ppm As	ppm Bi
Thompson 1C ore body						
JL98-1C-19A	SMS-SED	33.30	25200	756.76	34	1
JL98-1C-20	MS-SED	37.30	24500	656.84	44	3
JL98-1C-25A	MS-SED	34.60	31100	898.84	84	4
JL98-1C-25B	MS-SED	33.60	27600	821.43	97	4
JL98-1C-25D	MS-SED	35.50	32200	907.04	86	5
Thompson 1D ore body						
JL98-1D-07	MS-SED	39.90	42200	1057.64	425	41
JL98-1D-14	SMS-SED	33.80	31500	931.95	323	35
JL98-1D-18A	SMS-SED	27.40	26600	970.80	264	
JL98-1D-20	SMS-SED	31.50	22600	717.46	321	28
Thompson T1 mine						
JL98-T1-09A	MS-UB	38.20	22200	581.15	13	5
JL98-T1-12	MS-UB	37.90	34300	905.01	87	4
JL98-T1-19	MS-SED	35.00	24400	697.14	114	6
JL99-T1-35	MS-SED	35.50	32000	901.41	108	
Birchtree Mine						
JL98-BT-02	MS-UB	37.30	22300	597.86	49	1
JL98-BT-10	MS-SED	37.70	19000	503.98	34	0
JL98-BT-15	MS-SED	33.30	23000	690.69	71	2
JL98-BT-16B	MS-UB	32.60	15700	481.60	96	
JL98-BT-20	MS-UB	37.00	17400	470.27	82	2

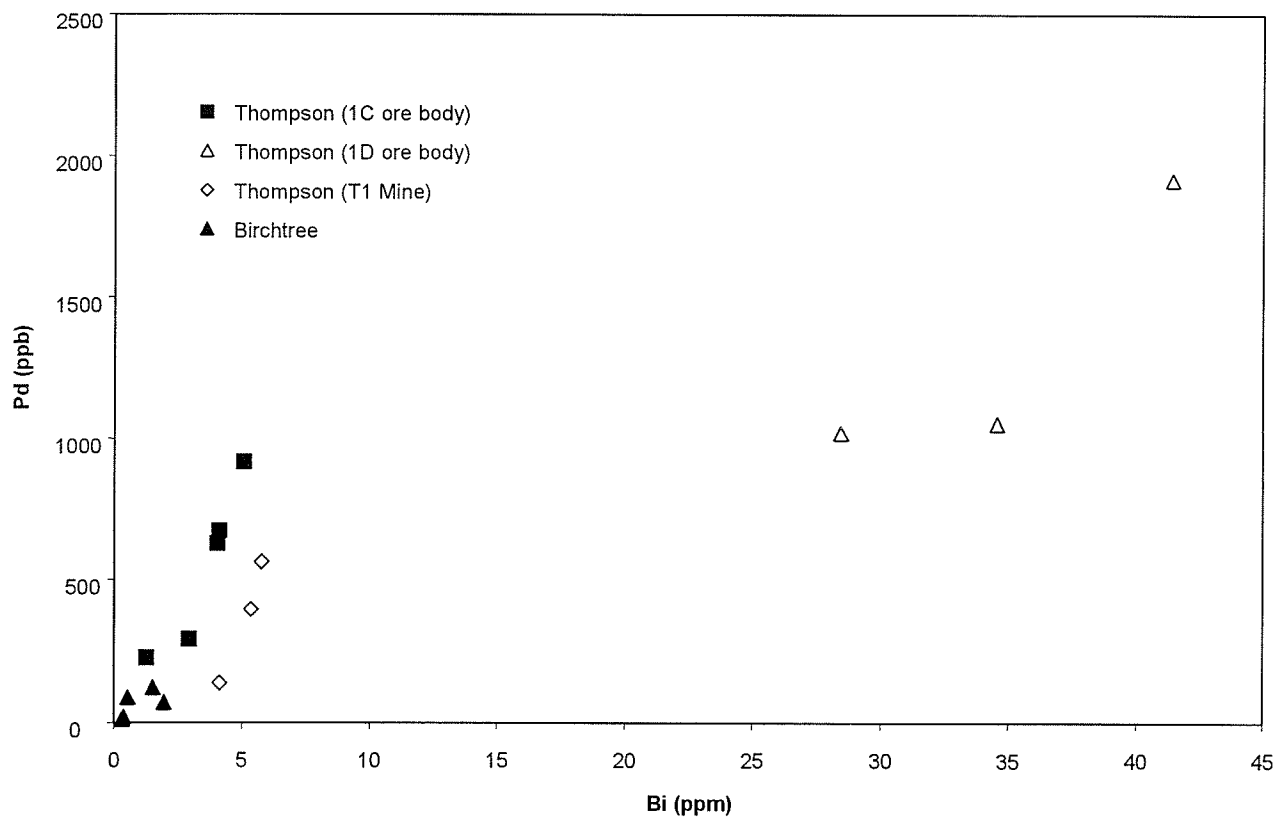
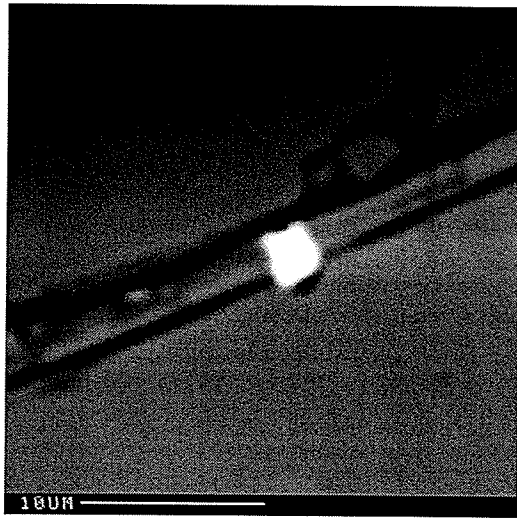
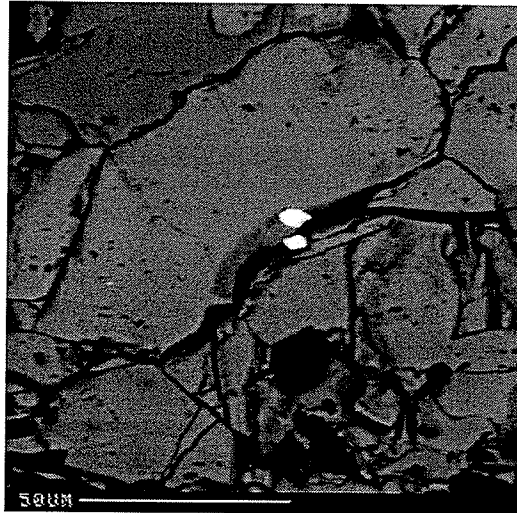


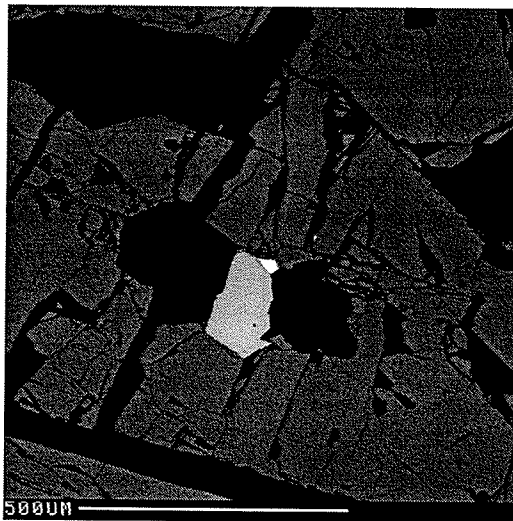
Figure 7.13. Pd and Bi concentrations in massive and semi-massive sulphide samples from the TNB.



a



b



c

Figure 7.14. Bismuthotellurides in massive sulphides from the 1D ore body, Thompson mine. a) Pd-Bi-Te-bearing mineral (white) in pentlandite. b) Bi-Te-bearing grain (white) in pentlandite. c) Bi-Te-bearing grain (white) adjacent to gersdorffite (light grey), in pentlandite.

by pyrrhotite. In one sample, a bismuthotelluride mineral was observed in association with euhedral gersdorffite; both minerals were hosted by pentlandite (Figure 7.14c).

A comparison of trace element concentrations in the Thompson 1D ore body, Birchtree, and Pipe 2 massive sulphides show a positive correlation between Ni and As (Figure 7.15), between Ni and Pd (Figure 7.16), and to a lesser extent, between Ni and Bi (Figure 7.17). These data suggest that the same processes that redistribute and concentrate As, Pd, and Bi may mobilize and concentrate nickel.

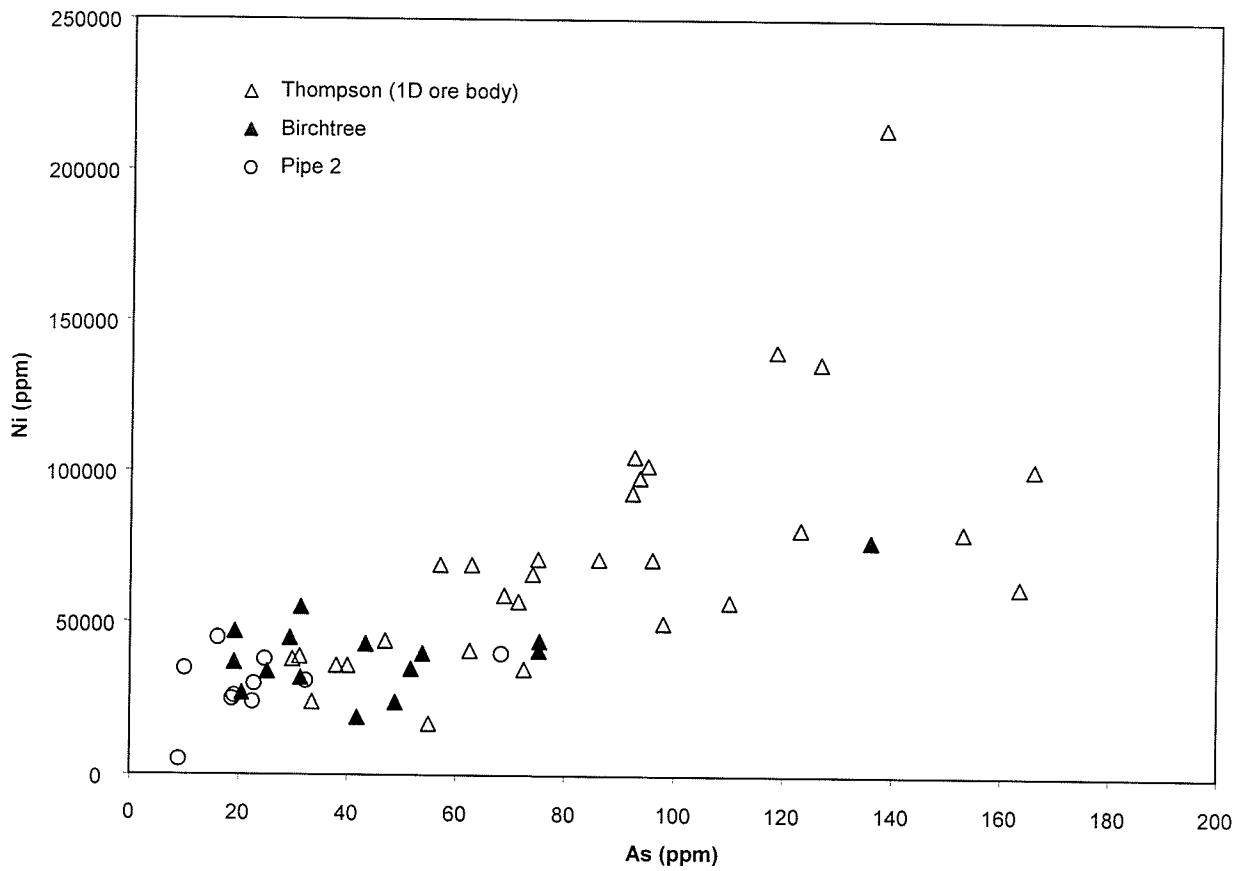


Figure 7.15. Ni and As concentration in massive and semi-massive sulphides from the TNB. Sulphide classes represented: MS-UB, MS-SED, SMS-SED.

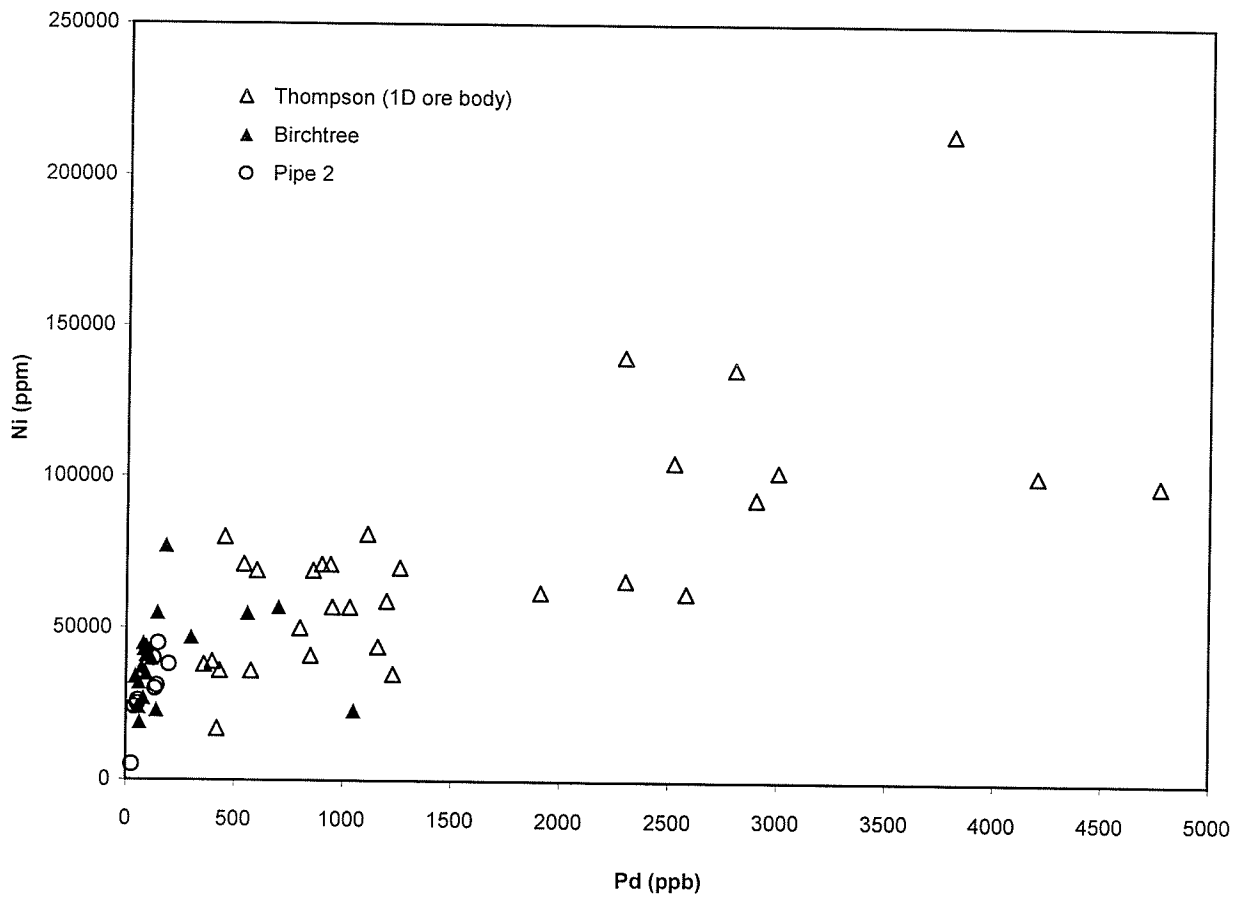


Figure 7.16. Ni and Pd concentration in massive and semi-massive sulphides from the TNB. Sulphide classes represented: MS-UB, MS-SED, SMS-SED.

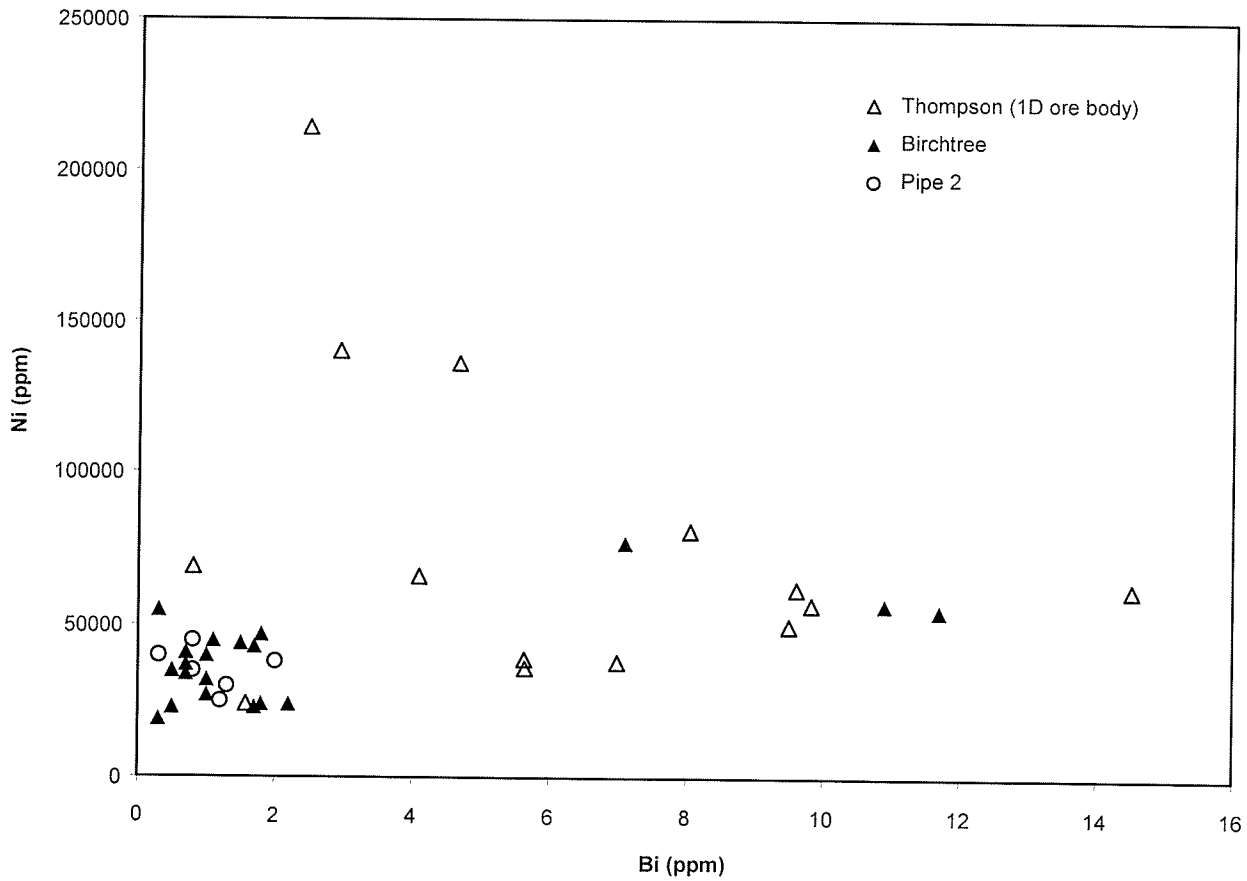


Figure 7.17. Ni and Bi concentration in massive and semi-massive sulphides from the TNB. Sulphide classes represented: MS-UB, MS-SED, SMS-SED.

CHAPTER 8: DISCUSSION

8.1 Metamorphic Textures in the TNB sulphides

The distribution of sulphide minerals in the massive ores from Thompson, Birchtree, and William Lake (MS-UB and MS-SED) shows evidence of metamorphic modification of the sulphides. In the Thompson Mine, particularly in the 1C ore body, massive sulphide horizons that occur both proximal and distal to ultramafic sills commonly consist of coarse-grained equant to ovoid pyrrhotite and pentlandite grains that are segregated into cm-scale bands (e.g. Figure 5.13b). Massive sulphide ore bodies that have undergone amphibolite facies metamorphism commonly show a pronounced planar fabric defined by the segregation of pentlandite and pyrite-rich bands on a scale of millimetres to centimetres (Barnes and Hill, 2000). Barrett *et al.* (1977) observed similar layering of coarse-grained pyrrhotite and pentlandite in the massive ores of the Nepean Mine, Western Australia. The authors attribute the banding to the segregation of more ductile pyrrhotite from pentlandite during deformation of *mss*-poor ore, prior to peak metamorphism. During peak metamorphism, the banded sulphides annealed, resulting in equant grains of pyrrhotite and pentlandite. Deformation of pyrrhotite-pentlandite ore, prior to peak metamorphism, is thus inferred for the banded ores of the Thompson deposit.

The concentration of chalcopyrite along the contact between massive sulphide horizons and the hosting metasediments is indicative of migration of Cu during metamorphism, rather than fractionation during magmatic cooling (Barrett *et al.*, 1977). The pyrite-chalcopyrite symplectites in the massive ores may be a result of cooling of a

metamorphically generated sulphide phase. During metamorphism, chalcopyrite-rich areas of the ore may have reverted to pyrite plus *iss* or a Cu-rich *iss* may have exsolved out of a metamorphic Fe-Ni-Cu-S *mss*; chalcopyrite may have then been re-formed by the reaction of *iss* with pyrite at lower, post-metamorphic temperatures (Barrett *et al.*, 1977).

The crystallization of euhedral to subhedral gersdorffite and pyrite among annealed pentlandite and pyrrhotite grains show that these minerals crystallized late in the paragenetic sequence. These observations indicate that alteration of the massive ores occurred prior to their final equilibration.

8.2 Discussion of Chalcophile Element Data

8.2.1 *Platinum Anomaly in TNB Massive Sulphides*

The Pt depletion in the Birchtree, Thompson, and Pipe massive ores (Figures 7.8, 7.9, and 7.10, respectively) indicates that Pt partitioned differently than the other platinum group elements. The partitioning of Pt may be attributed to:

- 1) The fractionation of noble metals into specific sulphide minerals.
- 2) Fractionation of Pt and Pd under reducing conditions.
- 3) Metamorphic or metasomatic processes that mobilized Pt from the massive ores.

Chyi and Crocket (1976) determined that, relative to pyrrhotite, Pd and Au are concentrated in pentlandite by a factor of ~14, and Pt and Ir are concentrated in chalcopyrite by a factor of ~6. The association of Pd and Au in pentlandite is attributed to solid solution of these metals in pyrrhotite at magmatic temperatures, and diffusion of the metals into pentlandite at relatively low subsolidus temperatures. The Pt and chalcopyrite

association suggests that Pt tends to fractionate in a Cu-rich magmatic liquid. The Pt anomaly could be related to the Cu-poor nature of the ores; evidence for what might be a complementary fractionated Cu-rich (and/or Pt-rich) magma has not been found in the Thompson region. However, if both Pt and Ir preferentially migrate with Cu, a negative Ir anomaly would likely occur with the negative Pt anomaly. Although a few of the Thompson massive sulphide samples seem to have a small negative Ir anomaly accompanying a negative Pt anomaly (Figure 7.9), the majority of the samples only show a Pt depletion. Therefore, the Pt anomaly in the Thompson, Birchtree, and Pipe samples may not necessarily be associated with the fractionation of a Cu-rich magma.

Experimental data from Bezmen *et al.* (1998) indicate that Pd and Pt can fractionate under strongly reducing conditions at magmatic temperatures. A decrease in oxygen fugacity in equilibrium with a hydrous silicate melt results in a considerable decrease in Pd solubility (Figure 8.1). Under the same conditions, the solubility of Pt also decreases, but near magnetite-wustite buffer at $X_{\text{H}_2\text{O}} \approx 0.1$, the slopes of the solubility curves for Pd and Pt diverge. This divergence is caused by the increase of water solubility in a silicate melt in the presence of hydrogen. These data suggest that the solubility of Pt increases under reducing conditions. Given the occurrence of graphitic schists in the Ospwagan Group stratigraphy, and the ubiquitous graphite in banded metasedimentary sulphides, it is possible that the ores may have been formed under reducing conditions. Incorporation of the graphite may have reduced the magma sufficiently to allow the Pt to remain in the silicate fraction of the melt.

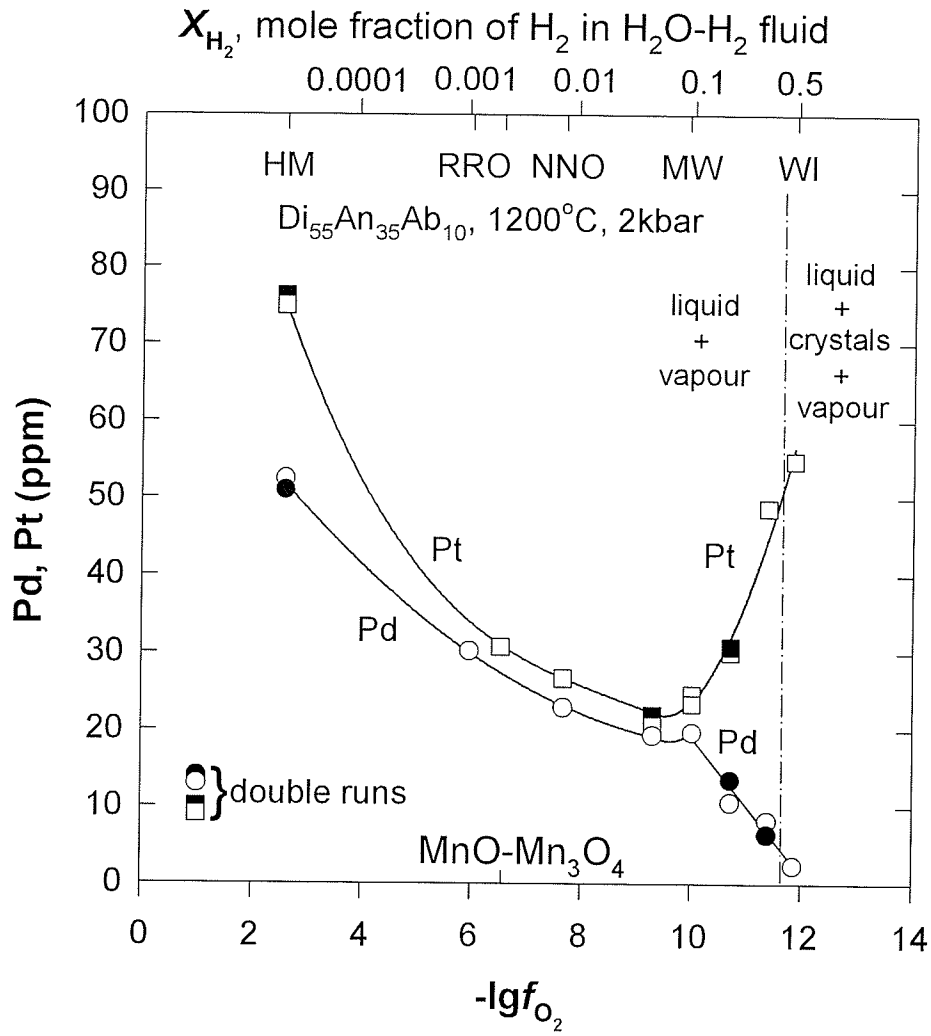


Figure 8.1. Solubility of Pd and Pt in the hydrous silicate melt *versus* oxygen fugacity (from Bezmen *et al.*, 1998).

It is also possible that Pt may have fractionated from the other PGE, particularly Pd, due to metamorphic or metasomatic processes. The argument for this hypothesis is presented in the following three sections.

8.2.2 *Effect of R Factor on the Distribution of Chalcophile Elements*

The range of chondrite-normalized metal concentrations for the Birchtree, Thompson, and Pipe massive sulphide samples is an order of magnitude lower than that of the other Archean and Proterozoic magmatic sulphide samples (Naldrett, 1989). Naldrett *et al.* (1979) attributed the significantly lower amounts of Cu, Ni, PGE, and Au in the Pipe deposit in comparison to other komatiite-related ores to a low magma/sulphide ratio (R factor) for Pipe ultramafic magma. That is, upon intrusion of the Pipe ultramafic sill, a high proportion of sulphide reacted with a relatively small amount of magma. This is consistent with the hypothesis that Pipe ores are the product of the localized assimilation of non-nickeliferous country-rock sulphide by a sulphide-undersaturated magma (Naldrett *et al.*, 1979).

The R factor model (Campbell and Naldrett, 1979), accounts for the fact that a metal will have a distribution coefficient (D) for the partitioning of that metal between an immiscible sulphide liquid and a silicate melt. If two metals have similar values of D , then variations in R would cause variations in the absolute levels of metals in sulphide ore without changing the ratio of one metal to the other greatly. However, if the two metals had greatly differing values in D , then variations in R would cause the ratio between the two metals to vary significantly (Figure 8.2). Distribution coefficients ($D^{\text{sulphide/silicate}}$) for

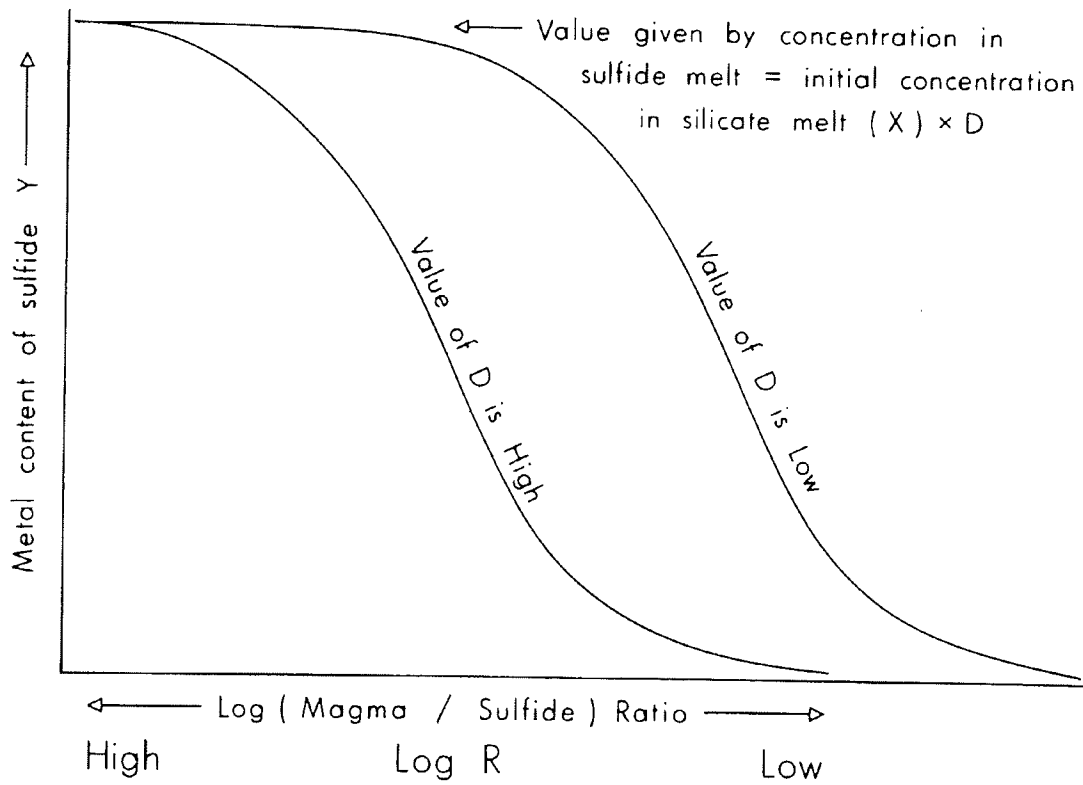


Figure 8.2. Schematic representation of the variation of the metal content of a sulphide melt as a function of R (magma/sulphide ratio) and D (Nernst distribution coefficient) (from Naldrett, 1989).

various chalcophile elements in natural and experimental mafic and ultramafic systems are: $D_{Ni} = 100-840$, $D_{Cu} = 50-1400$, $D_{Co} = 5-100$ (Leshner and Stone, 1996). Recent experimental data from Barnes and Maier (1999) show that average distribution coefficients for Pt and Pd are: $D_{Pt} = 10^4$, and $D_{Pd} = 10^4$. Because Pt and Pd partition into a sulphide melt much more readily than Ni, Cu, or Co, a low R factor for the Pipe deposit would result in a significant depletion in Pt and Pd. This is based on the assumption that the distribution coefficients for Pt and Pd are correct.

According to mass-balance calculations assessing the effect of mixing magmatic sulphides with sedimentary sulphides, as outlined by Bleeker (1990, p. 322-328), the Ni/Co ratio of massive magmatic sulphides exponentially increases with increased mixing of barren sedimentary sulphides and magmatic sulphides. This increase in Ni/Co ratio is in accordance with the fact that Ni, being more chalcophile than Co, will tend to enter an evolving sulphide liquid whereas Co will tend to stay in the parent silicate magma. Thus, if two massive sulphide bodies of similar texture and lithological association had different Ni/Co ratios, one could argue that the magmas that produced these two massive bodies had incorporated different amounts of sedimentary sulphides. For example, the Ni/Co ratios of Birchtree ores and Thompson T1 fold nose ores that are classified as MS-UB (massive sulphides in ultramafic breccia) are compared here. These breccia ores, which are proximal to their presumed ultramafic host rocks, are interpreted to be the best-preserved massive magmatic sulphides among the rocks sampled in this thesis. Birchtree breccia ores have Ni/Co ratios ranging from 24 to 32 (samples JL98-BT-02, JL98-BT-16B, and JL98-BT-20, Table 7.1), while Thompson T1 fold nose ores have Ni/Co ratios of ~45 (samples JL98-T1-09A and JL98-T1-12, Table 7.1). These data suggest that the

Birchtree ores may have less of a sedimentary sulphide component than the Thompson ores, i.e. a lower R factor.

The Birchtree and Thompson deposits can be further distinguished based on Ni/Co ratios of pentlandite grains from category DS-U (disseminated sulphides in ultramafic rocks). In disseminated sulphides with the assemblage pyrrhotite-pentlandite-magnetite, Co will partition into pentlandite, provided that pyrite is absent. Birchtree pentlandite grains in such an assemblage have Ni/Co ratios ranging from 6 to 27, while Thompson pentlandite grains in a similar assemblage have Ni/Co ratios ranging from 38 to 54 (Appendix 3). The marked difference between the Ni/Co values can be partially attributed to the fact that Birchtree pentlandite grains have 1 to 2 wt% Co, while Thompson pentlandite grains have <1 wt% Co. The low Ni/Co ratios in the Birchtree pentlandites could further indicate that the Birchtree magmas incorporated less sedimentary sulphide. Alternatively, these data could indicate that 1) the Birchtree magma is more fractionated than the Thompson magma, or 2) Thompson sulphides were enriched in Ni by metamorphic processes.

8.2.3 *Platinum Group Element Ratios*

Although the R factor model could partially explain the profile of the PGE plots for the Pipe deposit, it may not be able to explain the high Pd/Pt ratios of the Thompson and Birchtree massive ores (Table 7.1), compared to other massive sulphide deposits. Average Pd/Pt ratios for predominantly disseminated and net-textured Proterozoic sulphide ores (calculated from data compiled by Naldrett, 1989) are: Donaldson West, 3.76; Katiniq, 2.02; Bucko Lake, 2.04. Average Pd/Pt ratios for predominantly net-

textured Archean ores from the Kambalda mining camp (calculated from data compiled by Naldrett, 1989) are: Lunnon: 1.22; Hunt, 0.91; Juan, 1.02; Fisher, 1.23; Long, 1.59. In contrast to these disseminated and net-textured ores, average Pd/Pt ratios for massive and semi-massive sulphide ores from Birchtree and Thompson range from 24.22 to 92.90 (Table 7.1). Empirically, the differences in the Pd/Pt ratios between the massive ores and the disseminated to net-textured ores seem to correlate with a difference in ore texture. This textural distinction is further demonstrated in Figure 7.8, which shows the pronounced Pt depletion in Birchtree massive ores with respect to disseminated ultramafic-hosted Birchtree ores.

Theoretically, since Pt and Pd have the same partition coefficients ($\sim 10^4$), then Pd/Pt ratios for one magmatic sulphide deposit should be very similar to another magmatic sulphide deposit, even if they were produced at different R factors. If both the disseminated ores and the massive ores represent something approximating “primary” magmatic sulphides produced in the same event, then all the above Pd/Pt ratios should be similar (i.e., around 1.00 or 2.00). This assumption is based solely on the R factor model. Platinum typically behaves similarly to Pd in magmatic sulphide melts, yet Pt has clearly partitioned differently than Pd in the Thompson and Birchtree massive ores. This may indicate that a non-magmatic process is responsible for the high Pd/Pt ratios. Given that the Pt anomaly occurs only in the massive sulphides, and not in the ultramafic rocks of the Thompson Nickel Belt, it is more appropriate to attribute the Pd/Pt ratios to metamorphic and/or hydrothermal processes rather than “primary” magmatic processes.

8.2.4 PGE as Discriminants of Ore Genesis

The behaviour of Pd, in relation to other platinum group elements, particularly Pt and Ir, could help distinguish hydrothermal *versus* magmatic signature of sulphide ores. Barnes *et al.*, (1985) showed that hydrothermal alteration mobilizes Pd, the most soluble of the PGE. Sulphide ores from the Noril'sk deposit, believed to be magmatic ores that have been modified by some late-stage hydrothermal activity, have Pd/Pt ratios of about 3; the hydrothermal ores of the New Rambler Mine, Wyoming, have Pd/Pt ratios of about 18 (McCallum *et al.*, 1976). The enrichment of Pd relative to Pt in the New Rambler Mine is attributed to the tendency of Pd to preferentially form solution complexes with volatile elements (such as As, Sb, Te, and S) that fractionate to a low-temperature environment. The predominance of bismuthotellurides in the New Rambler Mine is consistent with a hydrothermal origin. Localization of the ore at the intersection of faults and shear zones suggests that fluids from dilatant fractures may have effectively focused activity of the mineralizing solutions.

Elevated Pd/Pt ratios for Thompson and Birchtree massive ores in this study (ranging from ~24 to 92) (Table 7.1), compared to ores of hydrothermal origin (e.g. Pd/Pt = ~18 at New Rambler Mine), may indicate that the Thompson Nickel Belt ores have been hydrothermally altered. However, it is important to note that the high Pd/Pt ratios in the Thompson Nickel Belt massive ores are largely the result of a pronounced depletion of Pt relative to all other PGE, more so than a pronounced enrichment of Pd in the ores.

Keays *et al.*, (1982) showed that Pd and Ir can be used to discriminate whether Australian Ni sulphide deposits associated with volcanic peridotites originated by a magmatic process or an ore forming-process aided by fluids (e.g. volcanic-exhalative,

hydrothermal/metasomatic, or metamorphic processes). The authors found that magmatic Ni sulphides contain high Ir and Pd contents, consistent with the Ir and Pd contents of their host rocks. In contrast, non-magmatic Ni sulphides contain extremely low Ir and low Pd when compared to magmatic ores. For example, typical magmatic Ni sulphide ore from Western Australia averages 1596 ppb Pd and 258 ppb Ir (normalized to 100 % sulphides); the hydrothermal Ni sulphides from the Otway propect, Nullagine, Western Australia average 76.4 ppb Pd and 0.8 ppb Ir. As Ir is an immobile element and is not readily leached or transported from source rocks, non-magmatic ores have much higher Pd/Ir ratios. The ores from the hydrothermal Otway prospect have an average Pd/Ir of 95.5, whereas ores from the magmatic Western Australian deposits have an average Pd/Ir of 6.19.

8.3 Fluid-Assisted Migration of Metals

8.3.1 Alteration of Thompson 1D ores

Fluid-assisted alteration is inferred specifically for the massive ores of the 1D ore body, Thompson Mine; these ores are interpreted to have undergone late brittle-ductile deformation. Massive ores from the 1D ore body have elevated Pd/Ir ratios (~18) in comparison to other areas in the mine (where Pd/Ir ranges from ~2 to 4). Although Pd/Ir ratios from unequivocal hydrothermal ores are typically >>20 (Keays *et al.*, 1982), there is a possibility that the originally magmatic 1D massive ores were modified by fluids.

The massive ores from the Thompson 1D ore body have slightly higher Se/S ratios than the Birchtree and Pipe massive ores (Figure 7.5). Hawley and Nichol (1959) showed that Se-enriched copper sulfide ores in the Noranda deposit are interpreted to have

acquired Se from vapors or later ore fluids during progressive fracturing and possibly recrystallization. The higher Se/S ratios in the Thompson 1D ores relative to the other Birchtree and Pipe ores may be the result of Se enrichment by late fluids. Alternatively, the Se/S ratios could reflect a lower degree of S loss from the Thompson ores, leaving a residual enrichment in selenium. The first explanation is most likely, as the sulphide minerals comprising the 1D massive ores have elevated absolute concentrations of Se compared to the minerals from other TNB deposits (Figures 6.15 and 6.16). These data indicate that the sulphide minerals from 1D became enriched in Se relative to S, rather than depleted in S relative to selenium.

Elevated Pd and Bi concentrations in the Thompson 1D ore, corresponding to the mineralization of Pd-bearing bismuthotellurides, could indicate fluid-assisted alteration of the ore. The fact that the ores have significant concentrations of As, attributed to the mineralization of late paragenetic phases like gersdorffite, niccolite and As-enriched pyrite, further suggests the possible modification of the ore by fluids. These fluids could have traveled through dilatant shear zones that prevail in that portion of the mine. Bleeker (1990) noted that the As concentrations of the Thompson deposit are anomalously high (>1000 ppm As) in samples that are associated with white vein quartz deposited along a fault that runs subparallel to the ore in the Thompson 1C pit. Fluid migration along this fault would have facilitated the mineralization of late paragenetic As-bearing phases.

The highly deformed Thompson 1D massive sulphides contain the highest Ni tenors among the deposits sampled in this thesis (Table 7.1). Deformation of massive sulphide ore may facilitate the permeability of the ores to As-, Pd- and Bi-enriched fluids that have complexed with nickel. With thermal metamorphism (above 300°C), Ni may be

incorporated into recrystallizing sulphide minerals. Naldrett *et al.* (1967b) showed that at temperatures as low as 300°C, pyrrhotite can accept in excess of 15 wt% Ni into solid solution. These observations indicate that elevated Ni contents in *mss* (e.g. 3 to 5 wt%) do not necessarily indicate deposition at magmatic temperatures. The higher degree of thermal metamorphism at Thompson, compared to Pipe and Birchtree (about 100 degrees higher; Bleeker, 1990), may have facilitated the incorporation of higher amounts of Ni into the sulphides comprising Thompson massive ore. As thermally metamorphosed sulphides cool, sulphide minerals may recrystallize with higher Ni concentrations than were possible before metamorphism.

Dillon-Leitch *et al.* (1986) found that dynamically metamorphosed rocks from the Donaldson West Deposit, Cape Smith Belt, Quebec, contained platinum group minerals and As-bearing minerals in late Cu-rich sulphide veins. The authors suggest that stress-induced dissolution of the sulphides could have released elements (such as Cu, Pd, Pt, Sb, Te, Au, Ag, Co, and As) that were transported hydrothermally and deposited in fractures. Similar processes may have caused the deposition of late paragenetic phases such as gersdorffite and Pd-bearing bismuthotellurides in the Thompson 1D ore body. The elevated Ni, As, Bi, and Pd concentrations of the Thompson 1D massive sulphides suggest that areas subjected to extreme deformation, particularly those areas containing shear zones and tension gashes, are most likely to facilitate the movement of metal-rich fluids and the subsequent crystallization of high Ni-tenor ores.

8.3.2 *The Role of Deformation in Fluid Movement*

In high-strain domains, tectonized planar sulphide ore bodies are commonly localized along major shear zones; these ore bodies can be up to 1-2 km from their original ultramafic host. Examples of such highly deformed deposits are at Perseverance (Barnes *et al.*, 1988) and the Widgiemooltha Dome in Western Australia (McQueen, 1981a, 1981b). McCallum *et al.* (1976) showed that sheared metagabbros from the New Rambler Mine, Wyoming, contained significantly higher concentrations of PGE and base metals than their unsheared counterparts. The authors attribute these observations to hydrothermal leaching of PGE and base metals from gabbroic rocks and the redeposition of the metals along shear zones to produce Pd- and Pt-rich sulphide ore.

Diffusion experiments show that S migrates much faster along fractures and in areas of high porosity, in comparison to more massive parts of the sample. Barrett *et al.* (1977) observed replacement of pyrrhotite and pentlandite by pyrite along grain boundaries in massive ore samples from the Juan Shoot, Western Australia; the authors attributed this mode of replacement to the movement of S along grain boundaries by vapour transport. The occurrence of pyrite lenses oriented parallel to the foliation of deformed massive ores in the Thompson Mine is interpreted as the result of stress-induced S diffusion. Fluids travelling along stress-induced zones of weakness in the Thompson massive ores could have facilitated the movement of S in the deposits.

This study shows that disseminated ultramafic-hosted sulphides contain predominantly hexagonal pyrrhotite, whereas associated massive sulphides contain predominantly monoclinic pyrrhotite; a metamorphically-induced transformation from hexagonal to monoclinic pyrrhotite is inferred. A sulphurization process could facilitate a

conversion of hexagonal pyrrhotite to monoclinic pyrrhotite in the massive ore horizons of the Thompson Mine. Furthermore, sulphurization or a similar vapour phase transformation could possibly aid the mobilization and concentration of Ni in highly deformed areas.

As illustrated in the 1C type section (Chapter 6.2), pentlandite grains from massive ores that have undergone higher degrees of deformation have higher Ni/Co ratios than their less deformed equivalents. Birchtree pentlandites from massive ultramafic breccia ores are markedly low ($\text{Ni/Co} < 40$) in comparison to the Thompson 1D pentlandites from massive sediment-hosted ores ($\text{Ni/Co} > 60$). Furthermore, whole-rock Ni/Co ratios from the Thompson 1D massive ores are elevated in comparison to the Birchtree and Pipe ores. These differences in Ni/Co ratios could reflect the higher degree of dislocation of the Thompson ores from their parent ultramafic rocks.

The high Ni tenors of the Thompson 1D ores, in comparison to the Pipe and Birchtree ores, may also be attributed to the more extensive remobilization of the Thompson ores from their ultramafic source. Some massive sulphide bodies in the Birchtree Mine have Ni tenors as high as those in Thompson, but these are typically distal from their ultramafic source (Gary Sorensen from INCO, pers. comm.). These observations are consistent with the presumption that fluids travelling through permeable pathways in attenuated ores can mobilize and redeposit nickel.

8.3.3 Compositional and Mineralogical Haloes

As shown in a type section from the Thompson 1C ore body, Ni concentrations in pyrrhotite and co-existing pentlandite grains that are disseminated within ultramafic rocks

increase with increasing serpentinization (Figures 6.3 and 6.4). Other authors have documented this phenomenon. Donaldson (1981) showed that magmatic disseminated Ni sulphide ores in dunites were significantly upgraded in sulphide Ni content with serpentinization. Barrett *et al.* (1977) found that disseminated sulphides from the Yilgarn Block, Western Australia, were more Ni-, Co-, and S-rich than co-existing sulphide-rich ores. These authors attributed these data to the loss of Ni from the silicate phase and the uptake Ni by the sulphide phase during serpentinization, combined with an increase in f_{O_2} and f_{S_2} during metamorphism.

In this study, metasedimentary pyrrhotite and pentlandite grains from the Thompson 1C ore zone were enriched in Ni (>0.2 wt % Ni) within about 20 metres of the ultramafic sill and within about 20 metres of the adjacent massive sulphide horizons (Chapter 5.4). This Ni enrichment in pyrrhotite and pentlandite coincides with an increased modal percentage of pentlandite in the metasediments. Monoclinic pyrrhotite dominates over hexagonal pyrrhotite in the massive sulphides and in metasediments within tens of metres of the massive sulphides. The Ni halo around the massive sulphide horizons is therefore interpreted to be both compositional and modal.

During high-temperature metamorphism, new mineral assemblages and metamorphic textures can be recognized around ore-masses. Syngenetic compositional haloes around metamorphosed deposits have been studied. Nesbitt and Kelly (1980) and Nesbitt (1982) showed that at the height of metamorphism, $\log f_{S_2}$ and $\log f_{O_2}$ within the orebodies at Ducktown, Tennessee, were -2.5 and -18.5 , respectively, whereas the values in the country rocks were -7.0 and -21.4 , respectively. These data show that the ore

bodies were more oxidizing and more sulphidizing than the host rocks, causing oxygen and S to move from the ore to the adjacent rocks.

Work by Vaughan *et al.* (1971) on pyrrhotite grains from the Strathcona Mine, Sudbury, showed that Ni concentration in both hexagonal and monoclinic pyrrhotites increased toward the centre of the ore body and decreased toward top and bottom. Nickel concentration in pentlandite grains from the same ore zone also increased toward the centre of the ore body, accompanied by a decrease in Co concentration. The Ni concentration of pentlandite is dependent on the activities of FeS and NiS in coexisting pyrrhotite and pentlandite (Vaughan *et al.*, 1971); as a_{FeS} decreases and pyrrhotite becomes more S-rich, Ni concentration in coexisting pentlandite increases. Pentlandite grains within metasediments in the Thompson 1C ore body contain increasing Ni concentrations with increasing proximity to massive ore (Figures 6.6 and 6.7). These observations may suggest that the metasediments hosting the massive ore experienced an increase in sulphur fugacity during its crystallization history. This increase in sulphur fugacity may facilitate the mobilization of Ni from the massive ore to the metasediments, and the subsequent crystallization of Ni-enriched metasedimentary sulphides.

8.4 Revised Model for the Thompson Nickel Belt Sulphides

A revised ore deposit model for the Thompson Nickel Belt deposits is presented here to account for trends in the texture and the chemistry of the sulphides (Figure 8.3). The stages listed below represent major events in the history of the deposition and post-magmatic modification of the ores.

Stage 1: Ultramafic magmatism associated with a rifting event led to the intrusion of ultramafic sills into the Oswagan Group metasediments. Based on the similarity in Se/S ratios from the Birchtree and Thompson ores, the two deposits may have been generated from a similar magmatic source. However, pentlandite grains disseminated within ultramafic rocks from Birchtree have distinctly low Ni/Co ratios in comparison to Thompson pentlandite grains of similar texture. This distinction in Ni/Co ratios could indicate that: 1) the Birchtree magmas had a different composition from the Thompson magmas, or 2) the Birchtree magmas had a lower *R* factor than the Thompson magmas.

Given the structural, lithological, and chemical similarities in the Birchtree and Pipe deposits, both deposits are considered to have undergone similar magmatic processes. The Pt depletion in massive sulphides from the two deposits, as well as the Thompson deposit, could indicate that the ultramafic magmas that produced the massive ores were intruded in reducing conditions. Such conditions would be encountered in the graphitic units of the Oswagan Group, thereby indicating that the ores may largely be stratigraphically controlled.

The high Se/S ratios of the William Lake ultramafic bodies, in comparison to the rest of the TNB bodies, suggests that the magmatic source for William Lake may have been more juvenile than the sources that generated the Birchtree, Pipe, and Thompson ores.

Stage 2: *Folding and stretching of the massive magmatic sulphides and boudinage of the ultramafic boudins, accompanied by high-grade metamorphism (>600 °C).*

Upon mobilization of the sulphides from their ultramafic hosts, it is possible that fluids, generated from the metamorphism of the ore zones, mobilized Ni along strike of the ore horizon and away from the base of the ultramafic rocks. These metamorphic fluids may have also caused Pt to partition from the other PGE; how the Pt partitioned, or where the bulk of the Pt is residing in the mines is uncertain.

Birchtree and Pipe massive breccia ores are not as highly metamorphosed, nor mobilized as far from their ultramafic host rocks as the Thompson massive ores. The markedly higher Ni/Co ratios in the Thompson massive ores, in comparison to the Birchtree and Pipe massive ores, may reflect a metamorphic enrichment of Ni in Thompson relative to Birchtree and Pipe. However, these ratios may also reflect 1) a difference in the initial compositions between Thompson and Birchtree/Pipe magmas, or 2) a difference in *R* factor. It is possible that the higher Ni tenor of Thompson ore, relative to Birchtree and Pipe ore, is a result of both primary magmatic processes and metamorphic alteration.

Stage 3: *Late stage ductile-brittle deformation of the sulphides.* The cooled (or cooling) massive sulphides were locally concentrated into late tension gashes and shear zones, and milled to finer-grained sulphides. Unsheared portions of the massive sulphide horizons remain coarse-grained. In the Thompson 1D ore body, the extent of shearing and brittle deformation appears to be on a mine scale, based on the predominance of fine-grained sulphides in association with extreme brecciation of the host rocks in that part of the mine. The Thompson 1D ore body is interpreted to represent the most remobilized sulphides in the Thompson structure, while the T1 fold nose area hosts the most preserved or least deformed sulphides in the Thompson deposit. The elevated As, Bi, Pd, and Ni

concentrations in the Thompson 1D ore body, compared to the rest of the Thompson Mine, suggest that the deposition of these elements is structurally and metasomatically controlled.

Stage 4: *Final cooling of the sulphides after a high temperature metamorphic event.* Fine-grained, milled sulphides that were sampled from late tension gashes in the Thompson deposit show evidence of recrystallization. These observations suggest that a high temperature metamorphic event followed late ductile-brittle deformation of the sulphides. During final cooling of the sulphides from high temperatures, the following processes may have occurred:

- crystallization of Ni-enriched pyrrhotite and pentlandite in the most deformed sulphides
- crystallization of late paragenetic bismuthotellurides and arsenic-bearing minerals
- migration of Cu into stringers at the contacts between massive sulphide horizons and metasedimentary hosts
- development of chalcopyrite-pyrite symplectite textures
- fluid-assisted diffusion of Ni from massive sulphide horizons to the hosting metasediments

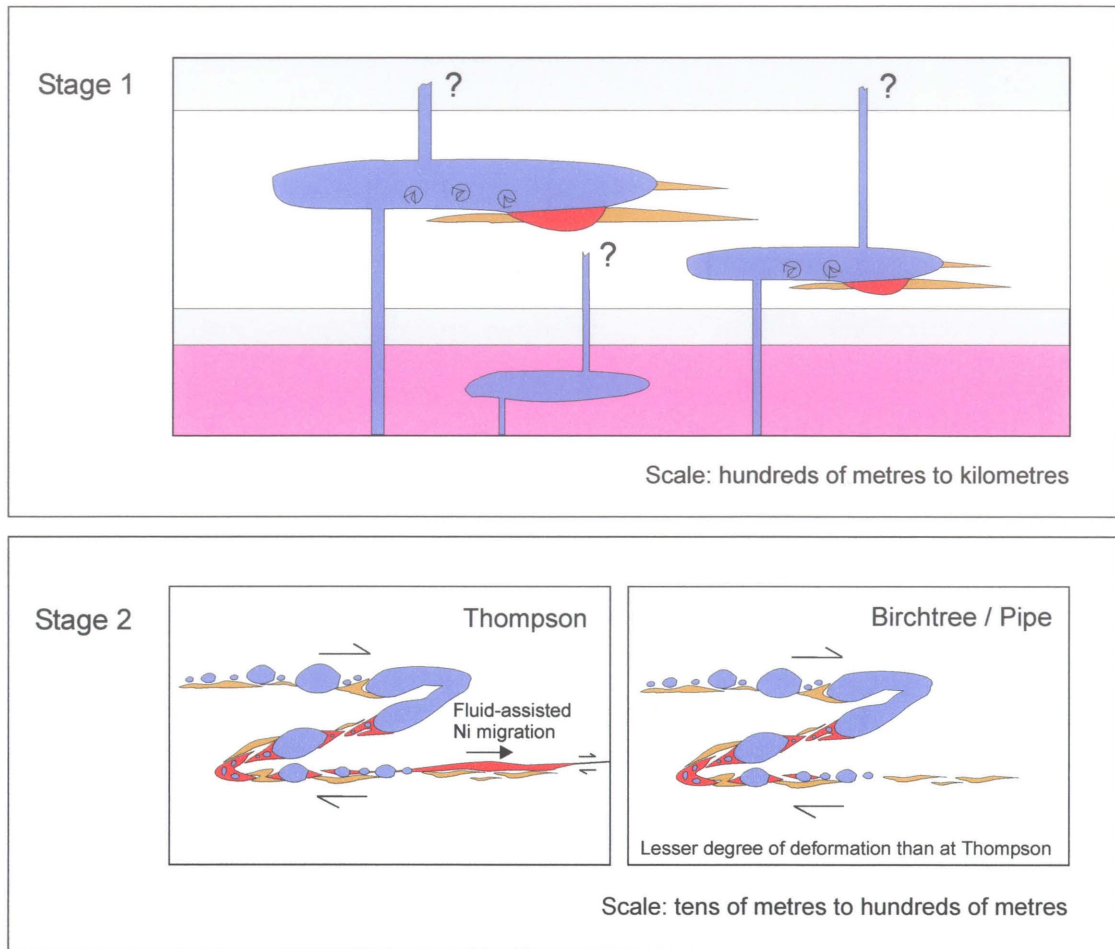
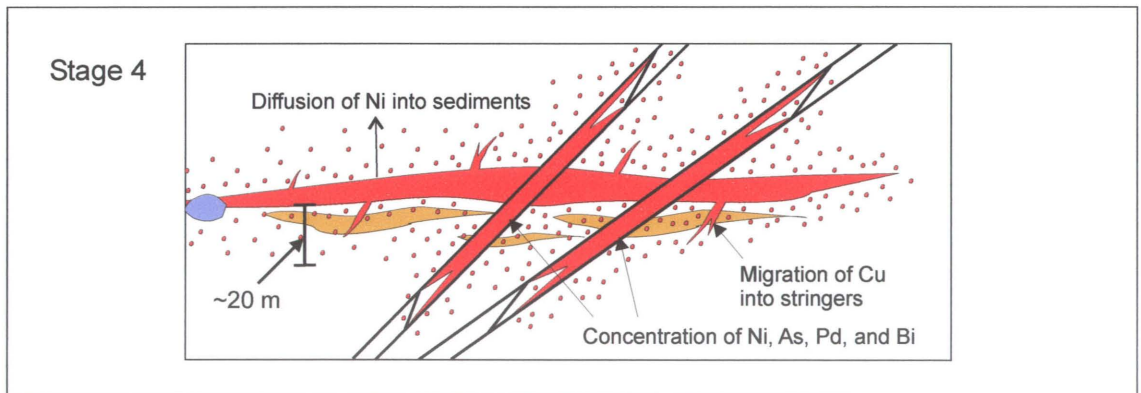
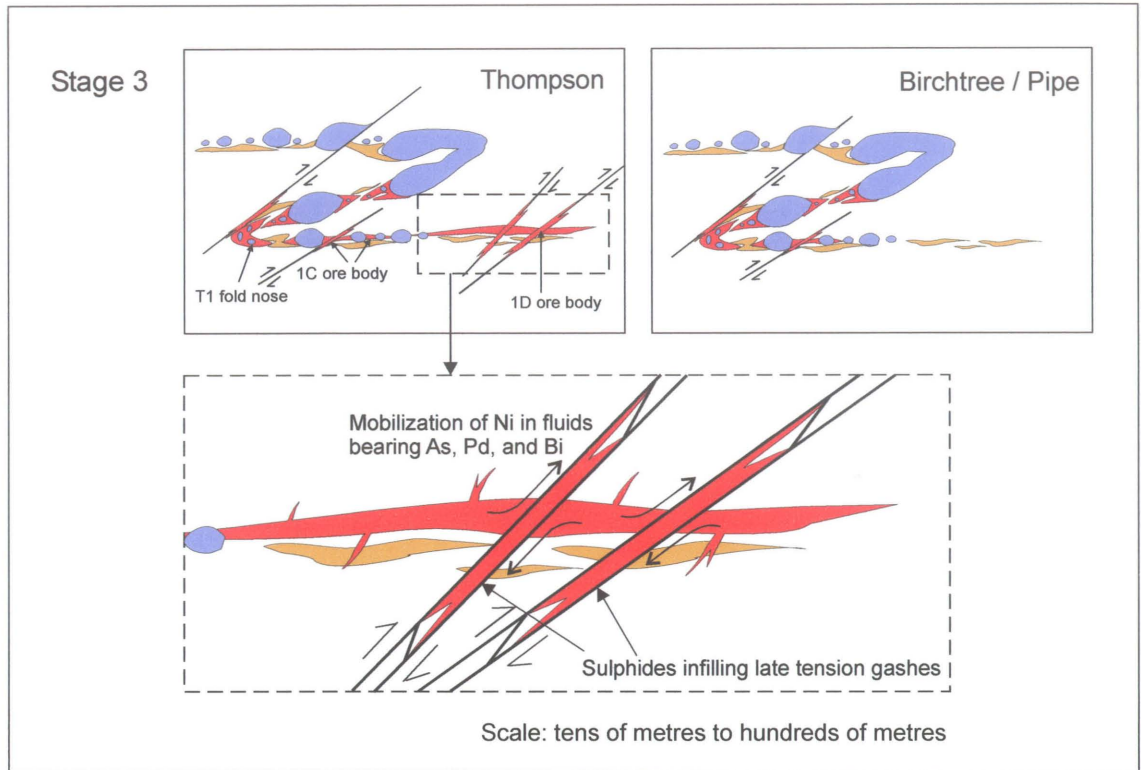


Figure 8.3. An ore deposit model representing the history of the deposition and post-magmatic modification of the ores from the Thompson Nickel Belt. Stage 1: Ultramafic magmatism associated with a rifting event led to the intrusion of ultramafic sills in the Oswagan Group metasediments. Stage 2: Folding and stretching of the massive magmatic sulphides and boudinage of the ultramafic boudins, accompanied by high-grade metamorphism (>600 degrees celcius). Stages 3 and 4 are continued on the following page. See text for further explanation.



- Pipe Formation
- Sulphide Facies Iron Formation
- Ultramafic Rocks
- Masssive Sulphides
- Ni-enriched Sedimentary Sulphides

Figure 8.3 (continued). Stage 3: Late stage ductile-brittle deformation of the sulphides. Stage 4: Final cooling of the sulphides after a high temperature metamorphic event, resulting in the development of a nickel halo around massive sulphide horizons. See text for further explanation.

CHAPTER 9: CONCLUSION

9.1 Summary

The chemical character of the deposits from the Thompson Nickel Belt has largely been attributed to magmatic processes. However, textural and geochemical analyses of the Thompson Nickel Belt sulphides show the following:

1. Metamorphic and metasomatic processes have modified the massive ores of the Thompson Nickel Belt.
2. Nickel may be mobilized across strike of an ore zone by fluid-assisted diffusion on a scale of tens of metres.
3. Nickel concentrations in deformed massive sulphides can be upgraded by metasomatic processes. Nickel may be complexed by As-, Pd-, and Bi-enriched fluids travelling through stress-induced weaknesses in deformed ores, subsequently re-deposited in massive sulphides distal to ultramafic sills, and incorporated into thermally metamorphosed sulphides.

The data presented in this thesis show that economic concentrations of sulphide ore in the Thompson Nickel Belt are structurally, stratigraphically, and metamorphically controlled.

9.2 Implications for Exploration

Correlations between structural, stratigraphic, and chemical data are important in assessing potential economic concentrations of sulphides in the Thompson Nickel Belt. High Ni-tenor sulphides are found in the most complexly deformed and sheared parts of the Thompson Mine, i.e. the 1D ore body. These high Ni-tenor sulphides show elevated

concentrations of As, Bi, and Pd (As > 300 ppm, Bi > 25 ppm, Pd > 1100 ppb). These massive sulphides also have the highest Ni/Co and Pd/Ir ratios in the Thompson Mine (Ni/Co = 57-113; Pd/Ir = 13-22). Elevated As, Bi, Ni/Co, and Pd/Ir in highly deformed massive sulphide horizons within Oswagan Group metasediments may indicate the presence of high-grade Ni ore nearby. If this ore is located on a limb of an F₃ fold structure, similar to the Thompson structure, it may be possible to locate large, relatively lower Ni-tenor ores preserved in the fold nose (e.g. T1 Mine).

A Pt depletion in massive ores from localities other than the Thompson, Birchtree, or Pipe deposits may indicate ore formation in a reducing environment; such a depletion may indicate that the ore is located in a stratigraphic setting (especially within Oswagan Group metasediments) that is favourable for an economic deposit to occur. Alternatively, the Pt depletion in massive sulphides may indicate that the sulphides underwent a metamorphic or metasomatic process that allowed Pt to partition differently than the other PGE. Whether stratigraphically controlled or metamorphically controlled, a Pt depletion in a potential deposit may indicate a genetic link between that deposit and the ores of Thompson, Pipe, and Birchtree mines.

According to this study, the Ni halo around sediment-hosted massive sulphide horizons does not exceed a scale of tens of metres. Therefore, testing proximity to ore in the metasediments of the Oswagan Group using low-resolution exploration drilling data may not be very feasible.

REFERENCES

- Arnold, R.G., 1971. Evidence for liquid immiscibility in the system FeS-S. *Economic Geology*, v. 66, p. 1121-1130.
- Barnes, S.J., and Hill, R.E.T., 2000. Metamorphism of komatiite-hosted nickel sulfide deposits. *Reviews in Economic Geology*, v. 11, p. 203-215.
- Barnes, S.J., Gole, M.J., and Hill, R.E.T., 1988. The Agnew nickel deposit, Western Australia: Part I. Stratigraphy and structure. *Economic Geology*, v. 83, p. 524-536.
- Barnes, S.J. and Maier, W.D., 1999. The fractionation of Ni, Cu, and the noble metals in silicate and sulphide liquids. *In Dynamic Processes in Magmatic Ore Deposits and Their Application in Mineral Exploration. Edited by R.R. Keays, C.M. Lesher, P.C. Lightfoot, and C.E.G. Farrow. Geological Association of Canada, Short Course Volume 13, p. 69-106.*
- Barnes, S.J., Naldrett, A.J., and Gorton, M.P., 1985. The origin of the fractionation of platinum-group elements in terrestrial magmas. *Chemical Geology*, v. 53, p. 303-323.
- Barrett, F.M., Binns, R.A., Groves, D.I., Marston, R.J., and McQueen, K.G., 1977. Structural history and metamorphic modification of Archaean volcanic-type nickel deposits, Yilgarn Block, Western Australia. *Economic Geology*, v. 72, p. 1195-1223.
- Batt, A.P., 1972. Nickel distribution in hexagonal and monoclinic pyrrhotite. *Canadian Mineralogist*, v. 11, p. 892-897.
- Bezmen, N.I., Naldrett, A.J., and Asif, M., 1998. Solubilities of Pt and Pd in the hydrous silicate melt. *Experiment in GeoSciences*, v. 7, p.17-18.
- Bleeker, W., 1990. Evolution of the Thompson Nickel Belt and Its Nickel Deposits, Manitoba, Canada. Unpublished Ph.D. Thesis, University of New Brunswick, Fredericton, New Brunswick.
- Boulet, M.P., and Larocque, A.C.L., 1997. Mineralogy and texture of barren sulphide and sulphide ore from the Birchtree Mine, Thompson Nickel Belt, Manitoba. *Geological Association of Canada – Mineralogical Association of Canada Joint Annual Meeting Abstracts, May 1997, Ottawa.*
- Cabri, L.J., 1988. Applications of proton and nuclear microprobes in ore deposit mineralogy and metallurgy. *Nuclear Instruments and Methods in Physics Research*, v. B30, p. 459-465.
- Cabri, L.J., Campbell, J.L., Laflamme, J.H.G., Leigh, R.G., Maxwell, J.A., and Scott, J.D., 1985. Proton-microprobe analysis of trace elements in sulfides from some massive-sulfide deposits. *The Canadian Mineralogist*, v. 23, p. 133-148.

- CAMIRO, 2000a. CAMIRO 97E-02 Thompson Nickel Belt Project. Digital Publication v. Feb 2000 (Confidential), Manitoba Energy and Mines.
- CAMIRO, 2000b. CAMIRO 97E-02 Thompson Nickel Belt Project Annual Report. Year 3, June 2000, Manitoba Energy and Mines.
- Campbell, I.H., and Naldrett, A.J., 1979. The influence of silicate: sulfide ratios on the geochemistry of magmatic sulfides. *Economic Geology*, v. 74, p. 1503-1506.
- Carpenter, R.H., and Desborough, G.A., 1964. Range in solid solution and structure of naturally occurring troilite and pyrrhotite. *American Mineralogist*, v. 49, p.1350-1365.
- Chyi, L.L., and Crocket, J.H., 1976. Partition of platinum, palladium, iridium, and gold among coexisting minerals from the Deep Ore Zone, Strathcona Mine, Sudbury, Ontario. *Economic Geology*, v. 71, p. 1196-1205.
- Coats, C.J.A., 1966. Serpentinized Ultramafic Rocks of the Manitoba Nickel Belt. Unpublished Ph.D. Thesis. University of Manitoba, Winnipeg.
- Corkery, M.T., 1985. Geology of the lower Nelson River project area. Manitoba Energy and Mines, Geological Report GR82-1, 66 p.
- Cowden, A., Donaldson, M.J., Naldrett, A.J., and Campbell, I.H., 1986. Platinum-group elements in the komatiite-hosted Fe-Ni-Cu sulfide deposits at Kambalda, Western Australia. *Economic Geology*, v. 81, p. 1226-1235.
- Cranstone, D.A. and Turek, A., 1976. Geological and geochronological relationships of the Thompson nickel belt, Manitoba. *Canadian Journal of Earth Science*, v. 13, p. 1058-1069.
- Czamanske, G.K., Kunilov, V.E., Zientek, M.L., Cabri, L.J., Likhachev, A.P., Calk, L.C., and Oscarson, R.L., 1992. A proton-microprobe study of magmatic sulfide ores from the Noril'sk-Talnakh district, Siberia. *The Canadian Mineralogist*, v. 30, p. 249-287.
- Dillon-Leitch, H.C.H., Watkinson, D.H., and Coats, C.J.A, 1986. Distribution of platinum-group elements in the Donaldson West Deposit, Cape Smith Belt, Quebec. *Economic Geology*, v. 81, p. 1147-1158.
- Donaldson, M.J., 1981. Redistribution of ore elements during serpentinization and talc-carbonate alteration of some Archean dunites, Western Australia. *Economic Geology*, v. 76, p. 1698-1713.
- Durazzo, A., and Taylor, L.A., 1982. Exsolution in the *mss*-pentlandite system: Textural and genetic implications for Ni-sulfide ores. *Mineralium Deposita*, v. 17, p. 313-332.

- Eckstrand, O.R., 1996. Magmatic nickel-copper-platinum group elements. *In* *Geology of Canadian Mineral Deposit Types*. Edited by O.R. Eckstrand, W.D. Sinclair, and R.I. Thorp. Geological Survey of Canada, *Geology of Canada*, no. 8, p. 583-614.
- Eckstrand, O.R., Grinenko, L.N., Krouse, H.R., Paktunc, A.D., Schwann, P.L., and Scoates, R.F.J., 1989. Preliminary data on sulphur isotopes and Se/S ratios and the source of sulphur in magmatic sulphides from the Fox River Sill, Molson Dykes and Thompson nickel deposits, northern Manitoba. *In* *Current Research, Part C*, Geological Survey of Canada, Paper 89-1C, p. 235-242.
- Ermanovics, I.F. and Fahrig, W.F., 1975. The petrochemistry and paleomagnetism of the Molson dikes, Manitoba. *Canadian Journal of Earth Science*, v. 12, p. 1564-1575.
- Good, D.J., 1985. Petrology and geochemistry of the Bucko Lake nickel deposit, Thompson Nickel Belt, Manitoba. Unpublished M.Sc. thesis, University of Toronto, Toronto, Ontario.
- Hawley, J.E., and Nichol, I., 1959. Selenium in some Canadian sulfides. *Economic Geology*, v. 54, p. 608-628.
- Heaman, L.M., Machado, N., Krogh, T., and Weber, W., 1986. Precise U-Pb zircon ages for the Molson dyke swarm and the Fox River sill: Implications for Early Proterozoic crustal evolution in NE Manitoba, Canada. *Contributions to Mineralogy and Petrology*, v. 94, p. 82-89.
- Huston, D.L., Sie, S.H., Suter, G.F., Cooke, D.R., and Both, R.A., 1995. Trace elements in sulfide minerals from Eastern Australian volcanic-hosted massive sulfide deposits: Part I. Proton microprobe analyses of pyrite, chalcopyrite, and sphalerite, and Part II. Selenium levels in pyrite: comparison with $\delta^{34}\text{S}$ values and implications for the source of sulfur in volcanogenic hydrothermal systems. *Economic Geology*, v. 90, p. 1167-1196.
- Jonasson, I.R., and Sangster, D.F., 1975. Selenium in sulphides from some Canadian base metal deposits. *Geological Survey of Canada Paper*, 75-1, Part C, p. 231-232.
- Keays, R.R., Nickel, E.H., Groves, D.I., and McGoldrick, P.J., 1982. Iridium and Palladium as discriminants of volcanic-exhalative, hydrothermal, and magmatic nickel sulfide mineralization. *Economic Geology*, v. 77, p. 1535-1547.
- Kissin, S.A., 1974. Phase relations in a portion of the Fe-S System. Ph.D. Thesis, University of Toronto, Canada.
- Kissin, S.A., and Scott, S.D., 1982. Phase relations involving pyrrhotite below 350°C. *Economic Geology*, v. 77, p. 1739-1754.

Larocque, A.C.L., and Boulet, M.P., 1998. Applications of microbeam analysis of sulfides to the discrimination of ore types at Inco's Birchtree deposit, Thompson Nickel Belt, Manitoba. Geological Association of Canada – Mineralogical Association of Canada Joint Annual Meeting Abstracts, May 1998, Quebec City.

Leshner, C.M., and Stone, W.E., 1996. Exploration geochemistry of komatiites. *In* Igneous Trace Element Geochemistry Applications for Massive Sulphide Exploration. *Edited by* D.A. Wyman. Geological Association of Canada, Short Course Notes, v. 12, p.153-204.

Macdonald, A. J. and Cherry, M. E., 1988. The platinum group of elements in Ontario. Ontario Geological Survey, Open File Report 5681, 279 p.

Machado, N., Krogh, T.E., and Weber, W., 1990. U-Pb geochronology of basement gneisses in the Thompson Belt (Manitoba): Evidence for pre-Kenoran and Pikwitonei-type crust and Early Proterozoic basement reactivation in the western margin of the Archean Superior province. *Canadian Journal of Earth Science*, v. 27, p. 794-802.

Marshall, B., Vokes, F.M., and Larocque, A.C.L., 2000. Regional metamorphic remobilization: Upgrading and formation of ore deposits. *In* Metamorphosed and Metamorphogenic Ore Deposits. *Edited by* P.G. Spry, B. Marshall, and F.M. Vokes. *Reviews in Economic Geology*, v. 11, p. 19-37.

Maxwell, J.A., Campbell, J.L., and Teesdale, W.J., 1989. The Guelph PIXE software package. *Nuclear Instruments and Methods in Physics Research*, B43, p. 218-230.

McCallum, M.E., Loucks, R.R., Carlson, R.R., Cooley, E.F., and Doerge, T.A., 1976. Platinum Metals Associated with Hydrothermal Copper Ores of the New Rambler Mine, Medicine Bow Mountains, Wyoming. *Economic Geology*, v. 71, p. 1429-1450.

McQueen, K.G., 1981a. The nature and metamorphic history of the Wannaway nickel deposit, Western Australia. *Economic Geology*, v. 76, p. 1444-1468.

McQueen, K.G., 1981b. Volcanic-associated nickel deposits from around the Widgiemooltha Dome, Western Australia. *Economic Geology*, v. 76, p. 1417-1443.

McQueen, K.G., 1987. Deformation and remobilization in some Western Australian nickel ores. *Ore Geology Reviews*, v. 2., p. 269-286.

Naldrett, A.J., 1981. Pt group element deposits. *In* Platinum Group Elements: Mineralogy, Geology, Geochemistry. *Edited by* L.C. Cabri. Canadian Institute of Mining and Metallurgy Special Volume 23, p. 197-232.

Naldrett, A.J., 1989. Magmatic Sulphide Deposits. New York: Oxford University Press, 186 p.

Naldrett, A.J., and Duke, J.M., 1980. Platinum metals in magmatic sulfide ores. *Science*, v. 208, p. 1417-1428.

Naldrett, A.J., Craig, J.R., and Kullerud, G., 1967a. The central portion of the Fe-Ni-S system and its bearing on pentlandite exsolution in iron-nickel sulfide ores. *Economic Geology*, v. 62, p. 826-847.

Naldrett, A.J., Craig, J.R., and Kullerud, G., 1967b. Pentlandite exsolution in iron-nickel sulfide ores. Abstract, Geological Society of America Special Paper 101, p. 149.

Naldrett, A.J., and Kullerud, G., 1967. A study of the Strathcona Mine and its bearing on the origin of the nickel-copper ores of the Sudbury District, Ontario. *Journal of Petrology*, v. 8, p. 453-531.

Naldrett, A.J., Hoffman, E.L., Green, A.H., Chou, C., Naldrett, S.R., and Alcock, R.A., 1979. The composition of Ni-sulfide ores, with particular reference to their content of PGE and Au. *Canadian Mineralogist*, v. 17, p. 403-415.

Nesbitt, B.E. and Kelly, W.C., 1980. Metamorphic zonation of sulfides, oxides, and graphite in and around the orebodies at Ducktown, Tennessee. *Economic Geology*, v. 75, p. 1010-1021.

Nesbitt, B.E., 1982. Metamorphic sulfide-silicate equilibria in the massive sulfide deposits at Ducktown, Tennessee. *Economic Geology*, v. 77, p. 364-378.

Peredery, W.V., 1982. Geology and nickel sulphide deposits of the Thompson Belt, Manitoba. *In Precambrian Sulphide Deposits. Edited by R.W. Hutchinson, C.D. Spence, and J.M. Franklin. Geological Association of Canada, Special Paper 25, p. 165-209.*

Potrel, A., 2000. CAMIRO 97E-02 Thompson Nickel Belt Project Annual Report. Year 3, June 2000, Manitoba Energy and Mines.

Pouchou, J.L., and Pichoir, F., 1984. A new model for quantitative x-ray microanalysis: Part I: Application to the analysis of homogeneous samples. *La Recherche Aérospace*, v. 3, p. 13-38.

Ryan, C.G., and Griffin, W.L., 1993. The nuclear microprobe as a tool in geology and mineral exploration. *Nuclear Instruments and Methods in Physics Research*, v. B77, p. 381-398.

Scoates, R.F.J., 1981. Volcanic rocks of the Fox River Belt, northeastern Manitoba. Manitoba Department of Energy and Mines, Geological Paper GR81-1, 109 p.

Scoates, R.F.J., and Macek, J.J., 1978. Molson Dyke Swarm. Manitoba Mines Branch, Geological Paper 78-1, 53 p.

Scoates, R.F.J., Macek, J.J., and Russel, J.K., 1977. Thompson Nickel Belt Project. Manitoba Mineral Resources Division, Report of Field Activities 1977, p. 47-53.

Vaughan, D.J., Schwarz, E.J., and Owens, D.R., 1971. Pyrrhotites from the Strathcona Mine, Sudbury, Canada: A thermomagnetic and mineralogical study. *Economic Geology*, v. 66, p. 1131-1144.

Weber, W., 1990. The Churchill-Superior Boundary Zone, southeast margin of the Trans-Hudson Orogen: A review. *In* The Early Proterozoic Trans-Hudson Orogen of North America. *Edited by* J.G. Lewry and M.R. Stauffer. Geological Association of Canada Special Paper, 37, p. 42-55.

Weber, W., and Scoates, R.F.J., 1978. Archean and Proterozoic metamorphism in the northwestern Superior province and along the Churchill-Superior boundary, Manitoba. *In* Metamorphism in the Canadian Shield. *Edited by* J.A. Fraser and W.W. Heywood. Geological Survey of Canada, Paper 78-10, p. 5-16.

Zubrigg, H.F., 1963. Thompson Mine geology. Canadian Institute of Mining and Metallurgy Bulletin, v. 56, p. 451-460.

APPENDIX 1: SUMMARY OF THIN SECTIONS

Abbreviations:

Sulphide classes:

- DS-SED = disseminated sulphides in metasediments
- DS-U = disseminated sulphides in ultramafic rocks
- IS-U = interstitial sulphides in ultramafic rocks
- MS-U = massive sulphides in ultramafic breccia
- BMS-SED = barren massive sulphides in metasediments
- MS-SED = massive sulphides in metasediments
- SMS-SED = semi-massive sulphides in metasediments

Sample	Rock Type	% Sulph	Sulphide Texture	Field Interpretation of Protolith	Sulphide Class
Thompson 1C ore body					
JL98-1C-10	garnet-sillimanite-biotite gneiss	1	Diss	Metasediments.	DS-SED
JL98-1C-11	garnet-sillimanite-biotite gneiss	5	Diss, confined to biotitic layers	Metasediments.	DS-SED
JL98-1C-12	biotite quartzite (impure)	tr	Diss	Metasediments.	DS-SED
JL98-1C-15	biotite quartzite (impure)	1	Diss	Metasediments.	DS-SED
JL98-1C-16	biotite-sillimanite gneiss	tr	Diss	Metasediments.	DS-SED
JL98-1C-19	semi-massive sulphide horizon in sillimanite-garnet-biotite gneiss	30	Semi-massive; sulphide stringers in host gneiss	Remobilized sulphides in metasediments.	SMS-SED
JL98-1C-20	massive sulphide horizon in sillimanite-garnet-biotite schist	95	Massive	Remobilized sulphides in metasediments.	MS-SED
JL98-1C-21	semi-massive sulphide in highly tectonized biotite-sillimanite gneiss	30	Semi-massive, interstitial	Remobilized sulphides in metasediments.	SMS-SED
JL98-1C-22	biotite quartzite (impure)	4	Diss	Metasediments.	DS-SED
JL98-1C-23	garnet-biotite schist	2	Diss	Metasediments.	DS-SED
JL98-1C-24A	massive sulphide horizon in graphitic biotite gneiss	80	Massive	Remobilized sulphides in metasediments.	MS-SED
JL98-1C-25B	massive sulphide horizon in sillimanite-biotite schist	85	Massive	Remobilized sulphides in metasediments.	MS-SED
JL98-1C-25D	massive sulphide horizon in sillimanite-biotite schist	85	Massive	Remobilized sulphides in metasediments.	MS-SED
JL98-1C-28A	garnet-hornblende gneiss	10	Diss and stringer	Sulphidic ferruginous metasediments.	DS-SED
JL98-1C-28C	garnet-hornblende gneiss	5	Diss	Sulphidic ferruginous metasediments.	DS-SED
JL98-1C-29	biotite gneiss	1	Diss	Metasediments.	DS-SED
JL98-1C-30	semi-massive sulphide breccia in garnet-biotite schist	50	Semi-massive breccia	Remobilized sulphides in metasediments.	SMS-SED
JL98-1C-31	biotite gneiss	5	Foliated; stringer	Sulphidic metasediments.	DS-SED
JL98-1C-33	sillimanite-biotite schist	tr	Diss	Metasediments.	DS-SED
JL99-1C-35	massive sulphide ore	85	Massive, w/ c.g. pn eyes	Remobilized sulphide in metasediments	MS-SED
Thompson 1D ore body					
DM98-1C-02	serpentinized peridotite	25	Interstitial	Magmatic sulphides in um.	IS-U
DM98-1C-03	serpentinized peridotite	15	Interstitial	Magmatic sulphides in um.	IS-U
DM98-1C-04	serpentinized peridotite	7	Diss	Magmatic sulphides in um.	DS-U
DM98-1C-05	serpentinized peridotite	5	Diss	Magmatic sulphides in um.	DS-U
DM98-1C-06	serpentinized peridotite	3	Diss	Magmatic sulphides in um.	DS-U
DM98-1C-07	massive sulphide horizon	95	Massive	Remobilized sulphides between metasediments and um.	MS-SED
DM98-1C-08	garnet-biotite schist	3	Diss	Metasediments	DS-SED
DM98-1C-09	garnet-biotite schist	3	Diss	Metasediments	DS-SED
DM98-1C-11	biotite schist	tr	Diss	Metasediments	DS-SED
DM98-1C-12	biotite schist	tr	Diss	Metasediments	DS-SED
JL98-1D-01	garnet-biotite schist	1	Diss	Metasediments.	DS-SED
JL98-1D-03	biotite gneiss	5	Diss, mostly confined to biotite schist	Metasediments.	DS-SED
JL98-1D-04	biotite schist	10	Diss and stringer	Metasediments.	DS-SED
JL98-1D-08	garnet-biotite quartzite (impure)	1	Diss; also sulphide veins	Metasediments; also secondary sulphides.	DS-SED
JL98-1D-09	biotite gneiss	5	Diss and stringer	Metasediments.	DS-SED
JL98-1D-11	sillimanite-biotite augen gneiss	tr	Diss; locally patchy.	Metasediments.	DS-SED
JL98-1D-13A	semi-massive sulphide band in biotite gneiss	60	Semi-massive	Remobilized sulphides in metasediments.	SMS-SED
JL98-1D-13B	sillimanite-garnet-biotite schist	1	Diss	Metasediments.	DS-SED

Sample	Rock Type	% Sulph	Sulphide Texture	Field Interpretation of Protolith	Sulphide Class
JL98-1D-14	semi-massive sulphide in biotite gneiss	60	Semi-massive	Remobilized sulphides in metasediments.	SMS-SED
JL98-1D-15	semi-massive sulphide in biotite gneiss	60	Semi-massive, banded	Remobilized sulphides in metasediments.	SMS-SED
JL98-1D-16	semi-massive sulphide in biotite gneiss	25	Semi-massive	Remobilized sulphides in metasediments.	SMS-SED
JL98-1D-18A	semi-massive sulphide in biotite gneiss	50	Semi-massive	Remobilized sulphides in metasediments.	SMS-SED
JL98-1D-18B	sillimanite-garnet-biotite schist	2	Diss	Metasediments.	DS-SED
JL98-1D-19	sulphide veins and stringers in sillimanite-biotite schist	25	Veins and stringers	Remobilized sulphides in metasediments.	SMS-SED
JL98-1D-21	garnet-biotite gneiss	5	Diss and stringer	Metasediments.	DS-SED
JL98-1D-22	sillimanite-biotite schist	3	Diss and foliated	Metasediments.	DS-SED
JL99-1D-35	massive barren sulphide horizon	75	Massive	Remobilized sulphides in metasediments	BMS-SED
JL99-1D-37	massive barren sulphides	75	Massive	Remobilized sulphides in metasediments.	BMS-SED
JL99-1D-38	massive barren sulphides	50	Massive	Remobilized sulphides in metasediments.	BMS-SED
JL99-1D-39	massive barren sulphides	75	Massive	Remobilized sulphides in metasediments.	BMS-SED
Thompson T1 Mine					
JL98-T1-04	semi-massive sulphide in serpentinite	40	Semi-massive	Remobilized sulphides in um.	MS-UB
JL98-T1-06	garnet-biotite gneiss	tr	Diss and foliated.	Metasediments.	DS-SED
JL98-T1-07	massive sulphide breccia	80	Massive sulphide breccia; matrix to serpentinite clasts	Remobilized sulphides in um.	MS-UB
JL98-T1-09A	massive sulphide band in breccia zone	90	Massive band	Remobilized sulphides in um.	MS-UB
JL98-T1-09B	serpentinized peridotite	3	Diss	Magmatic sulphides in um.	DS-U
JL98-T1-10	serpentinized peridotite	10	Diss.	Magmatic sulphides in um.	DS-U
JL98-T1-11	net-textured sulphide in metapyroxenite with "jack straw texture"	25	Net-textured	Recrystallized magmatic sulphides in altered um.	IS-U
JL98-T1-12	massive sulphide breccia	80	Massive	Remobilized sulphides in um.	MS-UB
JL98-T1-13	serpentinite	15	Diss and interstitial	Magmatic sulphides in um.	IS-U
JL98-T1-15	garnet-hornblende biotite gneiss	15	Banded and stringer	Sulphidic ferruginous metasediments.	DS-SED
JL98-T1-16	garnet-hornblende gneiss	20	Banded and stringer	Sulphidic ferruginous metasediments.	DS-SED
JL98-T1-19	massive sulphide horizon in biotite schist	80	Massive	Remobilized sulphides in metasediments.	MS-SED
JL98-T1-20	biotite gneiss	1	Diss	Metasediments.	DS-SED
JL99-T1-25	massive barren sulphide	95	Massive	Remobilized sulphide in metasediments	BMS-SED
JL99-T1-26	massive barren sulphide	95	Massive	Remobilized sulphide in metasediments	BMS-SED
Birchtree Mine					
JL98-BT-01	serpentinized peridotite	3	Diss	Magmatic sulphides in um.	DS-U
JL98-BT-02	massive sulphide vein in serpentinite	80	Massive	Remobilized sulphides in um.	MS-UB
JL98-BT-03	serpentinite	12	Diss and interstitial	Magmatic sulphides in um.	IS-U
JL98-BT-05	garnet-biotite schist	3	Diss	Metasediments.	DS-SED
JL98-BT-06	chlorite schist	tr	Diss	Metasediments.	DS-SED
JL98-BT-08	massive sulphide at contact with serpentinite	90	Massive ; diss and interstitial sulphide in serpentinite	Remobilized sulphides in um.	MS-UB
JL98-BT-09	serpentinite	tr	Diss	Magmatic sulphides in um.	DS-U
JL98-BT-10	massive sulphide body between serpentinite and biotite schist	97	Massive	Remobilized sulphides in um and metasediments.	MS-SED
JL98-BT-11	pyroxenite (altered to actinolite)	3	Diss and interstitial	Magmatic sulphides in um.	DS-U
JL98-BT-12	hbl-d-bio schist	tr	Diss	Metasediments.	DS-SED
JL98-BT-13	ga-bio gneiss	2	Diss	Metasediments.	DS-SED

Sample	Rock Type	% Sulph	Sulphide Texture	Field Interpretation of Protolith	Sulphide Class	
JL98-BT-15	massive sulphide horizon in biotite schist	93	Massive	Remobilized sulphides in metasediments. Magmatic sulphides in um. Remobilized sulphides in um. Metasediments. Recrystallized magmatic sulphides in altered um.	MS-SED	
JL98-BT-16A	serpentinite at contact with massive sulphide	5	Diss		DS-U	
JL98-BT-16B	massive sulphide at contact with serpentinite	85	Massive		MS-UB	
JL98-BT-18	biotite-muscovite schist	tr	Diss		DS-SED	
JL98-BT-22	net-textured sulphides in peridotite	25	Net-textured		IS-U	
Bucko Lake						
JL99-BU-01	semi-massive sulphide stringers in pegmatite	40	Stringers	Remobilized sulphides in pegmatite at base of um body. Remobilized sulphides in um Magmatic sulphides in um. Magmatic sulphides in um Remobilized sulphides between pegmatite and um.	SMS-ARC	
JL99-BU-02	massive sulphide horizon in plagioclase amphibolite and altered um	95	Massive		MS-ARC	
JL99-BU-04	serpentinized dunite	10	Interstitial, almost net-textured		IS-U	
JL99-BU-05	serpentinized dunite	7	Interstitial		IS-U	
JL99-BU-08	semi-massive breccia at contact between pegmatite and um	25	Stringer to SMS		SMS-ARC	
Soab North						
JL99-SN-02	semi-massive sulphide breccia in amphibole-rich schist	20	Fine stringers, interstitial to silicates	Remobilized sulphides in metasediments. Remobilized sulphides in metasediments.	SMS-SED	
JL99-SN-03	semi-massive sulphide breccia in amphibole-rich schist	25	Fine stringers interstitial to silicates		SMS-SED	
William Lake						
JL98-WL-06	serpentinized peridotite	20	Interstitial	Magmatic sulphides in um. Remobilized sulphides in um. Magmatic sulphides in um. Magmatic sulphides in um. Remobilized sulphides in um and metasediments. Recrystallized sulphidic metasediments. Metasediments. Sheared and intruded by pegmatite dykes. Metasediments. Sulphidic metasediments, tectonized. Sulphidic metasediments. Metasediments. Metasediments. Magmatic sulphides in um. Recrystallized magmatic sulphides in altered um. Metasediments. Sulphidic metasediments. Sulphidic metasediments. Sulphidic metasediments. Remobilized sulphides in metasediments. Remobilized sulphides in metasediments. Remobilized sulphides in metasediments.	IS-U	
JL98-WL-07	matrix sulphide to serpentinized breccia	20	Massive breccia		MS-UB	
JL98-WL-09	serpentinized peridotite	15	Interstitial		IS-U	
JL98-WL-10	serpentinized peridotite	tr	Diss		DS-U	
JL98-WL-11	massive sulphide band in serpentinite and garnet-biotite gneiss	80	Massive band		MS-SED	
JL98-WL-13	massive framboidal pyrite in biotite gneiss and pegmatite	80	Massive, framboidal		BMS-SED	
JL98-WL-14	biotite gneiss	10	Diss		DS-SED	
JL98-WL-17	muscovite-biotite gneiss	1	Diss		DS-SED	
JL98-WL-18	semi-massive breccia in muscovite biotite gneiss	50	Semi-massive band		DS-SED	
JL98-WL-19	massive sulphide horizon in muscovite-sillimanite-biotite gneiss	80	Massive		BMS-SED	
JL98-WL-21	biotite gneiss	15	Stringer		BMS-SED	
JL98-WL-23	biotite gneiss	3	Diss		DS-SED	
JL98-WL-24	serpentinite	1	Diss		DS-SED	
JL98-WL-25	talc schist	10	Blebbly and diss		DS-U	
JL98-WL-26	biotite quartzite (impure)	7	Foliated and stringer		DS-U	
JL98-WL-30	massive sulphide horizon in biotite schist	80	Massive		DS-SED	
JL98-WL-31	massive sulphide horizon in biotite schist	70	Massive		BMS-SED	
JL98-WL-32	garnet-sillimanite-biotite schist	5	Foliated and banded		BMS-SED	
JL98-WL-33	massive sulphide horizon in pegmatite	85	Massive		DS-SED	
JL98-WL-34	massive sulphide horizon in garnet biotite gneiss	85	Massive		MS-SED	
					MS-SED	

Appendix 1

APPENDIX 2: CONDITIONS OF MICROPROBE TECHNIQUES

Electron Microprobe Analysis (EMPA)

EMPA was done using a Cameca SX-50 at the University of Manitoba. All analyses were done using the wavelength dispersive system (WDS), with a stationary point beam with 20 kV accelerating voltage, 20 nA beam current, and counting times on the peaks and backgrounds of 20 and 10 seconds, respectively. All sulphide minerals were analysed using the program "pr20" (S and Cu off chalcopyrite standard; Fe off magnetite standard; Ni off pentlandite standard). Data reduction was performed using the PAP procedure of Pouchou and Pichoir (1984).

Proton-Induced X-ray Emission (PIXE)

The operating parameters for the proton microprobe at the University of Guelph were: proton energy, 3 MeV; charge, 2.5 μC ; average current, 5.6 nA; average counting time, 505 seconds; beam size, $5 \times 10 \mu\text{m}^2$. A synthetic pyrrhotite standard (in wt. %: Fe 60.93, S 38.87, Se 0.09, Pd, 0.11) was used for calibration. Aluminum absorbers of the following thicknesses were used: 250 μm for pyrrhotite and pyrite, 357.5 μm for pentlandite, and 508 μm for chalcopyrite. Data reduction was performed with the GUPIX program developed at Guelph (Maxwell *et al.*, 1989).

APPENDIX 3: EMPA DATA

Data is sorted by mineral, then by ore body. Hexagonal or monoclinic character of pyrrhotite was determined by the metal:sulphur ratio (M/S), as calculated from electron microprobe data.

Abbreviations:

Mineral:

- po = pyrrhotite
- pn = pentlandite
- cp = chalcopyrite
- py = pyrite
- gd = gersdorffite
- ni = niccolite

Ore body

- 1C = 1C ore body, Thompson Mine
- 1D = 1D ore body, Thompson Mine
- T1 = T1 Mine, Thompson Mine
- BT = Birchtree Mine
- BU = Bucko Lake
- SN = Soab North
- WL = William Lake deposit

Sulphide classes:

- DS-SED = disseminated sulphides in metasediments
- DS-U = disseminated sulphides in ultramafic rocks
- IS-U = interstitial sulphides in ultramafic rocks
- MS-U = massive sulphides in ultramafic breccia
- BMS-SED = barren massive sulphides in metasediments
- MS-SED = massive sulphides in metasediments
- SMS-SED = semi-massive sulphides in metasediments

Sample	Mineral	Ore Body	W%(S)	W%(Fe)	W%(Co)	W%(Ni)	W%(Cu)	W%(As)	Total	Sulphide Class	Ni/Co	M/S	hex/mono
JL98-1C-10	po	1C	39.54	59.17	0.05	0.42	0.00	0.00	99.27	DS-SED	8.10	0.867	mono
JL98-1C-10	po	1C	39.65	60.03	0.05	0.43	0.02	0.00	100.20	DS-SED	9.31	0.876	mono
JL98-1C-10	po	1C	39.41	59.59	0.07	0.35	0.00	0.00	99.45	DS-SED	5.02	0.874	mono
JL98-1C-11	po	1C	38.58	60.55	0.05	0.08	0.02	0.00	99.34	DS-SED	1.59	0.904	hex
JL98-1C-11	po	1C	39.19	59.66	0.10	0.12	0.01	0.00	99.20	DS-SED	1.18	0.879	mono
JL98-1C-11	po	1C	39.19	59.41	0.07	0.09	0.09	0.01	98.95	DS-SED	1.29	0.875	mono
JL98-1C-11	po	1C	39.45	59.85	0.06	0.11	0.00	0.00	99.50	DS-SED	1.75	0.874	mono
JL98-1C-11	po	1C	38.62	60.26	0.11	0.12	0.00	0.01	99.20	DS-SED	1.16	0.900	hex
JL98-1C-11	po	1C	38.76	60.66	0.06	0.11	0.00	0.00	99.65	DS-SED	1.80	0.902	hex
JL98-1C-12	po	1C	39.32	59.88	0.06	0.12	0.00	0.01	99.46	DS-SED	1.89	0.878	mono
JL98-1C-12	po	1C	39.38	59.79	0.11	0.14	0.01	0.00	99.50	DS-SED	1.31	0.876	mono
JL98-1C-12	po	1C	39.47	59.90	0.08	0.12	0.00	0.00	99.59	DS-SED	1.55	0.874	mono
JL98-1C-12	po	1C	39.29	58.98	0.06	0.10	0.00	0.01	98.53	DS-SED	1.57	0.866	mono
JL98-1C-12	po	1C	39.56	59.84	0.03	0.14	0.01	0.00	99.68	DS-SED	5.17	0.872	mono
JL98-1C-12	po	1C	39.29	59.40	0.05	0.11	0.01	0.00	98.89	DS-SED	2.21	0.871	mono
JL98-1C-15	po	1C	39.25	59.35	0.04	0.05	0.01	0.01	98.94	DS-SED	1.17	0.873	mono
JL98-1C-15	po	1C	39.18	59.37	0.11	0.04	0.07	0.00	98.80	DS-SED	0.41	0.873	mono
JL98-1C-15	po	1C	38.52	59.74	0.12	0.08	0.02	0.00	98.55	DS-SED	0.71	0.894	mono
JL98-1C-15	po	1C	38.60	59.61	0.09	0.09	0.02	0.00	98.43	DS-SED	1.00	0.890	mono
JL98-1C-16	po	1C	38.58	60.24	0.11	0.11	0.02	0.03	99.11	DS-SED	1.05	0.901	hex
JL98-1C-16	po	1C	38.70	60.77	0.11	0.13	0.01	0.00	99.78	DS-SED	1.16	0.906	hex
JL98-1C-16	po	1C	38.87	59.31	0.09	0.08	0.00	0.00	98.41	DS-SED	0.86	0.879	mono
JL98-1C-16	po	1C	38.90	59.82	0.07	0.11	0.01	0.00	98.94	DS-SED	1.54	0.886	mono
JL98-1C-19	po	1C	39.37	60.14	0.06	0.49	0.00	0.01	100.15	SMS-SED	8.75	0.886	mono
JL98-1C-19	po	1C	39.63	60.26	0.01	0.39	0.03	0.00	100.39	SMS-SED	52.55	0.880	mono
JL98-1C-19	po	1C	39.42	60.37	0.04	0.45	0.00	0.00	100.36	SMS-SED	11.02	0.887	mono
JL98-1C-19	po	1C	39.31	59.92	0.04	0.50	0.00	0.00	99.79	SMS-SED	12.99	0.883	mono
JL98-1C-19	po	1C	39.29	59.62	0.03	0.38	0.00	0.00	99.36	SMS-SED	12.09	0.878	mono
JL98-1C-20	po	1C	39.39	59.89	0.06	0.25	0.00	0.03	99.69	MS-SED	4.18	0.878	mono
JL98-1C-20	po	1C	39.52	60.47	0.06	0.24	0.00	0.00	100.29	MS-SED	3.69	0.883	mono
JL98-1C-20	po	1C	39.51	60.07	0.02	0.32	0.00	0.00	100.00	MS-SED	14.89	0.879	mono
JL98-1C-21	po	1C	38.89	60.29	0.04	0.48	0.04	0.01	99.75	SMS-SED	13.75	0.898	mono
JL98-1C-21	po	1C	38.76	60.62	0.07	0.55	0.02	0.00	100.09	SMS-SED	8.16	0.908	hex
JL98-1C-21	po	1C	38.72	60.35	0.03	0.66	0.02	0.01	99.83	SMS-SED	19.55	0.906	hex

Appendix 3

Sample	Mineral	Ore Body	W%(S)	W%(Fe)	W%(Co)	W%(Ni)	W%(Cu)	W%(As)	Total	Sulphide Class	Ni/Co	M/S	hex/mono
JL98-1C-21	po	1C	38.78	59.71	0.05	0.66	0.05	0.01	99.36	SMS-SED	12.27	0.896	mono
JL98-1C-22	po	1C	39.70	60.23	0.07	0.12	0.00	0.00	100.18	DS-SED	1.63	0.875	mono
JL98-1C-22	po	1C	39.44	59.84	0.09	0.15	0.00	0.02	99.60	DS-SED	1.63	0.875	mono
JL98-1C-22	po	1C	39.49	60.12	0.10	0.12	0.02	0.02	99.91	DS-SED	1.23	0.878	mono
JL98-1C-22	po	1C	39.38	60.02	0.10	0.15	0.00	0.00	99.72	DS-SED	1.46	0.879	mono
JL98-1C-22	po	1C	39.60	59.75	0.11	0.30	0.00	0.00	100.11	DS-SED	2.74	0.876	mono
JL98-1C-22	po	1C	39.53	59.96	0.10	0.11	0.02	0.00	99.74	DS-SED	1.08	0.875	mono
JL98-1C-23	po	1C	38.91	60.13	0.07	0.52	0.03	0.00	99.79	DS-SED	7.31	0.897	mono
JL98-1C-23	po	1C	39.71	59.26	0.10	0.28	0.01	0.01	99.48	DS-SED	2.89	0.863	mono
JL98-1C-23	po	1C	39.76	60.47	0.05	0.22	0.00	0.03	100.58	DS-SED	4.16	0.878	mono
JL98-1C-23	po	1C	39.67	59.45	0.05	0.32	0.05	0.02	99.68	DS-SED	6.00	0.868	mono
JL98-1C-24A	po	1C	39.07	60.42	0.00	0.57	0.00	0.01	100.09	MS-SED	271.67	0.896	mono
JL98-1C-24A	po	1C	39.86	60.18	0.05	0.24	0.01	0.00	100.43	MS-SED	4.96	0.872	mono
JL98-1C-24A	po	1C	39.11	60.13	0.04	0.58	0.00	0.01	99.95	MS-SED	13.56	0.893	mono
JL98-1C-24A	po	1C	39.30	60.73	0.02	0.52	0.00	0.00	100.62	MS-SED	25.99	0.895	mono
JL98-1C-25B	po	1C	39.61	59.39	0.04	0.91	0.00	0.00	99.96	MS-SED	22.75	0.874	mono
JL98-1C-25B	po	1C	39.67	58.93	0.05	0.87	0.00	0.01	99.58	MS-SED	16.20	0.866	mono
JL98-1C-25B	po	1C	39.24	58.25	0.03	0.80	0.00	0.00	98.36	MS-SED	23.13	0.864	mono
JL98-1C-25B	po	1C	39.38	58.90	0.02	0.83	0.00	0.02	99.20	MS-SED	34.78	0.871	mono
JL98-1C-25B	po	1C	39.17	59.38	0.04	0.75	0.00	0.00	99.43	MS-SED	17.14	0.882	mono
JL98-1C-25B	po	1C	39.40	59.70	0.03	0.58	0.00	0.00	100.02	MS-SED	18.22	0.883	mono
JL98-1C-25B	po	1C	39.30	59.67	0.07	0.65	0.01	0.01	99.75	MS-SED	9.61	0.883	mono
JL98-1C-25B	po	1C	39.52	59.28	0.03	1.05	0.00	0.01	99.99	MS-SED	31.04	0.877	mono
JL98-1C-25D	po	1C	39.75	59.40	0.07	0.98	0.02	0.00	100.24	MS-SED	14.79	0.873	mono
JL98-1C-25D	po	1C	39.65	59.81	0.03	0.79	0.00	0.01	100.39	MS-SED	27.85	0.879	mono
JL98-1C-25D	po	1C	39.67	59.36	0.01	0.89	0.00	0.00	100.01	MS-SED	96.18	0.872	mono
JL98-1C-25D	po	1C	39.63	59.17	0.04	0.90	0.00	0.00	99.84	MS-SED	20.87	0.872	mono
JL98-1C-25D	po	1C	39.56	59.25	0.03	0.96	0.00	0.00	99.89	MS-SED	32.53	0.875	mono
JL98-1C-28A	po	1C	38.74	62.42	0.02	0.06	0.00	0.03	101.35	DS-SED	2.64	0.928	hex
JL98-1C-28A	po	1C	39.17	62.25	0.08	0.06	0.02	0.01	101.60	DS-SED	0.82	0.915	hex
JL98-1C-28C	po	1C	39.29	61.65	0.09	0.14	0.00	0.01	101.21	DS-SED	1.48	0.905	hex
JL98-1C-28C	po	1C	38.69	61.91	0.08	0.06	0.07	0.02	100.83	DS-SED	0.73	0.922	hex
JL98-1C-29	po	1C	38.99	60.02	0.07	0.22	0.00	0.00	99.35	DS-SED	3.04	0.888	mono
JL98-1C-29	po	1C	38.81	60.30	0.11	0.17	0.00	0.02	99.54	DS-SED	1.60	0.898	mono

Appendix 3

Sample	Mineral	Ore Body	W%(S)	W%(Fe)	W%(Co)	W%(Ni)	W%(Cu)	W%(As)	Total	Sulphide Class	Ni/Co	M/S	hex/mono
JL98-1C-29	po	1C	39.41	59.85	0.12	0.10	0.00	0.01	99.53	DS-SED	0.87	0.876	mono
JL98-1C-30	po	1C	39.53	60.26	0.07	0.31	0.00	0.00	100.28	SMS-SED	4.66	0.882	mono
JL98-1C-30	po	1C	39.43	58.20	0.05	0.32	0.00	0.00	98.05	SMS-SED	6.06	0.853	
JL98-1C-30	po	1C	39.57	59.06	0.05	0.40	0.00	0.02	99.13	SMS-SED	8.86	0.864	mono
JL98-1C-30	po	1C	39.35	59.16	0.03	0.33	0.00	0.02	98.97	SMS-SED	10.45	0.869	mono
JL98-1C-30	po	1C	39.48	59.07	0.03	0.33	0.00	0.00	98.94	SMS-SED	9.75	0.864	mono
JL98-1C-30	po	1C	39.56	59.17	0.06	0.37	0.05	0.00	99.28	SMS-SED	6.48	0.866	mono
JL98-1C-31	po	1C	38.98	58.89	0.07	0.09	0.01	0.00	98.06	DS-SED	1.21	0.870	mono
JL98-1C-33	po	1C	38.81	58.99	0.10	0.34	0.01	0.00	98.28	DS-SED	3.56	0.879	mono
JL98-1C-33	po	1C	38.62	59.46	0.10	0.34	0.02	0.00	98.56	DS-SED	3.26	0.891	mono
JL98-1C-33	po	1C	38.60	59.17	0.06	0.43	0.02	0.00	98.37	DS-SED	7.73	0.889	mono
JL98-1C-33	po	1C	38.72	60.84	0.11	0.26	0.01	0.00	100.02	DS-SED	2.43	0.908	hex
JL99-1C-35	po	1C	39.65	58.24	0.05	0.62	0.01	0.00	98.67	MS-SED	13.80	0.854	
JL99-1C-35	po	1C	40.05	58.08	0.10	0.64	0.00	0.02	98.97	MS-SED	6.46	0.844	
JL99-1C-35	po	1C	39.60	58.39	0.05	0.62	0.00	0.00	98.73	MS-SED	13.10	0.857	
JL98-1D-01	po	1D	39.18	60.02	0.09	0.13	0.00	0.00	99.48	DS-SED	1.39	0.883	mono
JL98-1D-01	po	1D	39.09	60.26	0.13	0.16	0.00	0.00	99.70	DS-SED	1.24	0.890	mono
JL98-1D-01	po	1D	39.06	59.48	0.09	0.10	0.01	0.04	98.88	DS-SED	1.06	0.879	mono
JL98-1D-01	po	1D	39.03	59.63	0.12	0.14	0.03	0.00	99.10	DS-SED	1.23	0.883	mono
JL98-1D-01	po	1D	39.14	60.13	0.15	0.14	0.00	0.02	99.63	DS-SED	0.91	0.887	mono
JL98-1D-01	po	1D	38.41	59.86	0.11	0.18	0.02	0.00	98.65	DS-SED	1.66	0.900	hex
JL98-1D-03	po	1D	39.55	61.66	0.11	0.20	0.00	0.00	101.58	DS-SED	1.75	0.900	hex
JL98-1D-03	po	1D	39.69	61.66	0.10	0.19	0.00	0.00	101.74	DS-SED	1.93	0.897	mono
JL98-1D-03	po	1D	39.65	61.13	0.10	0.12	0.00	0.00	101.07	DS-SED	1.18	0.889	mono
JL98-1D-03	po	1D	39.59	62.00	0.11	0.14	0.00	0.00	101.92	DS-SED	1.22	0.904	hex
JL98-1D-03	po	1D	39.95	61.07	0.12	0.21	0.00	0.02	101.46	DS-SED	1.79	0.884	mono
JL98-1D-03	po	1D	39.55	61.71	0.10	0.20	0.00	0.00	101.61	DS-SED	2.04	0.900	hex
JL98-1D-03	po	1D	39.66	61.32	0.12	0.14	0.01	0.00	101.29	DS-SED	1.16	0.892	mono
JL98-1D-03	po	1D	39.80	60.89	0.08	0.18	0.02	0.00	101.06	DS-SED	2.13	0.883	mono
JL98-1D-03	po	1D	39.48	61.77	0.06	0.17	0.01	0.00	101.54	DS-SED	3.01	0.902	hex
JL98-1D-03	po	1D	39.30	61.52	0.12	0.20	0.01	0.01	101.26	DS-SED	1.67	0.905	hex
JL98-1D-04	po	1D	39.60	61.69	0.08	0.19	0.00	0.00	101.66	DS-SED	2.54	0.899	hex
JL98-1D-04	po	1D	39.52	61.44	0.08	0.18	0.00	0.00	101.29	DS-SED	2.12	0.897	mono
JL98-1D-04	po	1D	39.78	60.77	0.06	0.17	0.02	0.00	100.86	DS-SED	2.72	0.881	mono

Sample	Mineral	Ore Body	W%(S)	W%(Fe)	W%(Co)	W%(Ni)	W%(Cu)	W%(As)	Total	Sulphide Class	Ni/Co	M/S	hex/mono
JL98-1D-04	po	1D	39.49	60.85	0.06	0.17	0.00	0.00	100.62	DS-SED	2.99	0.889	mono
JL98-1D-04	po	1D	39.55	60.22	0.07	0.12	0.01	0.02	100.09	DS-SED	1.66	0.878	mono
JL98-1D-04	po	1D	39.29	60.40	0.11	0.16	0.01	0.00	100.02	DS-SED	1.50	0.887	mono
JL98-1D-04	po	1D	39.28	61.07	0.09	0.19	0.00	0.00	100.68	DS-SED	2.23	0.897	mono
JL98-1D-04	po	1D	39.35	61.24	0.08	0.12	0.00	0.00	100.87	DS-SED	1.48	0.897	mono
JL98-1D-08	po	1D	39.14	58.72	0.14	0.17	0.02	0.00	98.30	DS-SED	1.24	0.867	mono
JL98-1D-08	po	1D	39.06	59.41	0.16	0.18	0.00	0.04	98.90	DS-SED	1.16	0.879	mono
JL98-1D-08	po	1D	39.17	59.88	0.09	0.18	0.04	0.00	99.45	DS-SED	1.93	0.883	mono
JL98-1D-08	po	1D	39.19	60.23	0.12	0.20	0.04	0.00	99.79	DS-SED	1.70	0.888	mono
JL98-1D-08	po	1D	38.62	60.83	0.09	0.47	0.03	0.00	100.09	DS-SED	5.44	0.913	hex
JL98-1D-08	po	1D	39.16	58.88	0.17	0.25	0.02	0.00	98.49	DS-SED	1.47	0.869	mono
JL98-1D-09	po	1D	39.68	60.59	0.05	0.11	0.01	0.00	100.50	DS-SED	2.36	0.880	mono
JL98-1D-09	po	1D	39.59	60.97	0.04	0.12	0.00	0.00	100.80	DS-SED	3.16	0.887	mono
JL98-1D-09	po	1D	39.63	60.51	0.06	0.14	0.03	0.02	100.43	DS-SED	2.19	0.881	mono
JL98-1D-09	po	1D	39.79	61.04	0.06	0.07	0.00	0.00	101.02	DS-SED	1.21	0.883	mono
JL98-1D-09	po	1D	39.87	59.10	0.06	0.10	0.01	0.00	99.16	DS-SED	1.54	0.854	mono
JL98-1D-09	po	1D	39.63	60.39	0.06	0.11	0.00	0.02	100.25	DS-SED	1.97	0.878	mono
JL98-1D-09	po	1D	39.62	60.72	0.08	0.12	0.00	0.00	100.59	DS-SED	1.53	0.883	mono
JL98-1D-09	po	1D	39.43	59.51	0.05	0.10	0.00	0.00	99.22	DS-SED	2.01	0.870	mono
JL98-1D-09	po	1D	39.67	61.00	0.05	0.10	0.02	0.00	100.86	DS-SED	1.89	0.886	mono
JL98-1D-11	po	1D	39.46	60.55	0.16	0.18	0.00	0.01	100.40	DS-SED	1.16	0.886	mono
JL98-1D-11	po	1D	39.34	59.84	0.15	0.20	0.06	0.02	99.70	DS-SED	1.29	0.880	mono
JL98-1D-11	po	1D	39.19	60.52	0.17	0.27	0.08	0.03	100.29	DS-SED	1.63	0.894	mono
JL98-1D-11	po	1D	39.50	61.03	0.13	0.23	0.05	0.00	100.99	DS-SED	1.79	0.893	mono
JL98-1D-11	po	1D	39.59	60.73	0.14	0.17	0.00	0.03	100.69	DS-SED	1.25	0.886	mono
JL98-1D-11	po	1D	38.75	61.71	0.09	0.31	0.00	0.00	100.88	DS-SED	3.52	0.920	hex
JL98-1D-13a	po	1D	39.83	60.20	0.05	0.43	0.04	0.01	100.61	SMS-SED	8.12	0.876	mono
JL98-1D-13a	po	1D	39.26	59.81	0.05	0.62	0.01	0.00	99.78	SMS-SED	11.51	0.884	mono
JL98-1D-13a	po	1D	39.52	60.47	0.07	0.57	0.00	0.03	100.69	SMS-SED	8.70	0.888	mono
JL98-1D-13a	po	1D	39.43	60.22	0.03	0.49	0.05	0.00	100.24	SMS-SED	17.15	0.885	mono
JL98-1D-13a	po	1D	39.65	60.80	0.04	0.34	0.00	0.00	100.89	SMS-SED	9.34	0.886	mono
JL98-1D-13a	po	1D	39.82	60.53	0.05	0.52	0.02	0.00	101.01	SMS-SED	10.11	0.882	mono
JL98-1D-13a	po	1D	39.39	60.12	0.06	0.52	0.00	0.00	100.13	SMS-SED	8.58	0.885	mono
JL98-1D-13a	po	1D	39.38	60.78	0.02	0.47	0.06	0.04	100.79	SMS-SED	20.34	0.895	mono

Appendix 3

Sample	Mineral	Ore Body	W%(S)	W%(Fe)	W%(Co)	W%(Ni)	W%(Cu)	W%(As)	Total	Sulphide Class	Ni/Co	M/S	hex/mono
JL98-1D-13b	po	1D	38.86	59.98	0.04	0.73	0.00	0.00	99.69	DS-SED	20.25	0.898	mono
JL98-1D-13b	po	1D	38.51	59.27	0.03	0.69	0.00	0.00	98.60	DS-SED	20.71	0.895	mono
JL98-1D-13b	po	1D	38.55	58.76	0.05	0.69	0.00	0.00	98.11	DS-SED	12.71	0.886	mono
JL98-1D-13b	po	1D	38.70	59.68	0.04	0.77	0.00	0.00	99.23	DS-SED	21.37	0.897	mono
JL98-1D-13b	po	1D	38.68	59.79	0.01	0.68	0.00	0.00	99.18	DS-SED	105.98	0.898	mono
JL98-1D-13b	po	1D	39.49	60.05	0.06	0.46	0.00	0.00	100.09	DS-SED	8.15	0.881	mono
JL98-1D-13b	po	1D	39.38	59.24	0.04	0.39	0.00	0.01	99.15	DS-SED	8.95	0.871	mono
JL98-1D-14	po	1D	39.45	60.37	0.05	0.62	0.00	0.00	100.53	SMS-SED	11.98	0.889	mono
JL98-1D-14	po	1D	39.48	60.20	0.05	0.62	0.02	0.00	100.47	SMS-SED	12.24	0.886	mono
JL98-1D-14	po	1D	39.55	59.69	0.05	0.65	0.00	0.00	99.98	SMS-SED	14.39	0.877	mono
JL98-1D-14	po	1D	39.48	59.99	0.02	0.68	0.00	0.00	100.21	SMS-SED	39.34	0.883	mono
JL98-1D-15	po	1D	39.47	60.13	0.06	0.60	0.00	0.01	100.33	SMS-SED	10.75	0.885	mono
JL98-1D-15	po	1D	39.26	60.37	0.05	0.43	0.05	0.00	100.26	SMS-SED	8.22	0.891	mono
JL98-1D-15	po	1D	39.24	59.87	0.01	0.48	0.02	0.01	99.72	SMS-SED	67.76	0.884	mono
JL98-1D-15	po	1D	39.20	60.51	0.02	0.49	0.00	0.00	100.30	SMS-SED	23.25	0.894	mono
JL98-1D-16	po	1D	39.31	60.03	0.04	0.38	0.03	0.01	99.87	SMS-SED	9.89	0.884	mono
JL98-1D-16	po	1D	39.11	61.09	0.02	0.40	0.03	0.01	100.70	SMS-SED	25.61	0.904	hex
JL98-1D-16	po	1D	39.58	61.62	0.04	0.36	0.06	0.00	101.69	SMS-SED	9.66	0.901	hex
JL98-1D-16	po	1D	39.40	60.47	0.02	0.44	0.03	0.02	100.44	SMS-SED	19.38	0.889	mono
JL98-1D-16	po	1D	39.58	60.62	0.04	0.40	0.07	0.00	100.81	SMS-SED	10.22	0.887	mono
JL98-1D-18A	po	1D	39.54	60.03	0.03	0.66	0.00	0.00	100.32	SMS-SED	20.84	0.882	mono
JL98-1D-18A	po	1D	39.27	60.37	0.05	0.72	0.00	0.00	100.46	SMS-SED	14.99	0.894	mono
JL98-1D-18A	po	1D	39.48	59.91	0.03	0.88	0.00	0.00	100.36	SMS-SED	26.45	0.885	mono
JL98-1D-18A	po	1D	39.41	60.44	0.02	0.72	0.00	0.01	100.69	SMS-SED	30.64	0.892	mono
JL98-1D-18A	po	1D	39.68	60.58	0.03	0.82	0.03	0.00	101.21	SMS-SED	27.06	0.890	mono
JL98-1D-18A	po	1D	39.58	60.17	0.04	0.91	0.02	0.00	100.79	SMS-SED	24.79	0.887	mono
JL98-1D-18B	po	1D	39.26	61.00	0.02	0.41	0.02	0.00	100.77	DS-SED	17.55	0.899	hex
JL98-1D-18B	po	1D	39.39	60.58	0.04	0.46	0.00	0.00	100.61	DS-SED	11.11	0.892	mono
JL98-1D-18B	po	1D	39.50	61.59	0.05	0.27	0.02	0.00	101.55	DS-SED	5.44	0.902	hex
JL98-1D-18B	po	1D	39.43	60.35	0.06	0.42	0.00	0.00	100.41	DS-SED	6.66	0.887	mono
JL98-1D-18B	po	1D	39.46	61.11	0.04	0.45	0.01	0.00	101.26	DS-SED	10.16	0.898	mono
JL98-1D-18B	po	1D	39.66	60.49	0.04	0.44	0.00	0.00	100.65	DS-SED	11.32	0.883	mono
JL98-1D-19	po	1D	39.66	60.95	0.02	0.34	0.01	0.00	100.99	SMS-SED	20.45	0.888	mono
JL98-1D-19	po	1D	39.62	59.68	0.00	0.36	0.00	0.02	99.74	SMS-SED	107.82	0.871	mono

Appendix 3

Sample	Mineral	Ore Body	W%(S)	W%(Fe)	W%(Co)	W%(Ni)	W%(Cu)	W%(As)	Total	Sulphide Class	Ni/Co	M/S	hex/mono
JL98-1D-19	po	1D	39.45	61.01	0.03	0.50	0.00	0.01	101.08	SMS-SED	17.51	0.896	mono
JL98-1D-19	po	1D	39.81	61.47	0.00	0.43	0.02	0.01	101.77	SMS-SED	4332.00	0.893	mono
JL98-1D-19	po	1D	39.75	61.12	0.05	0.37	0.00	0.01	101.35	SMS-SED	7.26	0.889	mono
JL98-1D-21	po	1D	39.48	59.57	0.04	0.41	0.01	0.03	99.59	DS-SED	10.08	0.873	mono
JL98-1D-21	po	1D	39.01	59.30	0.03	0.36	0.00	0.00	98.75	DS-SED	11.97	0.879	mono
JL98-1D-22	po	1D	38.89	59.36	0.09	0.14	0.00	0.01	98.61	DS-SED	1.52	0.881	mono
JL98-1D-22	po	1D	39.23	59.50	0.14	0.15	0.02	0.00	99.05	DS-SED	1.08	0.875	mono
JL98-1D-22	po	1D	38.45	60.30	0.08	0.10	0.03	0.00	99.01	DS-SED	1.26	0.904	hex
JL98-1D-22	po	1D	39.43	59.75	0.06	0.05	0.01	0.00	99.33	DS-SED	0.73	0.872	mono
JL99-1D-35	po	1D	39.63	61.45	0.06	0.08	0.02	0.01	101.31	BMS-SED	1.38	0.893	mono
JL99-1D-35	po	1D	39.12	61.30	0.00	0.08	0.02	0.00	100.58	BMS-SED	24.58	0.902	hex
JL99-1D-35	po	1D	39.60	61.18	0.04	0.09	0.01	0.01	100.93	BMS-SED	2.59	0.889	mono
JL99-1D-35	po	1D	39.42	61.39	0.06	0.08	0.02	0.00	101.02	BMS-SED	1.44	0.897	mono
JL99-1D-35	po	1D	39.00	61.54	0.05	0.08	0.04	0.00	100.80	BMS-SED	1.72	0.909	hex
JL99-1D-37	po	1D	39.01	60.75	0.03	0.63	0.00	0.00	100.45	BMS-SED	21.31	0.904	hex
JL99-1D-37	po	1D	38.94	60.83	0.06	0.56	0.00	0.00	100.44	BMS-SED	9.64	0.906	hex
JL99-1D-37	po	1D	38.99	60.69	0.04	0.65	0.00	0.00	100.41	BMS-SED	15.21	0.904	hex
JL99-1D-37	po	1D	39.38	60.40	0.06	0.62	0.00	0.00	100.52	BMS-SED	10.92	0.891	mono
JL99-1D-38	po	1D	39.45	60.64	0.07	0.65	0.00	0.00	100.83	BMS-SED	9.52	0.893	mono
JL99-1D-38	po	1D	39.48	60.52	0.04	0.64	0.05	0.02	100.86	BMS-SED	17.96	0.892	mono
JL99-1D-38	po	1D	39.31	60.70	0.02	0.64	0.01	0.00	100.80	BMS-SED	31.98	0.897	mono
JL99-1D-39	po	1D	39.67	60.17	0.05	0.35	0.00	0.01	100.31	BMS-SED	6.73	0.877	mono
JL99-1D-39	po	1D	39.23	60.60	0.04	0.55	0.00	0.00	100.48	BMS-SED	15.18	0.896	mono
JL99-1D-39	po	1D	39.24	60.73	0.05	0.54	0.00	0.00	100.56	BMS-SED	11.76	0.897	mono
JL98-BT-01	po	BT	39.78	58.94	0.02	0.52	0.02	0.04	99.36	DS-U	26.85	0.859	mono
JL98-BT-01	po	BT	39.51	57.97	0.04	0.55	0.02	0.00	98.14	DS-U	13.66	0.851	
JL98-BT-01	po	BT	39.80	59.01	0.06	0.47	0.01	0.00	99.66	DS-U	7.26	0.863	mono
JL98-BT-01	po	BT	39.80	59.09	0.06	0.53	0.00	0.00	99.58	DS-U	8.38	0.862	mono
JL98-BT-02	po	BT	39.05	59.06	0.01	0.29	0.00	0.00	98.47	MS-UB	42.57	0.873	mono
JL98-BT-02	po	BT	39.69	59.14	0.04	0.27	0.00	0.00	99.19	MS-UB	6.66	0.861	mono
JL98-BT-02	po	BT	39.40	59.18	0.05	0.26	0.00	0.04	99.03	MS-UB	5.00	0.869	mono
JL98-BT-02	po	BT	39.80	59.98	0.04	0.32	0.00	0.01	100.17	MS-UB	7.88	0.871	mono
JL98-BT-02	po	BT	39.48	59.13	0.02	0.23	0.00	0.00	98.92	MS-UB	9.89	0.864	mono
JL98-BT-02	po	BT	39.76	59.81	0.05	0.21	0.00	0.00	99.90	MS-UB	4.08	0.868	mono

Appendix 3

Sample	Mineral	Ore Body	W%(S)	W%(Fe)	W%(Co)	W%(Ni)	W%(Cu)	W%(As)	Total	Sulphide Class	Ni/Co	M/S	hex/mono
JL98-BT-02	po	BT	39.54	59.91	0.03	0.30	0.00	0.00	99.83	MS-UB	9.72	0.875	mono
JL98-BT-02	po	BT	39.51	59.75	0.07	0.17	0.02	0.02	99.57	MS-UB	2.57	0.872	mono
JL98-BT-02	po	BT	39.68	59.71	0.06	0.18	0.03	0.01	99.73	MS-UB	3.30	0.869	mono
JL98-BT-02	po	BT	39.52	60.27	0.07	0.28	0.02	0.00	100.24	MS-UB	4.26	0.882	mono
JL98-BT-02	po	BT	39.69	59.94	0.04	0.19	0.00	0.00	99.92	MS-UB	5.02	0.871	mono
JL98-BT-03	po	BT	39.13	60.94	0.07	0.12	0.00	0.00	100.37	IS-U	1.66	0.898	mono
JL98-BT-03	po	BT	39.57	61.00	0.05	0.16	0.00	0.00	100.90	IS-U	3.15	0.889	mono
JL98-BT-03	po	BT	39.39	61.01	0.05	0.16	0.00	0.00	100.66	IS-U	3.24	0.893	mono
JL98-BT-03	po	BT	39.67	61.10	0.05	0.13	0.00	0.03	101.02	IS-U	2.38	0.888	mono
JL98-BT-03	po	BT	39.40	61.09	0.05	0.14	0.00	0.00	100.72	IS-U	2.74	0.894	mono
JL98-BT-03	po	BT	39.50	60.96	0.00	0.15	0.02	0.02	100.68	IS-U	1525.00	0.889	mono
JL98-BT-03	po	BT	39.59	60.77	0.03	0.14	0.00	0.00	100.57	IS-U	4.37	0.884	mono
JL98-BT-05	po	BT	39.08	58.85	0.07	0.14	0.00	0.01	98.25	DS-SED	1.99	0.869	mono
JL98-BT-05	po	BT	38.96	58.68	0.13	0.15	0.00	0.02	98.07	DS-SED	1.18	0.871	mono
JL98-BT-06	po	BT	39.51	60.32	0.03	0.02	0.00	0.00	99.94	DS-SED	0.51	0.878	mono
JL98-BT-06	po	BT	39.11	60.22	0.03	0.03	0.00	0.04	99.47	DS-SED	1.03	0.886	mono
JL98-BT-06	po	BT	39.24	60.14	0.09	0.05	0.00	0.02	99.63	DS-SED	0.57	0.883	mono
JL98-BT-06	po	BT	39.34	60.15	0.10	0.01	0.02	0.00	99.67	DS-SED	0.12	0.880	mono
JL98-BT-06	po	BT	39.43	60.66	0.09	0.07	0.03	0.01	100.39	DS-SED	0.83	0.887	mono
JL98-BT-06	po	BT	39.41	60.84	0.07	0.09	0.02	0.01	100.48	DS-SED	1.25	0.889	mono
JL98-BT-06	po	BT	39.21	60.94	0.07	0.08	0.05	0.00	100.44	DS-SED	1.20	0.896	mono
JL98-BT-06	po	BT	39.52	60.36	0.05	0.10	0.00	0.00	100.07	DS-SED	1.89	0.880	mono
JL98-BT-06	po	BT	39.71	60.48	0.05	0.02	0.00	0.00	100.44	DS-SED	0.42	0.877	mono
JL98-BT-06	po	BT	39.23	60.28	0.06	0.06	0.00	0.04	99.73	DS-SED	1.10	0.885	mono
JL98-BT-06	po	BT	39.52	60.68	0.07	0.02	0.02	0.00	100.40	DS-SED	0.31	0.884	mono
JL98-BT-08	po	BT	39.57	59.99	0.04	0.12	0.00	0.04	99.81	MS-UB	2.94	0.874	mono
JL98-BT-08	po	BT	39.42	59.34	0.04	0.14	0.03	0.00	99.04	MS-UB	3.27	0.868	mono
JL98-BT-08	po	BT	39.07	59.10	0.05	0.14	0.00	0.00	98.42	MS-UB	2.82	0.872	mono
JL98-BT-08	po	BT	38.99	59.80	0.02	0.24	0.00	0.01	99.13	MS-UB	12.57	0.885	mono
JL98-BT-08	po	BT	39.02	59.91	0.04	0.28	0.00	0.01	99.34	MS-UB	7.34	0.887	mono
JL98-BT-10	po	BT	38.88	60.68	0.06	0.48	0.00	0.01	100.21	MS-SED	7.67	0.905	hex
JL98-BT-10	po	BT	38.95	61.45	0.06	0.27	0.00	0.01	100.83	MS-SED	4.29	0.912	hex
JL98-BT-11	po	BT	38.62	62.18	0.03	0.26	0.02	0.01	101.18	DS-U	9.41	0.930	hex
JL98-BT-11	po	BT	38.84	61.81	0.04	0.22	0.00	0.02	101.04	DS-U	5.11	0.919	hex

Sample	Mineral	Ore Body	W%(S)	W%(Fe)	W%(Co)	W%(Ni)	W%(Cu)	W%(As)	Total	Sulphide Class	Ni/Co	M/S	hex/mono
JL98-BT-11	po	BT	38.61	61.50	0.04	0.28	0.01	0.00	100.46	DS-U	7.15	0.920	hex
JL98-BT-11	po	BT	38.05	61.73	0.04	0.24	0.01	0.00	100.11	DS-U	6.41	0.936	hex
JL98-BT-11	po	BT	37.81	61.17	0.02	0.20	0.00	0.00	99.31	DS-U	8.30	0.934	hex
JL98-BT-11	po	BT	38.51	61.94	0.04	0.20	0.03	0.00	100.76	DS-U	4.44	0.928	hex
JL98-BT-11	po	BT	38.38	61.47	0.06	0.23	0.00	0.00	100.16	DS-U	3.92	0.924	hex
JL98-BT-11	po	BT	38.31	61.66	0.04	0.22	0.00	0.03	100.32	DS-U	5.04	0.929	hex
JL98-BT-12	po	BT	38.82	61.87	0.06	0.35	0.01	0.03	101.19	DS-SED	5.79	0.922	hex
JL98-BT-12	po	BT	38.89	61.95	0.04	0.38	0.00	0.00	101.27	DS-SED	8.52	0.921	hex
JL98-BT-12	po	BT	39.61	61.33	0.04	0.19	0.07	0.03	101.34	DS-SED	4.89	0.894	mono
JL98-BT-12	po	BT	39.27	61.49	0.09	0.28	0.04	0.00	101.22	DS-SED	3.31	0.905	hex
JL98-BT-12	po	BT	39.19	62.00	0.07	0.37	0.06	0.00	101.76	DS-SED	5.55	0.916	hex
JL98-BT-13	po	BT	38.84	62.04	0.07	0.22	0.00	0.00	101.26	DS-SED	3.08	0.922	hex
JL98-BT-13	po	BT	38.78	60.73	0.05	0.19	0.03	0.00	99.88	DS-SED	3.85	0.904	hex
JL98-BT-13	po	BT	38.98	61.45	0.05	0.24	0.00	0.01	100.87	DS-SED	4.46	0.911	hex
JL98-BT-13	po	BT	39.09	61.72	0.04	0.19	0.02	0.00	101.10	DS-SED	5.08	0.911	hex
JL98-BT-13	po	BT	38.79	61.42	0.05	0.21	0.01	0.00	100.60	DS-SED	4.36	0.915	hex
JL98-BT-13	po	BT	39.07	61.28	0.11	0.29	0.02	0.01	100.85	DS-SED	2.70	0.908	hex
JL98-BT-16A	po	BT	38.95	61.00	0.06	0.35	0.03	0.00	100.44	DS-U	5.90	0.906	hex
JL98-BT-16A	po	BT	38.67	60.10	0.04	0.35	0.03	0.02	99.34	DS-U	9.63	0.900	hex
JL98-BT-16B	po	BT	38.22	60.77	0.05	0.33	0.00	0.00	99.43	MS-UB	6.44	0.919	hex
JL98-BT-16B	po	BT	38.25	59.68	0.07	0.24	0.00	0.00	98.29	MS-UB	3.38	0.901	hex
JL98-BT-16B	po	BT	38.63	61.26	0.07	0.29	0.00	0.00	100.32	MS-UB	4.05	0.917	hex
JL98-BT-16B	po	BT	37.86	60.57	0.03	0.34	0.00	0.00	98.83	MS-UB	11.03	0.924	hex
JL98-BT-16B	po	BT	38.58	59.57	0.04	0.30	0.01	0.01	98.59	MS-UB	8.01	0.892	mono
JL98-BT-16B	po	BT	38.41	60.36	0.05	0.20	0.00	0.01	99.09	MS-UB	3.99	0.907	hex
JL98-BT-18	po	BT	38.14	61.83	0.04	0.17	0.00	0.00	100.23	DS-SED	4.14	0.934	hex
JL98-BT-18	po	BT	38.38	61.37	0.05	0.20	0.00	0.00	100.10	DS-SED	3.92	0.923	hex
JL98-BT-18	po	BT	38.08	61.57	0.06	0.18	0.02	0.00	100.00	DS-SED	2.89	0.933	hex
JL98-BT-18	po	BT	38.46	61.66	0.06	0.23	0.03	0.00	100.52	DS-SED	3.73	0.926	hex
JL98-BT-18	po	BT	38.67	61.70	0.08	0.18	0.06	0.01	100.78	DS-SED	2.24	0.922	hex
JL98-BT-18	po	BT	38.52	62.41	0.09	0.23	0.00	0.02	101.37	DS-SED	2.48	0.936	hex
JL98-BT-18	po	BT	38.71	62.56	0.09	0.21	0.00	0.00	101.67	DS-SED	2.29	0.933	hex
JL98-BT-18	po	BT	38.81	61.71	0.08	0.20	0.02	0.01	100.88	DS-SED	2.63	0.918	hex
JL98-BT-22	po	BT	38.17	60.63	0.06	0.30	0.00	0.00	99.19	IS-U	5.15	0.917	hex

Sample	Mineral	Ore Body	W%(S)	W%(Fe)	W%(Co)	W%(Ni)	W%(Cu)	W%(As)	Total	Sulphide Class	Ni/Co	M/S	hex/mono
JL98-BT-22	po	BT	38.44	61.06	0.03	0.30	0.00	0.00	99.89	IS-U	8.96	0.918	hex
JL98-BT-22	po	BT	38.06	60.10	0.05	0.26	0.00	0.00	98.49	IS-U	5.06	0.912	hex
JL98-BT-22	po	BT	38.16	60.58	0.05	0.24	0.04	0.01	99.15	IS-U	4.45	0.917	hex
JL99-BU-01	po	BU	38.96	61.02	0.05	0.33	0.00	0.02	100.41	SMS-ARC	6.11	0.905	hex
JL99-BU-01	po	BU	38.77	60.70	0.05	0.35	0.00	0.00	99.90	SMS-ARC	6.50	0.905	hex
JL99-BU-01	po	BU	39.49	60.99	0.06	0.30	0.01	0.00	100.90	SMS-ARC	4.92	0.892	mono
JL99-BU-02	po	BU	39.03	60.82	0.03	0.24	0.04	0.00	100.25	MS-ARC	9.14	0.900	hex
JL99-BU-02	po	BU	38.73	60.52	0.03	0.27	0.00	0.00	99.60	MS-ARC	8.83	0.902	hex
JL99-BU-02	po	BU	38.40	60.71	0.09	0.28	0.00	0.02	99.57	MS-ARC	3.23	0.914	hex
JL99-BU-02	po	BU	38.56	61.39	0.05	0.24	0.00	0.00	100.35	MS-ARC	4.96	0.919	hex
JL99-BU-04	po	BU	39.39	59.21	0.04	0.09	0.01	0.01	98.80	IS-U	2.59	0.866	mono
JL99-BU-04	po	BU	39.95	59.25	0.03	0.14	0.00	0.02	99.46	IS-U	4.48	0.855	
JL99-BU-04	po	BU	39.49	59.17	0.04	0.15	0.02	0.01	98.90	IS-U	3.54	0.864	mono
JL99-BU-05	po	BU	40.04	59.46	0.00	0.08	0.01	0.00	99.61	IS-U	138.50	0.854	
JL99-BU-05	po	BU	39.99	60.41	0.04	0.09	0.00	0.00	100.60	IS-U	2.44	0.870	mono
JL99-BU-05	po	BU	36.89	56.98	0.56	6.54	0.04	0.00	101.06	IS-U	11.74	0.993	hex
JL99-BU-05	po	BU	36.85	55.51	0.63	6.52	0.05	0.00	99.60	IS-U	10.43	0.972	hex
JL99-BU-08	po	BU	40.14	58.68	0.01	0.54	0.02	0.00	99.48	SMS-ARC	43.85	0.848	
JL99-BU-08	po	BU	39.64	58.44	0.07	0.37	0.01	0.00	98.61	SMS-ARC	5.45	0.854	
JL99-BU-08	po	BU	40.16	59.49	0.00	0.38	0.00	0.02	100.10	SMS-ARC	78.54	0.856	
JL99-BU-08	po	BU	40.27	60.09	0.02	0.40	0.00	0.02	100.89	SMS-ARC	20.34	0.864	mono
DM98-1C-02	po	1C	39.25	59.73	0.03	0.15	0.01	0.00	99.19	IS-U	4.45	0.877	mono
DM98-1C-02	po	1C	39.23	60.19	0.00	0.12	0.00	0.02	99.62	IS-U	1202.00	0.884	mono
DM98-1C-02	po	1C	39.13	60.05	0.01	0.14	0.03	0.00	99.40	IS-U	27.65	0.884	mono
DM98-1C-02	po	1C	38.64	59.29	0.00	0.18	0.01	0.03	98.15	IS-U	84.19	0.884	mono
DM98-1C-02	po	1C	39.46	59.87	0.03	0.19	0.02	0.03	99.69	IS-U	6.47	0.876	mono
DM98-1C-02	po	1C	38.88	60.00	0.00	0.30	0.00	0.00	99.26	IS-U	3008.00	0.891	mono
DM98-1C-02	po	1C	39.23	59.65	0.07	0.19	0.01	0.00	99.19	IS-U	2.80	0.877	mono
DM98-1C-03	po	1C	39.99	60.33	0.07	0.11	0.04	0.00	100.64	IS-U	1.57	0.871	mono
DM98-1C-03	po	1C	39.77	59.97	0.03	0.09	0.00	0.00	99.93	IS-U	2.77	0.868	mono
DM98-1C-03	po	1C	40.23	60.29	0.04	0.12	0.00	0.00	100.80	IS-U	3.05	0.864	mono
DM98-1C-04	po	1C	38.97	60.61	0.04	0.22	0.01	0.02	99.94	DS-U	6.18	0.898	mono
DM98-1C-04	po	1C	39.06	61.07	0.05	0.13	0.00	0.00	100.31	DS-U	2.73	0.900	hex
DM98-1C-04	po	1C	38.97	60.99	0.04	0.11	0.00	0.01	100.15	DS-U	2.48	0.901	hex

Sample	Mineral	Ore Body	W%(S)	W%(Fe)	W%(Co)	W%(Ni)	W%(Cu)	W%(As)	Total	Sulphide Class	Ni/Co	M/S	hex/mono
DM98-1C-05	po	1C	36.70	63.48	0.01	0.00	0.00	0.00	100.26	DS-U	0.01	0.994	hex
DM98-1C-05	po	1C	37.04	63.44	0.05	0.02	0.00	0.00	100.62	DS-U	0.32	0.985	hex
DM98-1C-05	po	1C	39.08	61.40	0.05	0.12	0.00	0.00	100.70	DS-U	2.53	0.905	hex
DM98-1C-06	po	1C	37.84	62.30	0.04	0.12	0.04	0.00	100.38	DS-U	2.79	0.949	hex
DM98-1C-06	po	1C	37.44	62.94	0.05	0.04	0.01	0.00	100.50	DS-U	0.79	0.967	hex
DM98-1C-06	po	1C	38.05	61.85	0.02	0.14	0.00	0.03	100.17	DS-U	5.75	0.937	hex
DM98-1C-07	po	1C	39.32	60.40	0.04	0.27	0.00	0.01	100.07	MS-SED	6.71	0.887	mono
DM98-1C-07	po	1C	39.58	60.66	0.03	0.32	0.02	0.00	100.73	MS-SED	12.69	0.886	mono
DM98-1C-07	po	1C	39.37	60.99	0.05	0.40	0.00	0.00	100.82	MS-SED	7.81	0.896	mono
DM98-1C-08	po	1C	39.50	59.53	0.07	0.33	0.00	0.00	99.46	DS-SED	4.46	0.871	mono
DM98-1C-08	po	1C	38.95	59.04	0.05	0.36	0.00	0.00	98.45	DS-SED	7.51	0.877	mono
DM98-1C-08	po	1C	39.59	59.64	0.00	0.30	0.01	0.01	99.61	DS-SED	2951.00	0.870	mono
DM98-1C-09	po	1C	39.82	59.60	0.02	0.37	0.00	0.00	99.90	DS-SED	14.75	0.866	mono
DM98-1C-09	po	1C	39.93	60.91	0.04	0.37	0.00	0.03	101.32	DS-SED	9.48	0.882	mono
DM98-1C-09	po	1C	39.83	61.56	0.06	0.32	0.05	0.00	101.84	DS-SED	4.91	0.894	mono
DM98-1C-09	po	1C	39.76	60.55	0.06	0.35	0.00	0.00	100.76	DS-SED	5.59	0.880	mono
DM98-1C-11	po	1C	38.88	61.91	0.08	0.26	0.00	0.03	101.25	DS-SED	3.41	0.921	hex
DM98-1C-11	po	1C	39.33	62.04	0.05	0.26	0.00	0.00	101.79	DS-SED	5.48	0.911	hex
DM98-1C-11	po	1C	39.00	62.14	0.06	0.21	0.00	0.01	101.45	DS-SED	3.32	0.919	hex
DM98-1C-11	po	1C	38.90	61.03	0.08	0.21	0.00	0.00	100.31	DS-SED	2.52	0.906	hex
DM98-1C-11	po	1C	38.82	61.28	0.10	0.23	0.00	0.00	100.50	DS-SED	2.26	0.912	hex
DM98-1C-11	po	1C	38.79	61.85	0.08	0.22	0.00	0.00	101.05	DS-SED	2.66	0.921	hex
DM98-1C-12	po	1C	40.04	60.23	0.02	0.32	0.00	0.00	100.64	DS-SED	15.13	0.869	mono
DM98-1C-12	po	1C	39.60	60.73	0.04	0.38	0.04	0.00	100.84	DS-SED	9.16	0.887	mono
DM98-1C-12	po	1C	39.67	60.55	0.06	0.33	0.01	0.00	100.71	DS-SED	5.27	0.883	mono
JL99-SN-01	po	SN	40.33	59.32	0.01	0.55	0.04	0.00	100.27	SMS-SED	68.00	0.853	
JL99-SN-01	po	SN	40.12	59.96	0.05	0.61	0.01	0.01	100.78	SMS-SED	13.58	0.868	mono
JL99-SN-01	po	SN	39.77	59.36	0.03	0.56	0.01	0.00	99.77	SMS-SED	20.67	0.866	mono
JL99-SN-02	po	SN	40.07	60.00	0.06	0.49	0.06	0.00	100.79	SMS-SED	7.53	0.869	mono
JL99-SN-02	po	SN	39.80	59.80	0.04	0.46	0.00	0.00	100.12	SMS-SED	11.35	0.870	mono
JL99-SN-02	po	SN	39.82	59.91	0.05	0.55	0.04	0.03	100.47	SMS-SED	11.55	0.874	mono
JL99-SN-03	po	SN	39.84	60.57	0.03	0.46	0.00	0.00	100.93	SMS-SED	18.52	0.880	mono
JL99-SN-03	po	SN	39.20	60.04	0.08	0.51	0.00	0.03	99.96	SMS-SED	6.76	0.889	mono
JL99-SN-03	po	SN	39.27	60.47	0.06	0.58	0.03	0.00	100.46	SMS-SED	9.59	0.894	mono

Appendix 3

Sample	Mineral	Ore Body	W%(S)	W%(Fe)	W%(Co)	W%(Ni)	W%(Cu)	W%(As)	Total	Sulphide Class	Ni/Co	M/S	hex/mono
JL98-T1-03	po	T1	39.66	60.38	0.06	0.01	0.01	0.00	100.18	DS-SED	0.10	0.876	mono
JL98-T1-03	po	T1	38.78	61.32	0.08	0.02	0.00	0.00	100.24	DS-SED	0.29	0.910	hex
JL98-T1-03	po	T1	39.29	60.16	0.04	0.00	0.05	0.00	99.61	DS-SED	0.05	0.881	mono
JL98-T1-03	po	T1	39.70	60.33	0.04	0.01	0.00	0.02	100.17	DS-SED	0.17	0.874	mono
JL98-T1-03	po	T1	39.22	59.80	0.08	0.00	0.04	0.03	99.16	DS-SED	0.01	0.877	mono
JL98-T1-03	po	T1	39.61	59.32	0.05	0.03	0.00	0.01	99.04	DS-SED	0.52	0.861	mono
JL98-T1-03	po	T1	39.16	60.32	0.01	0.01	0.01	0.00	99.56	DS-SED	1.23	0.885	mono
JL98-T1-03	po	T1	38.83	61.24	0.09	0.01	0.05	0.01	100.29	DS-SED	0.14	0.908	hex
JL98-T1-04	po	T1	38.24	60.77	0.04	0.32	0.00	0.00	99.42	MS-UB	7.11	0.918	hex
JL98-T1-04	po	T1	38.66	60.72	0.00	0.35	0.00	0.00	99.82	MS-UB	3484.00	0.908	hex
JL98-T1-04	po	T1	38.38	61.16	0.02	0.34	0.03	0.00	100.04	MS-UB	13.48	0.922	hex
JL98-T1-04	po	T1	38.37	61.20	0.01	0.40	0.00	0.01	100.01	MS-UB	58.65	0.922	hex
JL98-T1-04	po	T1	38.49	61.29	0.02	0.41	0.05	0.00	100.30	MS-UB	26.47	0.921	hex
JL98-T1-04	po	T1	38.75	62.18	0.04	0.43	0.02	0.00	101.52	MS-UB	10.69	0.929	hex
JL98-T1-04	po	T1	39.05	61.83	0.05	0.49	0.02	0.02	101.50	MS-UB	10.72	0.917	hex
JL98-T1-04	po	T1	38.85	62.09	0.01	0.44	0.00	0.00	101.46	MS-UB	33.02	0.925	hex
JL98-T1-04	po	T1	36.58	64.05	0.02	0.08	0.02	0.00	100.86	DS-U	4.80	1.009	
JL98-T1-04	po	T1	36.72	64.87	0.05	0.05	0.02	0.00	101.79	DS-U	0.92	1.017	
JL98-T1-04	po	T1	36.47	64.31	0.03	0.04	0.00	0.03	100.94	DS-U	1.22	1.015	
JL98-T1-04	po	T1	36.29	63.67	0.03	0.02	0.03	0.02	100.10	DS-U	0.50	1.009	
JL98-T1-04	po	T1	36.42	64.92	0.05	0.00	0.03	0.01	101.47	DS-U	0.00	1.025	
JL98-T1-04	po	T1	36.37	64.59	0.06	0.01	0.01	0.01	101.07	DS-U	0.20	1.021	
JL98-T1-04	po	T1	37.87	60.87	0.03	0.09	0.00	0.00	99.02	DS-U	3.56	0.927	hex
JL98-T1-06	po	T1	38.63	60.62	0.06	0.36	0.01	0.00	99.71	DS-SED	6.33	0.907	hex
JL98-T1-06	po	T1	38.74	61.52	0.04	0.41	0.00	0.00	100.78	DS-SED	9.90	0.919	hex
JL98-T1-06	po	T1	38.79	60.97	0.07	0.37	0.04	0.00	100.28	DS-SED	5.48	0.910	hex
JL98-T1-06	po	T1	38.83	61.61	0.06	0.35	0.01	0.05	100.99	DS-SED	6.27	0.918	hex
JL98-T1-06	po	T1	39.01	61.32	0.14	0.31	0.00	0.00	100.85	DS-SED	2.11	0.910	hex
JL98-T1-06	po	T1	38.81	61.04	0.08	0.31	0.00	0.00	100.34	DS-SED	3.67	0.910	hex
JL98-T1-07	po	T1	39.35	60.52	0.04	0.29	0.18	0.00	100.49	MS-UB	7.14	0.891	mono
JL98-T1-07	po	T1	39.51	60.43	0.01	0.25	0.00	0.00	100.27	MS-UB	28.06	0.883	mono
JL98-T1-07	po	T1	39.43	60.91	0.05	0.29	0.00	0.02	100.86	MS-UB	6.30	0.894	mono
JL98-T1-07	po	T1	38.94	60.42	0.05	0.31	0.13	0.02	99.97	MS-UB	6.65	0.899	hex
JL98-T1-07	po	T1	39.29	60.41	0.04	0.26	0.07	0.04	100.22	MS-UB	6.24	0.889	mono

Sample	Mineral	Ore Body	W%(S)	W%(Fe)	W%(Co)	W%(Ni)	W%(Cu)	W%(As)	Total	Sulphide Class	Ni/Co	M/S	hex/mono
JL98-T1-07	po	T1	38.67	61.54	0.05	0.41	0.02	0.00	100.68	MS-UB	8.22	0.920	hex
JL98-T1-09A	po	T1	38.81	61.29	0.06	0.44	0.03	0.00	100.67	MS-UB	6.99	0.915	hex
JL98-T1-09A	po	T1	38.77	61.62	0.03	0.44	0.01	0.00	100.91	MS-UB	12.96	0.920	hex
JL98-T1-09A	po	T1	39.37	61.66	0.04	0.26	0.02	0.02	101.39	MS-UB	7.01	0.904	hex
JL98-T1-09A	po	T1	38.94	61.74	0.05	0.46	0.00	0.00	101.24	MS-UB	8.75	0.918	hex
JL98-T1-09A	po	T1	38.69	59.34	0.06	0.50	0.01	0.00	98.66	MS-UB	8.91	0.890	mono
JL98-T1-09A	po	T1	39.15	60.76	0.01	0.25	0.01	0.00	100.21	MS-UB	32.10	0.895	mono
JL98-T1-09A	po	T1	39.37	61.09	0.03	0.32	0.00	0.01	100.82	MS-UB	9.66	0.896	mono
JL98-T1-09A	po	T1	38.65	61.81	0.01	0.30	0.00	0.01	100.90	MS-UB	24.85	0.924	hex
JL98-T1-09A	po	T1	39.32	61.62	0.03	0.22	0.03	0.01	101.35	MS-UB	7.58	0.905	hex
JL98-T1-09A	po	T1	39.07	61.07	0.03	0.26	0.03	0.00	100.55	MS-UB	9.39	0.903	hex
JL98-T1-09A	po	T1	39.26	61.53	0.05	0.21	0.00	0.01	101.10	MS-UB	4.63	0.904	hex
JL98-T1-09A	po	T1	39.30	61.26	0.01	0.20	0.00	0.00	100.80	MS-UB	14.55	0.898	mono
JL98-T1-09B	po	T1	39.27	61.42	0.05	0.11	0.01	0.04	101.04	DS-U	2.45	0.903	hex
JL98-T1-09B	po	T1	39.75	61.91	0.06	0.14	0.03	0.01	101.97	DS-U	2.28	0.899	hex
JL98-T1-09B	po	T1	39.14	61.84	0.02	0.23	0.03	0.01	101.32	DS-U	10.58	0.912	hex
JL98-T1-09B	po	T1	39.41	61.38	0.04	0.15	0.06	0.00	101.09	DS-U	3.30	0.898	mono
JL98-T1-09B	po	T1	39.11	61.01	0.06	0.22	0.01	0.01	100.43	DS-U	3.76	0.900	hex
JL98-T1-09B	po	T1	39.58	61.87	0.03	0.18	0.00	0.04	101.72	DS-U	6.63	0.901	hex
JL98-T1-10	po	T1	39.14	61.14	0.05	0.35	0.00	0.00	100.74	DS-U	7.56	0.904	hex
JL98-T1-10	po	T1	39.13	61.39	0.03	0.35	0.02	0.00	100.93	DS-U	12.05	0.907	hex
JL98-T1-10	po	T1	38.75	61.00	0.04	0.28	0.00	0.00	100.11	DS-U	7.71	0.909	hex
JL98-T1-10	po	T1	39.02	60.84	0.07	0.28	0.00	0.02	100.32	DS-U	4.09	0.901	hex
JL98-T1-10	po	T1	38.87	59.23	0.06	0.28	0.04	0.02	98.51	DS-U	4.52	0.881	mono
JL98-T1-11	po	T1	39.31	62.41	0.06	0.16	0.00	0.00	101.97	IS-U	2.68	0.915	hex
JL98-T1-11	po	T1	38.79	59.36	0.01	0.30	0.03	0.00	98.50	IS-U	25.61	0.883	mono
JL98-T1-11	po	T1	39.65	58.21	0.05	0.30	0.02	0.00	98.34	IS-U	6.07	0.849	
JL98-T1-11	po	T1	39.23	61.64	0.04	0.21	0.00	0.03	101.23	IS-U	5.12	0.907	hex
JL98-T1-11	po	T1	39.45	61.58	0.04	0.32	0.00	0.00	101.54	IS-U	7.44	0.903	hex
JL98-T1-12	po	T1	38.48	60.27	0.05	0.51	0.00	0.00	99.37	MS-UB	9.91	0.908	hex
JL98-T1-12	po	T1	38.70	60.35	0.00	0.54	0.00	0.03	99.66	MS-UB	5406.00	0.904	hex
JL98-T1-12	po	T1	38.75	61.36	0.02	0.48	0.00	0.00	100.67	MS-UB	20.13	0.917	hex
JL98-T1-12	po	T1	38.51	60.79	0.03	0.53	0.01	0.00	99.91	MS-UB	17.96	0.915	hex
JL98-T1-12	po	T1	39.39	60.76	0.06	0.31	0.00	0.00	100.53	MS-UB	5.13	0.891	mono

Sample	Mineral	Ore Body	W%(S)	W%(Fe)	W%(Co)	W%(Ni)	W%(Cu)	W%(As)	Total	Sulphide Class	Ni/Co	M/S	hex/mono
JL98-T1-12	po	T1	39.36	60.12	0.05	0.34	0.00	0.00	99.91	MS-UB	6.57	0.883	mono
JL98-T1-12	po	T1	38.73	61.74	0.03	0.51	0.02	0.02	101.13	MS-UB	18.59	0.924	hex
JL98-T1-12	po	T1	38.70	61.04	0.07	0.54	0.01	0.00	100.37	MS-UB	8.16	0.915	hex
JL98-T1-13	po	T1	39.45	59.25	0.00	0.22	0.01	0.02	98.97	IS-U	67.94	0.866	mono
JL98-T1-13	po	T1	39.70	60.12	0.03	0.26	0.03	0.01	100.16	IS-U	8.19	0.874	mono
JL98-T1-13	po	T1	39.34	59.43	0.04	0.21	0.05	0.00	99.18	IS-U	5.09	0.873	mono
JL98-T1-13	po	T1	39.48	59.72	0.05	0.27	0.07	0.01	99.62	IS-U	5.46	0.874	mono
JL98-T1-13	po	T1	39.63	60.75	0.03	0.18	0.00	0.01	100.63	IS-U	5.43	0.884	mono
JL98-T1-13	po	T1	39.65	60.26	0.03	0.30	0.02	0.00	100.29	IS-U	9.99	0.878	mono
JL98-T1-13	po	T1	39.28	60.97	0.04	0.28	0.01	0.00	100.61	IS-U	6.90	0.896	mono
JL98-T1-13	po	T1	39.72	60.82	0.04	0.19	0.01	0.00	100.82	IS-U	4.44	0.883	mono
JL98-T1-16	po	T1	38.40	61.23	0.04	0.08	0.00	0.05	99.88	DS-SED	2.09	0.919	hex
JL98-T1-16	po	T1	38.46	60.02	0.11	0.06	0.00	0.00	98.69	DS-SED	0.57	0.899	hex
JL98-T1-16	po	T1	38.52	62.20	0.05	0.07	0.01	0.02	100.98	DS-SED	1.32	0.931	hex
JL98-T1-16	po	T1	38.62	60.62	0.06	0.08	0.02	0.01	99.43	DS-SED	1.40	0.904	hex
JL98-T1-16	po	T1	38.68	62.28	0.05	0.07	0.03	0.00	101.16	DS-SED	1.27	0.927	hex
JL98-T1-16	po	T1	38.55	62.91	0.04	0.07	0.00	0.01	101.66	DS-SED	1.51	0.940	hex
JL98-T1-19	po	T1	39.29	60.76	0.03	1.03	0.02	0.00	101.17	MS-SED	38.15	0.903	hex
JL98-T1-19	po	T1	39.35	60.07	0.09	1.07	0.06	0.01	100.69	MS-SED	11.37	0.894	mono
JL98-T1-19	po	T1	39.21	58.23	0.08	0.89	0.01	0.00	98.46	MS-SED	11.23	0.867	mono
JL98-T1-19	po	T1	39.02	59.44	0.05	0.84	0.00	0.01	99.42	MS-SED	16.74	0.888	mono
JL98-T1-19	po	T1	39.23	58.61	0.09	0.95	0.01	0.00	99.04	MS-SED	10.83	0.874	mono
JL98-T1-19	po	T1	39.31	60.26	0.05	0.95	0.00	0.00	100.62	MS-SED	17.48	0.895	mono
JL98-T1-19	po	T1	39.13	61.21	0.05	0.88	0.01	0.01	101.36	MS-SED	16.15	0.912	hex
JL98-T1-20	po	T1	38.76	61.51	0.10	0.15	0.00	0.00	100.60	DS-SED	1.47	0.916	hex
JL98-T1-20	po	T1	38.79	61.87	0.07	0.12	0.00	0.00	100.87	DS-SED	1.66	0.919	hex
JL98-T1-20	po	T1	39.07	62.29	0.06	0.14	0.00	0.00	101.65	DS-SED	2.18	0.919	hex
JL99-T1-25	po	T1	38.49	61.14	0.05	0.19	0.00	0.00	99.90	BMS-SED	4.04	0.916	hex
JL99-T1-25	po	T1	39.07	60.43	0.06	0.23	0.00	0.03	99.90	BMS-SED	4.05	0.893	mono
JL99-T1-25	po	T1	39.21	61.08	0.07	0.22	0.01	0.00	100.65	BMS-SED	3.20	0.899	hex
JL99-T1-25	po	T1	39.47	60.64	0.04	0.28	0.00	0.01	100.45	BMS-SED	7.68	0.887	mono
JL99-T1-26	po	T1	39.45	59.88	0.07	0.18	0.00	0.00	99.61	BMS-SED	2.71	0.875	mono
JL99-T1-26	po	T1	38.95	60.17	0.03	0.20	0.00	0.01	99.39	BMS-SED	7.56	0.891	mono
JL99-T1-26	po	T1	39.30	60.95	0.01	0.19	0.00	0.02	100.52	BMS-SED	25.55	0.894	mono

Sample	Mineral	Ore Body	W%(S)	W%(Fe)	W%(Co)	W%(Ni)	W%(Cu)	W%(As)	Total	Sulphide Class	Ni/Co	M/S	hex/mono
JL99-T1-26	po	T1	39.01	60.80	0.05	0.17	0.00	0.00	100.15	BMS-SED	3.34	0.900	hex
JL98-WL-03	po	WL	39.03	59.28	0.02	0.71	0.03	0.00	99.13	IS-U	28.67	0.883	mono
JL98-WL-03	po	WL	39.14	59.20	0.04	0.55	0.00	0.01	98.97	IS-U	15.35	0.877	mono
JL98-WL-03	po	WL	39.35	59.83	0.03	0.62	0.05	0.01	99.94	IS-U	20.41	0.884	mono
JL98-WL-03	po	WL	39.51	59.87	0.07	0.44	0.00	0.01	99.97	IS-U	6.32	0.878	mono
JL98-WL-03	po	WL	39.78	59.53	0.04	0.59	0.00	0.00	99.99	IS-U	13.35	0.868	mono
JL98-WL-06	po	WL	39.39	57.91	0.02	0.64	0.01	0.00	98.06	IS-U	30.24	0.855	
JL98-WL-06	po	WL	39.21	59.89	0.04	0.64	0.00	0.00	99.86	IS-U	16.21	0.887	mono
JL98-WL-06	po	WL	39.43	59.12	0.04	0.80	0.01	0.02	99.51	IS-U	18.22	0.874	mono
JL98-WL-06	po	WL	39.30	59.04	0.02	0.73	0.00	0.00	99.18	IS-U	37.43	0.874	mono
JL98-WL-06	po	WL	39.34	58.52	0.03	0.72	0.00	0.00	98.67	IS-U	22.16	0.865	mono
JL98-WL-07	po	WL	39.46	59.54	0.06	0.73	0.00	0.00	99.90	MS-UB	11.60	0.878	mono
JL98-WL-07	po	WL	39.37	59.33	0.06	0.69	0.00	0.00	99.49	MS-UB	12.21	0.876	mono
JL98-WL-07	po	WL	39.76	59.46	0.07	0.69	0.00	0.00	100.00	MS-UB	10.42	0.869	mono
JL98-WL-07	po	WL	39.51	59.69	0.00	0.69	0.00	0.00	99.93	MS-UB	984.14	0.878	mono
JL98-WL-07	po	WL	39.24	59.45	0.04	0.80	0.01	0.00	99.56	MS-UB	20.74	0.882	mono
JL98-WL-07	po	WL	39.41	59.71	0.03	0.69	0.00	0.00	99.90	MS-UB	20.23	0.880	mono
JL98-WL-07	po	WL	39.54	59.34	0.04	0.75	0.01	0.00	99.71	MS-UB	18.52	0.873	mono
JL98-WL-09	po	WL	40.61	56.54	0.03	2.36	0.03	0.00	99.63	IS-U	68.13	0.832	
JL98-WL-09	po	WL	41.05	56.43	0.00	2.35	0.00	0.00	99.94	IS-U	1956.67	0.822	
JL98-WL-09	po	WL	39.62	60.19	0.04	0.72	0.00	0.00	100.64	IS-U	20.48	0.884	mono
JL98-WL-09	po	WL	39.53	60.83	0.03	0.64	0.01	0.00	101.16	IS-U	22.11	0.895	mono
JL98-WL-09	po	WL	39.44	60.84	0.03	0.64	0.04	0.00	101.06	IS-U	18.72	0.896	mono
JL98-WL-09	po	WL	41.08	57.77	0.08	1.41	0.03	0.00	100.52	IS-U	18.13	0.829	
JL98-WL-09	po	WL	41.04	57.98	0.05	2.25	0.03	0.04	101.41	IS-U	48.79	0.843	
JL98-WL-10	po	WL	40.96	56.44	0.04	2.14	0.02	0.01	99.77	DS-U	59.90	0.822	
JL98-WL-10	po	WL	40.51	58.18	0.05	1.06	0.04	0.01	99.92	DS-U	19.28	0.841	
JL98-WL-10	po	WL	39.38	60.40	0.02	0.59	0.04	0.00	100.48	DS-U	29.34	0.890	mono
JL98-WL-10	po	WL	39.16	60.25	0.01	0.60	0.00	0.01	100.09	DS-U	78.43	0.893	mono
JL98-WL-10	po	WL	39.41	60.55	0.04	0.58	0.06	0.03	100.70	DS-U	13.14	0.892	mono
JL98-WL-11	po	WL	39.57	60.41	0.01	0.94	0.16	0.02	101.16	MS-SED	68.07	0.892	mono
JL98-WL-11	po	WL	39.60	59.70	0.06	1.04	0.22	0.00	100.67	MS-SED	17.38	0.884	mono
JL98-WL-11	po	WL	39.51	60.29	0.05	0.29	0.21	0.03	100.44	MS-SED	5.32	0.885	mono
JL98-WL-13	po	WL	39.43	60.30	0.00	0.26	0.00	0.00	100.02	BMS-SED	1306.50	0.882	mono

Sample	Mineral	Ore Body	W%(S)	W%(Fe)	W%(Co)	W%(Ni)	W%(Cu)	W%(As)	Total	Sulphide Class	Ni/Co	M/S	hex/mono
JL98-WL-13	po	WL	39.42	59.35	0.04	0.20	0.00	0.01	99.05	BMS-SED	5.11	0.868	mono
JL98-WL-13	po	WL	39.57	60.43	0.02	0.27	0.01	0.03	100.41	BMS-SED	11.28	0.882	mono
JL98-WL-17	po	WL	39.89	61.26	0.08	0.14	0.00	0.04	101.48	DS-SED	1.87	0.886	mono
JL98-WL-17	po	WL	38.85	59.78	0.04	0.10	0.00	0.03	98.89	DS-SED	2.49	0.887	mono
JL98-WL-17	po	WL	39.17	60.43	0.04	0.12	0.00	0.00	99.78	DS-SED	3.10	0.889	mono
JL98-WL-18A	po	WL	38.62	59.59	0.05	0.33	0.01	0.00	98.67	BMS-SED	6.54	0.892	mono
JL98-WL-18A	po	WL	38.85	60.59	0.05	0.27	0.06	0.00	99.85	BMS-SED	5.14	0.901	hex
JL98-WL-18A	po	WL	39.18	60.14	0.04	0.24	0.01	0.01	99.66	BMS-SED	6.40	0.886	mono
JL98-WL-18A	po	WL	39.13	60.65	0.02	0.31	0.01	0.00	100.18	BMS-SED	20.66	0.895	mono
JL98-WL-18A	po	WL	39.23	61.06	0.02	0.29	0.00	0.00	100.67	BMS-SED	18.47	0.899	hex
JL98-WL-18A	po	WL	39.21	61.02	0.02	0.32	0.02	0.00	100.64	BMS-SED	15.86	0.899	hex
JL98-WL-19	po	WL	39.75	60.47	0.05	0.46	0.00	0.00	100.78	BMS-SED	9.27	0.881	mono
JL98-WL-19	po	WL	39.42	59.28	0.04	0.44	0.01	0.00	99.25	BMS-SED	10.67	0.871	mono
JL98-WL-19	po	WL	39.49	59.48	0.05	0.47	0.00	0.03	99.57	BMS-SED	9.02	0.873	mono
JL98-WL-19	po	WL	39.55	60.04	0.03	0.44	0.03	0.01	100.12	BMS-SED	14.67	0.879	mono
JL98-WL-19	po	WL	39.21	59.88	0.04	0.41	0.00	0.00	99.56	BMS-SED	10.68	0.883	mono
JL98-WL-21	po	WL	39.41	59.64	0.05	0.53	0.00	0.00	99.72	DS-SED	10.54	0.878	mono
JL98-WL-21	po	WL	39.45	60.99	0.05	0.57	0.00	0.00	101.10	DS-SED	11.05	0.897	mono
JL98-WL-21	po	WL	39.63	60.46	0.06	0.53	0.00	0.00	100.75	DS-SED	9.33	0.885	mono
JL98-WL-21	po	WL	39.52	60.82	0.06	0.49	0.01	0.02	100.96	DS-SED	8.32	0.892	mono
JL98-WL-23	po	WL	39.56	61.36	0.06	0.50	0.00	0.00	101.57	DS-SED	8.57	0.899	hex
JL98-WL-23	po	WL	39.48	59.11	0.05	0.46	0.01	0.00	99.21	DS-SED	9.29	0.868	mono
JL98-WL-23	po	WL	39.32	60.74	0.02	0.47	0.00	0.00	100.56	DS-SED	22.34	0.894	mono
JL98-WL-24	po	WL	38.73	60.45	0.04	0.54	0.00	0.00	99.77	DS-U	14.02	0.904	hex
JL98-WL-24	po	WL	39.40	60.19	0.03	0.24	0.11	0.00	100.08	DS-U	7.33	0.883	mono
JL98-WL-24	po	WL	39.42	60.21	0.07	0.32	0.00	0.02	100.12	DS-U	4.71	0.883	mono
JL98-WL-25	po	WL	39.67	59.71	0.04	0.25	0.00	0.03	99.74	DS-U	5.96	0.869	mono
JL98-WL-25	po	WL	39.49	60.27	0.06	0.16	0.01	0.00	100.06	DS-U	2.85	0.880	mono
JL98-WL-25	po	WL	39.82	60.49	0.02	0.20	0.00	0.00	100.55	DS-U	8.46	0.875	mono
JL98-WL-25	po	WL	39.76	59.57	0.07	0.30	0.01	0.00	99.78	DS-U	4.03	0.866	mono
JL98-WL-25	po	WL	39.44	60.02	0.04	0.32	0.00	0.03	99.91	DS-U	8.99	0.880	mono
JL98-WL-26	po	WL	39.38	60.04	0.03	0.53	0.00	0.00	100.02	DS-SED	18.10	0.884	mono
JL98-WL-26	po	WL	39.55	59.45	0.05	0.59	0.01	0.00	99.74	DS-SED	10.90	0.873	mono
JL98-WL-26	po	WL	39.28	58.32	0.02	0.57	0.02	0.03	98.39	DS-SED	24.02	0.863	mono

Sample	Mineral	Ore Body	W%(S)	W%(Fe)	W%(Co)	W%(Ni)	W%(Cu)	W%(As)	Total	Sulphide Class	Ni/Co	M/S	hex/mono
JL98-WL-26	po	WL	39.39	58.42	0.04	0.50	0.00	0.00	98.42	DS-SED	11.35	0.860	mono
JL98-WL-26	po	WL	39.45	59.27	0.03	0.58	0.01	0.01	99.38	DS-SED	22.30	0.872	mono
JL98-WL-30	po	WL	38.88	61.89	0.04	0.02	0.04	0.00	100.97	BMS-SED	0.53	0.916	hex
JL98-WL-30	po	WL	38.77	61.76	0.06	0.05	0.37	0.00	101.79	BMS-SED	0.87	0.931	hex
JL98-WL-30	po	WL	38.85	61.67	0.05	0.05	0.14	0.01	100.83	BMS-SED	0.94	0.916	hex
JL98-WL-30	po	WL	39.08	61.47	0.03	0.04	0.01	0.05	100.71	BMS-SED	1.18	0.905	hex
JL98-WL-30	po	WL	39.16	62.27	0.04	0.07	0.04	0.00	101.88	BMS-SED	1.68	0.919	hex
JL98-WL-30	po	WL	39.10	61.86	0.03	0.07	0.03	0.04	101.20	BMS-SED	2.39	0.911	hex
JL98-WL-30	po	WL	39.21	61.69	0.05	0.06	0.03	0.00	101.09	BMS-SED	1.13	0.906	hex
JL98-WL-30	po	WL	39.08	61.82	0.06	0.05	0.01	0.00	101.23	BMS-SED	0.89	0.913	hex
JL98-WL-30	po	WL	38.83	61.38	0.03	0.03	0.00	0.03	100.34	BMS-SED	0.96	0.909	hex
JL98-WL-31	po	WL	39.61	59.76	0.03	0.05	0.00	0.00	99.56	BMS-SED	1.63	0.869	mono
JL98-WL-31	po	WL	39.93	59.74	0.06	0.07	0.01	0.00	99.96	BMS-SED	1.17	0.863	mono
JL98-WL-31	po	WL	39.68	59.58	0.06	0.06	0.04	0.00	99.48	BMS-SED	1.07	0.865	mono
JL98-WL-31	po	WL	39.57	59.42	0.05	0.03	0.00	0.01	99.15	BMS-SED	0.66	0.864	mono
JL98-WL-32	po	WL	39.42	60.27	0.04	0.08	0.00	0.00	99.84	DS-SED	1.92	0.880	mono
JL98-WL-32	po	WL	39.52	60.28	0.06	0.04	0.00	0.00	99.96	DS-SED	0.61	0.878	mono
JL98-WL-32	po	WL	39.51	60.40	0.00	0.05	0.00	0.00	100.01	DS-SED	10.11	0.879	mono
JL98-WL-32	po	WL	39.58	59.18	0.08	0.08	0.01	0.00	98.99	DS-SED	1.05	0.862	mono
JL98-WL-33	po	WL	39.56	60.50	0.04	0.38	0.00	0.00	100.54	MS-SED	9.41	0.885	mono
JL98-WL-33	po	WL	39.64	60.31	0.05	0.34	0.00	0.01	100.39	MS-SED	6.61	0.880	mono
JL98-WL-33	po	WL	39.60	60.51	0.06	0.36	0.00	0.00	100.59	MS-SED	6.36	0.884	mono
JL98-WL-33	po	WL	39.16	59.56	0.05	0.34	0.00	0.02	99.20	MS-SED	6.29	0.879	mono
JL98-WL-33	po	WL	39.65	59.71	0.05	0.36	0.04	0.00	99.84	MS-SED	7.68	0.871	mono
JL98-WL-33	po	WL	39.92	60.82	0.06	0.35	0.00	0.00	101.18	MS-SED	5.57	0.881	mono
JL98-WL-34	po	WL	39.82	59.61	0.04	0.68	0.00	0.00	100.19	MS-SED	15.72	0.870	mono
JL98-WL-34	po	WL	39.55	58.14	0.08	1.11	0.02	0.00	98.94	MS-SED	13.39	0.862	mono
JL98-WL-34	po	WL	39.48	61.06	0.03	0.63	0.04	0.00	101.34	MS-SED	19.52	0.899	hex
JL98-WL-34	po	WL	39.56	61.54	0.00	0.53	0.00	0.00	101.72	MS-SED	333.88	0.902	hex
JL98-WL-34	po	WL	39.51	60.65	0.03	0.64	0.00	0.00	100.85	MS-SED	18.79	0.891	mono
JL98-WL-34	po	WL	39.33	60.83	0.06	0.76	0.00	0.02	101.09	MS-SED	12.88	0.901	hex
JL98-WL-34	po	WL	39.28	61.71	0.05	0.67	0.02	0.00	101.81	MS-SED	12.40	0.913	hex
JL98-WL-34	po	WL	39.52	60.78	0.04	0.71	0.00	0.02	101.11	MS-SED	19.47	0.894	mono
JL98-1C-19	pn	1C	33.13	30.84	0.57	35.71	0.03	0.02	100.41	SMS-SED	62.59		

Sample	Mineral	Ore Body	W%(S)	W%(Fe)	W%(Co)	W%(Ni)	W%(Cu)	W%(As)	Total	Sulphide Class	Ni/Co	M/S	hex/mono
JL98-1C-19	pn	1C	33.18	30.99	0.67	35.45	0.02	0.00	100.44	SMS-SED	52.98		
JL98-1C-19	pn	1C	32.89	30.56	0.57	36.50	0.00	0.04	100.67	SMS-SED	64.05		
JL98-1C-19	pn	1C	33.16	31.08	0.59	36.18	0.00	0.01	101.07	SMS-SED	61.72		
JL98-1C-19	pn	1C	33.19	30.97	0.57	36.13	0.00	0.01	100.96	SMS-SED	62.99		
JL98-1C-20	pn	1C	33.52	30.99	0.15	36.52	0.08	0.01	101.39	MS-SED	251.36		
JL98-1C-20	pn	1C	33.23	30.80	0.12	36.68	0.04	0.00	100.92	MS-SED	314.35		
JL98-1C-20	pn	1C	33.37	30.88	0.12	36.73	0.00	0.03	101.28	MS-SED	301.83		
JL98-1C-21	pn	1C	33.38	31.53	0.58	35.60	0.08	0.02	101.30	SMS-SED	61.24		
JL98-1C-21	pn	1C	33.10	31.03	0.59	35.46	0.05	0.00	100.37	SMS-SED	59.63		
JL98-1C-21	pn	1C	33.23	30.82	0.54	35.87	0.05	0.02	100.60	SMS-SED	65.88		
JL98-1C-21	pn	1C	33.22	31.10	0.50	35.34	0.00	0.00	100.26	SMS-SED	71.12		
JL98-1C-24A	pn	1C	33.55	30.89	0.35	35.12	0.02	0.02	100.03	MS-SED	100.72		
JL98-1C-24A	pn	1C	33.39	30.90	0.37	36.20	0.02	0.02	101.03	MS-SED	97.16		
JL98-1C-24A	pn	1C	33.13	30.81	0.39	36.33	0.03	0.02	100.78	MS-SED	92.53		
JL98-1C-24A	pn	1C	33.34	31.05	0.38	35.89	0.00	0.00	100.68	MS-SED	94.10		
JL98-1C-25B	pn	1C	33.24	29.59	0.81	36.60	0.03	0.01	100.40	MS-SED	45.19		
JL98-1C-25B	pn	1C	33.30	29.31	0.86	36.84	0.01	0.00	100.39	MS-SED	42.80		
JL98-1C-25B	pn	1C	33.40	28.35	0.87	37.25	0.03	0.02	100.04	MS-SED	42.98		
JL98-1C-25B	pn	1C	33.37	29.10	0.75	36.55	0.00	0.03	99.86	MS-SED	48.57		
JL98-1C-25B	pn	1C	33.23	29.76	0.74	36.45	0.02	0.02	100.30	MS-SED	49.45		
JL98-1C-25B	pn	1C	33.19	29.65	0.83	36.49	0.03	0.00	100.25	MS-SED	44.06		
JL98-1C-25B	pn	1C	33.23	30.30	0.78	36.53	0.01	0.00	100.96	MS-SED	47.06		
JL98-1C-25B	pn	1C	33.21	29.73	0.75	37.11	0.00	0.00	100.87	MS-SED	49.37		
JL98-1C-25D	pn	1C	33.29	29.47	0.70	37.17	0.01	0.03	100.76	MS-SED	52.88		
JL98-1C-25D	pn	1C	33.43	29.19	0.90	37.29	0.00	0.00	100.92	MS-SED	41.40		
JL98-1C-25D	pn	1C	33.63	29.86	0.81	37.00	0.05	0.00	101.47	MS-SED	45.58		
JL98-1C-30	pn	1C	33.20	31.34	0.65	34.33	0.00	0.00	99.62	SMS-SED	53.03		
JL98-1C-30	pn	1C	33.46	31.29	0.69	33.99	0.14	0.00	99.71	SMS-SED	49.10		
JL98-1C-30	pn	1C	33.46	30.97	0.70	34.34	0.31	0.00	99.88	SMS-SED	49.41		
JL98-1C-30	pn	1C	33.49	30.06	0.72	34.64	0.01	0.00	99.00	SMS-SED	48.20		
JL98-1C-30	pn	1C	33.37	30.01	0.60	34.63	0.00	0.00	98.74	SMS-SED	58.13		
JL98-1C-30	pn	1C	33.28	30.27	0.73	34.71	0.17	0.02	99.29	SMS-SED	47.32		
JL98-1C-30	pn	1C	33.27	30.36	0.71	35.21	0.03	0.01	99.67	SMS-SED	49.56		
JL98-1C-30	pn	1C	33.36	31.15	0.62	34.49	0.02	0.00	99.71	SMS-SED	55.96		

Appendix 3

Sample	Mineral	Ore Body	W%(S)	W%(Fe)	W%(Co)	W%(Ni)	W%(Cu)	W%(As)	Total	Sulphide Class	Ni/Co	M/S	hex/mono
JL98-1C-30	pn	1C	33.26	30.23	0.64	35.44	0.03	0.02	99.69	SMS-SED	55.72		
JL98-1C-30	pn	1C	33.23	30.86	0.64	34.68	0.04	0.00	99.62	SMS-SED	54.57		
JL99-1C-35	pn	1C	33.63	29.46	0.65	36.21	0.02	0.02	100.07	MS-SED	55.58		
JL99-1C-35	pn	1C	33.36	28.90	0.65	36.71	0.02	0.00	99.72	MS-SED	56.27		
JL99-1C-35	pn	1C	33.66	28.67	0.56	36.61	0.00	0.01	99.68	MS-SED	65.65		
JL98-1D-13a	pn	1D	33.33	30.81	0.20	35.76	0.04	0.00	100.27	SMS-SED	175.66		
JL98-1D-13a	pn	1D	33.40	30.84	0.19	35.44	0.01	0.00	99.94	SMS-SED	188.90		
JL98-1D-13a	pn	1D	33.52	30.31	0.22	36.52	0.01	0.02	100.68	SMS-SED	166.44		
JL98-1D-13a	pn	1D	33.45	30.51	0.24	36.31	0.00	0.00	100.59	SMS-SED	148.91		
JL98-1D-13a	pn	1D	33.63	30.97	0.30	36.33	0.03	0.00	101.34	SMS-SED	121.06		
JL98-1D-13a	pn	1D	33.32	30.49	0.22	36.31	0.00	0.02	100.41	SMS-SED	168.82		
JL98-1D-13a	pn	1D	33.44	31.20	0.21	36.66	0.00	0.01	101.59	SMS-SED	173.25		
JL98-1D-13a	pn	1D	33.52	31.24	0.25	36.59	0.02	0.00	101.71	SMS-SED	145.31		
JL98-1D-13b	pn	1D	33.64	30.89	0.46	35.28	0.02	0.02	100.38	DS-SED	77.23		
JL98-1D-13b	pn	1D	33.33	30.28	0.40	35.66	0.00	0.00	99.84	DS-SED	89.77		
JL98-1D-13b	pn	1D	33.45	30.78	0.47	35.30	0.05	0.02	100.23	DS-SED	75.76		
JL98-1D-13b	pn	1D	33.23	30.83	0.43	35.34	0.03	0.01	99.87	DS-SED	82.16		
JL98-1D-13b	pn	1D	33.50	30.96	0.45	35.71	0.03	0.00	100.76	DS-SED	80.06		
JL98-1D-13b	pn	1D	33.15	30.57	0.47	34.70	0.00	0.01	98.98	DS-SED	73.39		
JL98-1D-14	pn	1D	33.22	30.49	0.33	35.86	0.04	0.01	99.97	SMS-SED	109.92		
JL98-1D-14	pn	1D	33.56	30.63	0.35	35.63	0.02	0.01	100.25	SMS-SED	102.35		
JL98-1D-14	pn	1D	33.43	31.10	0.30	35.31	0.10	0.01	100.28	SMS-SED	119.57		
JL98-1D-14	pn	1D	33.47	30.87	0.32	35.43	0.02	0.00	100.22	SMS-SED	110.00		
JL98-1D-14	pn	1D	33.39	30.62	0.32	35.13	0.02	0.00	99.59	SMS-SED	108.97		
JL98-1D-14	pn	1D	33.49	30.88	0.25	35.46	0.00	0.01	100.21	SMS-SED	144.33		
JL98-1D-14	pn	1D	33.26	30.57	0.30	35.22	0.02	0.00	99.60	SMS-SED	116.66		
JL98-1D-15	pn	1D	33.31	30.72	0.16	35.98	0.02	0.00	100.36	SMS-SED	229.63		
JL98-1D-15	pn	1D	33.03	30.58	0.24	36.28	0.04	0.00	100.27	SMS-SED	152.70		
JL98-1D-15	pn	1D	33.19	30.47	0.14	36.70	0.04	0.00	100.57	SMS-SED	260.47		
JL98-1D-15	pn	1D	33.37	31.26	0.18	35.20	0.06	0.00	100.14	SMS-SED	192.04		
JL98-1D-15	pn	1D	33.07	31.35	0.15	35.62	0.02	0.00	100.27	SMS-SED	232.05		
JL98-1D-15	pn	1D	33.12	30.49	0.23	35.94	0.03	0.00	100.03	SMS-SED	157.84		
JL98-1D-16	pn	1D	33.08	30.99	0.30	36.70	0.09	0.03	101.21	SMS-SED	122.18		
JL98-1D-16	pn	1D	33.29	31.18	0.28	35.93	0.01	0.01	100.82	SMS-SED	127.32		

Appendix 3

Sample	Mineral	Ore Body	W%(S)	W%(Fe)	W%(Co)	W%(Ni)	W%(Cu)	W%(As)	Total	Sulphide Class	Ni/Co	M/S	hex/mono
JL98-1D-16	pn	1D	33.05	30.45	0.39	35.59	0.04	0.00	99.58	SMS-SED	92.08		
JL98-1D-18A	pn	1D	33.44	29.81	0.29	37.71	0.00	0.01	101.39	SMS-SED	131.22		
JL98-1D-18A	pn	1D	33.26	29.60	0.22	37.19	0.01	0.02	100.37	SMS-SED	168.52		
JL98-1D-18A	pn	1D	33.30	30.49	0.29	36.64	0.04	0.00	100.83	SMS-SED	125.70		
JL98-1D-18A	pn	1D	33.33	30.53	0.27	36.69	0.04	0.01	100.94	SMS-SED	136.35		
JL98-1D-18A	pn	1D	33.61	30.40	0.25	37.37	0.01	0.01	101.76	SMS-SED	147.59		
JL98-1D-18B	pn	1D	33.25	30.91	0.69	36.02	0.00	0.02	101.03	DS-SED	51.85		
JL98-1D-18B	pn	1D	33.39	31.34	0.65	36.03	0.03	0.00	101.49	DS-SED	55.85		
JL98-1D-18B	pn	1D	33.15	30.97	0.53	36.22	0.04	0.01	101.02	DS-SED	67.77		
JL98-1D-19	pn	1D	33.54	31.39	0.35	35.74	0.02	0.00	101.20	SMS-SED	102.42		
JL98-1D-19	pn	1D	33.65	31.42	0.35	36.17	0.00	0.00	101.65	SMS-SED	103.53		
JL98-1D-19	pn	1D	33.49	31.17	0.34	35.92	0.07	0.01	101.12	SMS-SED	104.50		
JL98-1D-19	pn	1D	33.39	30.68	0.38	35.87	0.00	0.00	100.43	SMS-SED	94.80		
JL98-1D-19	pn	1D	33.49	30.83	0.34	35.78	0.07	0.02	100.61	SMS-SED	105.78		
JL98-1D-19	pn	1D	33.63	31.05	0.36	36.56	0.05	0.00	101.74	SMS-SED	101.46		
JL98-1D-19	pn	1D	33.35	31.56	0.31	36.11	0.07	0.02	101.59	SMS-SED	116.53		
JL98-1D-19	pn	1D	33.42	31.31	0.30	36.23	0.01	0.00	101.34	SMS-SED	120.05		
JL98-1D-19	pn	1D	33.46	31.45	0.32	36.28	0.03	0.00	101.60	SMS-SED	113.60		
JL98-1D-21	pn	1D	32.82	30.44	0.32	34.56	0.11	0.03	98.38	DS-SED	108.23		
JL98-1D-21	pn	1D	33.12	29.21	0.29	35.48	0.07	0.00	98.25	DS-SED	122.65		
JL99-1D-37	pn	1D	33.92	32.51	0.71	32.78	0.00	0.00	100.00	BMS-SED	46.01		
JL99-1D-37	pn	1D	33.42	30.81	0.83	34.91	0.07	0.00	100.18	BMS-SED	42.01		
JL99-1D-37	pn	1D	33.51	31.18	0.77	34.59	0.02	0.03	100.20	BMS-SED	45.12		
JL99-1D-37	pn	1D	33.63	31.50	0.58	34.46	0.00	0.00	100.23	BMS-SED	59.50		
JL99-1D-38	pn	1D	33.53	30.90	0.89	34.85	0.00	0.00	100.29	BMS-SED	38.97		
JL99-1D-38	pn	1D	33.60	31.15	0.79	35.24	0.01	0.01	100.82	BMS-SED	44.34		
JL99-1D-38	pn	1D	33.52	30.74	0.92	34.95	0.00	0.00	100.20	BMS-SED	38.01		
JL99-1D-39	pn	1D	33.59	30.75	0.84	34.64	0.00	0.00	99.95	BMS-SED	41.21		
JL99-1D-39	pn	1D	33.62	31.19	0.81	34.56	0.00	0.01	100.27	BMS-SED	42.50		
JL99-1D-39	pn	1D	33.71	31.12	0.85	34.69	0.02	0.01	100.54	BMS-SED	40.81		
JL98-BT-01	pn	BT	33.44	27.95	2.81	35.39	0.04	0.00	99.80	DS-U	12.58		
JL98-BT-01	pn	BT	32.65	27.82	2.99	36.01	0.00	0.00	99.53	DS-U	12.04		
JL98-BT-01	pn	BT	33.46	27.82	3.13	34.98	0.05	0.02	100.08	DS-U	11.18		
JL98-BT-01	pn	BT	33.16	26.89	3.28	35.89	0.00	0.00	99.29	DS-U	10.93		

Appendix 3

Sample	Mineral	Ore Body	W%(S)	W%(Fe)	W%(Co)	W%(Ni)	W%(Cu)	W%(As)	Total	Sulphide Class	Ni/Co	M/S	hex/mono
JL98-BT-02	pn	BT	33.08	30.12	1.55	34.50	0.02	0.00	99.30	MS-UB	22.26		
JL98-BT-02	pn	BT	33.24	29.88	1.49	33.88	0.00	0.00	98.61	MS-UB	22.81		
JL98-BT-02	pn	BT	33.06	30.41	1.31	34.28	0.02	0.00	99.21	MS-UB	26.13		
JL98-BT-02	pn	BT	33.71	30.57	1.53	32.46	0.02	0.00	98.33	MS-UB	21.26		
JL98-BT-02	pn	BT	33.21	31.55	1.44	33.15	0.07	0.00	99.54	MS-UB	22.97		
JL98-BT-02	pn	BT	33.36	31.31	1.37	33.54	0.06	0.00	99.74	MS-UB	24.57		
JL98-BT-02	pn	BT	33.10	32.11	1.53	32.88	0.00	0.00	99.69	MS-UB	21.47		
JL98-BT-03	pn	BT	33.41	32.65	1.52	33.18	0.01	0.00	100.87	IS-U	21.80		
JL98-BT-03	pn	BT	33.33	32.49	1.61	33.66	0.00	0.00	101.16	IS-U	20.86		
JL98-BT-03	pn	BT	33.21	32.34	1.63	33.48	0.03	0.00	100.81	IS-U	20.51		
JL98-BT-03	pn	BT	33.41	32.65	1.61	33.34	0.02	0.00	101.03	IS-U	20.72		
JL98-BT-03	pn	BT	33.32	31.78	1.69	33.53	0.02	0.00	100.39	IS-U	19.87		
JL98-BT-03	pn	BT	33.43	31.52	1.89	33.50	0.20	0.00	100.59	IS-U	17.72		
JL98-BT-08	pn	BT	33.61	31.59	1.20	33.81	0.02	0.02	100.39	MS-UB	28.29		
JL98-BT-08	pn	BT	33.40	30.97	1.88	33.83	0.03	0.00	100.25	MS-UB	18.04		
JL98-BT-08	pn	BT	33.41	31.70	1.48	33.44	0.00	0.00	100.15	MS-UB	22.65		
JL98-BT-08	pn	BT	33.33	31.92	1.41	33.61	0.03	0.00	100.44	MS-UB	23.84		
JL98-BT-09	pn	BT	32.06	19.25	6.85	40.26	0.03	0.00	98.58	DS-U	5.88		
JL98-BT-09	pn	BT	32.87	19.33	6.98	40.42	0.00	0.00	99.72	DS-U	5.79		
JL98-BT-09	pn	BT	33.15	19.49	7.07	41.40	0.09	0.07	101.39	DS-U	5.86		
JL98-BT-09	pn	BT	33.13	18.90	6.82	41.29	0.02	0.00	100.27	DS-U	6.05		
JL98-BT-09	pn	BT	33.09	19.36	6.74	41.42	0.00	0.02	100.71	DS-U	6.14		
JL98-BT-10	pn	BT	33.59	30.34	1.34	35.36	0.07	0.00	100.83	MS-SED	26.40		
JL98-BT-10	pn	BT	33.36	31.41	1.57	34.51	0.00	0.00	100.95	MS-SED	22.03		
JL98-BT-11	pn	BT	33.53	32.76	1.35	32.79	0.01	0.01	100.59	DS-U	24.25		
JL98-BT-11	pn	BT	33.48	32.68	1.31	33.05	0.03	0.00	100.57	DS-U	25.26		
JL98-BT-11	pn	BT	33.84	32.37	1.22	33.14	0.04	0.00	100.71	DS-U	27.20		
JL98-BT-11	pn	BT	33.53	32.92	1.31	32.68	0.04	0.00	100.59	DS-U	24.97		
JL98-BT-11	pn	BT	33.46	32.42	1.83	32.45	0.00	0.00	100.24	DS-U	17.71		
JL98-BT-11	pn	BT	33.25	32.56	1.86	32.15	0.03	0.00	99.94	DS-U	17.32		
JL98-BT-11	pn	BT	33.34	32.88	1.86	32.37	0.00	0.00	100.53	DS-U	17.39		
JL98-BT-16A	pn	BT	33.45	30.15	1.94	35.55	0.02	0.00	101.24	DS-U	18.31		
JL98-BT-16A	pn	BT	33.09	30.97	1.84	35.22	0.01	0.00	101.23	DS-U	19.17		
JL98-BT-16A	pn	BT	33.13	31.45	1.47	35.59	0.00	0.00	101.66	DS-U	24.17		

Sample	Mineral	Ore Body	W%(S)	W%(Fe)	W%(Co)	W%(Ni)	W%(Cu)	W%(As)	Total	Sulphide Class	Ni/Co	M/S	hex/mono
JL98-BT-16B	pn	BT	32.86	30.59	1.25	34.81	0.11	0.02	99.73	MS-UB	27.93		
JL98-BT-16B	pn	BT	32.72	30.86	1.28	35.59	0.10	0.02	100.64	MS-UB	27.78		
JL98-BT-16B	pn	BT	32.81	31.28	1.36	34.10	0.05	0.00	99.71	MS-UB	25.13		
JL98-BT-16B	pn	BT	32.44	30.97	1.24	34.98	0.02	0.00	99.69	MS-UB	28.11		
JL98-BT-16B	pn	BT	32.95	31.57	1.29	35.95	0.00	0.00	101.81	MS-UB	27.95		
JL98-BT-16B	pn	BT	33.13	31.58	1.29	35.04	0.07	0.00	101.17	MS-UB	27.19		
JL98-BT-22	pn	BT	32.71	29.96	1.01	35.51	0.01	0.00	99.24	IS-U	35.18		
JL98-BT-22	pn	BT	32.60	30.63	1.06	35.81	0.00	0.00	100.26	IS-U	33.76		
JL98-BT-22	pn	BT	32.83	31.27	1.05	36.61	0.03	0.00	101.85	IS-U	34.87		
JL98-BT-22	pn	BT	32.70	30.05	1.09	36.47	0.00	0.00	100.45	IS-U	33.54		
JL99-BU-01	pn	BU	33.64	32.11	0.15	34.73	0.01	0.00	100.68	SMS-ARC	225.95		
JL99-BU-01	pn	BU	33.72	30.98	0.15	35.01	0.00	0.00	99.95	SMS-ARC	234.34		
JL99-BU-01	pn	BU	33.63	31.23	0.11	35.28	0.04	0.00	100.43	SMS-ARC	331.28		
JL99-BU-02	pn	BU	33.85	31.56	0.23	34.64	0.01	0.00	100.42	MS-ARC	147.91		
JL99-BU-02	pn	BU	33.82	31.82	0.25	34.91	0.00	0.00	100.87	MS-ARC	137.83		
JL99-BU-02	pn	BU	33.50	31.70	0.22	34.90	0.00	0.00	100.36	MS-ARC	160.62		
JL99-BU-02	pn	BU	33.99	31.67	0.23	34.72	0.00	0.00	100.71	MS-ARC	152.01		
JL99-BU-04	pn	BU	33.49	32.42	0.47	33.38	0.03	0.03	99.89	IS-U	70.61		
JL99-BU-04	pn	BU	33.69	32.64	0.43	33.11	0.07	0.00	100.08	IS-U	77.59		
JL99-BU-04	pn	BU	33.83	31.89	0.47	33.10	0.00	0.00	99.39	IS-U	70.92		
JL99-BU-04	pn	BU	33.93	33.02	0.51	33.13	0.01	0.01	100.67	IS-U	64.62		
JL99-BU-05	pn	BU	33.89	31.99	0.58	33.42	0.09	0.02	100.16	IS-U	58.04		
JL99-BU-05	pn	BU	34.32	32.64	0.61	33.59	0.00	0.00	101.28	IS-U	54.95		
JL99-BU-05	pn	BU	33.65	31.40	0.95	33.46	0.02	0.00	99.64	IS-U	35.11		
JL99-BU-05	pn	BU	33.77	31.39	1.00	33.15	0.02	0.00	99.48	IS-U	33.25		
JL99-BU-08	pn	BU	33.63	29.65	0.34	35.85	0.06	0.00	99.57	SMS-ARC	106.57		
JL99-BU-08	pn	BU	34.09	29.75	0.37	36.30	0.00	0.00	100.55	SMS-ARC	99.05		
JL99-BU-08	pn	BU	33.94	30.65	0.31	36.11	0.00	0.02	101.19	SMS-ARC	115.37		
JL99-BU-08	pn	BU	33.69	30.03	0.29	36.27	0.00	0.00	100.35	SMS-ARC	126.81		
DM98-1C-02	pn	1C	33.63	32.51	0.72	33.93	0.04	0.00	100.92	IS-U	47.40		
DM98-1C-02	pn	1C	33.56	32.76	0.67	34.07	0.06	0.02	101.20	IS-U	50.71		
DM98-1C-02	pn	1C	33.39	32.52	0.71	33.55	0.01	0.00	100.31	IS-U	47.27		
DM98-1C-02	pn	1C	33.42	32.25	0.64	33.52	0.03	0.00	99.94	IS-U	52.02		
DM98-1C-02	pn	1C	33.49	32.71	0.61	34.16	0.00	0.00	101.05	IS-U	55.96		

Appendix 3

Sample	Mineral	Ore Body	W%(S)	W%(Fe)	W%(Co)	W%(Ni)	W%(Cu)	W%(As)	Total	Sulphide Class	Ni/Co	M/S	hex/mono
DM98-1C-02	pn	1C	34.09	32.74	0.61	33.58	0.06	0.00	101.14	IS-U	55.43		
DM98-1C-02	pn	1C	33.44	32.91	0.63	33.41	0.02	0.02	100.59	IS-U	53.11		
DM98-1C-03	pn	1C	33.99	32.53	0.70	34.02	0.03	0.02	101.44	IS-U	48.77		
DM98-1C-03	pn	1C	34.04	32.86	0.71	33.97	0.00	0.00	101.69	IS-U	47.67		
DM98-1C-03	pn	1C	33.84	33.00	0.67	33.67	0.04	0.00	101.28	IS-U	50.40		
DM98-1C-04	pn	1C	33.61	33.07	0.60	33.16	0.01	0.00	100.59	DS-U	55.44		
DM98-1C-04	pn	1C	33.65	33.47	0.61	33.25	0.05	0.00	101.09	DS-U	54.95		
DM98-1C-04	pn	1C	33.51	33.30	0.66	32.97	0.05	0.00	100.59	DS-U	50.30		
DM98-1C-05	pn	1C	32.67	33.75	0.79	30.50	0.02	0.00	97.87	DS-U	38.63		
DM98-1C-05	pn	1C	34.05	34.96	0.81	31.42	0.03	0.01	101.34	DS-U	38.93		
DM98-1C-05	pn	1C	34.06	35.00	0.77	31.60	0.02	0.01	101.52	DS-U	41.03		
DM98-1C-06	pn	1C	33.55	34.20	0.76	32.38	0.01	0.00	101.02	DS-U	42.49		
DM98-1C-06	pn	1C	33.52	34.20	0.71	32.14	0.00	0.01	100.63	DS-U	45.42		
DM98-1C-06	pn	1C	33.73	34.40	0.85	32.19	0.00	0.00	101.32	DS-U	37.97		
DM98-1C-07	pn	1C	33.62	31.64	0.42	35.55	0.00	0.01	101.31	MS-SED	85.31		
DM98-1C-07	pn	1C	33.72	31.71	0.47	35.32	0.00	0.02	101.32	MS-SED	74.68		
DM98-1C-07	pn	1C	33.45	31.15	0.40	36.22	0.00	0.03	101.36	MS-SED	90.57		
DM98-1C-08	pn	1C	33.17	29.94	0.54	35.86	0.00	0.03	99.61	DS-SED	66.11		
DM98-1C-08	pn	1C	33.28	30.30	0.62	36.24	0.01	0.00	100.64	DS-SED	58.36		
DM98-1C-08	pn	1C	33.23	29.99	0.70	36.01	0.02	0.02	100.10	DS-SED	51.18		
DM98-1C-09	pn	1C	33.43	30.10	0.04	37.42	0.03	0.00	101.16	DS-SED	1025.27		
DM98-1C-09	pn	1C	34.04	30.11	0.02	37.56	0.04	0.00	101.92	DS-SED	1887.62		
DM98-1C-09	pn	1C	33.57	30.79	0.54	36.04	0.04	0.00	101.06	DS-SED	66.40		
DM98-1C-09	pn	1C	33.56	30.92	0.49	36.01	0.04	0.00	101.22	DS-SED	74.19		
DM98-1C-09	pn	1C	33.71	31.24	0.41	36.22	0.04	0.02	101.78	DS-SED	88.23		
JL99-SN-01	pn	SN	34.70	29.39	0.91	35.89	0.08	0.06	101.11	SMS-SED	39.62		
JL99-SN-01	pn	SN	33.53	28.55	0.90	37.45	0.02	0.00	100.54	SMS-SED	41.52		
JL99-SN-01	pn	SN	33.58	28.42	0.91	37.81	0.03	0.02	100.83	SMS-SED	41.33		
JL99-SN-02	pn	SN	33.57	28.98	0.86	36.84	0.03	0.00	100.40	SMS-SED	42.60		
JL99-SN-02	pn	SN	33.96	28.57	0.85	37.46	0.04	0.00	100.96	SMS-SED	43.83		
JL99-SN-02	pn	SN	33.68	28.56	0.91	37.59	0.06	0.00	100.89	SMS-SED	41.47		
JL99-SN-03	pn	SN	34.06	31.40	1.00	34.99	0.00	0.01	101.60	SMS-SED	34.84		
JL99-SN-03	pn	SN	33.70	31.28	1.07	35.31	0.02	0.00	101.45	SMS-SED	32.95		
JL99-SN-03	pn	SN	33.78	31.34	1.10	35.12	0.00	0.01	101.40	SMS-SED	32.02		

Appendix 3

Sample	Mineral	Ore Body	W%(S)	W%(Fe)	W%(Co)	W%(Ni)	W%(Cu)	W%(As)	Total	Sulphide Class	Ni/Co	M/S	hex/mono
JL99-SN-03	pn	SN	33.44	30.82	1.06	35.35	0.06	0.02	100.82	SMS-SED	33.49		
JL98-T1-04	pn	T1	33.13	31.15	0.74	33.85	0.00	0.00	98.91	MS-UB	45.98		
JL98-T1-04	pn	T1	33.13	31.46	0.76	34.63	0.01	0.01	100.05	MS-UB	45.72		
JL98-T1-04	pn	T1	33.45	31.71	0.81	34.69	0.00	0.00	100.80	MS-UB	42.66		
JL98-T1-04	pn	T1	33.38	30.87	0.81	35.12	0.02	0.00	100.28	MS-UB	43.59		
JL98-T1-04	pn	T1	33.30	30.71	0.79	34.81	0.01	0.00	99.75	MS-UB	44.34		
JL98-T1-04	pn	T1	33.45	31.08	0.83	34.47	0.00	0.01	99.99	MS-UB	41.77		
JL98-T1-04	pn	T1	33.38	31.65	0.78	35.79	0.06	0.00	101.83	MS-UB	45.86		
JL98-T1-04	pn	T1	33.45	31.74	0.83	34.28	0.02	0.01	100.40	DS-U	41.12		
JL98-T1-04	pn	T1	33.39	31.38	0.89	35.34	0.00	0.00	101.05	DS-U	39.85		
JL98-T1-04	pn	T1	33.73	32.57	0.84	33.94	0.16	0.00	101.33	DS-U	40.44		
JL98-T1-04	pn	T1	33.29	31.78	0.71	34.95	0.08	0.00	100.94	DS-U	49.23		
JL98-T1-04	pn	T1	33.20	31.27	0.74	35.01	0.03	0.03	100.36	DS-U	47.20		
JL98-T1-04	pn	T1	33.31	31.75	0.65	34.48	0.05	0.00	100.31	DS-U	52.95		
JL98-T1-07	pn	T1	33.43	31.50	0.81	34.70	0.01	0.03	100.58	MS-UB	42.72		
JL98-T1-07	pn	T1	33.34	31.72	0.72	35.09	0.04	0.00	101.06	MS-UB	48.60		
JL98-T1-07	pn	T1	33.51	31.80	0.82	35.21	0.02	0.02	101.41	MS-UB	43.01		
JL98-T1-07	pn	T1	33.38	30.86	0.78	35.19	0.04	0.02	100.32	MS-UB	44.99		
JL98-T1-07	pn	T1	33.36	30.96	0.55	35.35	0.04	0.00	100.30	MS-UB	64.76		
JL98-T1-07	pn	T1	33.36	31.87	0.79	35.09	0.04	0.00	101.21	MS-UB	44.47		
JL98-T1-09A	pn	T1	33.93	31.36	0.65	34.11	0.11	0.00	100.26	MS-UB	52.52		
JL98-T1-09A	pn	T1	33.16	30.63	0.64	35.24	0.03	0.01	99.73	MS-UB	55.06		
JL98-T1-09A	pn	T1	33.67	31.15	0.65	35.57	0.02	0.00	101.16	MS-UB	55.02		
JL98-T1-09A	pn	T1	33.22	31.41	0.71	35.17	0.02	0.01	100.60	MS-UB	49.38		
JL98-T1-09A	pn	T1	33.31	31.47	0.59	35.55	0.00	0.00	101.04	MS-UB	60.16		
JL98-T1-09A	pn	T1	33.34	31.53	0.56	35.72	0.03	0.00	101.28	MS-UB	64.22		
JL98-T1-09A	pn	T1	33.25	31.95	0.88	35.47	0.04	0.00	101.63	MS-UB	40.13		
JL98-T1-09A	pn	T1	33.33	31.87	0.82	35.75	0.00	0.00	101.84	MS-UB	43.55		
JL98-T1-09A	pn	T1	33.09	31.83	0.63	35.62	0.18	0.04	101.50	MS-UB	56.63		
JL98-T1-09B	pn	T1	33.49	33.21	0.89	34.03	0.02	0.00	101.73	DS-U	38.35		
JL98-T1-09B	pn	T1	33.15	32.01	0.94	34.44	0.04	0.01	100.71	DS-U	36.49		
JL98-T1-09B	pn	T1	32.69	32.14	0.63	34.31	0.02	0.00	99.88	DS-U	54.60		
JL98-T1-10	pn	T1	33.22	31.58	0.50	35.02	0.03	0.01	100.40	DS-U	69.99		
JL98-T1-10	pn	T1	33.58	32.60	0.46	33.74	0.01	0.00	100.50	DS-U	73.13		

Sample	Mineral	Ore Body	W%(S)	W%(Fe)	W%(Co)	W%(Ni)	W%(Cu)	W%(As)	Total	Sulphide Class	Ni/Co	M/S	hex/mono
JL98-T1-10	pn	T1	33.69	32.25	0.55	34.56	0.02	0.02	101.12	DS-U	63.17		
JL98-T1-10	pn	T1	33.51	32.31	0.44	34.44	0.04	0.00	100.82	DS-U	79.11		
JL98-T1-10	pn	T1	33.52	31.57	0.51	34.05	0.08	0.01	99.95	DS-U	67.39		
JL98-T1-11	pn	T1	33.50	32.14	0.68	35.36	0.05	0.02	101.82	IS-U	51.73		
JL98-T1-11	pn	T1	33.28	32.05	0.70	35.73	0.07	0.00	101.91	IS-U	51.25		
JL98-T1-11	pn	T1	33.46	30.63	0.74	35.59	0.03	0.00	100.60	IS-U	48.05		
JL98-T1-11	pn	T1	33.24	31.10	0.74	34.25	0.00	0.03	99.51	IS-U	46.09		
JL98-T1-12	pn	T1	33.14	31.66	0.61	34.43	0.09	0.04	100.08	MS-UB	56.11		
JL98-T1-12	pn	T1	33.11	31.24	0.55	34.65	0.07	0.05	99.75	MS-UB	63.03		
JL98-T1-12	pn	T1	33.04	31.60	0.52	34.66	0.00	0.01	99.91	MS-UB	67.16		
JL98-T1-12	pn	T1	33.27	30.78	0.68	34.61	0.02	0.00	99.46	MS-UB	50.56		
JL98-T1-12	pn	T1	33.41	30.64	0.66	33.99	0.05	0.00	98.81	MS-UB	51.55		
JL98-T1-12	pn	T1	33.02	31.41	0.52	34.34	0.00	0.00	99.39	MS-UB	65.80		
JL98-T1-12	pn	T1	33.04	31.13	0.57	34.81	0.00	0.00	99.63	MS-UB	60.79		
JL98-T1-12	pn	T1	32.92	31.60	0.58	33.92	0.00	0.01	99.19	MS-UB	58.50		
JL98-T1-12	pn	T1	33.10	31.18	0.69	34.15	0.00	0.02	99.18	MS-UB	49.66		
JL98-T1-12	pn	T1	32.71	31.62	0.74	33.85	0.00	0.00	99.06	MS-UB	45.99		
JL98-T1-12	pn	T1	33.07	31.02	0.64	34.21	0.04	0.00	99.02	MS-UB	53.42		
JL98-T1-12	pn	T1	33.11	31.18	0.63	33.79	0.22	0.00	98.99	MS-UB	53.66		
JL98-T1-13	pn	T1	33.16	31.34	0.81	34.41	0.01	0.03	99.86	IS-U	42.61		
JL98-T1-13	pn	T1	33.29	31.46	0.82	34.88	0.00	0.01	100.51	IS-U	42.44		
JL98-T1-13	pn	T1	33.09	30.97	0.92	34.47	0.04	0.00	99.62	IS-U	37.51		
JL98-T1-13	pn	T1	33.18	31.84	0.69	35.13	0.03	0.02	101.01	IS-U	51.22		
JL98-T1-13	pn	T1	33.16	30.97	0.69	35.71	0.03	0.01	100.66	IS-U	51.58		
JL98-T1-13	pn	T1	33.21	31.34	0.77	35.63	0.00	0.01	101.06	IS-U	46.14		
JL98-T1-13	pn	T1	33.27	31.74	0.73	34.18	0.07	0.01	100.07	IS-U	46.82		
JL98-T1-19	pn	T1	33.18	28.90	0.70	38.15	0.05	0.00	101.00	MS-SED	54.87		
JL98-T1-19	pn	T1	33.21	29.14	0.60	38.76	0.01	0.01	101.89	MS-SED	64.91		
JL98-T1-19	pn	T1	33.05	29.06	0.58	37.57	0.00	0.00	100.34	MS-SED	65.14		
JL98-T1-19	pn	T1	32.89	28.83	0.65	37.45	0.01	0.00	99.86	MS-SED	57.21		
JL98-T1-19	pn	T1	33.03	29.26	0.58	36.55	0.01	0.02	99.55	MS-SED	63.03		
JL98-WL-03	pn	WL	33.42	30.14	0.47	35.40	0.17	0.00	99.68	IS-U	75.72		
JL98-WL-03	pn	WL	33.84	30.50	0.38	35.62	0.03	0.00	100.44	IS-U	93.23		
JL98-WL-03	pn	WL	33.21	28.80	0.49	37.72	0.01	0.00	100.28	IS-U	76.59		

Appendix 3

Sample	Mineral	Ore Body	W%(S)	W%(Fe)	W%(Co)	W%(Ni)	W%(Cu)	W%(As)	Total	Sulphide Class	Ni/Co	M/S	hex/mono
JL98-WL-03	pn	WL	33.68	28.56	0.80	34.99	0.07	0.00	98.21	IS-U	43.66		
JL98-WL-06	pn	WL	33.20	27.55	0.34	37.74	0.02	0.00	98.96	IS-U	111.89		
JL98-WL-06	pn	WL	33.27	27.36	0.25	38.54	0.01	0.02	99.56	IS-U	152.64		
JL98-WL-06	pn	WL	33.29	27.87	0.41	38.67	0.18	0.00	100.48	IS-U	93.67		
JL98-WL-06	pn	WL	33.62	28.27	0.44	38.91	0.00	0.01	101.35	IS-U	88.32		
JL98-WL-07	pn	WL	33.31	28.32	0.33	38.50	0.03	0.00	100.59	MS-UB	115.26		
JL98-WL-07	pn	WL	33.25	28.76	0.31	38.09	0.04	0.00	100.52	MS-UB	121.18		
JL98-WL-07	pn	WL	33.27	28.11	0.27	38.47	0.01	0.02	100.29	MS-UB	143.18		
JL98-WL-07	pn	WL	33.31	28.23	0.21	38.73	0.06	0.00	100.61	MS-UB	183.54		
JL98-WL-07	pn	WL	32.87	28.45	0.41	38.52	0.00	0.00	100.29	MS-UB	94.39		
JL98-WL-07	pn	WL	33.09	28.41	0.37	38.16	0.00	0.00	100.13	MS-UB	104.25		
JL98-WL-07	pn	WL	33.19	28.91	0.37	38.35	0.02	0.00	100.92	MS-UB	103.78		
JL98-WL-07	pn	WL	33.02	28.27	0.38	38.68	0.01	0.00	100.46	MS-UB	102.13		
JL98-WL-09	pn	WL	33.10	28.51	0.71	36.62	0.03	0.00	99.02	IS-U	51.29		
JL98-WL-09	pn	WL	33.20	28.63	0.76	37.27	0.03	0.01	99.99	IS-U	48.87		
JL98-WL-09	pn	WL	33.33	28.58	0.72	38.12	0.02	0.02	100.92	IS-U	52.89		
JL98-WL-09	pn	WL	33.15	28.62	0.84	37.16	0.16	0.01	100.07	IS-U	44.30		
JL98-WL-10	pn	WL	33.14	27.88	0.85	37.90	0.04	0.04	99.97	DS-U	44.67		
JL98-WL-10	pn	WL	33.43	28.58	0.62	38.09	0.04	0.00	100.89	DS-U	61.22		
JL98-WL-24	pn	WL	33.74	30.54	0.66	35.80	0.08	0.04	101.05	DS-U	54.03		
JL98-WL-24	pn	WL	32.95	30.82	0.67	34.98	0.02	0.00	99.53	DS-U	51.93		
JL98-WL-24	pn	WL	33.26	30.77	0.69	35.84	0.00	0.05	100.69	DS-U	51.87		
JL98-WL-25	pn	WL	33.33	29.01	0.19	38.02	0.00	0.03	100.68	DS-U	198.00		
JL98-WL-25	pn	WL	33.80	28.34	0.20	38.02	0.00	0.00	100.49	DS-U	190.39		
JL98-WL-25	pn	WL	33.87	27.57	0.21	38.46	0.04	0.01	100.30	DS-U	185.90		
JL98-WL-25	pn	WL	33.36	28.30	0.12	39.10	0.04	0.00	101.02	DS-U	314.53		
JL98-WL-26	pn	WL	33.17	28.75	0.41	37.71	0.04	0.00	100.21	DS-SED	91.52		
JL98-WL-26	pn	WL	33.12	28.30	0.48	36.53	0.01	0.00	98.60	DS-SED	75.96		
JL98-WL-26	pn	WL	33.13	28.76	0.55	37.17	0.00	0.03	99.72	DS-SED	67.17		
JL98-WL-26	pn	WL	33.14	28.18	0.43	36.77	0.04	0.00	98.70	DS-SED	86.01		
JL98-WL-26	pn	WL	33.39	29.22	0.50	35.40	0.00	0.00	98.64	DS-SED	70.88		
JL98-WL-26	pn	WL	33.25	29.15	0.60	36.98	0.02	0.00	100.04	DS-SED	61.77		
JL98-WL-34	pn	WL	33.54	29.45	0.79	36.04	0.00	0.00	99.89	MS-SED	45.48		
JL98-WL-34	pn	WL	33.27	28.26	0.69	37.45	0.01	0.01	99.79	MS-SED	54.30		

Sample	Mineral	Ore Body	W%(S)	W%(Fe)	W%(Co)	W%(Ni)	W%(Cu)	W%(As)	Total	Sulphide Class	Ni/Co	M/S	hex/mono
JL98-WL-34	pn	WL	33.40	28.71	0.57	37.63	0.04	0.00	100.38	MS-SED	65.83		
JL98-WL-34	pn	WL	33.26	29.30	0.68	36.59	0.82	0.00	100.80	MS-SED	53.68		
JL98-1C-10	cp	1C	34.82	30.66	0.00	0.01	34.23	0.00	99.86	DS-SED	3.17		
JL98-1C-10	cp	1C	34.99	30.71	0.03	0.07	33.42	0.00	99.36	DS-SED	2.20		
JL98-1C-11	cp	1C	34.47	30.04	0.03	0.00	34.49	0.02	99.11	DS-SED	0.00		
JL98-1C-11	cp	1C	34.26	29.99	0.02	0.00	34.59	0.00	98.90	DS-SED	0.18		
JL98-1C-11	cp	1C	34.54	30.86	0.03	0.01	34.23	0.00	99.75	DS-SED	0.57		
JL98-1C-11	cp	1C	34.46	29.97	0.00	0.00	34.34	0.01	98.84	DS-SED	47.00		
JL98-1C-12	cp	1C	34.53	30.18	0.05	0.02	34.66	0.00	99.48	DS-SED	0.42		
JL98-1C-12	cp	1C	35.05	30.10	0.05	0.02	34.45	0.00	99.75	DS-SED	0.39		
JL98-1C-12	cp	1C	34.85	30.36	0.05	0.02	34.72	0.00	100.10	DS-SED	0.30		
JL98-1C-12	cp	1C	34.73	30.42	0.05	0.01	34.05	0.00	99.39	DS-SED	0.21		
JL98-1C-12	cp	1C	34.48	29.46	0.00	0.03	34.71	0.01	98.72	DS-SED	283.00		
JL98-1C-15	cp	1C	34.52	30.20	0.04	0.00	34.11	0.00	98.90	DS-SED	0.04		
JL98-1C-15	cp	1C	34.03	30.25	0.00	0.01	33.72	0.03	98.15	DS-SED	110.00		
JL98-1C-16	cp	1C	34.61	30.32	0.03	0.00	33.90	0.03	98.94	DS-SED	0.00		
JL98-1C-16	cp	1C	34.34	30.12	0.02	0.02	33.91	0.00	98.47	DS-SED	0.85		
JL98-1C-19	cp	1C	35.02	30.17	0.06	0.05	34.83	0.01	100.23	SMS-SED	0.78		
JL98-1C-19	cp	1C	34.65	31.00	0.04	0.00	35.26	0.00	101.02	SMS-SED	0.07		
JL98-1C-19	cp	1C	34.89	30.32	0.01	0.04	35.51	0.00	100.90	SMS-SED	5.35		
JL98-1C-19	cp	1C	34.75	30.83	0.02	0.00	35.45	0.00	101.14	SMS-SED	0.01		
JL98-1C-20	cp	1C	34.66	30.33	0.04	0.27	35.20	0.00	100.60	MS-SED	6.06		
JL98-1C-20	cp	1C	34.75	30.83	0.07	0.01	35.30	0.00	101.01	MS-SED	0.19		
JL98-1C-20	cp	1C	34.72	30.46	0.04	0.04	35.11	0.00	100.38	MS-SED	0.98		
JL98-1C-21	cp	1C	34.86	30.54	0.00	0.05	35.11	0.00	100.66	SMS-SED	78.00		
JL98-1C-21	cp	1C	35.05	30.27	0.04	0.56	34.57	0.00	100.58	SMS-SED	12.98		
JL98-1C-21	cp	1C	34.71	30.44	0.02	0.01	35.39	0.00	100.79	SMS-SED	0.50		
JL98-1C-21	cp	1C	35.14	30.07	0.03	0.03	35.33	0.03	100.70	SMS-SED	1.32		
JL98-1C-21	cp	1C	34.69	30.29	0.01	0.08	34.80	0.00	99.86	SMS-SED	10.80		
JL98-1C-22	cp	1C	34.46	30.47	0.03	0.01	34.53	0.01	99.59	DS-SED	0.17		
JL98-1C-22	cp	1C	34.89	30.04	0.02	0.00	34.34	0.00	99.47	DS-SED	0.01		
JL98-1C-22	cp	1C	34.64	30.74	0.03	0.03	33.82	0.03	99.78	DS-SED	0.94		
JL98-1C-22	cp	1C	34.99	30.32	0.03	0.05	34.82	0.00	100.23	DS-SED	1.51		
JL98-1C-23	cp	1C	34.95	30.14	0.03	0.02	34.41	0.01	99.69	DS-SED	0.48		

Appendix 3

Sample	Mineral	Ore Body	W%(S)	W%(Fe)	W%(Co)	W%(Ni)	W%(Cu)	W%(As)	Total	Sulphide Class	Ni/Co	M/S	hex/mono
JL98-1C-23	cp	1C	35.04	30.39	0.06	0.03	34.44	0.00	100.06	DS-SED	0.47		
JL98-1C-23	cp	1C	34.77	30.33	0.04	0.05	34.33	0.02	99.59	DS-SED	1.14		
JL98-1C-24A	cp	1C	34.60	30.40	0.01	0.01	34.81	0.01	99.86	MS-SED	1.74		
JL98-1C-24A	cp	1C	34.53	30.47	0.04	0.01	34.46	0.00	99.56	MS-SED	0.26		
JL98-1C-24A	cp	1C	34.95	30.67	0.04	0.05	34.36	0.02	100.25	MS-SED	1.42		
JL98-1C-25B	cp	1C	34.68	30.44	0.00	0.03	35.10	0.02	100.35	MS-SED	303.00		
JL98-1C-25B	cp	1C	34.63	30.29	0.01	0.04	34.68	0.00	99.91	MS-SED	2.52		
JL98-1C-25B	cp	1C	35.09	30.57	0.05	0.09	34.76	0.03	100.79	MS-SED	1.94		
JL98-1C-25B	cp	1C	34.42	30.23	0.05	0.26	33.79	0.00	99.00	MS-SED	5.09		
JL98-1C-25B	cp	1C	34.78	29.35	0.04	0.09	34.75	0.01	99.08	MS-SED	2.33		
JL98-1C-25B	cp	1C	34.74	30.01	0.02	0.32	34.37	0.00	99.55	MS-SED	14.82		
JL98-1C-25B	cp	1C	35.00	30.71	0.04	0.18	34.59	0.00	100.67	MS-SED	4.06		
JL98-1C-25B	cp	1C	35.04	30.36	0.00	0.06	35.10	0.03	100.66	MS-SED	569.00		
JL98-1C-25D	cp	1C	35.15	30.30	0.07	0.16	34.19	0.02	100.12	MS-SED	2.33		
JL98-1C-28A	cp	1C	34.98	30.84	0.00	0.02	34.56	0.01	100.51	DS-SED	164.00		
JL98-1C-28A	cp	1C	34.76	31.56	0.03	0.02	35.17	0.00	101.63	DS-SED	0.69		
JL98-1C-28C	cp	1C	34.91	32.17	0.04	0.00	34.67	0.01	101.91	DS-SED	0.00		
JL98-1C-28C	cp	1C	34.64	31.08	0.00	0.02	35.18	0.02	101.05	DS-SED	213.00		
JL98-1C-29	cp	1C	34.87	29.80	0.03	0.01	34.60	0.00	99.39	DS-SED	0.37		
JL98-1C-29	cp	1C	35.01	29.67	0.00	0.00	34.86	0.03	99.69	DS-SED	1.00		
JL98-1C-29	cp	1C	34.98	30.20	0.01	0.03	34.77	0.00	100.11	DS-SED	1.77		
JL98-1C-29	cp	1C	34.75	29.35	0.02	0.00	34.68	0.02	99.15	DS-SED	0.19		
JL98-1C-30	cp	1C	35.00	30.35	0.03	0.01	35.44	0.01	100.96	SMS-SED	0.20		
JL98-1C-30	cp	1C	34.89	30.55	0.04	0.02	34.73	0.00	100.31	SMS-SED	0.52		
JL98-1C-30	cp	1C	34.82	30.76	0.07	0.01	34.85	0.00	100.55	SMS-SED	0.15		
JL98-1C-30	cp	1C	34.79	29.85	0.06	0.03	34.68	0.00	99.44	SMS-SED	0.43		
JL98-1C-30	cp	1C	34.71	29.71	0.00	0.02	33.99	0.01	98.52	SMS-SED	161.00		
JL98-1C-33	cp	1C	35.03	30.27	0.02	0.04	33.92	0.00	99.35	DS-SED	1.56		
JL98-1C-33	cp	1C	34.79	30.03	0.01	0.01	33.58	0.00	98.48	DS-SED	0.57		
JL98-1C-33	cp	1C	34.79	30.26	0.02	0.00	34.85	0.00	99.95	DS-SED	0.00		
JL99-1C-35	cp	1C	35.41	29.27	0.04	0.05	34.58	0.00	99.51	MS-SED	1.31		
JL99-1C-35	cp	1C	35.07	29.23	0.01	0.04	34.57	0.00	99.01	MS-SED	4.67		
JL99-1C-35	cp	1C	34.79	29.54	0.01	0.06	33.99	0.00	98.41	MS-SED	10.46		
JL98-1D-01	cp	1D	34.85	29.99	0.05	0.00	34.51	0.01	99.45	DS-SED	0.05		

Appendix 3

Sample	Mineral	Ore Body	W%(S)	W%(Fe)	W%(Co)	W%(Ni)	W%(Cu)	W%(As)	Total	Sulphide Class	Ni/Co	M/S	hex/mono
JL98-1D-01	cp	1D	34.42	29.09	0.03	0.00	34.51	0.00	98.11	DS-SED	0.09		
JL98-1D-01	cp	1D	34.65	30.33	0.03	0.01	34.17	0.02	99.26	DS-SED	0.28		
JL98-1D-03	cp	1D	34.58	31.08	0.00	0.03	34.19	0.01	99.97	DS-SED	305.00		
JL98-1D-03	cp	1D	34.89	31.56	0.02	0.00	34.00	0.00	100.54	DS-SED	0.00		
JL98-1D-03	cp	1D	34.93	31.35	0.01	0.03	34.41	0.00	100.83	DS-SED	3.09		
JL98-1D-03	cp	1D	34.55	31.07	0.01	0.00	33.54	0.01	99.28	DS-SED	0.01		
JL98-1D-03	cp	1D	34.81	31.52	0.04	0.00	34.35	0.00	100.80	DS-SED	0.07		
JL98-1D-03	cp	1D	34.78	31.19	0.03	0.00	34.49	0.00	100.57	DS-SED	0.00		
JL98-1D-03	cp	1D	34.87	31.15	0.02	0.02	33.91	0.00	100.12	DS-SED	0.97		
JL98-1D-04	cp	1D	34.60	30.86	0.02	0.06	34.55	0.00	100.14	DS-SED	2.75		
JL98-1D-08	cp	1D	34.91	30.86	0.02	0.00	34.01	0.00	99.93	DS-SED	0.01		
JL98-1D-08	cp	1D	34.42	30.31	0.02	0.04	33.69	0.02	98.70	DS-SED	1.79		
JL98-1D-09	cp	1D	34.97	31.33	0.04	0.00	33.31	0.00	99.77	DS-SED	0.00		
JL98-1D-09	cp	1D	35.01	30.81	0.03	0.02	34.44	0.00	100.45	DS-SED	0.69		
JL98-1D-09	cp	1D	34.75	30.63	0.02	0.03	34.52	0.00	100.00	DS-SED	1.20		
JL98-1D-09	cp	1D	35.07	31.24	0.01	0.01	34.06	0.00	100.49	DS-SED	0.79		
JL98-1D-11	cp	1D	35.16	30.57	0.06	0.03	34.14	0.01	100.11	DS-SED	0.40		
JL98-1D-11	cp	1D	34.82	30.88	0.02	0.00	34.42	0.01	100.31	DS-SED	0.00		
JL98-1D-11	cp	1D	34.82	30.69	0.00	0.02	34.34	0.00	99.96	DS-SED	14.58		
JL98-1D-11	cp	1D	35.19	31.05	0.00	0.02	34.18	0.05	100.61	DS-SED	4.08		
JL98-1D-13a	cp	1D	34.63	30.89	0.07	0.00	34.37	0.03	100.08	SMS-SED	0.00		
JL98-1D-13a	cp	1D	34.61	31.35	0.07	0.03	33.32	0.00	99.44	SMS-SED	0.48		
JL98-1D-13a	cp	1D	34.67	30.84	0.04	0.02	33.88	0.00	99.62	SMS-SED	0.58		
JL98-1D-13a	cp	1D	34.63	30.97	0.00	0.01	34.44	0.00	100.18	SMS-SED	4.84		
JL98-1D-13a	cp	1D	34.85	30.48	0.02	0.04	34.76	0.00	100.28	SMS-SED	1.90		
JL98-1D-13a	cp	1D	34.77	30.65	0.00	0.04	34.51	0.00	100.06	SMS-SED	358.00		
JL98-1D-13b	cp	1D	35.06	30.03	0.01	0.02	34.65	0.00	99.88	DS-SED	3.45		
JL98-1D-13b	cp	1D	35.10	29.99	0.02	0.00	34.73	0.00	99.94	DS-SED	0.00		
JL98-1D-13b	cp	1D	35.35	30.30	0.00	0.00	35.15	0.02	100.89	DS-SED	1.00		
JL98-1D-13b	cp	1D	34.77	30.21	0.04	0.37	34.57	0.00	100.02	DS-SED	8.68		
JL98-1D-13b	cp	1D	34.53	30.44	0.04	0.04	34.90	0.00	100.09	DS-SED	1.04		
JL98-1D-14	cp	1D	34.95	31.16	0.00	0.04	34.00	0.01	100.27	SMS-SED	14.23		
JL98-1D-14	cp	1D	35.10	30.89	0.02	0.00	34.44	0.00	100.52	SMS-SED	0.02		
JL98-1D-14	cp	1D	35.05	30.63	0.03	0.02	34.59	0.04	100.42	SMS-SED	0.92		

Appendix 3

Sample	Mineral	Ore Body	W%(S)	W%(Fe)	W%(Co)	W%(Ni)	W%(Cu)	W%(As)	Total	Sulphide Class	Ni/Co	M/S	hex/mono
JL98-1D-14	cp	1D	35.07	30.99	0.05	0.06	34.15	0.00	100.39	SMS-SED	1.07		
JL98-1D-14	cp	1D	34.40	30.77	0.03	0.05	34.55	0.01	99.95	SMS-SED	1.65		
JL98-1D-14	cp	1D	34.86	30.39	0.03	0.05	34.57	0.03	100.11	SMS-SED	1.65		
JL98-1D-15	cp	1D	34.72	30.65	0.04	0.05	34.43	0.00	99.94	SMS-SED	1.23		
JL98-1D-15	cp	1D	34.59	30.75	0.03	0.00	34.48	0.01	99.88	SMS-SED	0.07		
JL98-1D-15	cp	1D	34.87	30.77	0.03	0.13	33.89	0.00	99.70	SMS-SED	4.41		
JL98-1D-16	cp	1D	34.69	29.86	0.00	0.01	34.81	0.00	99.44	SMS-SED	53.00		
JL98-1D-16	cp	1D	34.44	30.74	0.04	0.05	35.33	0.00	100.62	SMS-SED	1.28		
JL98-1D-16	cp	1D	35.34	30.43	0.02	0.00	34.86	0.00	100.74	SMS-SED	0.15		
JL98-1D-16	cp	1D	34.61	31.36	0.01	0.01	34.70	0.02	100.75	SMS-SED	1.45		
JL98-1D-16	cp	1D	34.85	30.35	0.03	0.04	34.52	0.00	99.88	SMS-SED	1.30		
JL98-1D-16	cp	1D	34.82	30.73	0.03	0.03	35.06	0.00	100.79	SMS-SED	1.06		
JL98-1D-16	cp	1D	34.93	30.77	0.01	0.00	35.07	0.01	100.89	SMS-SED	0.01		
JL98-1D-16	cp	1D	34.65	30.78	0.02	0.00	35.31	0.00	100.91	SMS-SED	0.09		
JL98-1D-16	cp	1D	34.98	31.06	0.01	0.00	35.28	0.02	101.50	SMS-SED	0.01		
JL98-1D-16	cp	1D	34.86	30.94	0.01	0.17	35.26	0.01	101.31	SMS-SED	26.29		
JL98-1D-16	cp	1D	34.82	30.70	0.03	0.00	35.32	0.00	100.93	SMS-SED	0.11		
JL98-1D-18A	cp	1D	34.75	30.44	0.03	0.03	33.60	0.00	98.88	SMS-SED	1.36		
JL98-1D-18A	cp	1D	34.84	30.45	0.05	0.02	34.79	0.00	100.27	SMS-SED	0.38		
JL98-1D-18A	cp	1D	35.32	31.06	0.02	0.18	35.21	0.02	101.86	SMS-SED	7.48		
JL98-1D-18B	cp	1D	35.20	30.74	0.03	0.00	34.53	0.00	100.63	DS-SED	0.00		
JL98-1D-18B	cp	1D	34.67	31.02	0.02	0.00	34.85	0.02	100.68	DS-SED	0.00		
JL98-1D-19	cp	1D	34.94	31.13	0.02	0.03	34.48	0.01	100.69	SMS-SED	2.19		
JL98-1D-19	cp	1D	35.15	30.89	0.03	0.04	34.64	0.00	100.76	SMS-SED	1.31		
JL98-1D-19	cp	1D	35.02	31.15	0.02	0.03	34.93	0.00	101.23	SMS-SED	1.76		
JL98-1D-19	cp	1D	34.95	30.90	0.05	0.02	34.80	0.00	100.84	SMS-SED	0.32		
JL98-1D-19	cp	1D	35.00	31.01	0.01	0.00	34.42	0.00	100.52	SMS-SED	0.01		
JL98-1D-21	cp	1D	34.79	30.27	0.00	0.00	34.94	0.01	100.02	DS-SED	0.02		
JL98-1D-21	cp	1D	34.81	29.79	0.04	0.00	34.52	0.02	99.28	DS-SED	0.00		
JL98-1D-21	cp	1D	34.45	29.92	0.04	0.06	35.04	0.02	99.64	DS-SED	1.27		
JL98-1D-21	cp	1D	34.54	29.60	0.03	0.00	34.22	0.03	98.45	DS-SED	0.00		
JL98-1D-21	cp	1D	34.45	29.95	0.06	0.05	34.49	0.00	99.19	DS-SED	0.87		
JL98-1D-22	cp	1D	35.19	29.72	0.02	0.00	34.31	0.00	99.33	DS-SED	0.01		
JL98-1D-22	cp	1D	35.21	29.68	0.03	0.01	34.60	0.00	99.55	DS-SED	0.39		

Sample	Mineral	Ore Body	W%(S)	W%(Fe)	W%(Co)	W%(Ni)	W%(Cu)	W%(As)	Total	Sulphide Class	Ni/Co	M/S	hex/mono
JL98-1D-22	cp	1D	34.41	29.40	0.00	0.03	34.45	0.03	98.34	DS-SED	270.00		
JL98-1D-22	cp	1D	35.04	29.73	0.01	0.03	34.07	0.00	98.96	DS-SED	1.83		
JL98-BT-02	cp	BT	34.78	30.05	0.02	0.00	34.59	0.01	99.53	MS-UB	0.01		
JL98-BT-02	cp	BT	34.85	29.50	0.02	0.01	34.02	0.02	98.46	MS-UB	0.64		
JL98-BT-03	cp	BT	34.90	31.19	0.11	0.59	33.33	0.00	100.15	IS-U	5.52		
JL98-BT-10	cp	BT	34.89	31.57	0.04	0.15	34.96	0.02	101.70	MS-SED	3.82		
JL98-BT-10	cp	BT	34.70	30.98	0.06	0.01	34.75	0.00	100.60	MS-SED	0.21		
JL98-BT-10	cp	BT	34.79	30.65	0.01	0.02	33.92	0.00	99.42	MS-SED	2.67		
JL98-BT-11	cp	BT	35.12	31.62	0.00	0.00	34.34	0.02	101.16	DS-U	0.03		
JL98-BT-11	cp	BT	35.32	31.43	0.02	0.05	33.34	0.00	100.25	DS-U	3.15		
JL98-BT-12	cp	BT	34.59	30.70	0.00	0.00	34.37	0.00	99.79	DS-SED	1.00		
JL98-BT-12	cp	BT	34.94	30.78	0.03	0.03	34.14	0.02	100.02	DS-SED	1.24		
JL98-BT-12	cp	BT	35.03	31.36	0.09	0.12	33.76	0.00	100.45	DS-SED	1.29		
JL98-BT-12	cp	BT	35.13	30.74	0.05	0.06	34.82	0.01	100.87	DS-SED	1.27		
JL98-BT-12	cp	BT	34.95	31.37	0.05	0.02	34.19	0.00	100.61	DS-SED	0.49		
JL98-BT-13	cp	BT	35.04	31.04	0.02	0.00	34.07	0.00	100.20	DS-SED	0.01		
JL98-BT-13	cp	BT	34.91	30.93	0.04	0.04	34.03	0.00	100.14	DS-SED	0.88		
JL98-BT-13	cp	BT	35.12	31.58	0.01	0.00	33.80	0.00	100.54	DS-SED	0.75		
JL98-BT-13	cp	BT	34.51	30.83	0.02	0.03	33.59	0.04	99.05	DS-SED	1.48		
JL98-BT-15	cp	BT	34.99	30.68	0.54	0.31	34.37	0.03	101.00	MS-SED	0.56		
JL98-BT-16A	cp	BT	34.15	30.06	0.00	0.02	34.60	0.02	98.93	DS-U	204.00		
JL98-BT-16A	cp	BT	34.50	31.14	0.02	0.03	34.67	0.00	100.43	DS-U	1.72		
JL98-BT-16B	cp	BT	34.23	30.54	0.01	0.13	34.38	0.00	99.38	MS-UB	16.31		
JL98-BT-16B	cp	BT	34.21	31.13	0.01	0.01	35.36	0.00	100.74	MS-UB	0.56		
JL98-BT-16B	cp	BT	34.10	30.63	0.02	0.01	35.09	0.00	99.91	MS-UB	0.69		
JL98-BT-16B	cp	BT	33.82	30.64	0.00	0.06	35.15	0.00	99.70	MS-UB	638.00		
JL98-BT-16B	cp	BT	33.90	30.81	0.03	0.02	34.15	0.00	99.01	MS-UB	0.62		
JL98-BT-16B	cp	BT	34.08	31.13	0.04	0.03	35.63	0.01	100.98	MS-UB	0.62		
JL98-BT-18	cp	BT	34.79	30.32	0.04	0.04	34.80	0.03	100.13	DS-SED	1.03		
JL98-BT-18	cp	BT	35.19	31.05	0.04	0.00	34.91	0.04	101.31	DS-SED	0.00		
JL98-BT-22	cp	BT	33.52	30.14	0.09	0.65	34.21	0.00	98.65	IS-U	7.00		
JL98-BT-22	cp	BT	33.83	30.13	0.07	0.42	34.40	0.00	98.95	IS-U	5.80		
JL98-BT-22	cp	BT	34.29	31.58	0.03	0.01	34.98	0.00	100.93	IS-U	0.23		
JL98-BT-22	cp	BT	33.66	31.66	0.03	0.00	34.45	0.00	99.86	IS-U	0.00		

Sample	Mineral	Ore Body	W%(S)	W%(Fe)	W%(Co)	W%(Ni)	W%(Cu)	W%(As)	Total	Sulphide Class	Ni/Co	M/S	hex/mono
JL98-T1-03	cp	T1	34.79	30.49	0.04	0.03	33.95	0.01	99.40	DS-SED	0.72		
JL98-T1-03	cp	T1	34.51	30.89	0.03	0.02	34.20	0.01	99.81	DS-SED	0.69		
JL98-T1-03	cp	T1	34.29	30.38	0.06	0.00	34.35	0.00	99.08	DS-SED	0.00		
JL98-T1-03	cp	T1	34.87	29.36	0.00	0.02	33.97	0.00	98.36	DS-SED	191.00		
JL98-T1-03	cp	T1	34.36	30.00	0.04	0.00	33.88	0.02	98.36	DS-SED	0.04		
JL98-T1-04	cp	T1	34.80	29.95	0.01	0.03	34.12	0.00	98.96	MS-UB	2.37		
JL98-T1-04	cp	T1	35.00	29.75	0.00	0.03	34.26	0.00	99.19	MS-UB	281.00		
JL98-T1-04	cp	T1	34.66	30.42	0.04	0.03	34.40	0.06	99.76	MS-UB	0.83		
JL98-T1-04	cp	T1	34.78	30.19	0.05	0.06	34.87	0.00	100.12	MS-UB	1.03		
JL98-T1-04	cp	T1	34.59	30.41	0.02	0.15	34.57	0.00	99.92	MS-UB	7.53		
JL98-T1-04	cp	T1	35.35	30.78	0.02	0.00	35.25	0.02	101.54	MS-UB	0.00		
JL98-T1-04	cp	T1	35.04	31.36	0.04	0.04	34.47	0.01	101.01	MS-UB	1.01		
JL98-T1-04	cp	T1	35.26	30.74	0.02	0.02	35.18	0.00	101.35	MS-UB	1.31		
JL98-T1-04	cp	T1	34.84	30.77	0.04	0.13	34.80	0.00	100.73	DS-U	3.25		
JL98-T1-04	cp	T1	34.88	30.80	0.04	0.07	34.94	0.00	100.86	DS-U	1.77		
JL98-T1-06	cp	T1	34.84	31.06	0.03	0.01	34.49	0.00	100.47	DS-SED	0.42		
JL98-T1-06	cp	T1	34.46	30.76	0.00	0.03	34.01	0.03	99.36	DS-SED	279.00		
JL98-T1-06	cp	T1	35.02	30.84	0.02	0.00	34.38	0.00	100.36	DS-SED	0.01		
JL98-T1-07	cp	T1	34.95	30.74	0.05	0.01	34.48	0.00	100.26	MS-UB	0.18		
JL98-T1-07	cp	T1	34.76	30.58	0.00	0.05	34.01	0.01	99.59	MS-UB	467.00		
JL98-T1-07	cp	T1	35.04	30.53	0.03	0.70	33.78	0.00	100.24	MS-UB	22.79		
JL98-T1-07	cp	T1	34.90	30.63	0.04	0.35	34.38	0.00	100.30	MS-UB	9.78		
JL98-T1-07	cp	T1	35.29	30.80	0.04	0.04	34.14	0.00	100.39	MS-UB	0.78		
JL98-T1-07	cp	T1	34.87	30.63	0.03	0.03	34.52	0.01	100.23	MS-UB	1.03		
JL98-T1-07	cp	T1	34.67	31.03	0.25	0.15	34.19	0.02	100.47	MS-UB	0.60		
JL98-T1-09A	cp	T1	34.69	30.57	0.04	0.00	34.69	0.00	100.11	MS-UB	0.00		
JL98-T1-09A	cp	T1	34.52	30.05	0.03	0.05	34.53	0.00	99.26	MS-UB	1.81		
JL98-T1-09A	cp	T1	34.75	30.34	0.03	0.04	34.90	0.01	100.12	MS-UB	1.38		
JL98-T1-09A	cp	T1	34.95	31.24	0.00	0.05	34.75	0.04	101.10	MS-UB	506.00		
JL98-T1-09A	cp	T1	35.11	30.95	0.02	0.06	34.79	0.00	100.99	MS-UB	2.92		
JL98-T1-09A	cp	T1	34.44	30.65	0.02	0.06	34.60	0.01	99.78	MS-UB	4.00		
JL98-T1-09A	cp	T1	34.42	31.06	0.00	0.00	34.62	0.00	100.16	MS-UB	1.00		
JL98-T1-09A	cp	T1	34.48	31.37	0.01	0.18	34.57	0.00	100.75	MS-UB	13.42		
JL98-T1-11	cp	T1	34.83	31.76	0.03	0.00	34.27	0.00	101.00	IS-U	0.00		

Sample	Mineral	Ore Body	W%(S)	W%(Fe)	W%(Co)	W%(Ni)	W%(Cu)	W%(As)	Total	Sulphide Class	Ni/Co	M/S	hex/mono
JL98-T1-11	cp	T1	33.57	30.70	0.05	0.55	33.09	0.00	98.08	IS-U	10.91		
JL98-T1-11	cp	T1	35.02	30.89	0.04	0.00	34.74	0.04	100.81	IS-U	0.03		
JL98-T1-12	cp	T1	34.51	30.96	0.03	0.04	34.05	0.00	99.64	MS-UB	1.18		
JL98-T1-12	cp	T1	34.56	30.40	0.03	0.03	34.59	0.00	99.65	MS-UB	1.10		
JL98-T1-12	cp	T1	34.37	30.41	0.02	0.02	34.62	0.00	99.54	MS-UB	1.10		
JL98-T1-12	cp	T1	34.61	30.84	0.00	0.08	34.08	0.01	99.75	MS-UB	810.00		
JL98-T1-12	cp	T1	34.34	31.13	0.06	0.29	34.35	0.00	100.24	MS-UB	4.58		
JL98-T1-13	cp	T1	34.84	30.60	0.01	0.06	34.47	0.00	100.05	IS-U	7.85		
JL98-T1-13	cp	T1	34.79	30.92	0.02	0.04	34.48	0.00	100.26	IS-U	2.84		
JL98-T1-13	cp	T1	34.90	30.72	0.04	0.18	34.65	0.00	100.57	IS-U	4.37		
JL98-T1-16	cp	T1	34.57	29.64	0.02	0.02	33.88	0.00	98.26	DS-SED	0.62		
JL98-T1-16	cp	T1	34.73	29.93	0.02	0.00	33.46	0.01	98.22	DS-SED	0.00		
JL98-T1-16	cp	T1	34.62	30.73	0.02	0.03	34.14	0.00	99.65	DS-SED	1.39		
JL98-T1-16	cp	T1	34.66	30.82	0.00	0.01	34.52	0.00	100.16	DS-SED	72.00		
JL98-T1-16	cp	T1	34.47	30.40	0.01	0.01	34.25	0.00	99.24	DS-SED	0.70		
JL98-T1-16	cp	T1	34.76	30.93	0.01	0.02	34.87	0.00	100.67	DS-SED	2.00		
JL98-T1-19	cp	T1	34.41	30.24	0.00	0.29	33.98	0.02	99.10	MS-SED	2852.00		
JL98-T1-19	cp	T1	34.59	29.75	0.00	0.02	34.22	0.01	98.67	MS-SED	5.02		
JL98-T1-20	cp	T1	35.12	30.83	0.00	0.00	34.65	0.01	100.71	DS-SED	1.00		
JL98-T1-20	cp	T1	34.92	31.18	0.03	0.02	33.99	0.02	100.24	DS-SED	0.93		
JL98-T1-20	cp	T1	34.93	30.58	0.03	0.00	34.41	0.00	100.00	DS-SED	0.00		
JL99-T1-25	cp	T1	35.53	30.74	0.00	0.02	34.42	0.00	100.77	BMS-SED	224.00		
JL99-T1-25	cp	T1	35.23	30.63	0.00	0.02	34.18	0.00	100.13	BMS-SED	195.00		
JL99-T1-26	cp	T1	35.76	29.85	0.02	0.00	34.29	0.00	100.25	BMS-SED	0.01		
JL99-T1-26	cp	T1	35.22	29.94	0.04	0.03	34.42	0.02	99.73	BMS-SED	0.62		
JL98-WL-03	cp	WL	34.65	30.18	0.02	0.12	34.52	0.00	99.54	IS-U	5.55		
JL98-WL-03	cp	WL	34.84	30.06	0.08	0.15	34.75	0.01	100.07	IS-U	1.96		
JL98-WL-03	cp	WL	34.65	30.63	0.06	0.01	35.50	0.01	100.91	IS-U	0.18		
JL98-WL-06	cp	WL	34.80	29.67	0.00	0.06	35.37	0.00	100.06	IS-U	601.00		
JL98-WL-06	cp	WL	34.83	29.60	0.04	0.05	35.08	0.03	99.68	IS-U	1.34		
JL98-WL-06	cp	WL	35.18	30.20	0.03	0.21	34.99	0.00	100.76	IS-U	6.98		
JL98-WL-06	cp	WL	35.62	31.06	0.06	0.20	33.52	0.00	100.47	IS-U	3.35		
JL98-WL-07	cp	WL	34.57	30.45	0.02	0.23	34.08	0.00	99.42	MS-UB	12.50		
JL98-WL-07	cp	WL	35.13	30.65	0.03	0.19	34.18	0.00	100.28	MS-UB	6.93		

Appendix 3

Sample	Mineral	Ore Body	W%(S)	W%(Fe)	W%(Co)	W%(Ni)	W%(Cu)	W%(As)	Total	Sulphide Class	Ni/Co	M/S	hex/mono
JL98-WL-07	cp	WL	34.63	30.30	0.02	0.13	34.59	0.02	99.75	MS-UB	5.41		
JL98-WL-07	cp	WL	34.81	29.77	0.01	0.11	34.47	0.00	99.20	MS-UB	8.35		
JL98-WL-07	cp	WL	34.86	30.54	0.00	0.00	34.22	0.00	99.74	MS-UB	1.00		
JL98-WL-07	cp	WL	34.41	30.74	0.02	0.05	34.49	0.01	99.80	MS-UB	1.89		
JL98-WL-09	cp	WL	34.31	30.75	0.05	0.10	33.92	0.00	99.18	IS-U	2.07		
JL98-WL-09	cp	WL	34.48	30.04	0.02	0.32	33.74	0.00	98.71	IS-U	17.15		
JL98-WL-09	cp	WL	34.81	31.19	0.01	0.03	34.24	0.00	100.28	IS-U	2.72		
JL98-WL-09	cp	WL	34.67	30.95	0.04	0.05	34.29	0.00	100.05	IS-U	1.24		
JL98-WL-09	cp	WL	34.86	31.20	0.04	0.08	34.39	0.03	100.68	IS-U	2.15		
JL98-WL-09	cp	WL	34.83	30.91	0.01	0.01	34.84	0.00	100.65	IS-U	1.57		
JL98-WL-09	cp	WL	34.62	30.96	0.02	0.06	34.70	0.02	100.55	IS-U	2.62		
JL98-WL-09	cp	WL	34.80	30.90	0.03	0.02	34.84	0.00	100.67	IS-U	0.86		
JL98-WL-10	cp	WL	34.56	31.17	0.02	0.04	34.21	0.02	100.05	DS-U	2.52		
JL98-WL-10	cp	WL	34.73	30.89	0.02	0.01	34.24	0.01	99.97	DS-U	0.65		
JL98-WL-10	cp	WL	34.62	30.28	0.03	0.07	34.22	0.00	99.28	DS-U	2.03		
JL98-WL-10	cp	WL	34.84	30.73	0.01	0.07	34.23	0.00	99.94	DS-U	5.02		
JL98-WL-11	cp	WL	34.95	30.98	0.04	0.00	34.49	0.00	100.53	MS-SED	0.00		
JL98-WL-11	cp	WL	34.74	30.87	0.00	0.01	34.57	0.01	100.22	MS-SED	3.33		
JL98-WL-11	cp	WL	34.64	30.57	0.00	0.01	34.70	0.00	100.06	MS-SED	8.00		
JL98-WL-13	cp	WL	34.66	30.94	0.03	0.00	34.38	0.00	100.04	BMS-SED	0.00		
JL98-WL-13	cp	WL	35.15	30.84	0.03	0.00	34.23	0.03	100.32	BMS-SED	0.00		
JL98-WL-13	cp	WL	34.85	30.03	0.02	0.02	34.21	0.00	99.18	BMS-SED	1.25		
JL98-WL-18A	cp	WL	34.28	30.25	0.04	0.01	34.07	0.00	98.72	BMS-SED	0.41		
JL98-WL-18A	cp	WL	34.45	31.20	0.00	0.01	33.89	0.00	99.65	BMS-SED	121.00		
JL98-WL-19	cp	WL	34.78	30.90	0.03	0.01	34.75	0.00	100.53	BMS-SED	0.26		
JL98-WL-19	cp	WL	34.83	31.09	0.03	0.00	35.14	0.02	101.13	BMS-SED	0.00		
JL98-WL-19	cp	WL	34.96	30.51	0.02	0.02	35.88	0.00	101.48	BMS-SED	0.99		
JL98-WL-19	cp	WL	34.81	30.02	0.05	0.00	34.97	0.00	99.95	BMS-SED	0.00		
JL98-WL-19	cp	WL	34.70	30.59	0.00	0.02	34.52	0.04	100.00	BMS-SED	203.00		
JL98-WL-21	cp	WL	34.65	30.87	0.01	0.04	34.46	0.00	100.10	DS-SED	7.84		
JL98-WL-21	cp	WL	34.60	31.27	0.01	0.02	33.96	0.00	99.94	DS-SED	2.24		
JL98-WL-21	cp	WL	34.61	31.01	0.06	0.00	34.50	0.01	100.25	DS-SED	0.00		
JL98-WL-21	cp	WL	35.02	31.15	0.03	0.00	34.66	0.02	100.94	DS-SED	0.00		
JL98-WL-23	cp	WL	34.90	31.20	0.00	0.00	33.88	0.00	100.10	DS-SED	27.00		

Appendix 3

Sample	Mineral	Ore Body	W%(S)	W%(Fe)	W%(Co)	W%(Ni)	W%(Cu)	W%(As)	Total	Sulphide Class	Ni/Co	M/S	hex/mono
JL98-WL-23	cp	WL	34.72	30.47	0.02	0.03	33.94	0.00	99.25	DS-SED	1.42		
JL98-WL-23	cp	WL	34.81	30.16	0.03	0.02	34.22	0.00	99.34	DS-SED	0.73		
JL98-WL-24	cp	WL	34.69	30.42	0.02	0.18	34.10	0.00	99.53	DS-U	11.34		
JL98-WL-24	cp	WL	35.03	30.47	0.04	0.02	34.54	0.00	100.18	DS-U	0.44		
JL98-WL-25	cp	WL	34.89	30.89	0.05	0.24	33.89	0.00	100.06	DS-U	5.10		
JL98-WL-26	cp	WL	34.77	29.88	0.02	0.00	34.63	0.00	99.46	DS-SED	0.01		
JL98-WL-26	cp	WL	34.52	29.76	0.00	0.04	34.11	0.00	98.56	DS-SED	387.00		
JL98-WL-26	cp	WL	34.65	29.62	0.00	0.05	34.26	0.00	98.65	DS-SED	528.00		
JL98-WL-30	cp	WL	34.95	30.80	0.01	0.01	33.78	0.00	99.60	BMS-SED	1.08		
JL98-WL-30	cp	WL	34.82	31.44	0.03	0.00	34.20	0.00	100.59	BMS-SED	0.16		
JL98-WL-30	cp	WL	34.89	31.25	0.03	0.00	34.90	0.03	101.27	BMS-SED	0.00		
JL98-WL-30	cp	WL	34.77	30.74	0.00	0.03	34.86	0.00	100.47	BMS-SED	272.00		
JL98-WL-30	cp	WL	34.94	30.36	0.00	0.02	34.28	0.00	100.43	BMS-SED	205.00		
JL98-WL-30	cp	WL	34.79	30.98	0.01	0.00	34.12	0.00	99.99	BMS-SED	0.01		
JL98-WL-31	cp	WL	34.76	29.46	0.01	0.00	34.78	0.00	99.09	BMS-SED	0.32		
JL98-WL-31	cp	WL	35.01	29.38	0.04	0.00	34.42	0.00	98.91	BMS-SED	0.09		
JL98-WL-31	cp	WL	35.05	29.26	0.01	0.02	34.46	0.00	98.88	BMS-SED	1.65		
JL98-WL-33	cp	WL	34.51	30.41	0.03	0.02	34.42	0.00	99.51	MS-SED	0.48		
JL98-WL-33	cp	WL	35.15	30.59	0.04	0.02	34.48	0.01	100.35	MS-SED	0.38		
JL98-WL-33	cp	WL	34.84	30.70	0.00	0.03	34.66	0.00	100.37	MS-SED	337.00		
JL98-WL-33	cp	WL	34.72	30.67	0.01	0.02	34.34	0.00	99.85	MS-SED	2.96		
JL98-WL-34	cp	WL	34.87	30.82	0.03	0.00	34.84	0.00	100.66	MS-SED	0.00		
JL98-WL-34	cp	WL	34.91	30.52	0.00	0.01	34.64	0.00	100.22	MS-SED	128.00		
JL98-WL-34	cp	WL	34.65	30.90	0.00	0.03	34.70	0.00	100.34	MS-SED	316.00		
JL98-WL-34	cp	WL	34.71	31.56	0.06	0.03	33.94	0.00	100.45	MS-SED	0.51		
JL98-1C-10	py	1C	53.65	47.05	0.10	0.03	0.01	0.00	101.00	DS-SED	0.25		
JL98-1C-12	py	1C	53.86	44.50	2.15	0.03	0.00	0.04	100.62	DS-SED	0.01		
JL98-1C-12	py	1C	53.80	46.18	1.50	0.01	0.02	0.01	101.64	DS-SED	0.01		
JL98-1C-12	py	1C	53.48	44.95	0.03	0.02	0.01	0.00	98.57	DS-SED	0.76		
JL98-1C-20	py	1C	53.72	46.49	0.94	0.05	0.10	0.00	101.35	MS-SED	0.06		
JL98-1C-20	py	1C	53.75	46.22	1.50	0.03	0.00	0.02	101.61	MS-SED	0.02		
JL98-1C-20	py	1C	53.27	45.90	1.49	0.05	0.00	0.00	100.76	MS-SED	0.03		
JL98-1C-23	py	1C	53.91	47.43	0.15	0.02	0.00	0.01	101.56	DS-SED	0.11		
JL98-1C-23	py	1C	53.57	47.19	0.15	0.06	0.01	0.01	101.04	DS-SED	0.41		

Sample	Mineral	Ore Body	W%(S)	W%(Fe)	W%(Co)	W%(Ni)	W%(Cu)	W%(As)	Total	Sulphide Class	Ni/Co	M/S	hex/mono
JL98-1C-23	py	1C	53.92	47.58	0.00	0.00	0.01	0.00	101.57	DS-SED	1.00		
JL98-1C-29	py	1C	53.46	46.76	0.05	0.00	0.00	0.00	100.37	DS-SED	0.00		
JL98-1C-29	py	1C	53.51	47.04	0.01	0.00	0.00	0.04	100.69	DS-SED	0.01		
JL98-1C-29	py	1C	53.88	47.03	0.04	0.02	0.01	0.00	101.02	DS-SED	0.45		
JL99-1C-35	py	1C	53.93	44.50	0.38	0.93	0.06	0.01	99.84	MS-SED	2.43		
JL98-1D-01	py	1D	53.65	47.07	0.04	0.01	0.02	0.03	101.00	DS-SED	0.39		
JL98-1D-03	py	1D	53.52	48.30	0.03	0.00	0.01	0.03	101.93	DS-SED	0.00		
JL98-1D-04	py	1D	53.49	48.14	0.02	0.05	0.00	0.02	101.80	DS-SED	2.48		
JL98-1D-04	py	1D	53.79	47.67	0.10	0.02	0.00	0.03	101.69	DS-SED	0.20		
JL98-1D-04	py	1D	53.72	46.83	0.08	0.75	0.00	0.00	101.42	DS-SED	8.87		
JL98-1D-04	py	1D	53.64	47.79	0.05	0.02	0.00	0.01	101.60	DS-SED	0.41		
JL98-1D-04	py	1D	53.57	47.75	0.04	0.04	0.00	0.00	101.46	DS-SED	0.94		
JL98-1D-04	py	1D	53.51	46.19	0.03	0.04	0.00	0.00	99.85	DS-SED	1.32		
JL98-1D-08	py	1D	53.43	46.69	0.02	0.06	0.01	0.00	100.30	DS-SED	3.12		
JL98-1D-08	py	1D	53.40	46.68	0.06	0.36	0.00	0.00	100.54	DS-SED	5.96		
JL98-1D-08	py	1D	53.48	47.53	0.01	0.00	0.05	0.00	101.10	DS-SED	0.01		
JL98-1D-18A	py	1D	53.62	47.98	0.02	0.03	0.04	0.01	101.73	SMS-SED	1.58		
JL98-1D-19	py	1D	53.64	48.05	0.04	0.00	0.00	0.00	101.80	SMS-SED	0.00		
JL98-BT-06	py	BT	53.66	47.64	0.06	0.01	0.03	0.00	101.43	DS-SED	0.08		
JL98-BT-06	py	BT	53.72	47.36	0.01	0.00	0.00	0.00	101.15	DS-SED	0.01		
JL98-BT-18	py	BT	53.67	47.96	0.02	0.00	0.01	0.00	101.76	DS-SED	0.07		
JL98-BT-18	py	BT	53.77	48.04	0.02	0.01	0.01	0.01	101.90	DS-SED	0.27		
JL98-BT-18	py	BT	52.27	46.82	0.04	0.04	0.00	0.00	99.26	DS-SED	0.91		
JL99-BU-01	py	BU	54.17	43.80	3.34	0.63	0.01	0.01	102.01	SMS-ARC	0.19		
JL99-BU-01	py	BU	54.01	43.13	4.54	0.46	0.00	0.00	102.21	SMS-ARC	0.10		
JL99-BU-01	py	BU	53.85	46.04	0.52	0.64	0.03	0.02	101.17	SMS-ARC	1.23		
JL99-BU-01	py	BU	54.43	46.65	0.85	0.35	0.02	0.00	102.40	SMS-ARC	0.41		
JL99-BU-02	py	BU	54.64	43.09	3.83	0.25	0.02	0.03	101.89	MS-ARC	0.07		
JL99-BU-02	py	BU	54.07	46.38	1.27	0.17	0.02	0.00	101.99	MS-ARC	0.13		
JL99-BU-02	py	BU	54.24	45.26	2.67	0.10	0.00	0.02	102.32	MS-ARC	0.04		
JL99-BU-02	py	BU	54.08	45.71	1.24	0.18	0.00	0.00	101.27	MS-ARC	0.14		
JL99-BU-08	py	BU	54.19	44.86	2.01	0.17	0.04	0.00	101.33	SMS-ARC	0.08		
JL99-BU-08	py	BU	53.77	43.63	3.30	0.19	0.00	0.00	100.92	SMS-ARC	0.06		
DM98-1C-07	py	1C	54.22	46.77	0.65	0.36	0.00	0.00	102.04	MS-SED	0.56		

Sample	Mineral	Ore Body	W%(S)	W%(Fe)	W%(Co)	W%(Ni)	W%(Cu)	W%(As)	Total	Sulphide Class	Ni/Co	M/S	hex/mono
DM98-1C-07	py	1C	53.88	46.37	0.79	0.87	0.00	0.00	102.00	MS-SED	1.11		
DM98-1C-07	py	1C	53.81	45.64	1.94	0.43	0.05	0.00	101.92	MS-SED	0.22		
DM98-1C-09	py	1C	54.30	43.89	2.70	0.24	0.03	0.02	101.29	DS-SED	0.09		
DM98-1C-09	py	1C	53.23	45.97	0.20	1.12	0.00	0.00	100.54	DS-SED	5.57		
DM98-1C-11	py	1C	53.86	46.88	0.03	1.14	0.01	0.05	102.04	DS-SED	41.23		
DM98-1C-11	py	1C	54.12	47.63	0.27	0.03	0.00	0.06	102.24	DS-SED	0.12		
DM98-1C-11	py	1C	54.27	47.98	0.05	0.01	0.05	0.03	102.46	DS-SED	0.21		
DM98-1C-12	py	1C	54.09	46.05	1.84	0.00	0.00	0.00	102.03	DS-SED	0.00		
DM98-1C-12	py	1C	53.99	47.57	0.02	0.61	0.02	0.01	102.23	DS-SED	26.99		
DM98-1C-12	py	1C	54.07	45.61	1.96	0.00	0.00	0.00	101.77	DS-SED	0.00		
DM98-1C-12	py	1C	53.30	47.94	0.03	0.11	0.02	0.00	101.43	DS-SED	3.26		
JL98-WL-06	py	WL	52.98	45.19	0.04	0.46	0.03	0.00	98.76	IS-U	11.83		
JL98-WL-06	py	WL	53.05	46.09	0.05	0.29	0.00	0.01	99.55	IS-U	6.32		
JL98-WL-07	py	WL	52.68	47.24	0.04	0.41	0.00	0.01	100.38	MS-UB	9.69		
JL98-WL-07	py	WL	52.71	46.90	0.04	0.51	0.03	0.00	100.29	MS-UB	14.01		
JL98-WL-07	py	WL	52.80	47.03	0.03	0.67	0.07	0.00	100.68	MS-UB	22.20		
JL98-WL-13	py	WL	53.36	47.14	0.08	0.73	0.07	0.00	101.49	BMS-SED	9.22		
JL98-WL-13	py	WL	53.47	46.97	0.05	0.52	0.00	0.00	101.16	BMS-SED	10.60		
JL98-WL-13	py	WL	52.86	46.70	0.05	0.35	0.01	0.04	100.05	BMS-SED	6.45		
JL98-WL-13	py	WL	53.59	46.41	0.02	0.34	0.00	0.01	100.44	BMS-SED	15.00		
JL98-WL-14	py	WL	52.33	45.97	0.04	0.23	0.02	0.00	98.61	DS-SED	6.08		
JL98-WL-14	py	WL	52.65	47.28	0.01	0.39	0.00	0.00	100.43	DS-SED	30.44		
JL98-WL-14	py	WL	52.27	46.98	0.04	0.32	0.00	0.00	99.66	DS-SED	8.43		
JL98-WL-14	py	WL	53.07	46.03	0.06	0.01	0.00	0.00	99.26	DS-SED	0.20		
JL98-WL-14	py	WL	52.57	47.20	0.00	0.04	0.00	0.01	99.90	DS-SED	216.00		
JL98-WL-14	py	WL	52.43	47.52	0.06	0.25	0.06	0.00	100.40	DS-SED	3.93		
JL98-WL-14	py	WL	52.36	47.33	0.03	0.17	0.00	0.00	99.95	DS-SED	4.81		
JL98-WL-14	py	WL	53.02	48.27	0.03	0.00	0.00	0.00	101.36	DS-SED	0.00		
JL98-WL-14	py	WL	53.51	47.29	0.04	0.00	0.00	0.00	100.90	DS-SED	0.00		
JL98-WL-14	py	WL	52.75	47.33	0.02	0.22	0.11	0.00	100.46	DS-SED	14.27		
JL98-WL-14	py	WL	52.43	47.89	0.04	0.27	0.00	0.01	100.68	DS-SED	6.79		
JL98-WL-18A	py	WL	53.47	46.95	1.28	0.00	0.00	0.02	101.80	BMS-SED	0.00		
JL98-WL-23	py	WL	53.31	46.93	0.03	0.02	0.01	0.00	100.40	DS-SED	0.50		
JL98-WL-23	py	WL	53.30	48.04	0.00	0.00	0.00	0.00	101.39	DS-SED	0.07		

Sample	Mineral	Ore Body	W%(S)	W%(Fe)	W%(Co)	W%(Ni)	W%(Cu)	W%(As)	Total	Sulphide Class	Ni/Co	M/S	hex/mono
JL98-WL-23	py	WL	53.35	47.59	0.03	0.16	0.00	0.00	101.16	DS-SED	6.02		
JL98-WL-23	py	WL	53.51	47.90	0.01	0.02	0.02	0.00	101.53	DS-SED	2.14		
JL98-WL-23	py	WL	53.09	47.20	0.02	0.10	0.25	0.00	100.72	DS-SED	4.81		
JL98-WL-23	py	WL	53.11	44.45	0.05	0.18	0.31	0.00	98.20	DS-SED	3.75		
JL98-1C-19	gd	1C	18.70	6.28	8.61	20.87	0.00	45.66	100.47	SMS-SED	2.42		
JL98-1C-19	gd	1C	18.21	5.90	7.62	22.34	0.00	46.18	100.63	SMS-SED	2.93		
JL98-1C-19	gd	1C	18.47	6.18	8.08	21.31	0.03	45.44	99.85	SMS-SED	2.64		
JL98-1C-25B	gd	1C	18.53	6.11	8.75	20.03	0.13	46.33	100.18	MS-SED	2.29		
JL98-1C-25B	gd	1C	18.22	6.24	8.04	20.81	0.08	46.69	100.36	MS-SED	2.59		
JL98-1C-25B	gd	1C	17.83	5.63	7.55	21.90	0.01	47.16	100.46	MS-SED	2.90		
JL98-1C-25D	gd	1C	18.29	6.51	8.84	20.29	0.03	46.76	101.06	MS-SED	2.30		
JL98-1C-25D	gd	1C	17.85	5.74	7.46	20.82	0.04	46.88	99.13	MS-SED	2.79		
JL98-1C-25D	gd	1C	18.06	6.34	8.34	20.82	0.04	46.95	100.91	MS-SED	2.50		
JL98-1D-13a	gd	1D	18.31	4.21	4.27	26.53	0.02	46.53	100.21	SMS-SED	6.22		
JL98-1D-13a	gd	1D	18.39	4.16	4.08	26.27	0.00	46.27	99.54	SMS-SED	6.45		
JL98-1D-13a	gd	1D	18.33	4.59	4.59	26.40	0.04	46.29	100.52	SMS-SED	5.75		
JL98-1D-14	gd	1D	18.66	4.79	4.51	26.02	0.03	46.23	100.55	SMS-SED	5.77		
JL98-1D-14	gd	1D	18.55	4.96	4.87	25.33	0.02	46.30	100.39	SMS-SED	5.20		
JL98-1D-14	gd	1D	18.67	4.33	4.49	25.89	0.00	46.25	99.98	SMS-SED	5.77		
JL98-1D-14	gd	1D	18.76	5.52	6.12	23.64	0.04	46.02	100.44	SMS-SED	3.86		
JL98-1D-14	gd	1D	18.16	4.14	4.34	25.51	0.03	46.67	99.18	SMS-SED	5.88		
JL98-1D-15	gd	1D	18.34	4.41	4.65	26.13	0.05	46.31	100.20	SMS-SED	5.62		
JL98-1D-15	gd	1D	18.09	4.38	4.45	26.41	0.00	46.71	100.49	SMS-SED	5.94		
JL98-1D-15	gd	1D	18.04	4.39	4.51	26.17	0.04	46.37	99.96	SMS-SED	5.80		
JL98-1D-15	gd	1D	18.28	4.38	4.58	26.05	0.01	46.46	100.30	SMS-SED	5.69		
JL98-1D-15	gd	1D	18.05	4.31	4.31	26.44	0.01	46.51	99.94	SMS-SED	6.13		
JL98-1D-16	gd	1D	18.07	4.34	4.32	27.40	0.12	46.28	100.92	SMS-SED	6.34		
JL98-1D-16	gd	1D	17.96	4.56	4.47	27.24	0.14	46.50	101.19	SMS-SED	6.10		
JL98-1D-16	gd	1D	18.17	4.40	4.14	26.78	0.22	45.96	100.01	SMS-SED	6.47		
JL98-1D-16	gd	1D	18.20	4.54	4.44	27.08	0.12	46.55	101.27	SMS-SED	6.10		
JL98-1D-18A	gd	1D	18.45	4.64	4.51	26.26	0.04	45.73	100.02	SMS-SED	5.83		
JL98-1D-18A	gd	1D	18.59	4.91	4.77	26.19	0.00	45.51	100.36	SMS-SED	5.48		
JL98-BT-10	gd	BT	19.30	5.76	19.41	9.58	0.04	45.18	99.55	MS-SED	0.49		
JL98-BT-10	gd	BT	19.22	6.29	19.40	9.62	0.01	45.27	100.06	MS-SED	0.50		

Sample	Mineral	Ore Body	W%(S)	W%(Fe)	W%(Co)	W%(Ni)	W%(Cu)	W%(As)	Total	Sulphide Class	Ni/Co	M/S	hex/mono
JL98-BT-15	gd	BT	18.85	6.63	14.19	14.67	0.00	46.14	100.79	MS-SED	1.03		
JL98-BT-15	gd	BT	18.83	6.79	14.77	14.48	0.01	46.30	101.49	MS-SED	0.98		
JL98-T1-07	gd	T1	18.67	7.19	8.78	19.63	0.07	45.87	100.54	MS-UB	2.23		
JL98-T1-07	gd	T1	19.14	7.62	9.40	18.71	0.12	44.96	100.38	MS-UB	1.99		
JL98-T1-11	gd	T1	17.71	6.73	6.38	22.79	0.01	47.59	101.53	IS-U	3.57		
JL98-T1-11	gd	T1	17.54	6.29	6.45	22.87	0.05	47.30	100.88	IS-U	3.55		
JL98-T1-12	gd	T1	18.41	7.24	8.50	19.05	0.00	46.09	99.54	MS-UB	2.24		
JL98-T1-12	gd	T1	18.07	7.12	7.85	20.01	0.01	46.41	99.74	MS-UB	2.55		
JL98-T1-13	gd	T1	18.38	6.86	8.48	19.35	0.04	45.40	98.76	IS-U	2.28		
JL98-T1-13	gd	T1	18.20	6.40	6.70	21.50	0.00	46.13	99.23	IS-U	3.21		
JL98-T1-19	gd	T1	18.20	6.10	7.21	22.18	0.08	45.59	99.66	MS-SED	3.07		
JL98-T1-19	gd	T1	18.20	5.81	5.88	23.02	0.04	46.81	100.18	MS-SED	3.92		
JL98-T1-19	gd	T1	17.78	5.88	6.25	22.13	0.02	46.09	98.53	MS-SED	3.54		
JL98-T1-19	gd	T1	17.99	5.88	6.87	22.23	0.02	46.35	99.66	MS-SED	3.24		
JL98-T1-19	ni	T1	0.26	0.06	0.01	45.60	0.00	54.56	100.90	MS-SED	5560.85		
JL98-T1-19	ni	T1	0.23	0.05	0.02	44.69	0.00	54.83	100.36	MS-SED	2468.82		
JL98-T1-19	ni	T1	0.22	0.02	0.04	44.63	0.05	54.27	99.83	MS-SED	1206.11		

APPENDIX 4: PIXE DATA

Data is sorted by mineral, then by ore body.

Abbreviations:

Mineral:

- po = pyrrhotite
- pn = pentlandite
- cp = chalcopyrite
- py = pyrite
- gd = gersdorffite
- ni = niccolite

Ore body

- 1C = 1C ore body, Thompson Mine
- 1D = 1D ore body, Thompson Mine
- T1 = T1 Mine, Thompson Mine
- BT = Birchtree Mine
- BU = Bucko Lake
- SN = Soab North
- WL = William Lake deposit

Sample	Mineral	Ore Body	Fe (ppm)	Co (ppm)	Ni (ppm)	Cu (ppm)	Zn (ppm)	As (ppm)
JL98-1C-19	po	1C	591958	6858	4402	36	9	0
JL98-1C-19	po	1C	587544	6932	4879	37	1	4
JL98-1C-19	po	1C	581647	6310	4723	52	10	4
JL98-1C-19	po	1C	586171	7355	4650	30	6	7
JL98-1C-19	po	1C	586833	6662	5197	45	6	0
JL98-1C-20	po	1C	582020	6183	3589	29	6	1
JL98-1C-20	po	1C	583040	6748	3652	9	9	1
JL98-1C-20	po	1C	584399	6876	3357	14	7	1
JL98-1C-24A	po	1C	597361	6842	6395	35	4	4
JL98-1C-24A	po	1C	595345	6870	6215	35	11	0
JL98-1C-24A	po	1C	592865	7150	5847	45	12	1
JL98-1C-25B	po	1C	580907	6108	11474	56	12	1
JL98-1C-25B	po	1C	582467	6198	11467	63	7	8
JL98-1C-28A	po	1C	601648	8335	464	17	2	5
JL98-1C-28A	po	1C	598982	7150	516	9	1	0
JL98-1C-28A	po	1C	595536	7756	471	11	0	0
JL98-1C-33	po	1C	600996	7551	1979	23	5	4
JL98-1C-33	po	1C	599644	7981	3477	37	2	4
JL98-1C-33	po	1C	602103	7480	2566	30	4	0
JL98-1D-01	po	1D	606435	8325	2083	19	4	8
JL98-1D-01	po	1D	608160	7526	1909	93	3	5
JL98-1D-13A	po	1D	591503	7171	7632	61	14	1
JL98-1D-13A	po	1D	588626	6894	6857	28	8	3
JL98-1D-13B	po	1D	590208	7274	6319	43	9	5
JL98-1D-13B	po	1D	586988	6696	4744	39	8	1
JL98-1D-13B	po	1D	598025	6438	7677	50	4	0
JL98-1D-16	po	1D	590222	6632	4720	80	15	1
JL98-1D-16	po	1D	587173	6691	5221	67	4	4
JL98-1D-16	po	1D	592847	6510	7106	51	7	5
JL98-1D-18A	po	1D	586258	5808	9573	39	3	2
JL98-1D-18A	po	1D	584656	6533	9738	46	14	5
JL98-1D-18A	po	1D	588400	6878	9073	60	12	1
JL98-1D-18B	po	1D	589908	7038	4192	41	7	0
JL98-1D-18B	po	1D	586553	6793	3803	49	9	3
JL98-1D-18B	po	1D	587356	6443	4156	25	15	0
JL98-1D-21	po	1D	588708	6436	3982	39	6	2
JL98-1D-21	po	1D	586473	6848	3934	33	13	1
JL98-1D-21	po	1D	589063	7115	3738	17	2	4
JL98-BT-01	po	BT	584955	6007	7088	72	1	2
JL98-BT-02	po	BT	588436	6812	2919	29	11	2
JL98-BT-02	po	BT	588227	7311	1817	25	3	7
JL98-BT-02	po	BT	584138	5865	2319	3	13	0
JL98-BT-03	po	BT	589030	7322	1488	31	5	3
JL98-BT-03	po	BT	589065	6656	2412	12	31	6
JL98-BT-05	po	BT	592065	7538	1328	27	1	4
JL98-BT-05	po	BT	594346	8153	1123	75	2	0
JL98-BT-08	po	BT	583898	7903	1218	21	1	2
JL98-BT-08	po	BT	585187	6762	1371	22	0	2
JL98-BT-10	po	BT	593708	6721	3151	25	2	1
JL98-BT-10	po	BT	597673	7146	4750	27	6	1
JL98-BT-10	po	BT	598980	6589	5203	35	13	4
JL98-BT-10	po	BT	595495	6579	5136	20	9	2
JL98-BT-11	po	BT	601134	7100	2769	19	9	5
JL98-BT-11	po	BT	614031	6568	2382	12	3	1

Sample	Mineral	Ore Body	Fe (ppm)	Co (ppm)	Ni (ppm)	Cu (ppm)	Zn (ppm)	As (ppm)
JL98-BT-13	po	BT	602599	6568	2252	63	16	1
JL98-BT-13	po	BT	603827	6780	2396	36	4	1
JL98-BT-13	po	BT	598762	6019	2671	103	16	2
JL98-BT-14	po	BT	598976	8490	1574	12	2	2
JL98-BT-14	po	BT	587670	7585	1528	23	1	6
JL98-BT-14	po	BT	599656	7577	1384	11	3	3
JL98-BT-15	po	BT	602338	6752	6329	22	6	0
JL98-BT-15	po	BT	589207	6974	3395	22	0	0
JL98-BT-15	po	BT	593898	6511	5326	24	3	2
JL98-WL-06	po	WL	590278	5581	7363	29	8	4
JL98-WL-06	po	WL	587051	7083	6782	40	2	0
JL98-WL-06	po	WL	590264	7058	6349	47	10	0
JL98-WL-07	po	WL	585631	6255	6313	44	0	0
JL98-WL-07	po	WL	587059	6435	6604	38	1	0
JL98-WL-12	po	WL	596429	6479	7085	77	3	4
JL98-WL-12	po	WL	598256	6775	7206	52	16	4
JL98-WL-12	po	WL	595973	6726	6598	49	6	6
JL98-WL-19	po	WL	599074	7727	4514	38	7	4
JL98-WL-19	po	WL	598116	6766	4332	31	0	2
JL98-WL-19	po	WL	597832	6351	4277	43	4	3
JL98-WL-30	po	WL	599109	7302	495	0	1	0
JL98-WL-30	po	WL	595786	7436	476	19	0	2
JL98-WL-31	po	WL	583185	7168	413	4	0	2
JL98-WL-33	po	WL	602150	7068	3705	34	10	0
JL98-WL-33	po	WL	602668	7547	3954	25	13	0
JL98-WL-34	po	WL	590005	6435	7250	49	7	2
JL98-WL-34	po	WL	592949	7166	6191	34	8	4
JL98-1C-19	pn	1C	306650	11059	364033	0	11	0
JL98-1C-19	pn	1C	303730	9554	365887	15	22	0
JL98-1C-19	pn	1C	309762	8893	368193	93	47	5
JL98-1C-19	pn	1C	300162	9518	362488	91	27	6
JL98-1C-19	pn	1C	308726	9239	366184	2	34	8
JL98-1C-20	pn	1C	308182	4484	358585	0	20	0
JL98-1C-20	pn	1C	305585	4059	362841	28	17	7
JL98-1C-20	pn	1C	307695	4806	363190	17	13	10
JL98-1C-24A	pn	1C	304326	6848	365837	24	24	3
JL98-1C-24A	pn	1C	306108	7478	366196	0	15	3
JL98-1C-24A	pn	1C	304391	6894	361185	72	20	3
JL98-1C-25B	pn	1C	294664	10952	375569	62	0	0
JL98-1C-25B	pn	1C	294976	10419	375186	8	0	4
JL98-1C-25B	pn	1C	298307	11280	373197	22	22	0
JL98-1D-13A	pn	1D	305394	6439	376023	48	20	11
JL98-1D-13A	pn	1D	310484	5771	373081	95	29	6
JL98-1D-13A	pn	1D	304626	6507	371696	19	24	0
JL98-1D-16	pn	1D	306122	7008	370469	0	0	0
JL98-1D-16	pn	1D	303005	6133	365458	109	4	5
JL98-1D-18A	pn	1D	294631	6997	383371	0	14	8
JL98-1D-18A	pn	1D	293211	6824	379158	24	16	13
JL98-1D-18A	pn	1D	295894	6945	382102	0	13	4
JL98-BT-02	pn	BT	308310	16222	333961	35	18	4
JL98-BT-02	pn	BT	306210	17962	336245	75	23	7
JL98-BT-02	pn	BT	310710	17164	340165	23	9	4
JL98-BT-02	pn	BT	307162	17465	333885	18	20	0
JL98-BT-08	pn	BT	317943	19571	331463	0	27	5

Sample	Mineral	Ore Body	Fe (ppm)	Co (ppm)	Ni (ppm)	Cu (ppm)	Zn (ppm)	As (ppm)
JL98-BT-08	pn	BT	318197	19391	327671	0	22	0
JL98-BT-08	pn	BT	318280	19549	328617	0	0	0
JL98-BT-10	pn	BT	307741	20068	344408	33	0	6
JL98-BT-10	pn	BT	307816	20157	340056	33	28	7
JL98-BT-10	pn	BT	304753	20509	342983	0	24	1
JL98-BT-11	pn	BT	318666	16474	324641	92	20	1
JL98-BT-11	pn	BT	317209	17968	334560	0	1	7
JL98-BT-15	pn	BT	303534	16617	356169	75	17	1
JL98-BT-15	pn	BT	303871	16403	362646	14	14	0
JL98-BT-15	pn	BT	306558	16688	357086	46	44	5
JL98-WL-34	pn	WL	291358	11876	380421	38	40	0
JL98-WL-34	pn	WL	298667	11874	358506	26	0	0
JL98-1C-19	cp	1C	306718	6398	0	346582	320	0
JL98-1C-25B	cp	1C	322529	3173	0	339646	168	0
JL98-1C-25B	cp	1C	325200	2853	42	341187	47	0
JL98-1D-13A	cp	1D	312270	5295	0	345131	505	0
JL98-1D-13A	cp	1D	297233	4807	71	344783	247	1
JL98-1D-13A	cp	1D	312716	3758	0	348812	311	0
JL98-1D-16	cp	1D	308201	3955	565	347746	352	0
JL98-BT-02	cp	BT	321235	7336	989	338855	0	11
JL98-BT-02	cp	BT	327947	6874	416	329571	76	12
JL98-BT-08	cp	BT	302972	3309	63	344723	251	1
JL98-BT-08	cp	BT	304362	6386	1544	339065	145	0
JL98-BT-08	cp	BT	315586	6535	539	342508	89	0
JL98-BT-10	cp	BT	318586	7131	0	343269	273	8
JL98-WL-11	cp	WL	299143	6336	0	340067	134	0
JL98-WL-34	cp	WL	321219	2915	200	344853	90	13
JL98-WL-34	cp	WL	306957	399	0	344675	114	0
JL98-1C-20	py	1C	451961	19385	201	17	4	10
JL98-1C-20	py	1C	450505	16760	354	41	1	197
JL98-1C-20	py	1C	434601	19191	406	102	4	409
JL98-1D-13A	py	1D	453407	15192	3734	51	1	1
JL98-1D-13A	py	1D	454387	18066	4025	957	14	10
JL98-1D-18A	py	1D	466101	5454	42	0	9	37
JL98-1D-18A	py	1D	462369	4921	13	0	0	153
JL98-1D-18A	py	1D	465110	5164	44	14	8	18
JL98-BT-05	py	BT	472465	5375	2074	32	0	42
JL98-BT-05	py	BT	471477	5438	1581	27	3	30
JL98-BT-05	py	BT	473098	5644	554	5	3	58
JL98-WL-11	py	WL	456702	10506	603	411	8	0
JL98-WL-11	py	WL	458372	8955	264	67	2	6

APPENDIX 5: WHOLE-ROCK GEOCHEMICAL DATA

Abbreviations:

Sulphide classes:

- DS-SED = disseminated sulphides in metasediments
- DS-U = disseminated sulphides in ultramafic rocks
- IS-U = interstitial sulphides in ultramafic rocks
- MS-U = massive sulphides in ultramafic breccia
- BMS-SED = barren massive sulphides in metasediments
- MS-SED = massive sulphides in metasediments
- SMS-SED = semi-massive sulphides in metasediments.

Sample	Sulph Class	wt% SiO2	wt% TiO2	wt% Al2O3	wt% Fe2O3	wt% MnO	wt% MgO	wt% CaO	wt% Na2O	wt% K2O	wt% P2O5	wt% CO2	wt% LOI
Thompson 1C ore body													
JL98-1C-06	DS-SED	52.03	0.76	13.48	11.52	0.187	8.36	7.65	2.46	0.78	0.03		3.04
JL98-1C-07	DS-SED	49.36	0.98	12.75	13.04	0.263	12.91	3.94	0.69	3.20	0.08		2.95
JL98-1C-10	DS-SED	60.17	0.78	20.73	7.42	0.165	2.35	1.65	2.27	2.74	0.03		1.983
JL98-1C-11	DS-SED	63.47	0.55	16.29	8.02	0.055	1.85	1.23	2.06	4.05	0.03		2.5
JL98-1C-12	DS-SED	85.63	0.11	7.46	1.06	0.011	0.31	1.24	1.74	1.27	0.01		1.07
JL98-1C-14	DS-SED	76.00	0.41	10.94	3.72	0.053	1.13	1.92	2.24	1.48	0.04		2.15
JL98-1C-17	DS-SED	86.60	0.13	6.99	1.34	0.007	0.61	0.49	1.86	1.92	0.02		0.423
JL98-1C-18	DS-SED	51.54	0.84	14.22	12.81	0.196	8.66	7.56	2.34	0.50	0.06		1.616
JL98-1C-19A	SMS-SED		0.06	2.65	74.06	0.143	0.23	0.39	0.08	0.56	0.20	0.23	
JL98-1C-19B	SMS-SED	57.44	0.84	19.49	8.98	0.296	2.94	1.64	2.83	3.43	0.03		1.86
JL98-1C-20	MS-SED		0.00	0.87	80.71	0.031	0.02	0.75	0.03	0.06	0.21	0.91	
JL98-1C-25A	MS-SED		0.11	1.79	77.39	0.041	0.21	0.19	0.08	0.50	0.20	0.21	
JL98-1C-25B	MS-SED		0.07	2.40	77.66	0.050	0.24	0.34	0.28	0.43	0.21	0.29	
JL98-1C-25D	MS-SED		0.04	1.69	76.55	0.062	0.17	0.23	0.12	0.34	0.21	0.3	
JL98-1C-26B	DS-SED	80.70	0.18	9.58	2.62	0.009	0.72	1.68	2.84	1.11	0.02		0.8
JL98-1C-28A	DS-SED	60.13	0.17	4.39	25.65	1.268	3.57	3.13	0.35	0.04	0.46		1.62
JL98-1C-29	DS-SED	67.47	0.52	14.13	5.43	0.047	1.94	2.42	3.67	1.91	0.03		2.32
JL98-1C-33	DS-SED	62.40	0.67	19.28	6.92	0.055	1.96	1.23	2.10	3.55	0.04		1.758
Thompson 1D ore body													
JL98-1D-01	DS-SED	59.04	1.14	16.78	10.21	0.160	2.39	4.28	2.51	2.27	0.11		1.11
JL98-1D-03	DS-SED	66.53	0.51	14.11	7.13	0.084	1.47	1.94	3.40	2.14	0.01		2.541
JL98-1D-05	DS-SED	51.98	0.97	13.56	12.63	0.200	8.44	8.29	1.43	0.74	0.08		1.593
JL98-1D-08	DS-SED	60.66	0.65	17.37	7.65	0.130	2.15	2.32	4.35	1.80	0.02		2.85
JL98-1D-09	DS-SED	57.26	0.38	13.48	13.02	0.024	1.14	1.18	2.66	4.12	0.01		6.963
JL98-1D-11	DS-SED	65.32	0.50	16.61	5.56	0.061	1.61	1.80	3.42	2.45	0.03		2.981
JL98-1D-12	DS-SED	62.62	0.87	16.60	8.32	0.156	1.81	3.23	3.42	2.20	0.05		0.947
JL98-1D-14	SMS-SED		0.12	2.95	60.52	0.021	0.25	0.19	0.12	0.75	0.18	0.23	
JL98-1D-18A	SMS-SED		0.09	4.52	48.55	0.018	0.04	0.47	0.68	0.97	0.17		
JL98-1D-18B	DS-SED	59.11	0.79	19.23	8.33	0.217	2.53	1.27	2.29	3.68	0.06		2.82

Sample	Sulph Class	wt% SiO2	wt% TiO2	wt% Al2O3	wt% Fe2O3	wt% MnO	wt% MgO	wt% CaO	wt% Na2O	wt% K2O	wt% P2O5	wt% CO2	wt% LOI
JL98-1D-20	SMS-SED		0.07	3.37	61.90	0.019	0.06	0.47	0.51	0.67	0.19	4.06	
JL98-1D-21	DS-SED	58.77	0.41	14.66	13.60	0.759	3.06	2.47	2.56	1.66	0.07		2.15
JL98-1D-22	DS-SED	58.65	0.78	16.64	9.87	0.016	2.37	2.04	3.38	3.23	0.04		3.11
JL98-1D-23	DS-SED	63.84	0.57	18.15	7.60	0.131	1.89	0.78	1.62	3.74	0.02		1.82
JL99-1D-31	DS-SED	66.92	0.49	14.25	6.76	0.106	1.70	1.89	3.17	2.29	0.02		2.55
JL99-1D-32	DS-SED	61.23	0.73	17.26	8.49	0.125	2.36	1.73	2.74	2.63	0.02		2.8
JL99-1D-33	DS-SED	65.07	0.61	17.64	6.32	0.205	1.93	1.01	1.51	3.87	0.02		2.14
JL99-1D-34	SMS-SED		0.38	11.83	22.77	0.043	1.87	2.02	2.79	2.19	0.13		
JL99-1D-35	BMS-SED		0.06	1.55	64.88	0.018	0.03	0.32	0.23	0.28	0.23		
JL99-1D-36	DS-SED	67.76	0.35	14.85	6.05	0.152	1.33	2.05	3.48	1.70	0.02		2.23
JL99-1D-37	BMS-SED		0.15	3.97	50.02	0.029	1.59	0.56	0.55	1.08	0.11	9.27	N.M.
JL99-1D-38	BMS-SED		0.38	6.84	37.28	0.078	3.38	0.32	0.54	2.04	0.09	1.62	N.M.
JL99-1D-39	BMS-SED		0.10	1.72	61.60	0.015	0.38	0.45	0.57	0.37	0.13	16.3	N.M.
Birchtree Mine													
JL98-BT-01	DS-U	32.59	0.01	0.32	10.79	0.093	39.10	0.04	0.31		0.01		16.27
JL98-BT-02	MS-UB		0.01	0.93	85.57	0.037	0.73	0.09	0.02	0.10	0.23	0.09	
JL98-BT-03	IS-U	34.18	0.17	1.63	18.84	0.052	34.99	0.09	0.81			0.09	8.59
JL98-BT-04	DS-SED	60.05	0.45	11.94	15.50	0.847	3.82	1.55	0.88	2.96	0.10		2.238
JL98-BT-05	DS-SED	60.39	0.34	9.10	17.51	0.585	4.98	0.94	0.29	1.82	0.16		3.62
JL98-BT-08B	MS-UB		0.01	0.83	86.18	0.028	1.91	0.18	0.02	0.02	0.22	0.1	
JL98-BT-09	DS-U	37.22	0.10	2.63	9.79	0.090	35.88	0.25	0.49		0.01		13.2
JL98-BT-10	MS-SED			0.31	87.28	0.015	0.12	0.08	0.01		0.22	0.06	
JL98-BT-11	DS-U	48.47	0.18	5.04	11.53	0.221	26.17	3.95	0.39	0.03	0.03		3.69
JL98-BT-12	DS-SED	51.42	0.90	14.60	12.87	0.196	7.38	5.36	3.74	1.23	0.05		2.539
JL98-BT-15	MS-SED		0.01	0.77	83.68	0.022	0.63	0.28	0.02	0.05	0.23	0.08	
JL98-BT-16B	MS-UB		0.01	1.03	58.37	0.025	3.67	1.07	0.03	0.01	0.21		
JL98-BT-18	DS-SED	64.16	0.62	17.23	4.97	0.053	1.68	2.38	5.47	2.09	0.05		1.244
JL98-BT-20	MS-UB		0.02	1.19	82.33	0.035	0.79	0.24	0.03	0.16	0.24	0.12	
JL98-BT-25	DS-U	33.41	0.01	0.28	10.30	0.188	38.96	0.05	0.35				16.18

Sample	Sulph Class	wt% SiO2	wt% TiO2	wt% Al2O3	wt% Fe2O3	wt% MnO	wt% MgO	wt% CaO	wt% Na2O	wt% K2O	wt% P2O5	wt% CO2	wt% LOI
Thompson T1 Mine													
JL98-T1-03	DS-SED	82.63	0.01	0.29	9.18	0.023	1.97	2.79	0.37	0.01	0.14		2.801
JL98-T1-06	DS-SED	61.34	0.74	18.78	7.04	0.083	2.79	1.68	2.76	2.94	0.03		1.963
JL98-T1-09A	MS-UB			0.46	82.12	0.034	0.07	0.94	0.01	0.06	0.23	0.98	
JL98-T1-10	DS-U	36.48	0.07	2.00	12.29	0.184	38.26	0.24	0.70	0.14			8.29
JL98-T1-11	IS-U	31.89	0.07	2.01	22.20	0.199	31.28	0.51	0.05	0.57		0.08	9.08
JL98-T1-12	MS-UB			0.42	81.48	0.022	0.52	0.09	0.01	0.02	0.22	0.14	
JL98-T1-16	DS-SED	38.11	0.17	2.88	27.39	0.400	7.22	13.16	0.40	0.13	2.34	0.47	6.82
JL98-T1-17	DS-SED	63.58	0.72	18.77	6.63	0.042	1.90	0.92	1.80	3.69	0.06		2.09
JL98-T1-19	MS-SED		0.05	1.94	79.84	0.087	0.36	0.36	0.20	0.39	0.22	0.67	
JL98-T1-20	DS-SED	68.36	0.53	13.08	5.31	0.039	2.09	2.08	3.98	1.91	0.06		2.8
JL98-T1-22	MS-UB		0.37	8.40	29.24	0.093	2.69	2.55	0.36	2.01	0.16		
JL98-T1-23	DS-SED	68.32	0.54	14.34	5.96	0.243	2.03	2.14	2.63	2.78	0.04		1.268
JL99-T1-24	DS-SED	40.70	0.24	5.01	34.26	4.315	7.13	5.28	0.04	0.34	0.45		2.763
JL99-T1-25	BMS-SED		0.06	1.84	62.57	0.035		0.34	0.29	0.22	0.19		
JL99-T1-26	BMS-SED		0.03	0.12		0.026	0.12	0.05	0.10	0.14	0.09	11.9	N.M.
JL99-T1-27	DS-SED	64.78	0.39	14.83	7.52	0.080	2.49	2.92	2.81	1.85	0.15		2.452
JL99-T1-32	DS-SED	68.74	0.26	15.83	1.78	0.033	0.92	1.91	3.88	5.31	0.08		1.33
JL99-T1-33	DS-SED	51.51	0.95	13.81	12.72	0.341	10.81	3.24	0.29	4.15	0.07		2.41
JL99-T1-34	DS-SED	87.62	0.05	5.94	0.84	0.010	0.14	0.70	1.35	2.22	0.01		1.3
JL99-T1-35	MS-SED		0.02	1.01	57.27	0.026		0.19	0.08	0.20	0.18		
JL99-T1-36	DS-SED	62.45	0.66	16.69	7.17	0.041	2.04	1.67	3.02	2.18	0.02		3.938

Sample	Sulph Class	wt% S	ppm Cr	ppm Ni	ppm Co	ppm Cu	ppm Zn	ppb Ir	ppb Ru	ppb Rh	ppb Pt	ppb Pd	ppb Au	ppm Bi	ppb Se	ppm As
Thompson 1C ore body																
JL98-1C-06	DS-SED	2.70	418	102	66	125	109									
JL98-1C-07	DS-SED	0.01	375	395	59	2	126									
JL98-1C-10	DS-SED	0.06	118	80	54	4	100									
JL98-1C-11	DS-SED	1.56	97	39	64	188	88									
JL98-1C-12	DS-SED	0.21	23	20	103	4	27									
JL98-1C-14	DS-SED	0.64	65	49	78	54	60								2000	
JL98-1C-17	DS-SED	0.19	34	18	98	13	25								1100	
JL98-1C-18	DS-SED	0.03	294	227	75	26	103									
JL98-1C-19A	SMS-SED	33.30	312	75120	1336	2560		113.4	368.8	120.0	7.7	226.6	3.8	1.27	25200	33.5
JL98-1C-19B	SMS-SED	0.29	155	1133	39	75	169							0.03	326	
JL98-1C-20	MS-SED	37.30	670	82280	1071	628		141.0	458.8	131.0	7.8	291.6	13.9	2.92	24500	44.3
JL98-1C-25A	MS-SED	34.60	1530	66600	1323	3376	62	163.0	431.8	143.0	22.6	627.6	10.0	4.02	31100	84.2
JL98-1C-25B	MS-SED	33.60	1170	66240	1496	3042		138.0	396.8	141.0	28.7	672.6	18.3	4.1	27600	97
JL98-1C-25D	MS-SED	35.50	860	86400	1955	3078		144.0	446.8	156.0	27.3	915.6	14.9	5.06	32200	85.5
JL98-1C-26B	DS-SED	0.36	38	38	104	47	47									
JL98-1C-28A	DS-SED	0.52	46		7	438	135							0.12	396	
JL98-1C-29	DS-SED	0.76	82	43	21	153	226							0.06	233	
JL98-1C-33	DS-SED	0.57	122	65	50	104	113									
Thompson 1D ore body																
JL98-1D-01	DS-SED	0.43	56	57	27	69	121									
JL98-1D-03	DS-SED	1.18	101	69	54	100	72								4000	
JL98-1D-05	DS-SED	0.17	368	233	65	65	103	0.1	0.6	0.7	6.9	18.4	0.9			
JL98-1D-08	DS-SED	0.87	115	43	44	215	115									
JL98-1D-09	DS-SED	5.99	64	96	174	328	64								2500	1.4
JL98-1D-11	DS-SED	0.63	80	72	39	174	77									
JL98-1D-12	DS-SED	0.29	62	36	31	0	115									
JL98-1D-14	SMS-SED	33.80	268	108840	1535	3200		47.5	265.8	116.0	10.3	1050.6	49.5	34.57	31500	323
JL98-1D-18A	SMS-SED	27.40	245	84040	744	856		114.0	181.9	136.0	360.8	1587.5	95.6		26600	264
JL98-1D-18B	DS-SED	0.52	121	515	38	290	130							0.07	177	

Sample	Sulph Class	wt% S	ppm Cr	ppm Ni	ppm Co	ppm Cu	ppm Zn	ppb Ir	ppb Ru	ppb Rh	ppb Pt	ppb Pd	ppb Au	ppm Bi	ppb Se	ppm As
JL98-1D-20	SMS-SED	31.50	141	114120	1325	1842		57.0	97.8	92.0	15.0	1017.6	28.6	28.46	22600	321
JL98-1D-21	DS-SED	2.22	120	2224	23	253	131	0.0	0.2	0.3	3.5	29.0	8.4	0.14	3400	1.2
JL98-1D-22	DS-SED	2.77	94	157	30	308	112	0.1	0.1	0.2	4.4	4.8	3.0	0.15	396	
JL98-1D-23	DS-SED	0.39	118	62	54	21	98									
JL99-1D-31	DS-SED	0.82	96	49	52	79	91									
JL99-1D-32	DS-SED	0.74	125	154	62	220	112									
JL99-1D-33	DS-SED	0.18	96	72	68	14	98									
JL99-1D-34	SMS-SED	8.71	100	328	77	666	106								1400	6.5
JL99-1D-35	BMS-SED	33.40	27	430	103	314	71								12700	1.7
JL99-1D-36	DS-SED	1.04	162	29	53	48	80								1000	
JL99-1D-37	BMS-SED	24.60	110	9570	125	591	129								11100	26.2
JL99-1D-38	BMS-SED	15.80	242	6152	93	796	229								7400	7.4
JL99-1D-39	BMS-SED	31.80	21	12821	157	264	104								11900	9.8
Birchtree Mine																
JL98-BT-01	DS-U	0.22	2155	6794	153	104	43	5.5	9.6	2.1	13.5	13.1	0.5	0.14	478	
JL98-BT-02	MS-UB	37.30	800	49280	2034	588		57.4	148.8	27.2	26.4	88.6	21.2	0.52	22300	49.1
JL98-BT-03	IS-U	3.03	2863	6600	135	190	76	9.0	12.3	4.4	32.8	8.5	19.4	0.14	1770	
JL98-BT-04	DS-SED	0.68	103	31	48	51	102									
JL98-BT-05	DS-SED	2.84	70		10	173	22							0.83	2400	8.3
JL98-BT-08B	MS-UB	37.40	558	23840	940	238	28	25.2	71.8	15.5		12.1	3.9	0.31	21900	8.1
JL98-BT-09	DS-U		3078	4120	83	14	51	2.8	5.1	1.1	5.2	5.2	7.4	0.12	69	
JL98-BT-10	MS-SED	37.70	91	42280	1774	426		12.0	47.6	10.1	0.6	19.7		0.37	19000	34.3
JL98-BT-11	DS-U	0.89	2600	2511	76	95	200	2.2	2.2	0.6	1.7	4.0	1.8	0.07	466	
JL98-BT-12	DS-SED	0.32	292	215	68	278	108									
JL98-BT-15	MS-SED	33.30	340	50560	1825	1010		56.1	145.8	27.7	2.5	123.6	4.2	1.52	23000	71.3
JL98-BT-16B	MS-UB	32.60	1250	43760	1370	7720	4	31.4	96.9	21.3	2.3	51.9	1432.6		15700	95.5
JL98-BT-18	DS-SED	0.12	93	57	56	62	72								1300	
JL98-BT-20	MS-UB	37.00	307	48520	1901	1538		49.9	140.8	36.0	5.4	71.1	13.8	1.95	17400	81.5
JL98-BT-25	DS-U	0.19	2038	3478	97	77	28	7.3	9.3	2.4	9.5	17.0	1.9	0.14	414	

Sample	Sulph Class	wt% S	ppm Cr	ppm Ni	ppm Co	ppm Cu	ppm Zn	ppb Ir	ppb Ru	ppb Rh	ppb Pt	ppb Pd	ppb Au	ppm Bi	ppb Se	ppm As
Thompson T1 Mine																
JL98-T1-03	DS-SED	4.15	17	11	127	155	44									
JL98-T1-06	DS-SED	0.77	112	57	58	136	183									
JL98-T1-09A	MS-UB	38.20	26	79920	1785	2810		3.9	4.4	38.1	5.1	395.6	10.4	5.36	22200	12.9
JL98-T1-10	DS-U	1.79	4081	11720	142	268	538	11.0	32.5	9.5	50.8	66.9	27.1	0.5	2600	50.1
JL98-T1-11	IS-U	8.89	7136	16120	388	2112	98	22.6	40.5	37.0	13.3	149.6	163.9	1.49	9200	50
JL98-T1-12	MS-UB	37.90	92	70240	1521	2054		23.6	38.0	28.7	1.7	138.6	1.1	4.12	34300	86.5
JL98-T1-16	DS-SED	6.57	10	74	35	1022	38							1.11	2200	12.8
JL98-T1-17	DS-SED	0.01	94	86	72	2	95									
JL98-T1-19	MS-SED	35.00	370	52720	952	345		110.0	370.8	130.0	28.9	564.6	51.6	5.74	24400	114
JL98-T1-20	DS-SED	0.94	70	41	8	70	74							0.09	342	
JL98-T1-22	MS-UB	16.00	734	24680	424	1370	85	96.0	247.9	100.0	30.6	555.5	47.6		11800	69.6
JL98-T1-23	DS-SED	0.37	119	81	82	95	114									
JL99-T1-24	DS-SED	4.50	53	45	55	366	136									
JL99-T1-25	BMS-SED	30.70	25	1778	65	770	133								10100	15
JL99-T1-26	BMS-SED	37.00	30	1590	18	876	165								10300	23.8
JL99-T1-27	DS-SED	2.10	78	52	80	64	296									
JL99-T1-32	DS-SED	0.03	49	37	85	3	119									
JL99-T1-33	DS-SED	0.06	405	302	72	1	126								900	
JL99-T1-34	DS-SED	0.15	18	22	141	3	25								2000	
JL99-T1-35	MS-SED	35.50	262	7660	1093	2502		157.0	439.9	198.0	32.4	848.5	17.0		32000	108
JL99-T1-36	DS-SED	1.84	109	66	80	73	83									